STUDY II

STUDY ON STATE OF THE ART AND NEXT GENERATION PHOTOVOLTAICS

THE CIRCA GROUP EUROPE

January 2013

TABLE OF CONTENTS

Table of Figure ... 3

Table of Tables ... 12

1 Introduction ... 14

1.1 Study II: State of the art and next generation photovoltaic ... 14

1.1.1 Study goals and objectives ... 14

1.1.2 Reasons for the doing this study ... 14

1.1.3 Scope ... 15

1.1.4 Methodology and Information sources ... 15

1.2 Summary Layout ... 16

1.3 Overview of the report ... 17

1.3.1 Background ... 17

1.3.2 The highest independently confirmed efficiencies for solar cells and modules ... 19

1.3.3 Costs, targets and learning curve ... 23

2 State of the art analysis of currently employed and next generation PV technologies 25

2.1 Crystalline silicon ... 25

2.1.1 Trends in raw material: mono-, multi-, quasi-mono- crystalline silicon ... 26

2.1.2 Trends in crystalline silicon wafering technology ... 39

2.1.3 Review of trends in p-type and n-type wafers applications ... 54

2.1.4 Solar cells ... 57

2.1.5 Module manufacturing ... 70

2.2 Thin Film ... 83

2.2.1 Overview of main trends ... 83

2.2.2 Cadmium Telluride photovoltaic technology ... 91

2.2.3 Copper–indium–gallium–diselenide (CIGS) photovoltaic technology ... 100

2.2.4 Thin film silicon modules ... 105

2.3 Concentrator photovoltaics ... 122

2.3.1 Conclusions: CPV ... 136

2.4 Emerging photovoltaics ... 137

2.4.1 Organic /Polymer solar cells ... 139

2.4.2 Dye-sensitized solar cells 153
2.4.3 New technologies for PV cell production 166
2.4.4 Conclusions: emerging photovoltaics 186
3 Complementary technology: energy storage 188
3.1 Needs for electric energy storage 188
3.2 Electricity Storage: technology overview 190
3.2.1 Larger energy storage systems: comparison of technical features 192
3.2.2 Operational and planned large scale battery energy systems 194
3.2.3 Comparison of economic features 197
3.2.4 Short-term storage: nanomaterial supercapacitors 198
3.2.5 Conclusions: energy storage 200
4 Forecast of related RTD activities and scientific potential development 203
4.1 Specific technology goals and R&D issues 203
4.1.1 Crystalline silicon 204
4.1.2 Thin films 207
4.1.3 Emerging technologies and novel concepts 209
4.1.4 Concentrator technologies (CPV) 210
4.2 Expected impact of roadmaps and research agendas 210
5 Conclusions 213

TABLE OF FIGURE

Figure 1: Areas of Activity in PV value chain 17

Figure 2: Global annual PV Installation by technology in 2011. The global solar PV installations reached about 32 GW in 2012. Source: Fraunhofer ISE, 2012 18

Figure 3: Efficiency Comparison of Technologies: Best Lab Cells vs. Best Lab Modules. Source: Franhofer ISE, 2012 19

Figure 4: Price learning curve by technology cumulative production up to 2012. Learning Rate: Each time the cumulative production doubled, the price went down by 19.6 %. Source: Fraunhofer ISE, 2012 23

Figure 5: The primary steps of the wafer-based c-Si module supply chain. Source: A. Goodrich, 2012 25

Figure 6: Price learning curve for crystalline Si modules as function of installed capacity (Sources: National Renewable Energy Laboratory, European Photovoltaic Industry Association, Navigant Consulting.) 26

Figure 7: Alternative routes for solar grade silicon, *(Source: New Feedstock Materials, Aud Waernes et al, Proceedings NREL/BK-520-40423)* 27

Figure 8: Generalized process flow for the production of solar grade polysilicon feedstock via the *Siemens* process. Source: A. Goodrich, 2012 29

Figure 9: Expected change in share of poly-Si production technologies. Source: ITRPV, 2012 31

Figure 10: Schematic setup of a Czochralski crystal puller. Source: S. Meroli, 2012 32

Figure 11: Estimated Cz-wafer costs, minimum sustainable price standard (U.S. and China) and high-lifetime (U.S.) processing route (170 µm wafer thickness, 130 µm kerf-loss, $35/kg poly price) Source: Photovoltaic Specialists Conference (PVSC), 2012 38th IEEE 33

Figure 12: Growth over the last five years in the size of ingots cast using DSS. Source: Fisher et al, 2012 34

Figure 13: Crystalline silicon market share by technology. Sourece: PV Magazine, 2012 36

Figure 14: Crystalline silicon wafer technology by efficiency 36

Figure 15: Different categories of quasi-mono wafer in the same ingot. Source: PV magazine, 2012 37

Figure 16: Cell with grains with different colours. Source: PV magazine, 2012 38

Figure 17: Process and materials flow for standard Cz growth of monocrystalline silicon ingots and subsequent cropping, squaring, and wafering. Typical material losses in production are shown on the outside of the processing steps, where the solid scrap

generated through sawing of the boule crown, tail, and chords is recycled for further ingot pulls; but the kerf loss in sawing is not. The given 'Capex' numbers within each step refer to the associated capital equipment expenses divided by the annual production capacity of the facility, with an assumed solar cell power conversion efficiency of 16.7%. Source: A. Goodrich, 2012 39

Figure 18: Projected trend in minimum wafer thickness processed in mass production of solar cells (Source: International Technology Roadmap for Photovoltaics, SEMI PVGroup/ITRPV, 2011) 40

Figure 19: With sufficient passivation to reduce surface recombination velocity, cell efficiency may be optimized with cell thickness of around 20–60 μm [48], [49]. (Source: J. Fossum, University of Florida and Stuart Bowden, Arizona State University) 41

Figure 20: Multi-wire slurry saw process. Kerf loss and wafer thickness are set by the wire guide roller (WGR), wire diameter and carrier/abrasive grit selection (Source: Henley, F.J., 2010) 42

Figure 21: Alternative wafering technologies using the three available phases of silicon (Source Henley, F.J., 2010) 43

Figure 22: Upstream silicon source connection to the three phases of wafering (Source Henley, F.J., 2010) 44

Figure 23: Silicon Genesis Corporation PolyMax™ Process and 20μm / 50μm wafers 51

Figure 24: Schematic representation of the differences in recombination at impurities for p-type versus n-type solar cells. Typical transition metal impurities are donor-type, resulting in a large capture cross-section for electrons, but a much smaller one for holes. Therefore they are effective minority carrier recombination centres in p-type cells, but not in n-type cells. In addition, in p-type Cz, boron-oxygen-related defects are present, which are important recombination centres 55

Figure 25: Process flow for fabricating a standard c-Si solar cell. Source: NREL, 2012 57

Figure 26: Schematic illustration of the back-contacted back-junction n-type silicon solar cells with a large emitter coverage (A) and small emitter coverage (B) featuring a passivating and insulating thin film on the rear side (top). Also shown is a schematic top view of the emitter and back surface field diffusions on the rear side (bottom) including the active solar cell area as well as the interdigitated metallization and the busbar area (dotted lines). The distance between the n-metal and the p-metal fingers, that is, the pitch (metal fingers), is smaller than the pitch distance. Source: John Wiley & Sons, Ltd., 2012 59

Figure 27: Front-side metallization on a p-type Cz wafer (20–22% cell efficiency). Source: NREL, 2012 66

Figure 28: Interdigitated back contact (IBC) c-Si solar cell (≈25% cell efficiency). Source: NREL, 2012 67

Figure 29: Heterojunction with intrinsic thin layer (HIT) cell (≈24% cell efficiency). Source: NREL, 2012 68

Figure 30: Expected market share of different c-Si cell concepts. Source: ITRPV, 2012 .. 68

Figure 31: Top: Cost model results for completed modules: a compilation of estimated costs for manufacturing standard modules and advanced modules within the full c-Si supply chain, assuming all products are transferred at minimum sustainable prices. The numbers underneath each cell type indicate the assumed module efficiency and wafer thickness for each. The long-term scenario reflects the projected costs and prices for modules made with cells on 80-μm wire-sawn kerfless wafers at minimum sustainable polysilicon prices. Bottom: efficiency-adjusted module prices for the different cell types, in consideration of balance-of-systems savings (HIT and IBC) or costs. The BOS efficiency adjustments to the module prices are normalized against the 20% module efficiency targeted within the U. S. Department of Energy's SunShot Initiative. Source: NREL, 2012 72

Figure 32: The target system for state-of-the-art PV production (Technology leadership and integrated automation drives TCO). Source: Manufacturing the solar future, 2012 . 74

Figure 33: 6-M representation of the factors influencing uptime. Source: Manufacturing the solar future, 2012 75

Figure 34: The P V system with elements in the box (1), between the boxes (2) and out of the box (3) is encompassed by the MES automation system (4), thus representing the second order of cybernetic feedback systems and fulfilling the requirements for an integrated, intelligent MES automation system. Source: Manufacturing the solar future, 2012 77

Figure 35: The blue curve shows the benefit of integrated systems with fast ramp-up and very short response times vs. the light grey curve which represents very low automation integration with a high risk of expensive trial and error processes. Manufacturing the solar future, 2012 78

Figure 36: Expected yield trend in module manufacturing (ratio of good cells in good modules out to good cells in) (Green Industrial solution exists and is being optimized in production. Yellow Industrial solution is known but not yet in mass production.Red Industrial solution is not known). Source: ITRPV, 2012 79

Figure 37: Expected improvement in throughput for module manufacturing equipment (Green Industrial solution exists and is being optimized in production, Yellow Industrial solution is known but not yet in mass production, Orange Interim solution is known, but too expensive or not suitable for production). Source: ITRPV, 2012 80

Figure 38: Market share of different c-Si module types as fraction of worldwide production. Source: ITRPV, 2012 82

Figure 39: Market share of different module sizes. Source: ITRPV, 2012 82

Figure 40: Estimation of market shares of thin film materials CdTe, a-Si/uc-Si and CIGS in 2008 84

Figure 41: Updated estimation of market shares of thin film materials CdTe, a-Si/f.lc-Si and CIGS, 2012, by B. Dimmler 85

Figure 42: Expectations of experts of the evolution of efficiencies on cell (dashed lines) and module level (solid lines) in the future 88

Figure 43: Cost structure according to detailed calculations of Manz AG for a CIGS module production of 200 MWp/a today 89

Figure 44: Main impacts on production cost for large-scale CIGS manufacturing 89

Figure 45: A cross-sectional representation of a monolithically integrated layer stack used in commercial (single-junction, polycrystalline) CdTe cells. Source: NREL 2012 91

Figure 46: Projecting paths for CdTe photovoltaics. The concerns about Te availability limiting CdTe PV module production assume that the layer thickness will be maintained at 3 μm. Projections of maximum market share attainable are shown based on modest increases in Te production (from 1% growth per year in copper production, its main supply route) and module efficiency (15%), but substantial decreases in CdTe active-layer thickness. The blue and purple lines are market-share maxima if 10% of the world electricity is made from PV in 2030, with layer thicknesses of 0.67 and 0.2 μm, respectively. Similar projections (orange and green) are for 25% world electricity production by PV in 2030. In all cases, with thin enough CdTe, nearly 100% market share might be attained. The inset shows tellurium in its native form. Source: K. Zweibel, 2010 92

Figure 47: Light absorption and current generation characteristics of CdTe solar cells. (a) The plot on the left displays the absorption coefficient of CdTe, and the curve on the right (b) portrays the relative amount of current that can be expected (normalized from the current density at the cell's maximum power point) as a function of the CdTe layer thickness. The curve is derived from the spectral output seen after AM 1.5 light has been attenuated by front glass reflection and absorption from 600 Å CdS on 1.0 μm SnO_2. Source NREL 2012 95

Figure 48: Projected roadmap Te intensity for module production over time. The rates of improvement in efficiency and CdTe thickness were set at +0.4% per year and −75 nm per year, respectively. Source NREL 2012 97

Figure 49: Overview of module manufacturing cost model results for monolithically integrated CdTe in rigid glass. Source NREL 2012 98

Figure 50: Simulated CdTe module manufacturing costs as a function of changing the input efficiency, WACC, and CdTe thickness. The simulation was run without changing the Te price or capital costs. Gradual reductions in the CdTe thickness are represented, as is the WACC in anticipation that the required rate of return for investments in PV companies will be lowered in the future as the industry matures and is given the

expected benefit of a reduced risk profile. Some of the technical improvement opportunities that are available are shown within the figure captions. In coordination with Table 12, they have been put forth here as examples that may achieve the efficiency targets shown. Source NREL 2012 98

Figure 51: Waterfall chart to represent how CdTe module manufacturers could conceivably address dramatic increases in the price for Te and still meet a module price target that may be competitive against the projected long-term price of c-Si. All other material and depreciation expenses are assumed to be constant. Source NREL 2012 99

Figure 52: Monolithically interconnected CIGS solar cells 100

Figure 53: Monolithically interconnected CdTe solar cells 100

Figure 54: Schematics of example commercial thin-film silicon PV module device structures. (a) A single-junction a-Si PV module with Al back contact (e.g. Applied Materials a-Si turn-key products) (b) Dual-junction a-Si/a-Si module, (c) Tandem-junction a-Si/μc-Si "micromorph" PV module with ZnO:Al backcontact and white paste reflector (e.g. Oerlikon micromorph turn-key products), and (d) Triple-junction a-Si/a-SiGe/a-SiGe PV cell built on stainless steel foil (e.g. Uni-Solar (Energy Conversion Devices)). 106

Figure 55: Schematic drawing of a silicon electron–beam evaporation chamber. Courtesy: Oerlikon Solar AG, 2012 116

Figure 56: Absorption spectra of a solid phase crystallized 2 μm-periodic poly-Si microhole array (black) and a planar poly-Si film (grey) with a nominal layer thickness of 2.1 μm. The microhole array (see inset) was fabricated via a bottom-up process on a nanoimprint-textured glass substrate. Courtesy: Oerlikon Solar AG, 2012 118

Figure 57: Absorption spectra of a liquid phase crystallized poly-Si thin-film on a 2 μm-periodically structured glass substrate (black) and a reference film on a planar glass substrate, both with a nominal thickness of 6 μm. The inset shows a cross-sectional SEM micrograph of the LPC poly-Si thin-film on nanoimprint-textured glass substrate. Courtesy: Oerlikon Solar AG, 2012 119

Figure 58: Schematic of the electron gun (top) and picture of the crystallization process (bottom). Courtesy: Helmholtz-Zentrum Berlin, 2012 120

Figure 59: Progression of various terrestrial concentrator solar cell designs, beginning with today's 3-junction C3MJ+ and 40% C4MJ cells, and increasing efficiency to over 50% under the concentrated AM1.5D spectrum 125

Figure 60: (a) Cross-sectional diagram and (b) illuminated *I–V* curves for subcells and the full multijunction cell for a 3-junction, upright metamorphic (MM) GaInP/GaInAs/Ge concentrator solar cell (C4MJ), with modeled production average efficiency of 40.0% at 500 suns (50.0 W/cm^2). Source: Source: Wiley Interdisciplinary Reviews, 2012 127

Figure 61: Calculated efficiencies for ideal two-terminal triple-junction cells at 100X. The black dots are calculated using real spectrum at Golden, CO, USA in 2002. The red line is

calculated under a simple assumption that air mass is the only factor that affects spectrum 128

Figure 62: (a) Cross-sectional diagram and (b) illuminated *I*–*V* curves for subcells and the full multijunction cell for a 4-junction, upright metamorphic (MM) AlGaInP/AlGaInAs/GaInAs/Ge concentrator solar cell, with modeled production average efficiency of 44.4% at 500 suns (50.0 W/cm^2). Source: Wiley Interdisciplinary Reviews, 2012 130

Figure 63: (a) Cross-sectional diagram and (b) illuminated *I*–*V* curves for subcells and the full multijunction cell for a 5-junction, lattice-matched AlGaInP/AlGaInAs/GaInAs/epitaxial Ge/Ge concentrator solar cell, with modeled production average efficiency of 43.2% at 500 suns (50.0 W/cm^2). Source: Wiley Interdisciplinary Reviews, 2012 131

Figure 64: (a) Cross-sectional diagram and (b) illuminated *I*–*V* curves for subcells and the full multijunction cell for a 5-junction, lattice-matched AlGaInP/AlGaInAs/GaInAs/dilute nitride GaInNAs(Sb)/Ge concentrator solar cell, with modeled production average efficiency of 47.4% at 500 suns (50.0 W/cm^2). Source: Wiley Interdisciplinary Reviews, 2012 132

Figure 65: (a) Cross-sectional diagram and (b) illuminated *I*–*V* curves for subcells and the full multijunction cell for a 6-junction, inverted metamorphic (IMM) cell and three transparent graded buffer regions (MMX3), with an AlGaInP/AlGaAs/AlGaAs/GaInAs/GaInAs/GaInAs structure, and with modeled production average efficiency of 50.9% at 500 suns (50.0 W/cm^2). Source: Wiley Interdisciplinary Reviews, 2012 133

Figure 66: (a) A typical reflective CPV module structure; (b) a typical refractive CPV module structure. Source: Wiley Interdisciplinary Reviews, 2012 135

Figure 67: Spectral analysis of the minimum losses for a silicon solar cell (band-gap = 1.1 eV). These are the losses accounted for in the Shockley-Queisser limit and represent an upper limit for solar cells made from single-junction bulk semiconductors. Thermalization represents the largest loss in this analysis, and it increases for the higher energy portions of the solar spectrum. Courtesy by G. Conibeer and S. Huang 138

Figure 68: Basic research underway with the technology developments required to achieve the desired applications. Source: Nanotechnology for the energy Challenge, J. G. Martinez, 2010 139

Figure 69: Year wise progress of different solar cell technologies. Source: National Renewable Energy Laboratory, 2012 141

Figure 70: The power conversion efficiency values obtained as a function of publication year, the inset shows the distribution of power conversion efficiency values. Courtesy by M. Jørgensen 143

Figure 71: Optical losses due to polymer bandgap mismatch with solar spectrum. Source: W. Cai et al. Solar Energy Materials & Solar Cells, 2010 144

Figure 72: Schematic illustration of organic solar cells can be manufactured by standard printing processes. Source: R. Gaudiana et al. Nat. Photonics, 2008 148

Figure 73: A graphical overview of the field of stability and degradation of polymer solar cells. Source: W. Cai et al. Solar Energy Materials & Solar Cells, 2010 150

Figure 74: Dye-sensitized solar cell device schematic and operation: a, Liquid-based DSCs are comprised of a transparent conducting oxide (such as fluorine-doped tin oxide, FTO) on glass, a nanoparticle photoanode (such as titania) covered in a monolayer of sensitizing dye, a hole-conducting electrolyte and a platinum-coated, FTO-coated glass back-contact. b, Energy level and device operation of DSCs; the sensitizing dye absorbs a photon (energy $h\nu$), the electron is injected into the conduction band of the metal oxide (titania) and travels to the front electrode (not shown). The oxidized dye is reduced by the electrolyte, which is regenerated at the counter-electrode (not shown) to complete the circuit. VOC is determined by the Fermi level (EF) of titania and the redox potential (I_3^-/I^-) of the electrolyte. Source: Nature Photonics, 2012 154

Figure 75: Best-in-class dye-sensitized solar cells: the external quantum efficiency versus wavelength (a) and photocurrent density versus voltage (b) for the ruthenium dye (CYC-B11)/iodide redox couple, the co-sensitized donor–pi–acceptor dye (YD2-o-C8 and Y123)/cobalt redox couple and a solid-state system comprised of the Y123 dye and the hole conductor spiro-OMeTAD. Absorbing into the NIR region of the spectrum increases the photocurrent density from 20 mA cm−2 to 30 mA cm−2. c, Chemical structures of the best-performing ruthenium-based complex CYC-B11, together with donor–pi–acceptor dyes YD2-o-C8 and Y123. d, Chemical structures of the iodide redox couple, a cobalt redox mediator and the solid-state hole conductor spiro-OMeTAD. Source: Nature Photonics, 2012 155

Figure 76: DSC containing ERDs: ERDs mixed inside the liquid electrolyte (a) and co-sensitized to the titania surface (b). Typical absorption process for lower energy (red) photons in DSCs: light is absorbed by the sensitizing dye (i), after which an electron is transferred to the titania and a hole is transported to the back contact through the electrolyte. The ERD process is similar except that higher energy (blue) photons are first absorbed by the ERD and then undergo Förster resonant energy transfer (FRET; ii) at rate k_{ET} to the sensitizing dye, which is responsible for charge separation (iii) involving electron injection (rate k_{inj}) and hole regeneration (rate k_{reg}). Source: Nature Photonics, 2012 164

Figure 77: (a) SEM image of amorphous Si:H nanocones prepared by nanosphere lithography. (b) Measured value of absorption on samples with a-Si:H thin film, nanowire arrays, and nanocone arrays as the top layer over a large range of wavelengths at normal incidence. (c) Schematic of a dual-diameter nanopillar array embedded in anodic aluminum oxide templates. (d) Experimental absorption spectra of a dual-diameter nanopillar array with D_1 = 60 nm and D_2 = 130 nm, and single-diameter

nanopillar arrays with diameters of 60 and 130 nm. Source: Nanoscale , 2012, 4 M.Yu 169

Figure 78: Schematic of carrier collection in a planar thin film single junction solar cell (a) and a 3D nanowire/pillar solar cell (b). (c) Spectral response of typical photo-etched planar and nanorod array photo-electrochemical cells with the external quantum yield normalized to its highest value. Source: Nanoscale , 2012, 4 M.Yu 171

Figure 79: (a) SEM image of the hollow-tip arrays, and (b) an optical image of the water droplet profile (5 mL) on the silicon hollow-tip array surface. Source: The Royal Society of Chemistry, 2009 172

Figure 80: (a) Tilted cross-sectional SEM image of the Si nanowire solar cell. (b) The side view (45°) SEM image of the ordered Si NCF arrays, with scale bar 800 nm. (c) Cross-sectional schematic of ZnO-nanorod/a-Si:H solar cells. Source American Institute of Physics, 2011 173

Figure 81: (a) Cross-sectional SEM image of Ge dual-diameter nanopillars after the growth in anodic aluminum oxide (AAO) membranes. (b) SEM of a single Ge dual-diameter nanopillar. (c) SEM image of the GaAs core/shell nanowires. Source: American Chemical Society, 2010 174

Figure 82: (a) SEM image of as grown array of vertically aligned CNT towers. (b) Cutaway view of individual CNT tower (black) coated with CdTe (gray) and CdS. (c) The corresponding increase in efficiency for CNT-cell with respect to azimuthal angle. Source: Springer-Verlag, 2007 175

Figure 83: (a) Schematic of a solar nanopillar cell consisting of an array of CdS nanopillars partially embedded in a CdTe thin film. (b) The open-circuit voltage slightly increases with the intensity and the solar energy conversion efficiency is nearly independent of the illumination intensity for 17–100 mW cm^{-2}. (c) Schematic diagram of a bendable solar nanopillar cell module embedded in PDMS. Source: American Institute of Physics, 2010 176

Figure 84: (a) Schematic diagram of a ZnO nanowire array DSSC. (b) Schematic view of a flexible ZnO nanowire array DSSC. (c) Schematic architecture of planar waveguide-nanowire integrated 3D DSSC. (d) Detailed structure of a unit waveguide-nanowire 3D DSSC. Source: Springer Group, 2011 177

Figure 85: (a) SEM image of ZnO nanoparticles on the surface of ZnO nanowires in the hybrid ZnO nanowire–nanoparticle photoanode, scale bars 100 nm. (b) Schematic representation of the possible electron path way (along the nanowire) in the hybrid nanowire–nanoparticle photoanode. Source: American Institute of Physics, 2010........ 179

Figure 86: SEM images of (a) ZnO nanotetrapods. (b) Branched ZnO nanowires, (c) ZnO nanotrees and, and (d) ZnO aggregates consisting of nanocrystallites for DSSC applications. Source: WILEY-VCH Verlag GmbH & Co. KGaA, 2008 180

Figure 87: (a) SEM image of a TiO_2 fiber showing an islands-in-a-sea morphology with nanofibrils. (b) SEM image of TiO_2 nanorod electrode. (c) SEM image of ZnO nanofiber mats hot pressed at 120 °C and calcined at 450 °C. The inset exhibits the networks of twisted nanofibers composed of individual grains of ~30 nm. Source: American Institute of Physics, 2007 181

Figure 88: Schematic illustration of a nanofiber-nanoparticle composite solar cell Source: Royal Society of Chemistry, 2010 182

Figure 89: (a) Schematic diagram of a quasi-solid-state DSSC with electrospun PVDF-HFP membrane electrolyte. (b) Normalized light-to-electricity conversion efficiency variation of the DSSCs with liquid electrolyte and electrospun PVDF-HFP membrane electrolyte Source: American Chemical Society, 2008 183

Figure 90: Carbon nanotube solar cells; comparison to Dye-Sensitized Solar Cells (DSSC), construction, and energeticts. a) DSSC. b) Carbon Nanotube Solar Cell, CNSC. c) Layout of a CNSC. The top and bottom glass slides (light blue) are covered in carbon nanotube films which are electrically connected by the iodide-triiodide electrolyte (light red) that is contained by the silicone separator (white). The top film (green) is the photoactive electrode, while the bottom electrode (grey) is the counter electrode. The inset is an Atomic Force Micrograph of the height of a 2×2 m section of a carbon nanotube film. d) Band diagram of the CNSC. Source: PLoS ONE 7(5): e37806 184

Figure 91: Three different generic QD Solar Cell Configurations: Photoelectrodes Composed of Quantum Dot Arrays (top), Quantum Dot-Sensitized Nanocrystalline TiO2 Solar Cells (middle) and Quantum Dots Dispersed in Organic Semiconductor Polymer Matrices (bottom). Source: Chemical Reviews, 2010 184

Figure 92: HC schematic diagram. Source: Physica E, 42, 2010 186

Figure 93: Total Load, Wind and Solar Power Output in Germany, September 2011. Source: The German Energy Transition – Issues and Perspectives, J. Keil, 2012 189

Figure 94: Daily and Annual Patterns. Source: The German Energy Transition – Issues and Perspectives, J. Keil, 2012 189

Figure 95: Classification of energy storage applications in electric power systems. 191

Figure 96: Efficiency and reliability in discharge cycles for diverse energy storage technologies. Source: A. Nourai, 2002 191

Figure 97: Application of energy storage systems in terms of discharge time and rated power. Source: A. Nourai, 2002 192

Figure 98: Clasification of supercapacitors. 199

Figure 99: Photovoltaic technology status and prospects 203

Figure 100: Application of international standards in Photovoltaic industry 211

TABLE OF TABLES

Table 1: Confirmed terrestrial cell and submodule efficiencies measured under the global AM1.5 spectrum (1000 W/m2) at 25 °C (IEC 60904-3: 2008, ASTM G-173-03 global) at 25 °C (IEC 60904-3: 2008, ASTM G-173-03 global). Source: Progress in Photovoltaics, 2013 20

Table 2: Confirmed terrestrial module efficiencies measured under the global AM1.5 spectrum (1000 W/m2) at a cell temperature of 25°C (IEC 60904–3: 2008, ASTM G-173-03 global). Source: Progress in Photovoltaics, 2013 21

Table 3: 'Notable Exceptions': 'top ten' confirmed cell and module results, not class records measured under the global AM1.5 spectrum (1000 Wm^{-2}) at 25 °C (IEC 60904–3: 2008, ASTM G-173-03 global) 22

Table 4: The general trends for crystalline silicon substrate technology 40

Table 5: Comparison of Various Wafering Methods 45

Table 6: Comparison of Energy Expended Between Selected Wafering Processes 52

Table 7: Wafering Process Comparison with Slurry Sawing 53

Table 8: Overview of several technical improvement opportunities. Source: NREL, 2012 69

Table 9: Overview of companies with operating capacities larger than 30 $\mathrm{MW_P}$/a for CIGS modules worldwide 86

Table 10: Overview of companies producing thin film modules based on CdTe worldwide 87

Table 11: Snapshot of typical 2011 parameters for estimating the Te intensity of CdTe module production and the effect of the metalloid's price upon module costs. The typical, and publicly available, input parameters are cited and used for the calculations. Source NREL 2012 93

Table 12: Overview of some technical improvement opportunities that are available to improve the efficiency of single-junction polycrystalline CdTe modules. Source NREL 2012 96

Table 13: Maximum open circuit voltages, efficiencies and grain sizes of poly-Si thin-film solar cells prepared by diverse methods. Source: Applied Physics Letters, 2012 111

Table 14: Terrestrial concentrator cell and module efficiencies measured under the ASTM G-173-03 direct beam AM1.5 spectrum at a cell temperature of 25 °C 125

Table 15: Photovoltaic performance of some of the important organic solar cells by employing different device designs. Source: Wiley Interdisciplinary Reviews, 2012 142

Table 16: OPV fabrication methods and environment 147

Table 17: Representative device performance of various single-junction nanostructured photovoltaic cells under 1-sun illumination. Source: Adv. Mater. 2011 166

Table 18: Comparison of large scale energy storage systems. Source: Applied Energy, 2011 193

Table 19: Technical characteristics of large scale energy storage systems. Source: Environmental Innovation and Societal Transitions, 2012 193

Table 20: Technical suitability of large scale energy storage systems. 194

Table 21: Worldwide operational large scale battery systems 195

Table 22: Planned large scale battery systems in the world 197

Table 23: Economical and environmental characteristics of large scale energy storage systems 197

Table 24: A comparison of electrostatic capacitors, supercapacitors and batteries 198

Table 25: General technology target 204

Table 26: Technology goals and key R&D issues for crystalline silicon technologies 205

Table 27 Technology goals and key R&D issues for thin film technologies 208

Table 28 Prospects and key R&D issues for concentrating PV, emerging and novel technologies 210

1 INTRODUCTION

1.1 Study II: State of the art and next generation photovoltaic

1.1.1 Study goals and objectives

The aim of this study is to provide an analysis on prospective photovoltaic (PV) technologies throughout the PV value chain, technology maturity, competitiveness in PV market and the main trends in PV technology evolution.

This is Study number 2.

This study provides the technology related insight for a series of related photovoltaic studies and critically assesses the different aspects and maturity of the photovoltaic technologies.

The other studies are:

- Mid-term and long-term trends of global photovoltaic industry development (Study I)
- Present and prospective PV applications and challenges for the PV industry (Study III)
- The dynamics of PV industry: integration and competitiveness in the energy sector (Study IV)
- State of the art analysis of Lithuanian PV technology cluster and potential for its development (Study V)

This study is aimed at audience of PV manufacturers, technology staff, researchers and other interested stakeholders. The study covers the current photovoltaic technologies by the materials employed for solar cells manufacturing and the main trends, as well the challenges and future prospects. Moreover, the complementary technology on energy storage is analysed.

1.1.2 Reasons for the doing this study

Lithuania has an active photovoltaic technology cluster (PTC). It has 26 members, which include both commercial companies and research institutes. It was founded in 2008 with the aim to establish systematic background for international competitiveness and development of PTC members and a Lithuanian PV industry. The main PTC objective is to increase the added value produced by PTC members and Lithuanian PV technology and enhance companies' competitiveness by integrating RTD into the business model. The main PTC activity areas are (i) photovoltaic RTD and industry development and (ii) development of interface between photovoltaic and other areas of research and industry, where the achieved results in PV technology could be deployed.

PTC became a member of the European Photovoltaic Industry Association (EPIA) in 2009, and is the representative of Lithuania in European Photovoltaic Technology platform "Mirror" and "Research and Technology" working groups.

But the Lithuanian PV industry is currently only at an early stage of development and evolution. This study and its related studies are important contributions to the PTC's further development and the sustainable development of the Lithuanian PV industry by preparing the long-term development strategy and optimising the synergy of business and research and technological innovation (RTI) from both Lithuanian research centres and the research area of the European Union.

1.1.3 Scope

The scope of this report is on state of the art and next generation photovoltaic technologies. The on-going efforts in PV technology development are mapped against the PV supply chain. The periods covered depends on the technology – as some of the mature technologies have a long history, and some technological concepts are newly emerged and counts only several years. The potential future developments are described for 2020, 2030 time horizons.

1.1.4 Methodology and Information sources

The core method of research for Study 2 is the use of a wide and extensive range of secondary sources, including:

- Peer-reviewed scientific publications (Progress in Photovoltaics: Research and Applications, Solar Cells, Solar Energy Materials & Solar Cells, Journal of Photovoltaics and oth.);
- Presentations and conference proceedings (IEEE Photovoltaic Specialists Conference, European PV Solar Energy Conference and Exhibition and oth.);
- Roadmaps, working papers and publications of photovoltaic technology platforms, clusters and associations (ITRPV, EUPVTP; EPIA and oth.);
- Relevant websites and Specialised information of Photovoltaic technology related online magazines;
- Reports of technological foresights on PV.

Further information on the references quoted or used for background information are listed in the References in the annexes.

The report was prepared by three very experienced senior consultants. The team leader was Circa Group's Managing Director. The process used to prepare this report was that:

- An outline of the report was prepared by the team working together and initial research was undertaken. This formed the basis of the two monthly progress report submitted to VsI "Perspektyviniu technologiju taikomųju tyrimų institutas".
- The research was divided between the team members which allowed for a degree of overlap thus ensuring at least two of the team would cover the same ground.

- More detailed research was undertaken, then the team met to review the layout and develop a more detailed format. The writing was allocated to the team members.
- Detailed research was then undertaken and initial draft chapters were written.
- These drafts were circulated and reviewed by the team.
- The chapters were redrafted and a final content and presentation agreed.
- The whole report was formally proofed and the final edits undertaken.

It was submitted to VsI "Perspektyviniu technologiju taikomųju tyrimų institutas" in January 2013.

1.2 Summary Layout

The layout of the report is outlined in the following paragraphs.

Chapter 1 includes the following sections:

- Introduction – which includes the study goals and objectives, reasons for the study, scope and format, methodology and information sources
- Summary layout of the study
- An overview of the content of the study

Chapter 2 covers the overview of state of the art analysis of currently employed and next generation PV technologies. It includes the following sections:

- Crystalline silicon, including: trends in raw material: mono-, multi-, quasi-mono-crystalline silicon, trends in crystalline silicon wafering technology, review of trends in p-type and n-type wafers applications, solar cells and module manufacturing
- Thin Film, including overview of main trends, Cadmium Telluride photovoltaic technology, Copper–indium–gallium–diselenide (CIGS) photovoltaic technology and Thin film silicon modules
- Concentrator photovoltaics
- Emerging photovoltaics, including Organic /Polymer solar cells, Dye-sensitized solar cells and new technologies for PV cell production

Chapter 3 covers the overview of status and technology trends of energy storage as complementary technology. Its main sections are:

- Needs for electric energy storage
- Electricity Storage technology overview

Chapter 4 analysis the strategic documents shaping the future of PV technologies and research. It includes:

- Forecast of related RTD activities and scientific potential development, including specific technology goals and R&D issues

Chapter 5 provides the conclusions to the study.

Finally the annex includes the list of references.

1.3 Overview of the report

1.3.1 Background

The on-going efforts in PV technology development are mapped against a schematic of the PV supply chain for visualisation how wide they are spread across of it (Figure 1).

Figure 1: Areas of Activity in PV value chain[1]

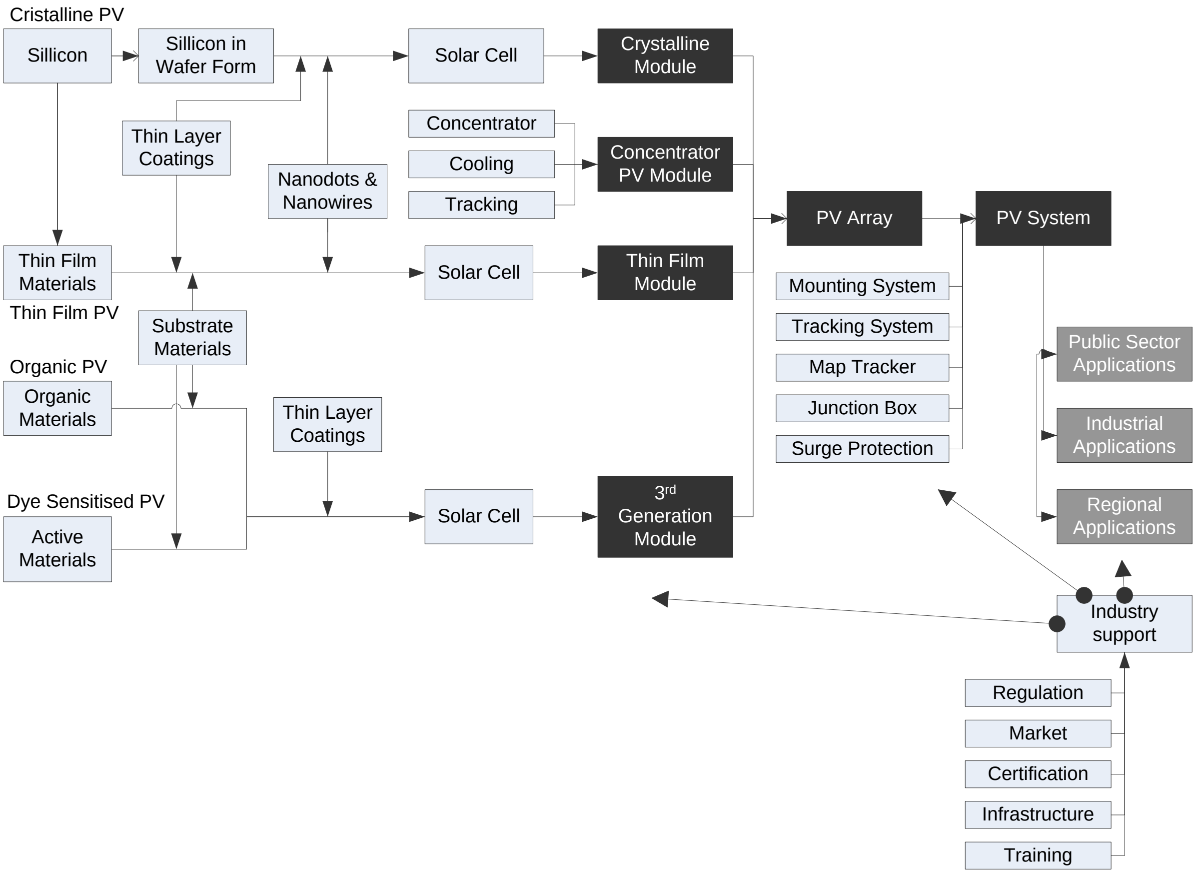

Silicon is a leading technology (Figure 2) in making solar cell due to its high efficiency. However, due to its high cost, most researchers are trying to find new technology to reduce the material cost to produce solar cell and to till date, thin film technology can be seen as a suitable substitute. The reasons behind the low cost of thin film technology are because it uses less material and the layers are much thinner compared to mono- and polycrystalline solar cell thus lowering the manufacturing cost. However, the efficiency of this technology based solar cells is still low. Three materials that have been given much attention under thin film technology are amorphous silicon, CdS/CdTe and CIS, but researchers are continuously putting in more effort to enhance the efficiency. However, all of these materials have some bad impact on the environment. Another

---

[1] S. Fantechi. Photovoltaics and nanotechnology: from innovation to industry. The European Photovoltaics Clusters. European Commission/ Research and Innovation policy. 2011

solution for thin film technology has been carried out by researchers by using polymer or organic as a solar cell material. Polymer materials have many advantages like low cost, lightweight and environmental friendly. The only problem is it has very low efficiency compared to other materials with just 4–5%.

Figure 2: Global annual PV Installation by technology in 2011. The global solar PV installations reached about 32 GW in 2012. Source: Fraunhofer ISE, 2012

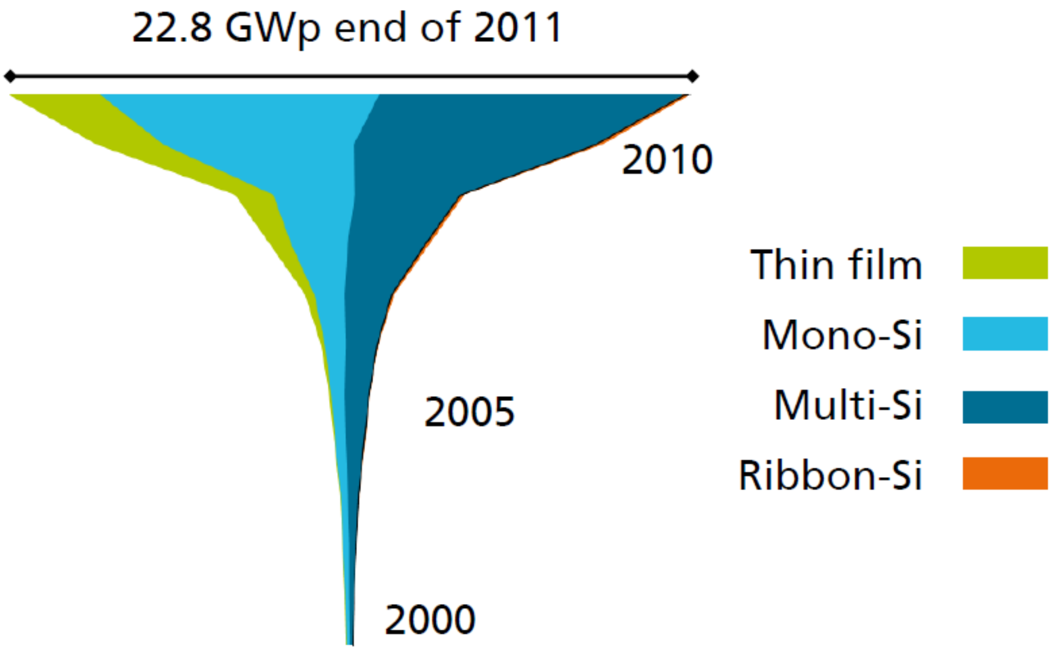

The main trends and maturity of PV technologies could be summarised as follows:

- Crystalline silicon (c-Si) modules represent 85-90% of the global annual market today. C-Si modules are subdivided in two main categories: i) single crystalline (sc-Si) and ii) multi-crystalline (mc-Si).
- Thin films currently account for 10% to 15% of global PV module sales. They are subdivided into three main families: i) amorphous (a-Si) and micromorph silicon (a-Si/μc-Si), ii) Cadmium-Telluride (CdTe), and iii) Copper-Indium-Diselenide (CIS) and Copper-Indium-Gallium-Diselenide (CIGS).
- Concentrator technologies (CPV) use an optical concentrator system which focuses solar radiation onto a small high-efficiency cell. CPV technology is currently being tested in pilot applications.
- Emerging technologies encompass advanced thin films and organic cells. The latter are about to enter the market via niche applications.
- Novel PV concepts aim at achieving ultra-high efficiency solar cells via advanced materials and new conversion concepts and processes. They are currently the subject of basic research.

1.3.2 The highest independently confirmed efficiencies for solar cells and modules

Highest confirmed 'one sun' cell and module results for 2012 are summarised in Figure 3 and reported in Table 1 and Table 2.[2] Table 1 summarises the best measurements for cells and submodules whereas Table 2 shows the best results for modules. Table 3 contains what might be described as 'notable exceptions', although not conforming to the requirements to be recognised as a class record. The cells and modules in Table 3 have notable characteristics (significant and timely) that are of interest to target groups of the photovoltaic community.

Figure 3: Efficiency Comparison of Technologies: Best Lab Cells vs. Best Lab Modules. Source: Franhofer ISE, 2012

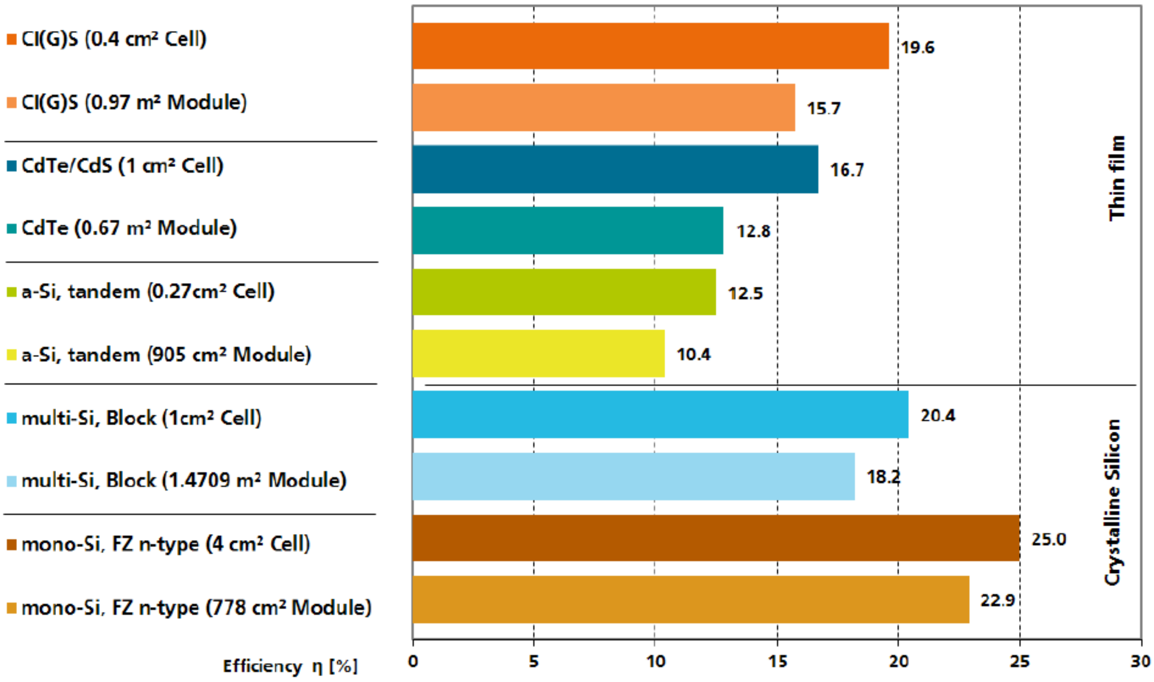

---

[2] M.A. Green, K. Emery, Y. Hishikawa, W. Warta, E.D. Dunlop. Solar cell efficiency tables (version 41). Progress in Photovoltaics: Research and Applications. Volume 21, Issue 1, pages 1–11, January 2013

Table 1: Confirmed terrestrial cell and submodule efficiencies measured under the global AM1.5 spectrum (1000 W/m2) at 25 °C (IEC 60904-3: 2008, ASTM G-173-03 global) at 25 °C (IEC 60904-3: 2008, ASTM G-173-03 global). Source: Progress in Photovoltaics, 2013

Classification[a]	Effic.[b] (%)	Area[c] cm^2	V_{oc} (V)	J_{sc} (mA/cm^2)	FF[d] (%)	Test center[e] (date)	Description
SILICON							
Si (crystalline)	25.0 ± 0.5	4.00 (da)	0.706	42.7[f]	82.8	Sandia (3/99) [g]	UNSW PERL
Si (multicrystalline)	20.4 ± 0.5	1.002 (ap)	0.664	38.0	80.9	NREL (5/04)[g]	FhG-ISE
Si (thin film transfer)	20.1 ± 0.4	242.6 (ap)	0.682	38.14[h]	77.4	NREL (10/12)	Solexel (43 µm thick)
Si (thin film submodule)	**10.5 ± 0.3**	**94.0 (ap)**	**0.492i**	**29.7[i]**	**72.1**	**FhG-ISE (8/07)[g]**	**CSG Solar (1–2 µm on glass; 20 cells)**
III–V CELLS							
GaAs (thin film)	28.8 ± 0.9	0.9927 (ap)	1.122	29.68[j]	86.5	NREL (5/12)	Alta Devices
GaAs (multicrystalline)	18.4 ± 0.5	4.011 (t)	0.994	23.2	79.7	NREL (11/95)[g]	RTI, Ge substrate
InP (crystalline)	22.1 ± 0.7	4.02 (t)	0.878	29.5	85.4	NREL (4/90)[g]	Spire, epitaxial
THIN FILM CHALCOGENIDE							
CIGS (cell)	19.6 ± 0.6[k]	0.996 (ap)	0.713	34.8[l]	79.2	NREL (4/09)	NREL, on glass
CIGS (submodule)	17.4 ± 0.5	15.993 (da)	0.6815[i]	33.84[i]	75.5	FhG-ISE (10/11)	Solibro, 4 serial cells
CdTe (cell)	**18.3 ± 0.5**	**1.005 (ap)**	**0.857**	**26.95[h]**	**77.0**	**NREL (10/12)**	**GE Global Research**
AMORPHOUS / NANOCRYSTALLINE SI							
Si (amorphous)	10.1 ± 0.3[m]	1.036 (ap)	0.886	16.75[f]	67.8	NREL (7/09)	Oerlikon Solar Lab, Neuchatel
Si (nanocrystalline)	10.1 ± 0.2[n]	1.199 (ap)	0.539	24.4	76.6	JQA (12/97)	Kaneka (2 µm on glass)
PHOTOCHEMICAL							
Dye sensitised	11.9 ± 0.4[o]	1.005 (da)	0.744	22.47[h]	71.2	AIST (9/12)	Sharp
Dye sensitised (submodule)	9.9 ± 0.4[o]	17.11 (ap)	0.719[i]	19.4[i, l]	71.4	AIST (8/10)	Sony, 8 parallel cells
ORGANIC							
Organic thin-film	10.7 ± 0.3[o]	1.013 (da)	0.872	17.75[h]	68.9	AIST (10/12)	Mitsubishi Chemical(4.4 mm × 23.0 mm)
Organic (submodule)	**6.8 ± 0.2[o]**	**395.9 (da)**	**0.798[i]**	**13.50[h,i]**	**62.8**	**AIST (10/12)**	**Toshiba (15 series cells)**
MULTIJUNCTION DEVICES							
InGaP/GaAs/InGaAs	**37.7 ± 1.2**	**1.047 (ap)**	**3.014**	**14.57[h]**	**86.0**	**AIST (9/12)**	**Sharp**
a-Si/nc-Si/nc-Si (thin film)	13.4 ± 0.4[p]	1.006 (ap)	1.963	9.52[h]	71.9	NREL (7/12)	LG Electronics
a-Si/nc-Si (thin film cell)	12.3 ± 0.3%[q]	0.962 (ap)	1.365	12.93[r]	69.4	AIST (7/11)	Kaneka
a-Si/nc-Si (thin film submodule)	11.7 ± 0.4[n, s]	14.23 (ap)	5.462	2.99	71.3	AIST (9/04)	Kaneka

Table 2: Confirmed terrestrial module efficiencies measured under the global AM1.5 spectrum (1000 W/m2) at a cell temperature of 25°C (IEC 60904–3: 2008, ASTM G-173-03 global). Source: Progress in Photovoltaics, 2013

Classification[a]	Effic. [b] (%)	Area [c] cm^2	V_{oc} (V)	I_{sc} (A)	FF[d] (%)	Test center (and date)	Description
Si (crystalline)	22.9 ± 0.6	778 (da)	5.60	3.97	80.3	Sandia (9/96)[e]	UNSW/Gochermann
Si (large crystalline)	21.4 ± 0.6	15780 (ap)	68.6	6.293	78.4	NREL (10/09)	SunPower
Si (multicrystalline)	18.5 ± 0.4	14661 (ap)	38.97	9.149[f]	76.2	FhG-ISE (1/12)	Q-Cells (60 serial cells)
Si (thin-film polycrystalline)	8.2 ± 0.2	661(ap)	25.0	0.320	68.0	Sandia (7/02)[e]	Pacific Solar (1–2 μm on glass)
GaAs (thin film)	**24.1 ± 1.0**	**858.5 (ap)**	**10.89**	**2.255[g]**	**84.2**	**NREL (11/12)**	**Alta Devices**
CIGS	15.7 ± 0.5	9703 (ap)	28.24	7.254[h]	72.5	NREL (11/10)	Miasole
CIGSS (Cd free)	13.5 ± 0.7	3459 (ap)	31.2	2.18	68.9	NREL (8/02)[e]	Showa Shell
CdTe	15.3 ± 0.5	6750.9 (ap)	64.97	2.183[f]	72.9	NREL (1/12)	First Solar
a-Si/a-SiGe/nc-Si (tandem)	**10.5 ± 0.4[i]**	**14316 (t)**	**224.3**	**0.991**	**67.9**	**AIST (9/12)[g]**	**LG Electronics**

1. Any changes in the tables from those previously published are set in bold type.
2. [a] CIGSS, CuInGaSSe; a-Si, amorphous silicon/hydrogen alloy; a-SiGe, amorphous silicon/germanium/hydrogen alloy; nc-Si, nanocrystalline or microcrystalline silicon.
3. [b] Effic., efficiency.
4. [c] (t), total area; (ap), aperture area; (da), designated illumination area.
5. [d] FF, fill factor.
6. [e] Recalibrated from original measurement.
7. [f] Spectral response and/or current–voltage curve reported in Version 40 of these Tables.
8. [g] Spectral response and current–voltage curve reported in present version of these Tables.
9. [h] Spectral response reported in Version 37 of these Tables.
10. [i] Stabilised at the manufacturer under the light-soaking conditions of IEC61646.

Table 3: 'Notable Exceptions': 'top ten' confirmed cell and module results, not class records measured under the global AM1.5 spectrum (1000 Wm^{-2}) at 25 °C (IEC 60904–3: 2008, ASTM G-173-03 global)

Classification [a]	Effic. [b] (%)	Area [c] (cm^2)	V_{oc} (V)	J_{sc} (mA/cm^2)	FF[d] (%)	Test centre (and date)	Description
CELLS (SILICON)							
Si (MCZ crystalline)	24.7 ± 0.5	4.0 (da)	0.704	42.0	83.5	Sandia (7/99)[d]	UNSW PERL, SEH MCZ substrate
Si (large crystalline)	24.2 ± 0.7	155.1(t)	0.721	40.5[e]	82.9	NREL (5/10)	Sunpower *n*-type CZ substrate
Si (large crystalline)	23.9 ± 0.6	102.7(t)	0.748	38.89[f]	82.2	AIST (2/12)	Panasonic HIT, *n*-type
Si (large multicrystalline)	19.5 ± 0.4	242.7(t)	0.652	39.0[e]	76.7	FhG ISE (3/11)	Q-Cells, laser fired contacts
CELLS (other)							
CIGS (thin film)	20.3 ± 0.6	0.5015 (ap)	0.740	35.4[e]	77.5	FhG-ISE (6/10)	ZSW Stuttgart, CIGS on glass
CZTSS (thin film)	11.1 ± 0.3	0.4496 (ap)	0.4598	34.54[g]	69.8	Newport (2/12)	IBM solution grown
CZTS (thin film)	**8.4 ± 0.2**	**0.4463 (ap)**	**0.661**	**19.5[h]**	**65.8**	**Newport (4/11)**	**IBM, thermal evaporation**
Organic (thin film)	**11.1 ± 0.3[i]**	**0.159 (ap)**	**0.867**	**17.81[f, h]**	**72.2**	**AIST (10/12)**	**Mitsubishi Chemical**
Luminescent submodule	7.1 ± 0.2	25 (ap)	1.008	8.84[e]	79.5	ESTI (9/08)	ECN Petten, GaAs cells

1. Any changes in the tables from those previously published are set in bold type.
2. [a] CIGS, $CuInGaSe_2$; CZTSS, $Cu_2ZnSnS_{4-y}Se_y$; CZTS, Cu_2ZnSnS_4.
3. [b] Effic., efficiency.
4. [c] (ap), aperture area; (t), total area; (da), designated illumination area.
5. [d] Recalibrated from original measurement.
6. [e] Spectral response reported in Version 37 of these Tables.
7. [f] Spectral response and current–voltage curve reported in Version 40 of these Tables.
8. [g] Spectral response and current–voltage curves reported in Version 39 of these Tables.
9. [h] Spectral response and current–voltage curves reported in the present version of these Tables.
10. [i] Stability not investigated.

1.3.3 Costs, targets and learning curve

Photovoltaic (PV) is one of the fastest growing electricity generation technologies in the world. Average annual growth rates of global PV-installations have reached around 45% for the last 15 years, which triggered a fast and ongoing reduction of production cost in PV industry (Figure 4).

Figure 4: Price learning curve by technology cumulative production up to 2012. Learning Rate: Each time the cumulative production doubled, the price went down by 19.6 %. Source: Fraunhofer ISE, 2012

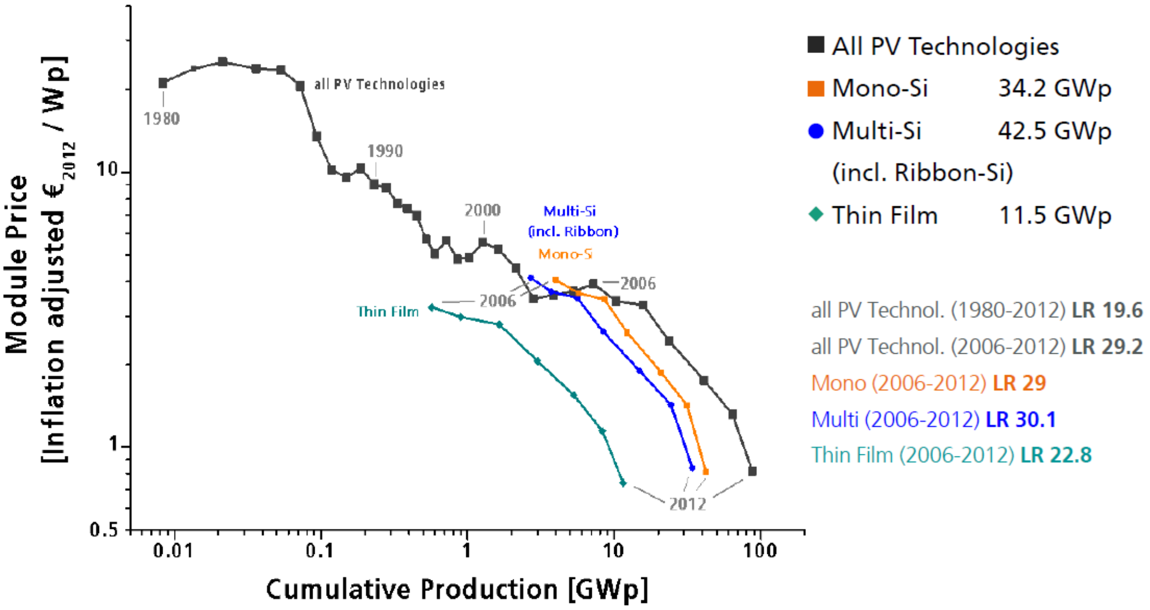

For c-Si modules a valid learning rate of 17% is found based on a meta-analysis of various studies. In early years, even a learning rate of 30% is observed. As an example for thin-film PV, CdTe module cost reduce by 16% as the cumulated production output doubles. Interestingly, efficiency improvements contribute only in second order to the overall cost reduction for both technologies, emphasising the relevance of production excellence and economies of scale. On PV system level, a cost reduction of 14% per doubling of cumulated installed capacity is derived. However, the variations of learning rate are only of minor influence on the overall global PV market potential.[3] It is expected that future learning rates should continue to accelerate as manufacturing moves to ever larger, more automated plants. The prices are expected to decrease in ten coming years by 36-51% depending on the segment resulting PV solar as a low-cost source of new electricity generating capacity in most of the world, before 2020. However, the required costs decrease per Watt peak (Wp) of PV modules is by 8%-12% per year and despite of a huge potential for further generation cost decline the previously demonstrated linear learning rate it is hardly being achieved. Looking at analysis for Germany today yields a

---

[3] F. Kersten, R. Doll, A. Kux, D. M. Huljic, M. A. Görig, C. Breyer, J. W. Müller, P. Wawer. PV Learning curves: past and future drivers of cost reduction. Proceedings of 26th European Photovoltaic Solar Energy Conference, 5 - 9 September 2011, Hamburg, Germany

learning rate for PV of only 7%[4] as costs are driven by technical factors, such as scale effect, R&D, learning-by-doing brought by the accumulation of experience. In contrast, the profit margin component - the difference between price and cost - are more driven by market based elements, such as competition, demand and supply balance and strategic behaviours. Scaling of PV installations to the needed terawatt scale, however, will require significant improvements in the cost-effectiveness of installed PVs, including improvements in their power conversion efficiencies (PCE) as well as reductions in the cost of PV module installation through streamlined fabrication and innovations in rapid and lightweight PV deployment. In order to help the PV industry achieve sustainable progress without relying on the large subsidy from the government, more radical decline of PV system cost is needed. Although the influence of market scaling is relatively stable and predictable, the more exploration space from the R&D side should be found.

---

[4] J. Kessler. Germany's feed-in-tariff has failed at reducing Photovoltaic costs. The Breakthrough July 27, 2011

2 STATE OF THE ART ANALYSIS OF CURRENTLY EMPLOYED AND NEXT GENERATION PV TECHNOLOGIES

2.1 Crystalline silicon

With average annual growth rates in excess of 40% over the past decade, the success of the PV industry can largely be attributed to the steadfast growth of wafer-based multicrystalline and monocrystalline silicon. This growth has been sustained through a powerful combination of three critical competitive advantages: (1) industry-leading full module area sunlight power conversion efficiencies (to date, monocrystalline silicon continues to provide the highest power conversion efficiency among all commercially demonstrated single junction PV modules); (2) product 'bankability' from the appropriately qualified suppliers (with warranties for 80% of original performance after 25 years of service now being standard); and (3) a consistent ability to offer competitively priced modules, which has been enabled through an ability to realize cost reductions throughout the c-Si module supply chain (Figure 5).

Figure 5: The primary steps of the wafer-based c-Si module supply chain. Source: A. Goodrich, 2012

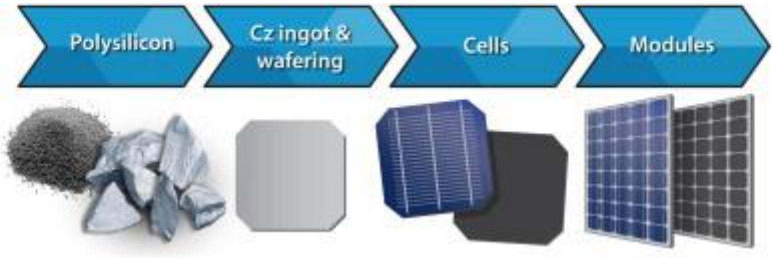

A significant portion of these cost reductions have come about due to 'economies-of-scale' benefits. But there is a point of diminishing returns when trying to lower costs by simply expanding production capacity. Based on the three decades of high volume PV manufacturing, the technology learning curve for silicon (Si) PV (Figure 6) shows that the price of technology (€/Wp) has decreased by 20% for each doubling of cumulative installed capacity.[5]

---

[5] Fisher et al. Silicon Crystal Growth and Wafer Technologies. Proceedings of the IEEE | Vol. 100, May 13th, 2012

Figure 6: Price learning curve for crystalline Si modules as function of installed capacity (Sources: National Renewable Energy Laboratory, European Photovoltaic Industry Association, Navigant Consulting.)

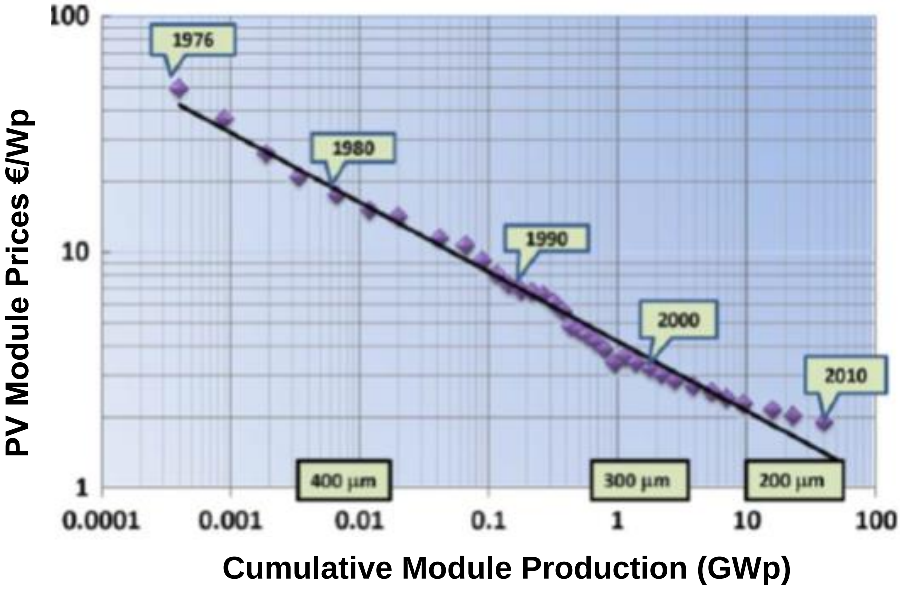

The challenge is to sustain this rate of technology and cost improvements, and bring PV to grid parity without feed-in-tariffs and other subsidies. With limited opportunity for dramatic improvements in PV efficiency, there is an industry-wide push to reduce the active Si content of the cell in combination with improved light management. With increased manufacturing volumes, there is limited scope for cost reduction through manufacturing efficiencies alone; the input cost of module materials, especially the amount of Si used, becomes a bigger factor. Thus, at the raw material and wafer level, the development of thin crystalline silicon wafers and reducing the consumption of silicon or replacing the monosilicon with less expensive materials or higher bulk lifetime of the substrates (different doping), for maintaining energy conversion efficiency comparable to thicker c-Si solar cells are the main drivers for solar Si wafers, so is the need for new and improved silicon feedstock and wafer (and wafer equivalent) manufacturing technologies.

2.1.1 Trends in raw material: mono-, multi-, quasi-mono- crystalline silicon

2.1.1.1 Solar grade silicon

The silicon value chain to feedstock for solar cells is shown in Figure 7 with the traditional route to semiconductor silicon shown on the left hand side. Semiconductor grade silicon for electronic devices is made through the Siemens process and has a higher requisite purity still (9N). Because of the nature of the process, electronic silicon production is slow and costly and involves use of toxic and corrosive reagents. Moreover, semiconductor grade wafers are not needed for PV.

Figure 7: Alternative routes for solar grade silicon, *(Source: New Feedstock Materials, Aud Waernes et al, Proceedings NREL/BK-520-40423)*

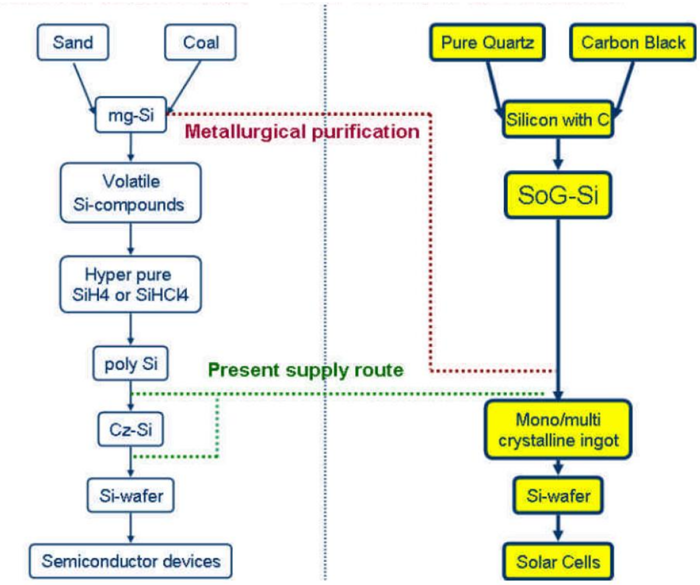

There is not a shortage of silicon in the world today as it was estimated in period of 2005-2009. The global polysilicon capacity is forecasted to double by 2013 over 2010 levels (< 385,000 tons) causing over-supply in today's market of waning PV demand.[6] Feedstock supply for solar companies has historically been obtained from the oversupply or offspec electronic silicon (scrap, rejected, and non-prime material from this production is the main supply route of today). Considering the high cost and the difference in silicon purity requirements for the electronics and PV industries, interest had grown in the development of technologies for direct production of low-cost solar-grade silicon (SoG-Si). In principle, there are several different ways to the silicon called solar grade silicon (SoG-Si), which is required for photovoltaic industry (Figure 7 right side). Crude silicon with 98% to 99% purity, known as metallurgical-grade silicon (MG-Si), is produced on a large scale (capacity of 900,000 ton/y) through carbothermic reduction of silica. The requirement for solar cells is for a much higher purity of around 6 N to 7 N, with many dopant and other deleterious metallic elements needing to be at levels<1 ppm. Thus, additional refining to target these impurities is needed to produce SoG-Si from MG-Si.

Several companies (Wacker, ASIMI, etc) were making a big effort to economize the chemical route by shifting from rod decomposition of trichlorosilane to fluidized bed in the last step of the poly-silicon production. Several companies (Elkem, FerroAtlantica etc) were working on the purification of metallurgical silicon to SoG-Si. The last potential source of solar grade silicon might be from the direct carbothermic reduction of quartz and carbon as indicated on the right hand side of Figure 7 (the Solsilc route and RSI Silicon are examples of this). All the investigations in metallurgical Si refining show, however, that each method is selective in removing one or a small group of

---

[6] B. Prior, C. Campbell. Polysilicon 2012-2016: Supply, Demand & Implications for the Global PV Industry. GTM Research 2012

impurity elements.[7] Vaporization of volatile elements such as P or B compounds is a feasible method for their removal but is often a slow process requiring excessively high temperatures and may be accompanied with Si loss. Thus, cost becomes an issue. Solvent refining has proved successful in removing a wide range of impurities, with Al being the most suitable alloying agent among those studied (Fe, Al, Cu, Sn, Sb, and Ni). Small addition of other elements such as Ti and Ca to target specific impurities (B and P) has shown promising results, although there is always the issue of separating the refined silicon from the solidified matrix. Slag treatment is an effective method in lowering the concentration of impurities that are highly responsive to oxidation (e.g., Al, Ti, etc.). While refining of MG-Si to lower P and B requires prohibitively large amounts of slag, use of Cu-Si alloy has shown very large LB, overcoming this problem, although the issue of separating silicon from the alloy remains. Electrorefining can lower the concentration of a wide range of impurities, but the final product is still distinct from SoGSi.

It became evident that a one-step metallurgical process to produce SoG-Si is unlikely to be realized. So far, all the efforts had not resulted in a commercially viable process for a feedstock to solar cells, as the lowest price achieved is on average of 20€/kg, when the average polysilicon prices are forecast to start to stabilize in 2013 at around 17€/kg.[6]

2.1.1.2 The Siemens process for producing polysilicon

The very first step in the fabrication of a c-Si wafer is the production of metallurgical grade silicon via the high-temperature reduction of silica (the source of which is typically lumpy quartz, not sand). With coke serving as the reducing agent, the process is most typically carried out in an electric arc furnace with carbon electrodes. The elemental purity of this metallurgical grade silicon, which currently sells for around 1.87€/kg, is approximately 98%. But the material purity requirement for the highest efficiency c-Si devices can approach 99.9999999% (9N). The most widely used process for the production of the much more pure polysilicon feedstock material is a chemical vapor deposition (CVD) method called the *Siemens* process, whose processing sequence is broadly represented in Figure 8.

---

[7] M. D. Johnston et al. High-Temperature Refining of Metallurgical-Grade Silicon: A Review. JOM, Vol. 64, No. 8, 2012

Figure 8: Generalized process flow for the production of solar grade polysilicon feedstock via the *Siemens* process. Source: A. Goodrich, 2012

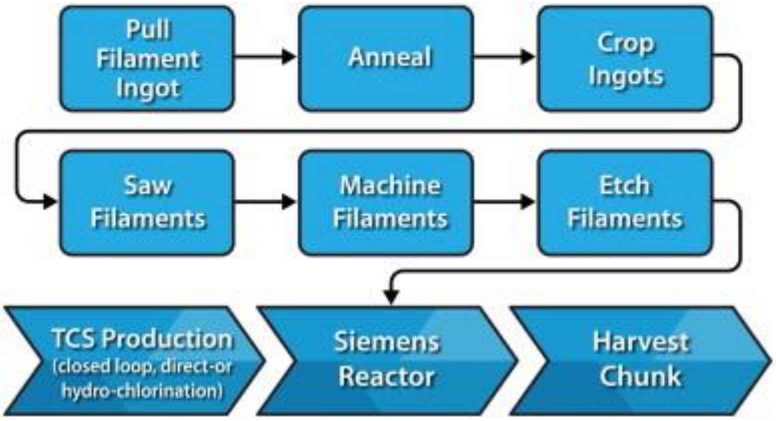

In order to remove the impurities contained within metallurgical grade silicon, the first step in the *Siemens* CVD process involves the production and distillation of trichlorosilane (TCS). Facilities that manufacture more than 2000 metric tons per annum (MTPA) of polysilicon generally manufacture their own TCS onsite. The production of TCS can be achieved by the reaction of metallurgical grade silicon with hydrochloric acid at moderate temperatures. Most of the impurities that were present within the metallurgical grade Si are left behind while the TCS is distilled. Solid polysilicon is then produced in a batch process as TCS is converted over the surface of silicon rods that have been placed inside of large bell jars, or '*Siemens* reactors' as they are commonly called. These silicon rods—or 'filaments'—are produced from ingots made from either the *Czochralski* (*Cz*) or Float Zone (*FZ*) approaches. The as-produced filaments of today are typically a 7 mm×7 mm×2500 mm elongated square, which have been sawn lengthwise from the ingots using slurry-based wire saws. The cropped ingot scrap can be reused for making other ingots, but, due to inclusions of chemical impurities from the wire-sawing slurry, and because it remains in the form of a very fine powder that is extremely difficult to mechanically separate from the SiC based slurry used during the cutting process, the approximately 10–15% of the ingot removed as sawing—or 'kerf'—loss has essentially no value. As final steps before the CVD chamber is sealed, the filaments are mechanically shaped to fit the electrical contacts made for each, a bridge of filament material is set in place between each parallel pair, and the native oxide is etched off using a dilute aqueous HF solution. Electrical current is passed through the resistive U-shaped silicon filaments to reach a temperature that approaches 1150 °C. This rather high temperature serves to activate the growth of solid polysilicon, Si (*ps*), on the surface of these filaments as a result of the hydrogenation of TCS with an HCl catalyst. The decomposition of trichlorosilane to produce dichlorosilane (SiH_2Cl_2) is one of several side reactions that also occur in the course of this growth process. Fortunately, this intermediate can also react to make polysilicon, and so—even though the TCS stream usually contains 6–9% DCS—most polysilicon producers choose not to separate the two. A leading high-pressure 500-MTPA reactor made in 2012 would accommodate 72 rods; the *Siemens* process would typically stopped once a diameter of 125 mm is reached for each. In a reactor of that size, approximately 125 kg of hydrogen is consumed during each hour of polysilicon growth, and the process is approximately 20% efficient in its use of TCS for each pass through the chamber. A total processing time of approximately 60 h per batch is typical, including a total time of around 24 h for filament placement, oxide etching, and for harvesting of the U-shaped polysilicon rods. As final steps, the polysilicon rods are smashed into chunks and packaged in nitrogen- or argon-filled bags for shipping. In order to drive the reaction sequence toward the production of polysilicon, it is helpful to remove the H_2 and $SiCl_4$ as they are produced within the bell jar. Fortunately, these effluents are actually useful in that they can be recycled for the production of trichlorosilane (which can, of course, be used again in later rounds of polysilicon production). The hydrogenation of silicon tetrachloride, more commonly called the ‘direct chlorination’ method. Or the H_2 and $SiCl_4$ can be reacted with metallurgical grade Si in the ‘hydrochlorination’ process. The yields for the hydrochlorination route are generally more difficult to control and it is a more technically challenging process. Thus, those companies having less experience—but also a desire to quickly scale up and establish a presence in this upstream step of the supply chain—are more likely to adopt the direct chlorination approach. The direct chlorination method does, however, require nearly double the capital equipment investment and uses significantly more energy: 120–200 kWh/kg for direct chlorination versus 65–90 kWh/kg for hydrochlorination.

2.1.1.3 The fluidized bed reactor (FBR) process for producing polysilicon

The process of polysilicon production via the fluidized bed process is an altogether *physically* different approach from the *Siemens* process. The end product is also quite different in that polysilicon granules, ranging in size from 100 to 1500 µm, are produced instead of the much larger chunks. A fluidized bed reactor is a cone shaped reaction vessel containing small crystalline silicon seed particles that are suspended by an upward-flowing ‘fluidizing’ gas. This becomes physically possible once the upward drag force of the fluidizing gas is approximately equal to the downward gravitational pull on the particle, based upon its mass (W=mg). At the same time they are being fluidized, the particles must be heated above the decomposition temperature of a silicon precursor gas (commonly SiH_4) that is introduced into the vessel. Once the necessary decomposition temperature is reached, with hydrogen serving as the fluidizing gas purified crystalline silicon layers build up layer-upon-layer onto the suspended silicon beads. After reaching a size whereby their weight becomes greater than the upward drag force of the fluidizing gas, the heavier crystallized Si granules fall to the bottom of the cone where they are collected. There are several advantages to this approach in that it is much more efficient in the overall net use of the reactant gases; it does not require the fabrication, shaping, and placement of crystalline seed filaments; and it requires significantly less energy, at only around 12–20 kWh/kg. The material form factor of the FBR granules is also quite advantageous in the subsequent step of melting polysilicon because the granules can be continuously fed into *Cz* pullers to bear up to 3 daughter ingots per initial charge (versus having to reload polysilicon chunk in single batch processing). In addition, the semi-continuous feeding of granules enables the semi-continuous feeding of dopants; and this can be helpful in overcoming the well-known challenges of uniformly distributing dopants having low segregation coefficients. In spite of its numerous apparent advantages, however, there are also numerous technical challenges in qualifying new FBR facilities. In particular, it can be difficult to manage the heating of the fluidized beads in a controlled manner, without losing an important temperature differential between the reaction zone and the walls of the reactor cone. This at least partially explains why there are currently only a handful of companies that have the technical capability to provide this FBR material.

It is expected that FBR technology to increase its share against Siemens processing as shown in Figure 9.

Figure 9: Expected change in share of poly-Si production technologies. Source: ITRPV, 2012

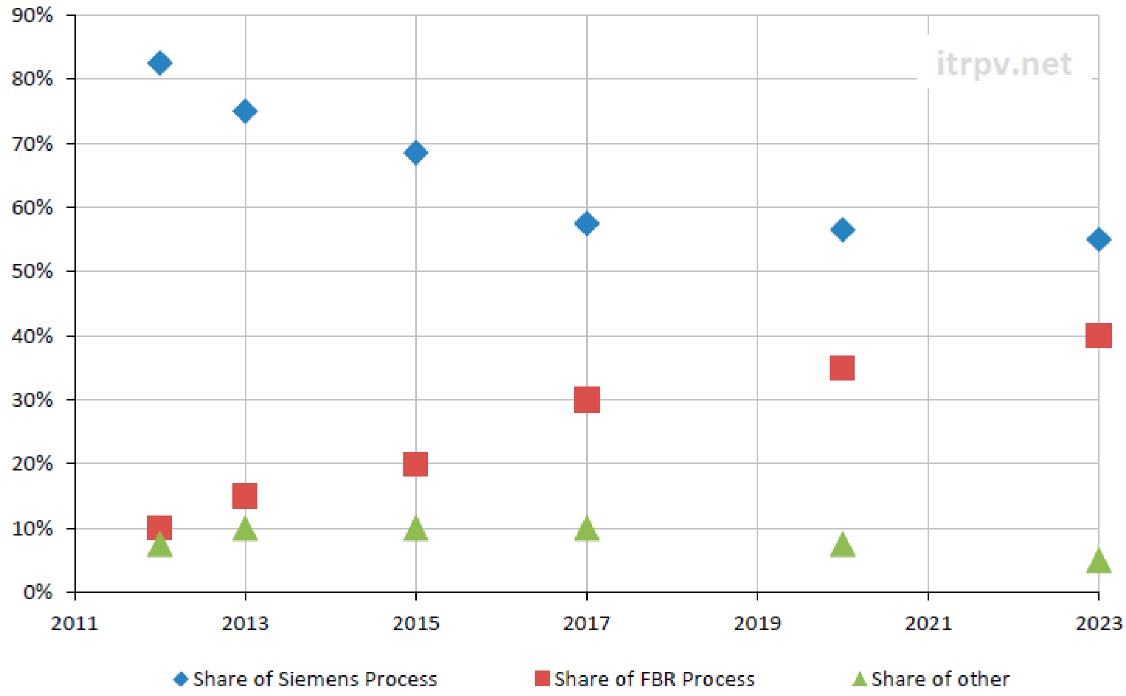

2.1.1.4 Czochralski silicon (CZ)

The Czochralski (CZ) process is generally used for growth of monocrystalline silicon ingots due to the better resistance of the wafers to thermal stress, the speed of production, the low cost and the high oxygen concentration. The industrial standard crystals range in diameter from 75 to 200 mm, are typically l m long and of < 100> orientation. A schematic diagram of a Czochralski-Si grower, called puller, is shown in Figure 10. The puller consists of three main components:

- a furnace, which includes a fused-silica crucible, a graphite susceptor, a rotation mechanism (clockwise as shown), a heating element, and a power supply;
- a crystal-pulling mechanism, which includes a seed holder and a rotation mechanism (counter-Clockwise); and

- an ambient control, which includes a gas source (such as argon), a flow control and an exhaust system.

The Czochralski method begins by melting high purity polysilicon (SGS) with additional dopants as required for the final resistivity in the rotating quartz crucible. A single crystal silicon seed is placed on the surface and gradually drawn upwards while simultaneously being rotated. This draws the molten silicon after it which solidifies into a continuous crystal extending from the seed. Temperature and pulling speed are adjusted to first neck the crystal diameter down to several millimetres, which eliminates dislocations generated by the seed/melt contact shock, and then to widen the crystal to full diameter. During the production process the quartz crucible (SiO_2) gradually dissolves, releasing large quantities of oxygen into the melt. More than 99% of this is lost as SiO gas from the molten surface, but the rest stays in the melt and can dissolve into the single crystal silicon. Another impurity, however with smaller concentrations, that is also introduced into the melt by the production process itself is carbon. The silicon monoxide evaporating from the melt surface interacts with the hot graphite susceptor and forms carbon monoxide that re-enters the melt. As the crystal is pulled from the melt, the impurity concentration incorporated into the crystal (solid) is usually different from the impurity concentration of the melt (liquid) at the interface. The ratio of these two concentrations is defined as the equilibrium segregation coefficient k0 =Cs/c1 where Cs and C1 are the equilibrium concentrations of the impurity in the solid and liquid near the interface, respectively.

Figure 10: Schematic setup of a Czochralski crystal puller. Source: S. Meroli, 2012

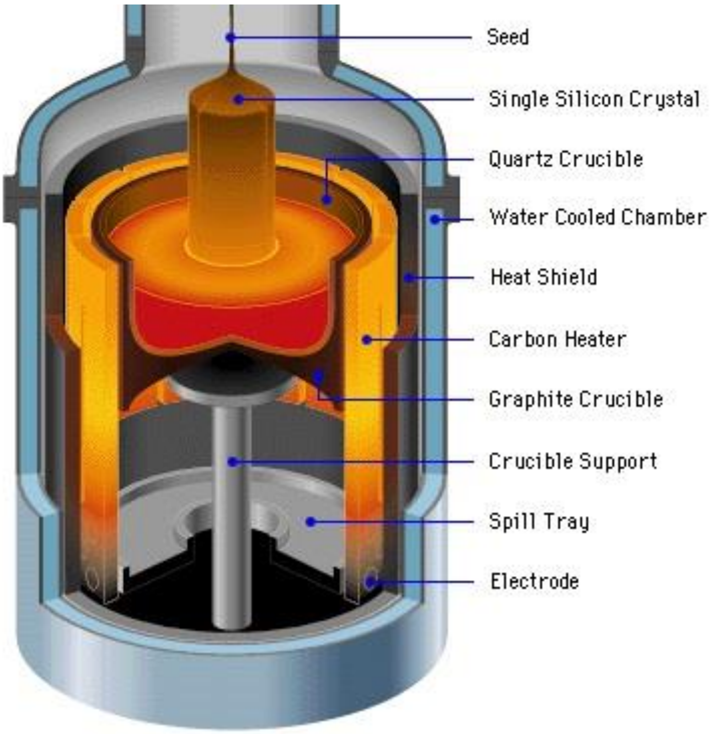

If utilizing p-type starting materials (wafers), the dominant loss mechanism appears to be defect-mediated recombination, specifically due to the presence of boron-oxygen pairs. Several methods exist to manage or eliminate these defects, thus enhancing the bulk lifetime of the substrate materials. The alternatives for common CZ process are the Magnetic-confined Czochralski (M-Cz), and Gallium doped Czochralski (Ga Cz) growth technologies (Figure 11). The first possible method, the Magnetic-confined Czochralski (M-Cz) process, has been found to significantly lower oxygen content, while adding capital expense (~149K€/station) for each Cz-puller. Alternative dopants, such as gallium greatly reduce the recombination within a wafer, but add other production challenges. For example, due to a lower segregation coefficient than boron, gallium is more difficult to manage during ingot formation – potentially limiting the usable as-grown length of Cz-ingots to around 50% (in comparison to the 80% that is achievable today using boron doping). Also, at least historically, the commercial viability of using boron-dopant alternatives, such as gallium has been limited by the complexities and cost of managing multiple material streams in high volume operations. To avoid cross-contamination, silicon materials from ingot and wafer lines running boron-doped feedstock would have to be run entirely separate from gallium-doped silicon lines. Perhaps until recently, production volumes did not justify the expense of running a dedicated gallium-silicon ingot and wafering line.

Figure 11: Estimated Cz-wafer costs, minimum sustainable price standard (U.S. and China) and high-lifetime (U.S.) processing route (170 µm wafer thickness, 130 µm kerf-loss, $35/kg poly price) Source: Photovoltaic Specialists Conference (PVSC), 2012 38th IEEE

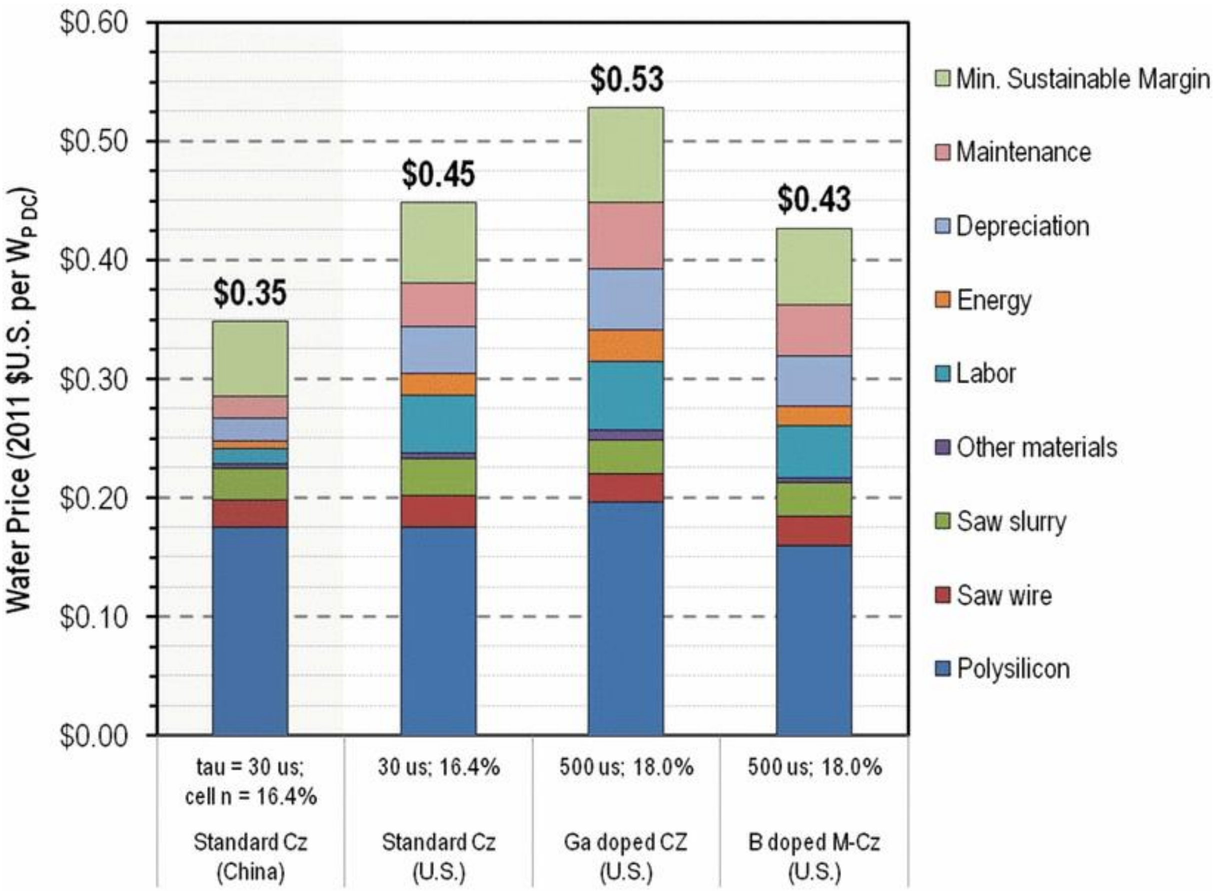

By increasing lifetime from 30 µs to 500 µs, the cell-efficiency is enhanced from 16.4% to 18.0%, which roughly corresponds to module efficiencies of 14.6% and 16.2%, respectively. The value of high lifetime p-type silicon produced via the M-Cz process is competitive with today's materials; the added cost of the magnets and energy are more than offset by the resulting gain in efficiency. High lifetime materials produced using alternative dopants, such as Gallium, however are not cost effective due to the negative impact on the Czochralski process yields.[8]

2.1.1.5 Casting

The most common casting method used for producing high purity multicrystalline silicon is directional solidification (DSS). The efficiency of this process depends on the segregation coefficient of the impurities between solid and liquid silicon. Most metallic impurities are readily removed by directional solidification, but other elements such as B and P are unresponsive due to their high segregation coefficients of 0.8 and 0.35, respectively. There have been significant advances in DSS technology that allows for casting larger charge size multicrystalline ingots, improved crystalline quality, and significantly reduced cost. There is considerable opportunity for DSS technology to improve wafer quality by reducing dislocation density, increasing grain size, and reducing the carbon concentration below saturation level. For example, Figure 12 highlights the exceptional progress in manufacturing, with the size of the mc-Si ingots increasing from 270 kg in 2006 to almost 2 tons in 2010. These large ingots allow for more wafers per cast, improved yields, and the potential for sizing wafers to larger dimensions (although the latter is currently not envisioned).

Figure 12: Growth over the last five years in the size of ingots cast using DSS. Source: Fisher et al, 2012

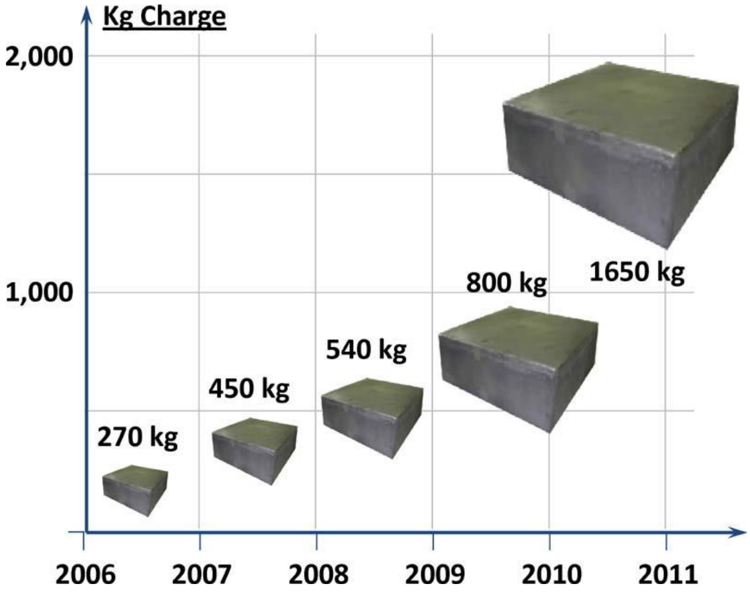

Although there seem to be no industry wide plans to go beyond 156-mm wafers, larger ingots do offer significant manufacturing improvements through increased wafer output per cast ingot. Within the last two years, mc-Si solar cell volume has expanded significantly and now has a larger market share than c-Si cells (more than 40 percent). The CZ monocrystalline silicon wafer is still holding its market share due to its higher

---

[8] A. Goodrich et al. The Value Proposition for High Lifetime (p-type) and Thin Silicon Materials in Solar PV Applications. Conference Paper NREL/CP-6A20-55477, IEEE Photovoltaic Specialists Conference, US, June 3–8, 2012

cell conversion efficiency. The difference in the cell conversion efficiency between the mono and multisilicon modules is typically about 1.5%. Such a difference is a result of the surface property (about 0.5%) and the bulk crystal quality.

Also the new technology, in between multi-crystalline and monocrystalline, blurs those boundaries. That is a technology called quasi-monocrystalline, nearly-mono, castmono or monocast. The process for quasi-mono wafers is similar to that used for multi-crystalline wafers with two key differences: a monocrystalline wafer is used as a seed at the bottom of the crucible; and the temperature is carefully controlled. The idea for the quasi-mono technology is not new, but market conditions kept it in the lab for many years. The growth of single crystal silicon with the directional solidification (or casting) method and the application of the resulting mono (or quasi-mono) silicon wafers for solar cells was also carried out by numerous researchers in the past 20 years. However the first large-scale (pilot) application of quasi-mono wafers could be considered that which was implemented by BP Solar. As early as 2006, BP Solar branded its quasi-mono wafers and solar cells as “Mono2 TM.” However, the quasi-mono wafers didn’t receive much attention until 2011 (Figure 13). During 2012 a plethora of announcements emerged including Chinese companies ReneSola and JA Solar, German companies Q-Cells, Schmid and Schott, US company Tech Precision, US furnace manufacturer GT Advanced Technologies and Dutch metals company AMG IdealCast[9] because only relatively small investment to retrofit their current furnaces they can manufacture wafers closer in performance to conventional CZ monocrystalline wafers at a cost close to multi-crystalline wafers. Mono-like silicon material is an emerging new technology utilizing mc-Si crystallization equipment to grow silicon ingots which have larger volume fractions with mono crystalline properties. As this material is well suited for high efficiency cells we expect an increasing market share for mono-like silicon material within the next years.[10]

---

[9] N. Anscombe. Quasi-mono Silicon: The best of both worlds. Solar Novus Today 2012, April

[10] International Technology Roadmap for Photovoltaics (ITRPV), Results 2011

Figure 13: Crystalline silicon market share by technology. Sourece: PV Magazine, 2012

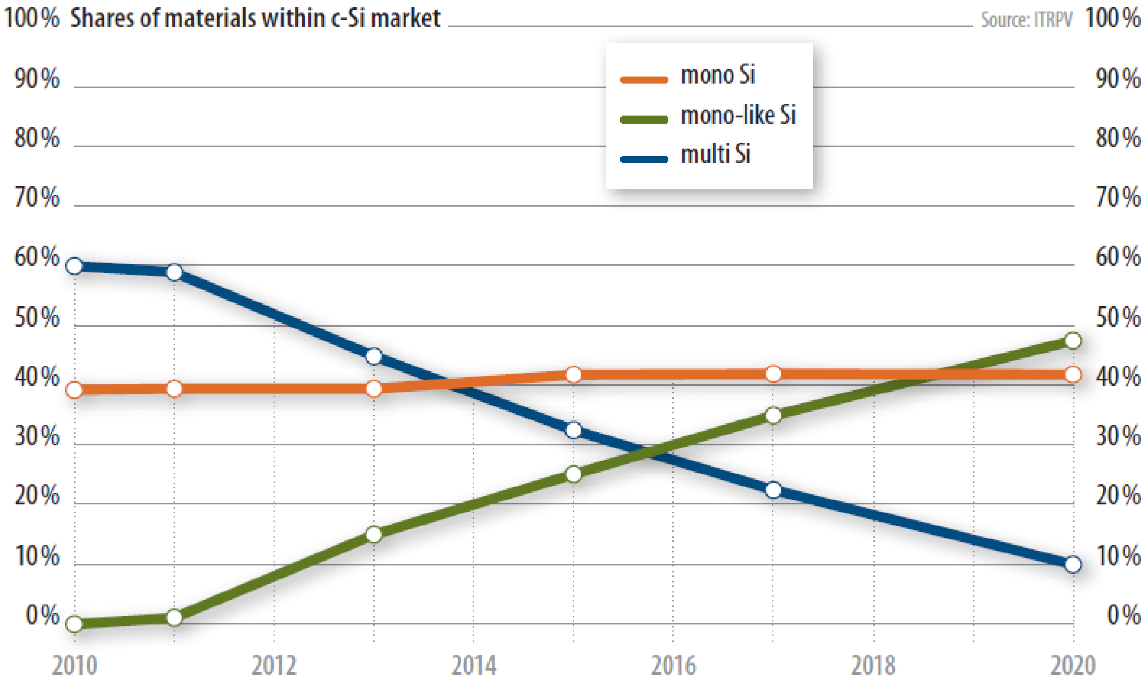

As the market shifted increasingly towards higher efficiency solar modules, and solar cell technology advanced to a much higher level, the requirements for high quality wafers became more pressing. Companies such as JA Solar, LDK Solar and ReneSola announced their quasi-mono products, and modules based on quasi-mono materials also found acceptance in the market. Since then, quasi-mono wafers have slowly gained market share.

Figure 14: Crystalline silicon wafer technology by efficiency[11]

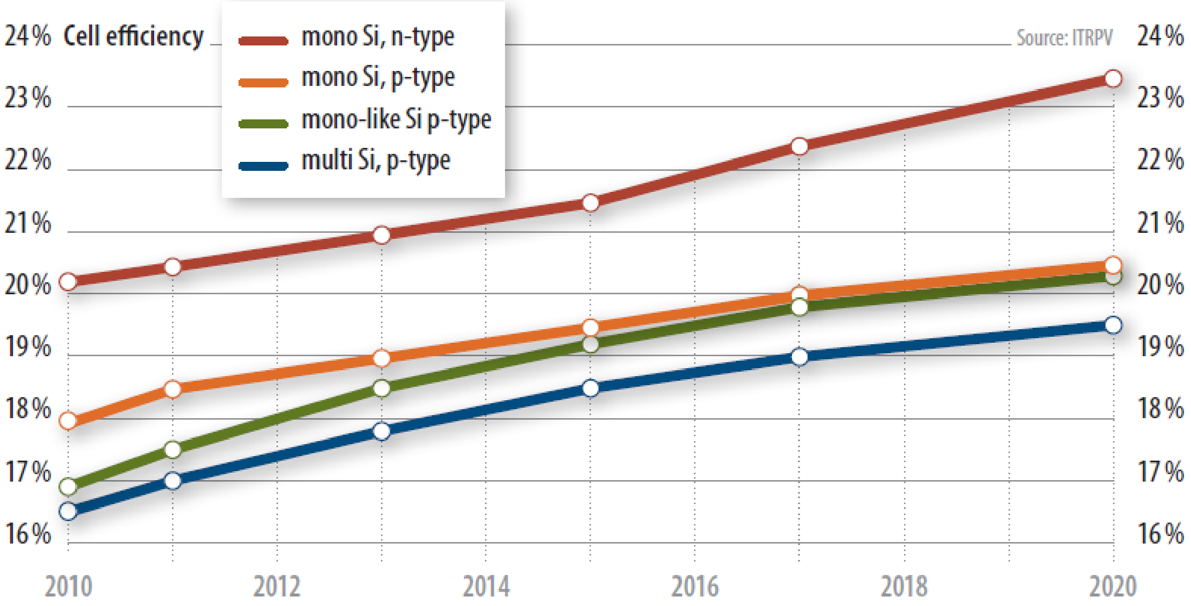

---

[11] Paving the way to acceptance. PV Magazine 09/2012, 94-99

As a new product, modules made of quasi-mono wafers are facing several challenges to gain market acceptance. The colour difference on the grains with different orientation after alkali texturing causes aesthetic concerns in residential applications. The endurance and attenuation of the electrical properties also remain causes for concern among some cautious customers. A consensus on the quality of the quasi-mono wafers is also still missing. There is even no standard name for this new type of wafer.

2.1.1.6 Properties of quasi-mono wafers

Quasi-monocrystalline silicon ingots can be made with current crystal growth furnaces for multicrystalline silicon ingots. In comparison to the growth pro process of multicrystalline silicon ingots, the major difference in the process is that a layer of monocrystalline silicon seeds are employed on the surface of the bottom side of the crucible. The seeds are usually made with the CZ process. Silicon feedstock and dopant are then loaded on top of the seed. In the process of melting, the silicon feedstock starts to melt from the top. The process is controlled so that the seeds will not be completely melted. When the solidification process begins, the remaining seeds act as the nucleation surface and the grown crystal will follow the orientation of the seeds and gradually form a large ingot consisting of crystals with some sections having multiple grains, especially in the areas close to the crucible and between the seeds. Due to this special growth process, the appearance and properties of a quasi-mono-wafer is different from that of a monocrystalline silicon wafer or a multicrystalline silicon wafer. Firstly, due to the seeding control the growth of quasi-mono is from the middle to the outside.

The crystalline silicon grown in the region close to the crucible surface is mostly multicrystalline silicon, while in other regions it forms mono-like crystals, in the case of good growth. As a result, wafers with very different characteristics can be obtained from the same ingot (Figure 15).

Figure 15: Different categories of quasi-mono wafer in the same ingot. Source: PV magazine, 2012

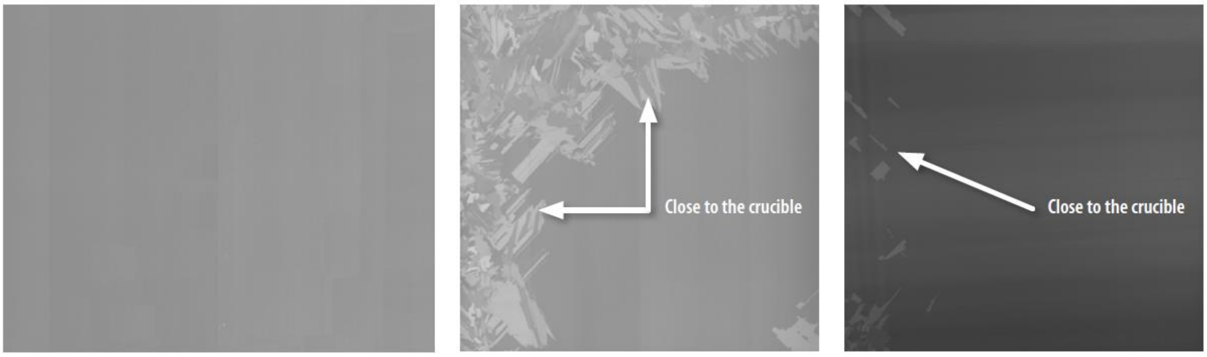

Secondly, as previously outlined, a layer of seed crystals of the same crystallographic directions are placed at the bottom of the crucible for quasi-mono casting. The crystals will merge together and become a large grain during the growth, and result in small angle sub-grain boundaries originating from the gap of the seeds. The surface of the mono-like crystal looks uniform, but in some cases a large number of sub-grain boundaries, which may cause a dislocation cluster, can be seen from an oblique direction. Besides, the oxygen content of quasi-mono is less than that of monocrystalline silicon, which can in turn reduce the effect of light induced degradation (LID) of quasi-mono solar cells. A quasi-mono wafer is a multicrystalline wafer with a large monocrystallinelike grain. To make full use of the surface of the mono-grain, the alkali texturing process can be applied so that the light reflection on the cell surface can be greatly reduced. In general, for different percentages of large single grains of the quasi-mono wafer, different texturing processes should be selected, to minimize the surface reflectivity and hence maximize the cell efficiency. For the high percentage of large single grains of quasi-mono wafer, alkali texturing can form an inverted pyramid texture surface and improve the efficiency of the solar cell. But due to the anisotropic etching of alkaline, the pyramids that form on the other grains, with an orientation different from that of the large grain, will have a different structure and orientation. This area will have a different reflectivity for the incoming light and exhibit different colours from that the large grain as shown in Figure 16.

Figure 16: Cell with grains with different colours. Source: PV magazine, 2012

And for a low percentage of large single grains of quasi-mono wafer, acid texturing can be applied. However the dislocation density, the concentration of oxygen and carbon, and the impurity made the efficiency obviously lower than that of a high percentage of large single grains. Typically if the efficiency of a monocrystalline silicon cell is 18.5%, the efficiency of a quasi-mono cell with a high large single grain percentage can reach about 17.5 to 18.2%. But for low single grain percentage quasi-mono cells, the efficiency can be about 16.6 to 17.0%.

2.1.2 Trends in crystalline silicon wafering technology

In Figure 17a typical process and material flow is shown for producing today's standard wafers having a thickness of 180 µm.

Figure 17: Process and materials flow for standard Cz growth of monocrystalline silicon ingots and subsequent cropping, squaring, and wafering. Typical material losses in production are shown on the outside of the processing steps, where the solid scrap generated through sawing of the boule crown, tail, and chords is recycled for further ingot pulls; but the kerf loss in sawing is not. The given 'Capex' numbers within each step refer to the associated capital equipment expenses divided by the annual production capacity of the facility, with an assumed solar cell power conversion efficiency of 16.7%. Source: A. Goodrich, 2012

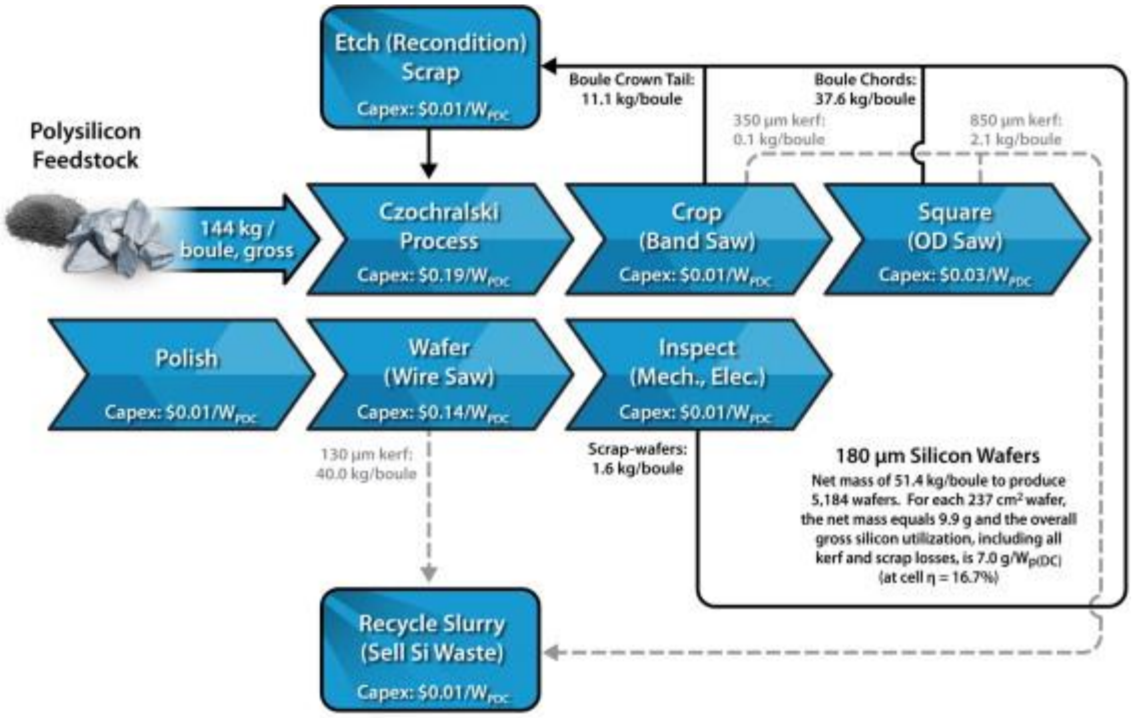

Currently, commercial PV wafers produced with wire slicing range in nominal thickness from about 150 to 200 µm, corresponding to silicon material use of about 5 g/Wp. Since the silicon wafer is the largest cost component of finished solar cell, it is widely accepted that reducing the cost of silicon through reduced wafer thicknesses will greatly benefit lower solar energy costs. Further reduction would require improvements in wafering processes and the development of new and alternate wafering technologies (Table 4).

Table 4: The general trends for crystalline silicon substrate technology

Crystalline silicon technology	2010-2015	2015-2020	2020-2030/50
Industry Manufacturing aspects	Silicon consumption <5g/W	Silicon consumption <3g/W	Silicon consumption <2g/W
Selected R&D Areas	Advanced silicon and solar cell processing Wafer thickness <150 µm	Alternate wafering technologies: - Low/zero kerf-loss - Avoid slurry recycling - Ability to slice down to < 100µm wafer thickness - Improved thickness consistency - Less micro-fractures	Wafer equivalent technologies, which could be defined as a means of making a starting substrate of silicon either from gas, liquid or solid phases of silicon Wafer thickness <50 µm

Source: summarised based on technology roadmaps from the International Energy Agency (IEA), and trade groups such as Semiconductor Equipment and Materials International (SEMI), European Photovoltaic Industry Association (EPIA) and EU PV Technology Platform

The various industry roadmaps project wafer thickness to reach 100 µm, possibly near the limit of wire slicing technology, by the end of the decade. Further reduction will require development of wafer equivalent technologies such as layer transfer techniques or epitaxial growth of thin wafers. Trends in wafer thickness estimates for the next ten years are shown in Figure 18.

Figure 18: Projected trend in minimum wafer thickness processed in mass production of solar cells (Source: International Technology Roadmap for Photovoltaics, SEMI PVGroup/ITRPV, 2011)

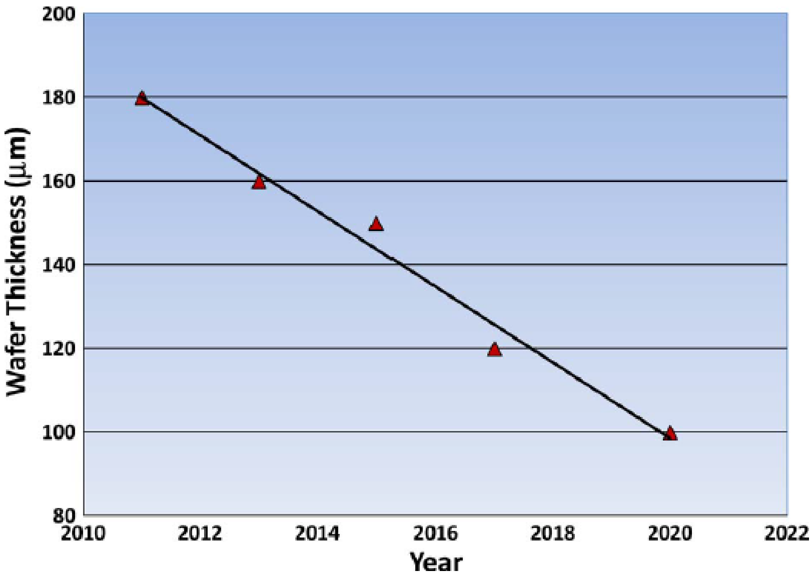

The reducing solar cell thickness improves the diffusion-length-to-cell-thickness ratio, thus improves the overall cell efficiency potential. With adequate light trapping and very good surface passivation, cell efficiency peaks in the 20–50 µm thickness range. Figure 19 gives cell efficiency as a function of cell thickness, which shows efficiency peaking around 40 µm silicon thickness.

Figure 19: With sufficient passivation to reduce surface recombination velocity, cell efficiency may be optimized with cell thickness of around 20–60 μm [48], [49]. (Source: J. Fossum, University of Florida and Stuart Bowden, Arizona State University)

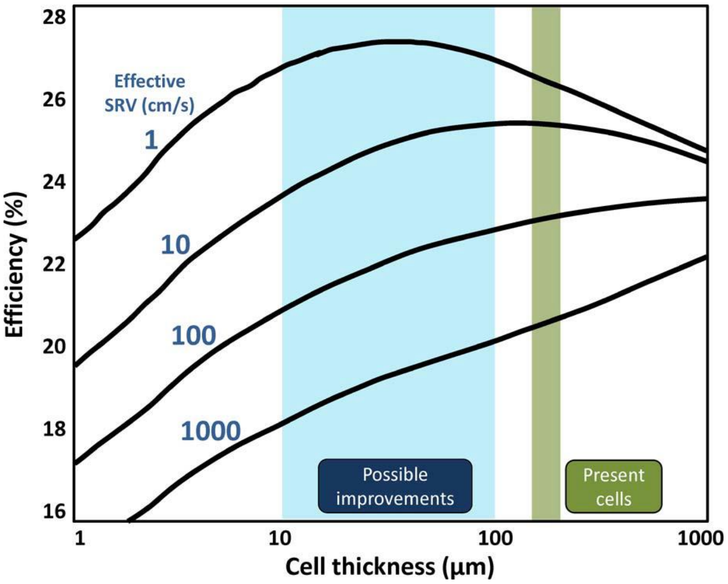

However, there has been a significant progress in demonstrating thin c-Si cells using different techniques, further improvements are needed for commercialization. Reducing the thickness of wafers further is a manufacturing challenge, with increasing kerf loss, reduced yield due to breakage, and more stringent wafer handling requirements, making them into high efficiency cells, thermal annealing to recover the degradation of carrier lifetime due to implant damage. For wafer thickness reduction, the two key elements are the cost of silicon, the ability to mitigate yield losses due to microcracks and throughput challenges.

2.1.2.1 Current industrial challenges

Above mentioned issues have been the drivers to find practical lower cost wafering alternatives as nearly all crystalline silicon wafers made today uses the Multi-Wire Slurry Saw (MWSS) sawing process (basic concept shown in Figure 20). Although the process has undergone impressive evolutionary improvements in the important areas of yield, quality, kerf loss, productivity and thickness reduction, the process remains one of the highest cost contributors to crystalline silicon PV manufacturing.

Figure 20: Multi-wire slurry saw process. Kerf loss and wafer thickness are set by the wire guide roller (WGR), wire diameter and carrier/abrasive grit selection (Source: Henley, F.J., 2010)

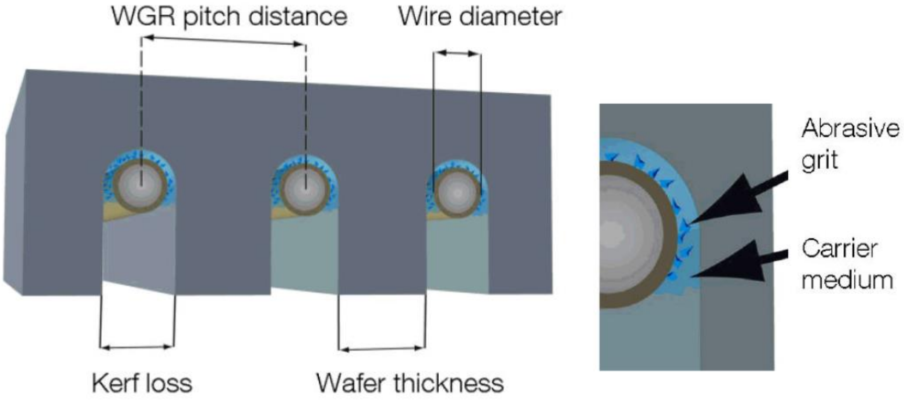

The main issues in using a sawing process for solar PV wafering are fourfold:[12]

- Kerf-loss is inherent. Kerf loss is a fundamental result of any sawing process and is currently 40-50% for 180-200μm thick wafers. Lower wafer thickness slicing can increase the kerf loss to ~70%. Since purified silicon accounts for >50% of the cost of a solar cell, kerf losses will continue to represent a large material inefficiency for MWSS processes.
- Significant thickness variation and wafer brittleness. The sawing process develops surface scratches and thickness non-uniformity. These quality issues lower wafer strength causing breakage and drive cost/quality issues in the downstream cell and module manufacturing steps.
- High operating expense. The sawing process requires on-going slurry and wire consumable expenses and additional satellite equipment for wet clean steps, wet singulation and slurry recycling. These increase cost of the wafering step.
- Barriers to produce ultra-thin wafers. In addition to higher kerf loss, sawing ever thinner large area wafers becomes increasingly difficult. Throughput and high post-sawing yield losses are but a few of the challenges. Other issues include catastrophic failure of the saw process due to wafer breakage. Due to the use of wire as the cutting medium, fundamental costs are irreducible and material inefficiencies exist and are likely to continue.

2.1.2.2 Alternative wafering processes: Wafer-Like Technologies

A number of techniques are being explored to produce thin crystalline silicon wafers. These include epitaxial growth and various exfoliation techniques that use ion implant, stress engineering, or electrochemical means to separate a thin crystalline layer from the parent substrate.

As depicted in Figure 21, alternative wafering can be defined as the conversion of one of the three phases of silicon into a silicon substrate of desired dimensional and electrical

---

[12] Henley, F.J. Kerf-free wafering: Technology overview and challenges for thin PV manufacturing. Photovoltaic Specialists Conference (PVSC), 2010 35th IEEE, 1184-1192

specifications. There are numerous methods that have been tried to cost-effectively fabricate a wafer from one of the three silicon states. The amount of work underlines the industry-wide need to find a more cost-effective and practical wafering substitute to the present sawing technology. Table 5 shows a summary of the major wafering alternative techniques that have been researched for solar PV kerf-free wafering.

Figure 21: Alternative wafering technologies using the three available phases of silicon (Source Henley, F.J., 2010)

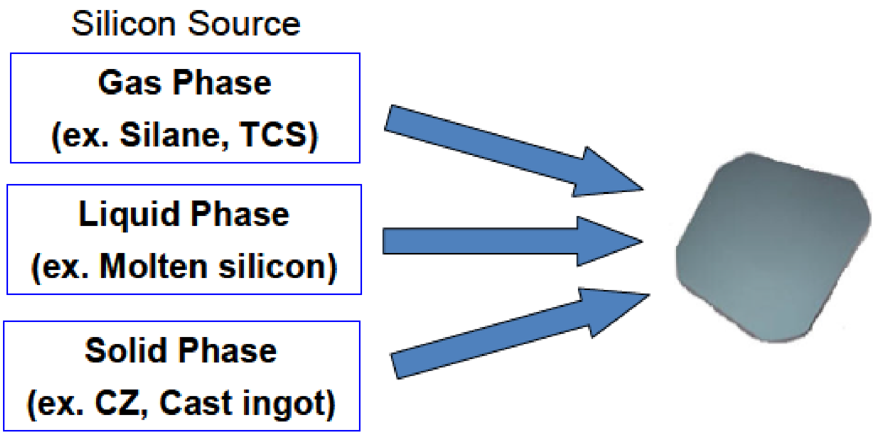

As shown in Figure 22, the simplest and most cost-effective method would use the silicon source in its purified gas phase as silane or a chlorosilane. By using direct deposition of the silicon bearing gas by chemical vapour deposition (CVD), these gas phase methods are attractive in eliminating the cost and complexity of using the Siemens process to produce polysilicon feedstock and the casting or CZ crystal pulling associated with solid phase wafering. Liquid phase wafering using polysilicon feedstock as a high-purity melt is also potentially cost effective compared to solid phase wafering by skipping the crystallization phase.

Figure 22: Upstream silicon source connection to the three phases of wafering (Source Henley, F.J., 2010)

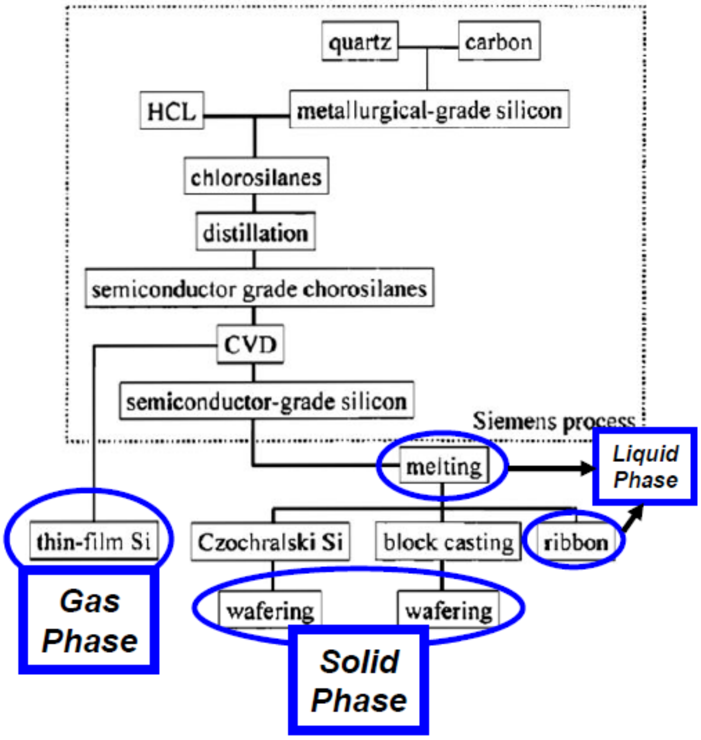

Moving progressively higher upstream to connect to the least processed purified silicon source introduces its own series of challenges however. More complex process steps, slower deposition rates and the generation of wafers having lower quality and PV conversion efficiency are but a few of the practical consequences associated with the use of liquid or gas phase wafering methods.

Table 5: Comparison of Various Wafering Methods

#	Phase	Deposition Source	Target Substrate	Detach Mechanism	Product	Name	Affiliation	Kerf-Free	Cost	Energy Efficiency Potential	Throughput Potential	Quality Potential	Cell Efficiency	Substrate Area Reported	Time to Ramp
1	Gas	CVD	Reusable substrate	Molten Interface	Film	Peeled Film Technology	Camegie-Mellon Univ.	Yes	Med	High	Med	Low-Med	N/A	None Reported	N/A
2	Gas	CVD	Reusable substrate	Stress Layer	Film	CLEF	MIT	Yes	Med	High	Med	Low-Med	N/A	None Reported	N/A
3	Gas	CVD	Substrate mask	Stressed interface	Film	EPILIFT	Univ. Canberra	Yes	Med	High	High	Med	N/A	None Reported	N/A
4	Gas	CVD	Reusable substrate	Porous Silicon	Fillm	SPS	Sony	Yes	Med-High	High	Med-High	Med	12-14%	4 cm^2 cell area	N/A
5	Gas	CVD	Reusable substrate	Via Hole Etch	Film	VEST	Mitsubishi	Yes	Med	High	Med-High	Med	13-16%	100mm Diameter	N/A
6	Gas	CVD	Reusable substrate	Porous Silicon	Film	PSI	ZAE-Bayem	Yes	Med	High	Med-high	Med-High	>12%	Few cm^2 to full wafers	Licensing activity (3-5 years?)
7	Gas	CVD	Reusable substrate	Porous Silicon	Porous Film	FMS, QMS	Stuttgart IMEC	Yes	Low-Med	High	Med-High	Low-Med	12-16%	Few cm^2	N/A
8	Gas	CVD	Inexpensive substrate	Porous silicon as reflector	Absorber on Substrate	EPI-on-porous silicon	IMEC	Yes	Med	High	Med-High	Med	13-14%	Full Wafers	N/A
9	Gas-Solid	Silicon Powder	Reusable substrate	Deposition and ZMR	Substrate	SDS (Silicon Dust Sheet)	SFMC	Yes	Gas-Solid + Med	High	Very High	Low-Med	10-11%	156mm Wafer 300um	Unlimited Production
10	Liquid	Melt	Reusable substrate	Porous Silicon	Film	SCLIPS	Canon	Yes	Med	High	High	Med	10%	125mm Diameter	N/A
11	Liquid	Melt	None	Laser cut singulation	Substrate	Ribbon (EFG, SR)	Evergreen, Wacker Schott	Yes	Low-Med	High	Med	Med	16-18%	Full Wafers	In Production
12	Liquid	Melt	Reusable substrate	Stressed interface	Substrate	CDS, RGS	Sharp, ECN	Yes	Low-Med	High	High	Med	14-16%	156mm Wafer	N/A

#	Phase	Deposition Source	Target Substrate	Detach Mechanism	Product	Name	Affiliation	Kerf-Free	Cost	Energy Efficiency Potential	Throughput Potential	Quality Potential	Cell Efficiency	Substrate Area Reported	Time to Ramp
														300um	
13	Liquid	Melt	None	Near Cold Plate	Substrate	Floating Silicon Method	Varian	Yes	Low-Med	High	High	Med	N/A	None Reported	N/A
14	Solid	CZ	Direct	Shock Cleaving	Substrate	Wafer Shock Cleaving	Purdue Research Foundation	Yes	CZ + Low	High	High	High	N/A	None Reported	N/A
15	Solid	CZ	Direct	Stress Cleaving	Substrate	Wafer Cleaving	Atlantic Richfield	Yes	CZ + Low	High	High	High	N/A	None Reported	N/A
16	Solid	CZ	Direct	Shock Cleaving	Substrate	E-Beam	Y.Y.L.	Yes	CZ + Med	High	High	High	N/A	None Reported	N/A
17	Solid	CZ/Cast	Direct	None	Substrate	Laser-induced stress cleaving	US Patent Appl.	Yes	CZ + Med	High	Medium/High	High	N/A	None Reported	N/A
18	Solid	CZ	Direct	Stressed Surface Layer	Thin Wafer	SLIM-Cut	IMEC	Yes	CZ + Med	High	Medium	Medium	10%	10cm²	N/A
19	Solid	CZ	Direct	Stressed Implant Layer	20-150um Wafer	DFT/Polymax	SiGen	Yes	CZ + Med	High	Medium-High	High	>16%	156mm Wafer 20-150um	1-2 years
20	Solid	CZ/Cast	Direct	None	Substrate	Chemical Assisted Laser Cutting	Frauhofer ISE	No	ZC + Med	Low-Med	Med	Med-High	N/A	None Reported	N/A
21	Solid	CZ/Cast	Direct	None	Substrate	Plasma Cutting	Toyo	No	CZ + Med	Low-Med	Low	Low-Med	N/A	None Reported	N/A
22	Solid	CZ/Cast	Direct	None	Substrate	Spark Cutting	Mitsubishi Nanjing Univ.	No	CZ + Med	Low-Med	Low	Low-Med	N/A	100mm Diameter	N/A
23	Solid	CZ/Cast	Direct	None	Substrate	Slurry Saw Cutting	Ex. Meyer Burger, HTC	No	CZ + Med	Low-Med	Medium-High	Med-High	>18%	156mm, 170-200um	In Production
24	Solid	CZ/Cast	Direct	None	Substrat	Diamond	Ex. Meyer	No	CZ +	Med	High	Med-	>18%	156mm,	1-2 years

#	Phase	Deposition Source	Target Substrate	Detach Mechanism	Product	Name	Affiliation	Kerf-Free	Cost	Energy Efficiency Potential	Throughput Potential	Quality Potential	Cell Efficiency	Substrate Area Reported	Time to Ramp
					e	Wire Cutting	Burger, HTC		Med			High		150-200um	

Silicon Gas Phase Wafering (Methods 1-9)

Growing a substrate directly from silane or a chlorosilane has the tremendous cost benefit of eliminating both the polysilicon (ex. Siemens process) and the cast/CZ crystallization upstream steps. The main approaches are to grow the absorber onto either a releasable substrate or an inexpensive target substrate:

- Releasable substrate approaches. CVD onto a releasable substrate accounts for most of the gas-phase wafering methods. The method requires the formation of a silicon absorber device onto a specially prepared silicon substrate. A layer or features are prepared onto the silicon substrate to allow the device film to be releasable onto a carrier substrate (depositing an absorber over a releasable surface layer having a lower melting point and the release is therefore made by heating the assembly to the point where the surface layer is molten and allows separation). More recent methods are listed in Table 5 (methods 3-8). These methods involve the development of a weaker substrate mask (EPILIFT), porous silicon cleave layers (SPS, ELTRAN and PSI) and etch lift-off layers (such as Mitsubishi's VEST technology).

  Offsetting the basic benefit of its access to the least costly source of silicon, all of these methods have the following challenges:
  - Process complexity (cleave plane and release process development, handling thin-films through bonding, new or modified cell process).
  - Use of non-standard equipment (CVD reactors, bond, cleave plane formation and separation equipment, ultra-thin wafer handling).
  - Low deposition rates which limit the absorber thickness and increases cell process complexity.
  - Reduced crystallinity of the absorber film despite additional process steps such as RTP and ZMR.
  - Limited or little segregation effect for reducing contaminants that lower lifetime, a hallmark of the CZ crystal pulling process.
  - Yields and releasable substrate re-use counts have not been shown in pilot production, let alone on an industrial scale.

  Two methods that eliminate the CVD process step are the Free-Standing Monocrystalline (FMS) silicon or Quasi-monocrystalline Si (QMS) processes. The technique uses the porous layer itself as the absorber. An additional benefit is the light trapping effect of the porous layer, once it is used to detach the absorber itself from a high-quality CZ substrate with multiple re-uses. The various efforts and approaches have thus focused on optimizing absorber quality without degrading the cost advantages, developing compatible high-efficiency cell designs and developing new production equipment. Although theoretically close to monocrystalline CZ, the achievable conversion efficiency has been typically 12-16% due to one or more of the aforementioned issues. Recent interest in further developing this technology using mask and porous silicon separation layers continue (ex. Solexel, San Jose Calif.), however practical production and high conversion efficiencies are still unreported.

- Inexpensive substrate approaches. High-temperature CVD deposition onto a permanent but inexpensive substrate has been researched with encouraging cell conversion efficiencies (>14%). Porous silicon has been used as a reflector to isolate cell efficiency from possible deleterious effects of the inexpensive substrate. Other approaches use seeded layers with aluminum induced crystallization but with disappointing results. The cost advantage of this technique is tied to the cost difference between the method (epitaxial growth substrate cost, surface preparation & CVD) and the cost of a suitable CZ substrate. Three main trends are lowering the advantages of this method:
    - The recent fall of polysilicon feedstock price from historical highs (€400/Kg in 2008 to an estimated 25€/Kg today).
    - Introduction of more efficient CZ pulling equipment such as continuous CZ methods recently industrialized by Solaicx (now MEMC) and Confluence Solar.
    - Adoption of thinner wafers from 300μm down to 200μm -180μm and continuing to below 150μm.

  All these trends will make the technique less attractive since there is a strong connection between the quality of the substrate as an effective homoepitaxial template and its cost. An interesting high-throughput variant of gas phase wafering uses direct gas-solid conversion from nucleating silane gas at atmospheric pressure. The advantages include fast growth, no use of a carrier or backing substrate and near contactless processing for contamination reduction. At best multicrystalline with porous substructure, the present minority carrier diffusion length is still low at 50-60μm.

Silicon Liquid Phase Wafering (Methods 10-13)

By far the most industrialized kerf-free wafering methods use a liquid silicon melt. The main advantage is the much faster effective deposition rates making 20 μm to 300 μm wafer thicknesses readily achievable in mass-production. In many cases the achievable production rates more than offset the use of the more costly source of silicon compared to gas-phase wafering. A liquid phase variant of the ELTRAN™ process by Canon, SCLIPS (Solar Cells by Liquid Phase Epitaxy over Porous Silicon) has been proposed to improve productivity. The technique has yielded about 10% cell efficiency using an 80 μm thick absorber layer. Work by Sharp (Crystallization on Dipped Substrate – CDS) and ECN's Ribbon Growth on Substrate (RGS) are examples of direct solidification of molten silicon onto high-temperature substrates such as ceramics. The CDS method promises to achieve both throughput and large wafer area due to its improved crystallization uniformity.

Direct crystallization from a melt has been achieved commercially using Edge-defined Film-fed Growth (EFG) and String Ribbon (SR). Commercially are available both the equipment and the products using this technology. Finally, a non-contact continuous process has been in development by Applied Materials, Inc. This floating silicon method forms ribbon-like silicon sheets by surface cooling a melt area via a cold plate in close proximity to the melt surface. The frozen silicon ribbon layer is pulled in a continuous manner and singulated into wafers.

Although kerf-free and directly grown from a melt, the methods have the following drawbacks:

- The rapid crystallization causes stress, high dislocation densities and multi-crystallinity in the resulting film with correspondingly lower cell efficiencies and increased brittleness.
- Lowered contaminant segregation compared to CZ ingot pulling or cast ingot growth can lower lifetime due to increased contamination.
- Lower efficiency ceiling of the technology can reduce or eliminate the basic cost advantages.

The minimum wafer thicknesses for these processes are either sub-80 µm with a backing substrate (such as SCLIPS) or 200-300 µm thick to be of sufficient strength for free-standing wafer processing. The combination of lower efficiency and a higher overall thickness continues to be the major issue with these methods. At some point the purpose of being kerf-free becomes moot if the liquid wafering substrate thickness exceeds next-generation MWSS yielding stronger high-efficiency 160-190 µm wafers.

Silicon Solid Phase Wafering (Methods 14-22)

Although solid phase wafering uses the most upstream (and highest cost) silicon processing, casting or Chrozalski (CZ) crystallization steps produce the highest quality source material for wafering. Another ancillary advantage to using CZ or cast blocks as a starting material is that little change is needed in the upstream high-volume equipment and processes to support new solid phase wafering technology. Noteworthy is the fact that most kerf-free methods in this class use a major crystallographic plane to guide or assist in guiding the cleave fracture. This explains why CZ pulled single-crystal ingots are preferred over cast blocks. If it can be done reliably, cleaving substrates directly from an ingot without a cleave plane is the simplest and most elegant wafering solution. Initiating and guiding a release fracture at the desired depth below the ingot surface is the main technical challenge and early work focused on applying stresses that drive a fracture guided along a major crystallographic plane. Shock waves generated from an impact, a laser beam or an electron beam impinging on the boule edge has also been described as a way to produce a cleaved surface.[13]

Recently, Silicon Genesis Corporation has modified this method using patterned implantation and advanced cleave technology to initiate and guide a fracture for efficient kerf-free wafering. The process is called PolyMax™ using Direct Film Transfer (DFT) technology. The kerf-free, dry wafering process uses a 2-step implant-cleave method

---

[13] 22] US Patents. No. 4244348, No. 7351282 and Patent Application No. 2009/0056513

shown in Figure 23 where high-energy light ion irradiation first forms a cleave plane followed by advanced controlled cleaving to initiate and propagate a fracture plane in a controlled manner along the cleave plane to release a large-area wafer from a shaped ingot. The ion beam-induced cleaving process has been used to demonstrate the slicing of full mono-crystalline silicon wafers ranging in thickness from 20µm to 150µm with good material quality. Figure 23 lower part shows 125mm pseudo-square substrates made using the PolyMax™ process. A high-volume manufacturing system is currently under construction.

Figure 23: Silicon Genesis Corporation PolyMax™ Process and 20µm / 50µm wafers

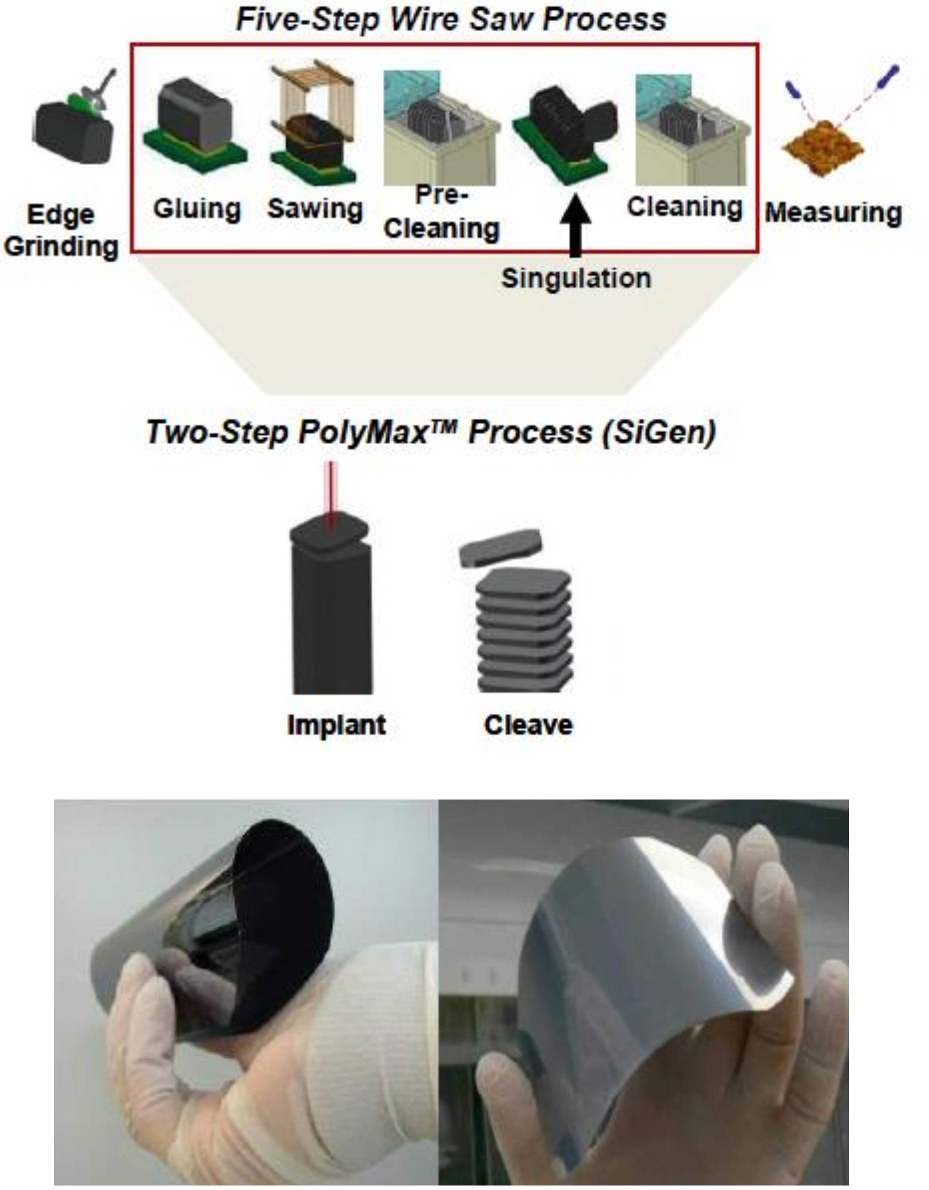

Alternative cutting methods (Table 5, Methods 20-22) have also been proposed that may promise a lower kerf alternative to the MWSS approach. Such techniques include laser assisted chemical etching, plasma cutting and spark cutting. Most reported data are for single test cuts and thus these methods have not been developed to the point where full wafers or test cell efficiency results are available.

From the numerous approaches listed in Table 5, certain near/medium term kerf-free processes stand out as potentially practical approaches in the important areas of cost, complexity, quality, ability to produce thin (< 150 μm) and ultra-thin (< 80 μm) wafers and high-volume manufacturing (HVM) scalability. These selected approaches are further analyzed in comparison to the slurry saw as a benchmark method (Table 6) estimating from the available data in the literature.[14] A rating of 1-5 was then applied to the estimates and entered as an energy efficiency rating in Table 7 resulting The overall comparison. It is immediately apparent that the processes have substantial differences in complexity which in turn will affect time to scale to mass-production. Taking the slurry saw as a benchmark, its process complexity is medium due to its need for satellite equipment such as singulation, clean benches and slurry recovery, but it does have the incumbent method’s advantage of having its constituent sub-processes available and highly engineered for high-volume manufacturing. Using CZ monocrystalline material as its source makes the quality high except for surface scratch induced brittleness and thickness variation. Its main weak points include kerf loss and its inability to support an ultrathin wafer thickness roadmap. Diamond wire is being successfully integrated in bricking and squaring operations. It has also been touted as a means of further improving the slurry saw manufacturing cost and the fundamental benefits of kerf-free wafering. Compared to the MWSS benchmark rating of 18, some kerf-free solutions do not fare as well as expected. The PSI process may have excellent silicon utilization and can support ultra-thin wafering, but high complexity and relatively low HVM compatibility makes it a marginal contender against the ever improving slurry sawing process. Although EFG and ribbon silicon processes have relatively low process complexity, they lack a proven ability to reduce silicon thickness to sub-200 μm and their use of fast crystallization from molten silicon reduces the electrical and mechanical quality of the wafer. Quality was given a 2X weight since conversion efficiency is linked to wafer material quality and impacts cost throughout the PV value chain.

Table 6: Comparison of Energy Expended Between Selected Wafering Processes

Method	Cost complexity	Effective Thickness	Effective gms/Wfr	Siemens Process	CZ Process	CVD/Crystallization	Wafering Energy	Total Energy	Obverall Rating
MWSS** (SAW)	Siemens + CZ/Cast + **MWSS + Clean + Singulate + Clean**	375	21	31	31	0	90	153	1
PSI	Gas + **CVD + LT + Special Cell Process**	50	3	0	0	4	20	24	5
SDS	**CVD + Anneal**	300	17	25	0	25	20	70	3

---

[14] S. Hopman & al., “First Results Of Wafering With Laser Chemical Processing”, 24th European Photovoltaic Solar Energy Conference plenary presentation 2BO.3.6 (2008)

Method	Cost complexity	Effective Thickness	Effective gms/Wfr	Siemens Process	CZ Process	CVD/Crystallization	Wafering Energy	Total Energy	Obverall Rating
EFG, SR	Siemens + **Grow + Singulate**	250	14	21	0	21	20	62	3
CDS, RGS	Siemens + **Grow + Singulate**	300	17	25	0	25	20	70	3
PolyMax (150 µm)	Siemens + CZ + **DFT**	150	8	13	13	0	37	62	3
PolyMax (50 µm)	Siemens + CZ + **DFT**	50	3	4	4	0	37	45	4

*Rating: 1-5 (5=Highest); Energy are in kJ/cm2; **: Includes ~50% kerf loss*

The SDS, RGS and CDS processes are interesting in their high-volume production potential, but again wafer quality may keep these processes from successfully competing on a €/Wp level against the higher quality (and thus higher efficiency potential) slurry saw method. The PolyMax™ process uses high-quality CZ ingots and thus can produce truly monocrystalline silicon wafers. Recent results suggest the process can maintain minority carrier lifetime/diffusion lengths comparable to the starting CZ material. It is also the only kerf-free process that has been demonstrated across an industrially interesting 20- 150 µm thickness range. The range allows a thickness roadmap from current crystalline wafering thicknesses to thin-film flexible substrates.

Table 7: Wafering Process Comparison with Slurry Sawing

Method	Phase	Energy Efficiency (Table 2)	Complexity	Quality (2x)	<80um Potential	HVM Compatibility	Overall Rating (Max 30)
MWSS (SAW)	Solid	1	3	8	1	5	18
PSI	Gas	5	1	6	5	2	19
SDS	Gas-Solid	3	4	4	3	5	19
EFG, SR	Liquid	3	3	6	2	3	17
CDS, RGS	Liquid	3	4	6	3	4	20
PolyMax (150 µm)	Solid	3	4	10	4	4	25
PolyMax (50 µm)	Solid	4	4	10	4	4	26

Rating: 1-5 (5=Highest); LT : Layer-Transfer; Underline: Method process content*

Kerf-free wafering alternatives for crystalline silicon solar PV manufacturing have been in development for over 40 years. Although the main attraction is the higher material utilization efficiency, supporting a wafer thickness roadmap from 150 µm to 50 µm or below is also of great value. Numerous kerf-free methods were reviewed and compared to current slurry saw wafering in important areas such as cost, quality, and ability to fabricate ultrathin wafers. Although CVD based kerf-free processes are attractive from an energy expended standpoint, more productive liquid phase wafering approaches or use of higher quality kerf-free wafering from CZ material is more able to meet the quality and productivity requirements with less process complexity.

Regardless, other materials, such as carbon nanotubes, graphene, molecular semiconductors, or some other exotic material, become the material of choice for the active devices of the sub-10-nm era, it is still likely that the substrate to support these materials will be silicon. The large wafer diameters, crystalline perfection, ultrahigh purity, mechanical and chemical robustness, extreme flatness and cleanliness and high-quality oxide insulator afforded by semiconductor silicon, combined with a rich infrastructure of deposition, etching and patterning processes and tools, guarantees silicon a central role in semiconductor device technology far into the future.

2.1.3 Review of trends in p-type and n-type wafers applications

Most industrial crystalline silicon solar cells are based on p-type wafers. Applying a phosphorous-diffused emitter and a back-surface field created by aluminium-silicon alloying, results in the common multicrystalline or monocrystalline silicon solar cells used in the vast majority of PV modules. The exceptions to this rule have been (for many years) the cells and modules produced by Sanyo, Sunpower Roth & Rau and PVGS who are using n-type wafers for their high-efficiency cells. Recently, Yingli Solar has also taken high-efficiency 'Panda' cells based on n-type wafers into production. In addition, practically all major research organizations and several companies, including Bosch, Suniva, Silfab, Siliken and Trina have started to report activities in cell processing from n-type wafers.

2.1.3.1 Differences in properties of p-type and n-type wafers

If utilizing p-type starting materials (wafers), the dominant loss mechanism appears to be defect-mediated recombination, specifically due to the presence of boron-oxygen pairs. Several methods exist to manage or eliminate these defects, thus enhancing the bulk lifetime of the substrate. The starting material (Si feedstock) for producing n-type silicon crystals is the same type of polysilicon as that used for p-type Si crystals (based on the Siemens process). The difference is in the doping process during crystallization: while for p-type Si usually boron is used as a dopant, for n-type Si crystals usually phosphorus is added to the Si melt. One of the most important characteristics of wafers used for solar cells is the minority carrier diffusion length, which is directly dependent on the minority carrier recombination lifetime or 'lifetime'. A long diffusion length and high lifetime allow for higher efficiencies. A characteristic of n-type doped crystalline silicon is that it generally reaches (much) higher lifetimes than p-type silicon. This is one of the reasons for the interest in n-type wafers for solar cell production (Figure 24).

Figure 24: Schematic representation of the differences in recombination at impurities for p-type versus n-type solar cells. Typical transition metal impurities are donor-type, resulting in a large capture cross-section for electrons, but a much smaller one for holes. Therefore they are effective minority carrier recombination centres in p-type cells, but not in n-type cells. In addition, in p-type Cz, boron-oxygen-related defects are present, which are important recombination centres[15]

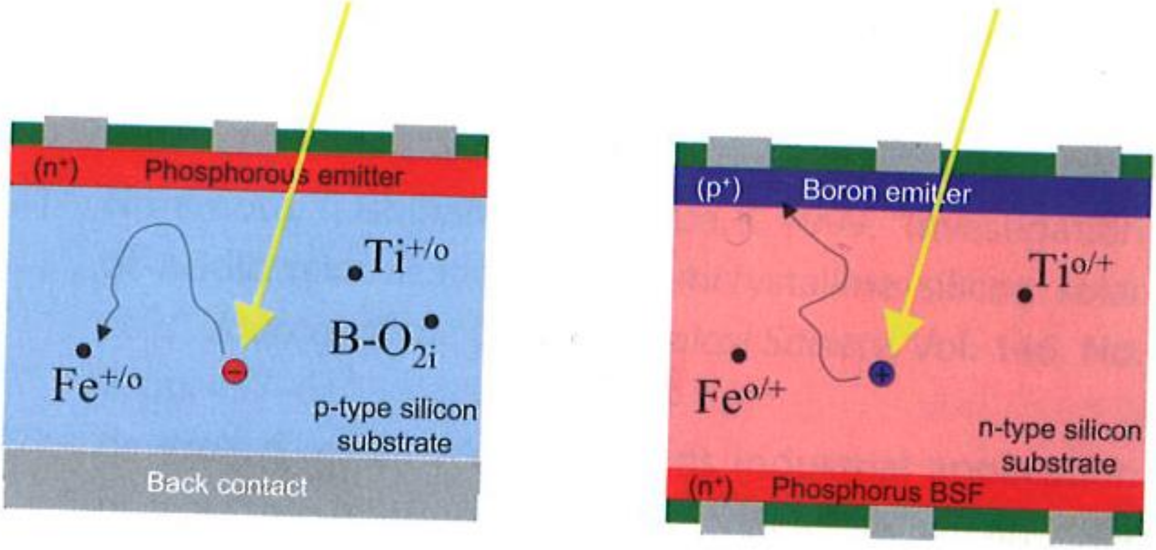

Boron-doped p-type Czochralski (Cz) wafers show lifetime degradation due to formation of a boron-oxygen related metastable defect, upon illumination or in general upon minority carrier injection. Since boron (dopant) and oxygen (growth process impurity) are abundant in typical p-type Cz wafers for solar cells, the effect is very important as they severely limit the potential cell efficiency in high-efficiency cell designs.[16]

Absence of boron or oxygen in wafers will avoid this boron-oxygen related lifetime reduction.[17] Oxygen reduction can be realized by magnetic Cz (MCz), for example, or floatzone (FZ) ingot growth; however these techniques are not yet available for low cost production. Boron can be avoided altogether by switching to Ga doping (Al-doping results in defects).[18] Ga-doped Cz for example is applied by Suntech in its high-efficiency Pluto cells. A technique to remove the boron-oxygen defect is so-called regeneration, which does not yet appear to be applied commercially.[19] Obviously, switching to n-type wafers will entirely avoid the boron dopant and the associated lifetime reduction.[20]

---

[15] LJ. Geerligs, N. Guillevin, I.G. Romijn. Progression of n-type base crystalline silicon solar cells. Manufacturing the solar future. Edited by Stefan Krauter. Solar Media Ltd. 2012

[16] S. Gunz et al. N-Type silicon – enabling efficiencies >20% in industrial production. Proc. 35th IEEE PVSC, Honolulu, Hawai, USA. 2010, 50-56

[17] T. Saitoh et al. Suppression of light-iduced degradation of minority carrier lifetimes in low-resistivity Cz-silicon wafers and solar cells. Proc. 16th EU PVSEC, Glasgow UK. 2000, 1206-1209

[18] J. Schmidt. Temperature- and injection-dependent lifetime spectroscopy for the characterization of defect centers in semiconductors. Appl. Phys.Lett, Vol. 82, 2178-2180

[19] B. Lim et al. Permanent deactivation of the boron-oxygen recombination center in silicon solar cells. Proc. 23rd EU PVSEC, Valencia, Spain. 2008, 1018-1022

[20] T. Schuz-Kuchly et al. Light0induced-degradation effects in boron-phosphorus compensated n-type Czochralski silicon. Appl. Phys. Lett. 2010 Vol. 93, 093505

In the last decade, another reason for higher lifetime in n-type wafers has become clear: the reduced impact of typical transition metal impurities (Fe, Cr, Au, Zn).[21]

In practice, lifetimes of many milliseconds are readily obtained in n-type Cz. Even in n-type mc-Si, very high lifetimes have been measured. However, the crystal defects in mc-Si appear to reduce the carrier lifetime more or less equally for n-type and for p-type. It is not currently clear whether there is a significant diffusion length advantage of n-type mc- Si over p-type mc-Si. For n-type Cz reduction of the diffusion length due to oxygen-induced crystal defects has been reported but it also that this can be minimized by suitable design of the cell thermal processing.[22]

In conclusion, for very high-efficiency cell concepts (requiring very long diffusion lengths, such as back-junction back-contact, or having exceptional surface passivation, such as Heterojunction with Intrinsic Thin layer (HIT)), n-type silicon as a base material has clear benefits. Nevertheless, it is possible that for particular cell designs (e.g., a diffused emitter on the front and dielectric passivation on the rear) and with particular care to avoid process-induced contamination, similar efficiencies can be reached in Ga-doped or MCz p-type, as in n-type silicon. After all, UNSW still holds the cell efficiency record with a cell based on a p-type FZ base.[23]

2.1.3.2 Differences between n-type and p-type cell processing

The reasons for the current industrial emphasis on p-type cells are manifold. Martin Green gives an historic perspective,[24] mentioning aspects such as the convenience of phosphorous gettering, and aluminium-silicon alloying to create a back- surface field (BSF), which applies to p-type substrates, and the complications of boron diffusion as a technology to form an emitter on an n-type substrate.

Until recently the passivation of a boron emitter was also considered a bottleneck, with only thermal oxidation available as a high quality passivating step, with some doubts about its long-term stability. Silicon nitride typically does not provide practical passivation for boron emitters. Also, the complexity and therefore cost of creating and isolating two separate diffusions (emitter and BSF) on either face of the cell may have been considered to be a bottleneck. In this respect the standard p-type cell process is very simple with only eight or nine process steps, and every additional process step means a cost increase that has to be paid for by increased cell efficiency.

However, for all these bottlenecks there has been much progress in recent years, and therefore interest and activities in n-type cells have increased dramatically. For passivation of the boron emitter there are now at least five methods that seem to work well, with coating by Al_20_3 via atomic layer deposition (ALD) - probably the best

---

[21] J. Schmidt et al. Recombination activity of interstitial chromium and chromiuim-boron pairs in silicon. K. Appl. Phys., 2008 Vol. 102, 123701

[22] A. Edler et al. High lifetime on n-type silicon wafers obtained after boron diffusion. Proc. 25th EU PVSEC, Valencia, Spain, 2010, 1905-1907

[23] J. Zhao, A. Wang, MA Green. 24.5% efficiency silicon PERT cells on MCZ substrates and 24,7% efficiency PERL cells on FZ substrates. Prog. Photovolt: Res Appl., 1999 Vol. 7, 471-474

[24] M. Green. Silicon solar cells at the crossroads. Prog. Photovolt: Res. Appl, 2000 Vol. 8, 443-450

documented. Several companies are actively developing equipment for the PV industry to deposit Al_20_3. Industrial boron emitters have now been reported with emitter recombination currents below 30 fA/cm^2 based on a variety of passivation layers, which compares favourably with industrial phosphorous emitters for which typical numbers appear to be somewhat higher. [25] Incidentally, this low recombination current shows that the boron emitter of n-type cells does not need to be influenced much by recombination due to impurities (e.g. Fe or boron-oxygen defect), or crystal defects induced by boron diffusion. It may be fortunate in this respect that the gettering of Fe by a boron emitter is not very good. A practical aspect of concern for n-type cell processing might be the resistivity variation through an n-type ingot, which will be larger than for a p-type ingot due to the different segregation coefficients of the dopants phosphorous (k=0.3) and boron (k~0.7). However, for high-efficiency cell designs, the typical resistivity variation in a phosphorous-doped ingot is acceptable.

Clearly, it is recognised in research and industry that n-type silicon offer advantages for creating very high efficiency cells, which is of high importance for reducing costs per Wp. Therefore, in addition to the very high-efficiency cells that Sunpower and Sanyo have been producing for a number of years, there are many new exiting developments and results of n-type cell technology, and it is very likely that n-type solar cells will rapidly gain a larger market share in the coming years.

2.1.4 Solar cells

2.1.4.1 *Structure of silicon solar cells*

The majority of c-Si solar cell production is currently based upon a very standardized process that is intended to make a *p-/n-* electrical junction on the entire front surface of the wafer and a full-area aluminum-based metallization on the back. A representative series of steps for making such cells is shown in Figure 25.

Figure 25: Process flow for fabricating a standard c-Si solar cell. Source: NREL, 2012

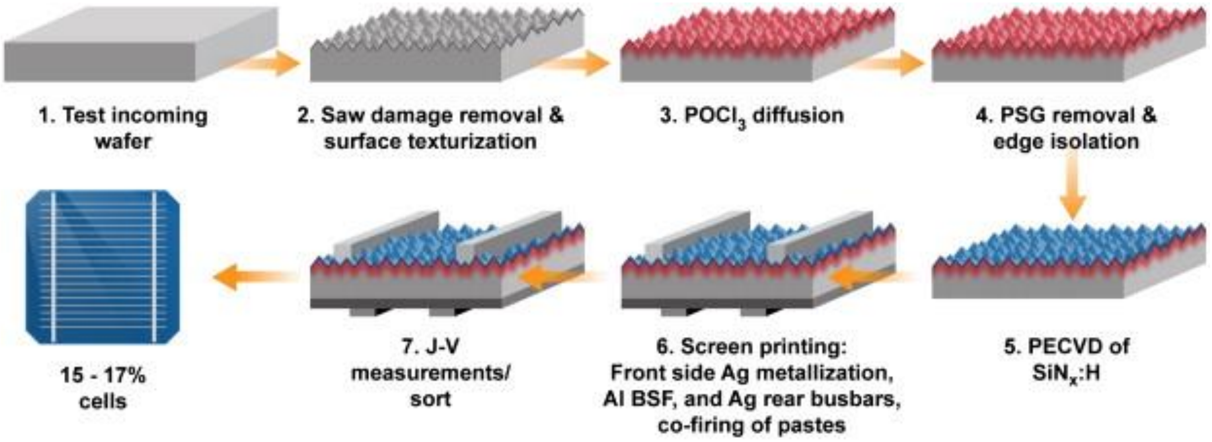

In the last decade, a lot of research has been done in the field of n-type Si-based PV. The results have proven its potential to outperform compared with the standard p-type Si PV

---

[25] V.D. Mihailetchi et al. Screen-printed n-type silicon solar cells for industrial application. Proc 25th EU PVSEC, Valencia, Spain, 2010. 1446-1448

in terms of efficiency. As a consequence, there is a growing interest in the development and the industrial implementation of n-type Si based cell and module technologies. According to the latest edition of the International Technology Roadmap for Photovoltaics (ITRPV 03/2012), its share could reach around 30 percent of the monocrystalline silicon solar module market by 2015.[26]

For back-contacted back-junction *n*-type silicon solar cells, the charge carrier collecting B-doped emitter and the P-doped back surface field (BSF) diffusions as well as the metallization for both polarities are located on the rear side. Thus, no optical shading due to metal fingers on the front side occurs, which leads to a higher photo-generated current density. However, the presence of the base region, usually consisting of the BSF and an undiffused gap on the rear side, reduces the area of the emitter below unity. As a result, the photo-generated minority charge carriers have to be transported, not only vertically to the wafer thickness but also, in addition, laterally to the collecting emitter. In dependence of the geometry, this two-dimensional or even three-dimensional transport can lead to an inefficient collection of minority charge carriers because of increased recombination in the non-collecting base area. This effect is known as electrical shading and limits the short-circuit current density potential of these solar cells.[27] To minimize electrical shading losses, the lateral distance of minority charge carriers to the collecting emitter has to be reduced significantly, and the non-collecting base area on the rear side has to be passivated effectively. On the one hand, this can be realized when the emitter coverage on the rear side is increased, and nearly the whole rear side is covered by the emitter. In this case, the majority charge carriers are collected by small point-like base contacts (Figure 26 A).

---

[26] PV magazine, Issue 06 / 2012. Switch from p to n

[27] Hermle M, Granek F, Schultz-Wittmann O, Glunz SW. Shading effects in back-junction back-contacted silicon solar cells. Proc. of the 33 rd IEEE Photovoltaic Specialists Conference, San Diego, California, USA, 2008; 1–4.

Figure 26: Schematic illustration of the back-contacted back-junction n-type silicon solar cells with a large emitter coverage (A) and small emitter coverage (B) featuring a passivating and insulating thin film on the rear side (top). Also shown is a schematic top view of the emitter and back surface field diffusions on the rear side (bottom) including the active solar cell area as well as the interdigitated metallization and the busbar area (dotted lines). The distance between the n-metal and the p-metal fingers, that is, the pitch (metal fingers), is smaller than the pitch distance. Source: John Wiley & Sons, Ltd., 2012

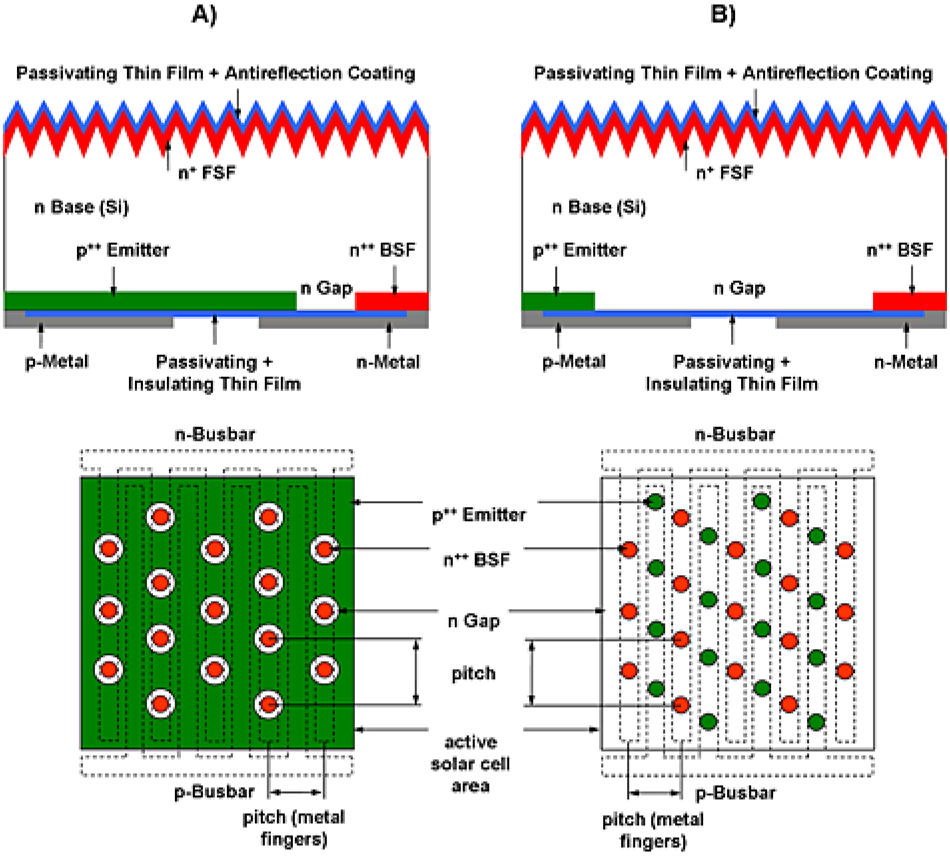

This solar cell design has been proposed by De Ceuster and Cousins[28] and is referred to as a solar cell with a large emitter coverage in this study. On the other hand, the aforementioned requirements are also met by a solar cell design with closely adjacent small point-like emitter diffusions and small point-like base contacts (Figure 26 B). The latter solar cell design has been introduced by Swanson *et al.*[29] and Sinton *et al.*[30] and is referred to as a solar cell with a small emitter coverage. For the solar cell design with a large emitter coverage (A), the lateral distance for the minority charge carriers is minimized, resulting in a predominantly vertical, that is, quasi one-dimensional, minority charge carrier transport to the collecting emitter area. In contrast, for the solar cell design with a small emitter coverage (B), the lateral distance for the minority charge carriers is only minimized for very small pitch distances.

Nevertheless, to maximize the performance of these solar cells, the electrical series resistance of the metallization has to be minimized, especially for large-area solar cells.

---

[28] *De Ceuster D, Cousins PJ, United States Patent Application, US2008/0017243 A1, 2008; 1–9*

[29] *Swanson RM, Beckwith SK, Crane RA, Eades WD, Kwark YH, Sinton RA, Swirhun SE. Point-contact silicon solar cells. IEEE Transaction on Electron Devices 1984; 31(5): 661–664.*

[30] *Sinton RA, Kwark Y, Swirhun S, Swanson RM, Silicon point contact concentrator solar cells. IEEE Electron Device Letters 1985; 6(8): 405–407.*

Hence, sophisticated two-level metallization schemes have been developed. The two-level metallization scheme is usually characterized by a first metal layer as the positive electrode to contact the emitter area and a second metal layer as the negative electrode to contact the base area through several vias in the first metal layer. Because the second metal layer is formed on top of the first metal layer, it is required that both metal layers have to be electrically isolated from each other by an insulating thin film. These insulating thin films should therefore be without defects, such as pinholes, cracks, or particle inclusions, to prevent shunts. The different metal layers are then connected to busbars in the perimeter region of the active area of the solar cell. The electrical insulation of the thin films also has to be guaranteed during annealing and contact sintering at elevated temperatures. Furthermore, the coverage of the substrate as well as the metal layer with the insulating thin films is of major concern. In general, for solar cells, relatively low-temperature processes for the thin film deposition are required to prevent minority charge carrier lifetime degradation and thus reduction of the bulk diffusion length. Moreover, degradation of surface passivation and hence an increase of the surface recombination velocity (SRV) has to be taken into account. Because the two-level metallization scheme is a highly sophisticated and demanding process, an easier to fabricate and more reliable single-level interdigitated metallization scheme with a higher yield is usually applied. The interdigitated metallization scheme is generally characterized by a number of interdigitated negative and positive electrodes or metal fingers connected to the busbars in the perimeter region of the active area of the solar cell. The positive and negative metal fingers are placed horizontally (side by side) and not on top of each other as in the case of the two-level metallization scheme. Thus, no thin films for electrical insulation of both metal fingers are required. However, the use of an interdigitated metallization scheme is generally associated with an increase in the electrical series resistance compared with the two-level metallization scheme. Therefore, it is required that both the positive and the negative metal fingers are sufficiently wide and high to conduct the current without enhanced electrical series resistance to the busbars. The implementation of an interdigitated metallization scheme to solar cells with a large and a small emitter coverage leads, in this case, to an overlap of the negative metal finger and the *p*-type emitter (Figure 26 A (top)) and the positive metal finger and the *n*-type base (Figure 26 B (top)). Hence, an insulating thin film is required when an interdigitated metallization scheme is applied to the solar cell designs presented in this study so that shunting is prevented and decoupling of the charge carrier collecting emitter and BSF diffusion and the metallization geometry on the rear side can be obtained.

For solar cells where the emitter and the BSF diffusions have the same width as the metal fingers of the interdigitated metallization scheme, insulating thin films are not required. The geometry of the charge carrier collecting diffusions on the rear side is, in this case however, determined by the metallization geometry. This consequently leads to a trade-off between minimizing electrical shading losses and thus maximizing the short-circuit current density and minimizing electrical series resistance of the metal fingers. Nevertheless, this trade-off can be avoided by overcompensating the B-doped emitter diffusion with the P-doped BSF diffusion. In this case, the additional *p-n* junction between the emitter and the BSF acts as an insulator and thus allows the geometry of the minority charge carrier collecting emitter diffusion on the rear side to be independent of the width of the BSF and the negative metal fingers. Hence, the emitter coverage can be increased significantly, leading to a reduction of electrical shading losses. The most challenging aspect for the fabrication of the presented solar cells with a large and a small emitter coverage featuring an interdigitated metallization scheme (Figure 26) is the formation of insulating thin films with excellent electrical insulation properties for large areas. In this regard, plasma-enhanced chemical vapor deposited (PECVD) SiO_2 insulating thin films with various thicknesses ranging from 100 to 2000 nm and deposited at different temperatures in the range from 150 to 350 °C have been investigated in this study. The electrical properties of these insulating thin films have been analyzed by metal-insulator-semiconductor (MIS) structures and leakage current density measurements. To account for annealing and contact sintering steps in the solar cell fabrication process, the leakage current density has also been determined after an additional annealing step at elevated temperatures ranging from 350 to 450 °C. Furthermore, the influence of different metal layers such as Al, Ti, Pd, Ag, and Cr on the insulation properties of the films has been analyzed. Insulating thin films with excellent insulation properties and passivating plasma-enhanced atomic layer deposited (PEALD) Al_2O_3 thin films have been applied to the aforementioned solar cell designs to further investigate the influence of the pitch distance on the short-circuit current J_{sc}, the fill factor FF, the open-circuit voltage V_{oc}, and the efficiency of solar cells with a large and a small emitter coverage.

The structures of the most basic n-type cells, with full-area emitter on front or rear, and contact grid on the front are:

- The cell with emitter on front and BSF on rear (BSF cell, or p^+nn^+ cell). It normally has a boron-diffused emitter and a phosphorous-diffused BSF.
- The Al rear-emitter cell with a front-surface field (FSF cell, or n^+np^+ cell). It normally has a phosphorous- diffused FSF, and is also known as PhosTop cell.

Both cell types have a variant with local junction formation on the rear, either local BSF or local emitter.

Many variations of this cell have been published, including the following types:

- bifacial BSF type cell (Figure 24): full area emitter on front and full area BSF on rear, which are contacted by contact grids. Front and rear-passivating dielectric coatings.
- PERT: passivated emitter rear totally-diffused. Can be identical to the above, but typically has rear point contacts with local heavier BSF diffusion and a full-area metal layer to interconnect the point contacts.

- PERL (Figure 24): passivated emitter rear locally-diffused; most of the rear area is undiffused. Local BSF diffusion under the rear contacts. Typically a full area metal layer to interconnect the point contacts.
- PERC: passivated emitter rear contact. Rear undiffused. Typically high density of rear point contacts and a full area metal layer to interconnect the point contacts. This will not yield a high efficiency unless the rear point contacts are passivated (for p-type this can be done by using aluminium point contact metallization where a local BSF is created by alloying).

In 1978, Sandia labs published excellent results for p^+nn^+ cells (probably not bifacial; the BSF appears to have been fully covered by metal contact).The Sandia paper explains the advantages of the structure: a transparent emitter; gettering as well as passivation by the BSF and a long hole diffusion length in the base.

In recent years the development of p^+nn^+ bifacial cells using simple industrial techniques such as screen-printing was pursued by many institutes. Yingli Solar has adopted and piloted the technology in a joint project with ECN and Amtech [32] and subsequently commercialized the concept, so far reporting a best cell efficiency in trial production of 19.5% (independently confirmed) and in production of 19.9%. Other companies like Bosch and Suniva have made public that they work on production technology of $p'nn^+$ type cells. Suniva reported 19.1% (independentlyconfirmed) using implantation in cooperation with Varian.

In addition to the cells with nearly 20% efficiency made by industrial techniques, there have also been efforts on laboratory cells, demonstrating new processes, materials and the potential of particular cell designs. In particular ISE has reached very high cell efficiencies upto 23.9% for a cell structure with full-area BSF, using emitter passivation by Al_20_3 (pioneered in collaboration with University of Eindhoven). Comparisons of different emitter profiles were reported. PERL as well as PERT laboratory cells have been reported. The rear-side recombination seems to be only marginally different between these two cell types, as their $l/_{oc}$s are very similar. Compared to conventional p-type Al-alloyed BSF cells, the high efficiencies obtained with p^+nn^+ cells are due to several factors. Ranked by approximate importance they are:

- Improved light trapping due to much better internal rear reflection than an AI-BSF provides.
- Improved diffusion length in the base.
- Improved rear-passivation due to BSF with passivating dielectric coating.
- Low emitter recombination current, probably somewhat better than for comparable phosphorous emitters on p-type wafers.

A valid question is whether or not with comparably more complex processing than the standard p-type cell process, it is also possible to create a p-type bifacial BSF cell (n^+pp^+ cell) with comparable advantages. One of the challenges in that case would be to obtain wafers with high diffusion length (e.g. Ga-doped or magnetic Cz), and maintain this high diffusion length during processing. Especially when applying a boron-diffused BSF, maintaining a high diffusion length in a p-type wafer might be challenging. The high temperature for boron diffusion easily contaminates a wafer with Fe, which is a severe lifetime killer for p-type wafers but not for n-type wafers. Siemens worked on p-type cells with boron BSF until several years ago. For p-type high-efficiency designs, it is more common to omit the full-area BSF and apply a PERC or PERL cell design, but this requires a finely spaced rear- contact grid for low series resistance losses, and therefore requires low recombination (high quality local BSF) under these contacts.

Aluminium rear-emitter cell

An alternative process to create n-type cells by a relatively simple process is by applying phosphorous front diffusion and Al-alloying on the rear, i.e., very close to the current industrial p-type cell process.

In its basic form this process has the disadvantage that it lacks the efficiency improving factors one, three and four of the bifacial BSF cell of the previous section. Without removal of the Al and Al-Si alloy layers on the rear, the V_{oc} of such cells is limited by the emitter recombination to about 640mV. In addition, conventional cell interconnection is impossible since the complete rear surface area should be Al-doped, as the commonly used Ag interconnection pads would be large areas with high recombination loss ('electrical shading' areas). Alternative interconnection might resolve this problem.

Despite the limited rear surface passivation, an efficiency of up to 19.3% was recently obtained on FZ material by using a plated front grid and SiO_x/SiN_x front-surface passivation and with full rear-area Al coverage (i.e., cutting off the cell edges on which emitter is absent). To improve the rear recombination and enable conventional interconnection, cell processes have been developed where, after Al-Si-alloying to create the emitter, the remaining Al layer and the Al-Si alloy are removed by wet chemistry and the rear surface is coated with a passivating layer such as a-Si, Al_20_3, or SiO_x. This can improve the cell efficiency to a level more comparable to the bifacial BSF type cell, as reported efficiencies well over 19% demonstrate. However, for lab cells the V_{oc}s are still significantly lower than for a B-emitter; this shows that the emitter recombination current is significantly higher ($J_{0(}$,=160-180fA/cm^2) than for a well- passivated B-emitter. A quick estimate shows that free carrier absorption in the Al-emitter is probably roughly the same as in the B-emitter. A variation of the Al rear-emitter cell that has been explored is based on the laser-fired contacts scheme. Here a dielectric rear-side passivation is applied with only local Al- emitter areas, created by laser-firing of an Al layer through the dielectric. However, for this elegant process scheme so far the results are lagging behind the full-area rear Al-emitter cells, due to non-optimal junction quality.

Back-contact n-type cells

Back-contact n-type cells require more complex processing but offer the significant advantages of reduced shading losses (higher cell efficiency) and lower losses in module interconnection.

Back-contact cells have the major advantage that interconnection in a module will be on one side of the cells only. This will reduce the stress exerted by the interconnection on the cells. It allows the use of thinner cells, or cells larger than six inches. Back-side interconnection also has efficiency advantages. The interconnection conduits can be optimized for best series resistance losses without the constraints related to normal front-to-back tabbed interconnection: shadow loss (i.e. width of tab) and stress on cells (i.e. thickness of tab). The reduction of series resistance losses at the module level can result in a significant reduction of efficiency loss from cell to module, compared to standard interconnection; for example, the FF loss can be reduced to 2%, about 1.5% better than for traditional tabbed modules. Only Sunpower is commercially producing back-contact n-type cells, of the back-junction back-contact type (also often referred to as interdigitated back-contact or IBC cells, although that term is rather ambiguous). Metal wrap-through (MWT) and emitter wrap-through (EWT) cells (cells where the back- contact is realized by connecting a front emitter to the back of the wafer through holes in the wafer) are in research phase. MWT and EWT cells have been under development for p-type cells for more than 10 years. Typically the cell process requires laser drilling of a small number (MWT) or a large number (EWT) of holes in the wafer. For MWT the front grid connects through these holes to contact pads on the rear, while for EWT there is no front grid, but the emitter is wrapped through these holes to contact pads on the rear. N-type EWT cells have to our knowledge not yet been reported. In principle, cell processing used for high efficiency p-type EWT cells such as RISE[31] might be applicable to n-type base material.

The bifacial n-type MWT cells hd been reported.[32] Depending on the front grid design and the number of holes, a cell efficiency gain of several tenths of a percentage point can be obtained. ECN have obtained up to 19.75% cell efficiency with low-cost industrial techniques on 156mm-size Cz wafers. This means that current technology allows low-cost back-contact cells of efficiency close to 20% or higher. Together with the possibility of using thinner wafers, and the benefit for module interconnection and efficiency, this is a promising route to low-cost high- efficiency modules. An advantage of MWT back-contact technology is that it should allow bifacial modules with quite good bifaciality, whereas IBC cells due to the requirement for finer grids on the back result in modules with rather low bifaciality.

Back-junction back-contact cells

IBC cells on n-type wafers have been around for more than 50 years. High efficiencies can be achieved on IBC cells because all current collecting contacts are located at the rear, eliminating all front shading losses. At the same time, the rear structure can be optimized for maximum collection efficiency and minimal resistive losses. However, as the minority carriers need to travel to the emitter contacts on the rear of the cell, the

---

[31] N.P. Harder et al. Laser-processed high-efficiency silicon RISE-EWT solar cells and characterisation. Physica Status Soliditi C, Vol 6, 20009, p. 736-743

[32] N. Giulevin et al. High efficiency n-type metal warp through Si solar cells for low-cost industrial production. Proc. 25th EU PVSEC, Valencia Spain, 2010, p.1429-1434

cells are very sensitive to wafer quality. Furthermore, the device structure needs excellent surface passivation on both sides. Currently the most successful approach is that used by Sunpower with cell efficiencies of over 24%.[33]

Recently, several institutes have published work on IBC cells[34,35] using low cost methods to fabricate the p+nn+ junctions and contacts at the rear surface. These methods range from screen-printing and laser processing to the RISE concept which is based on laser ablation and self-aligned metallization by a single evaporation step.[36] Efficiencies up to 21.3% have been reached on n-Cz and up to 22% on p-FZ. The latter process can be applied to n-type without a change in design. Most institutes so far demonstrated high efficiencies on relatively small areas (4cm2). ECN has worked in collaboration with Siliken to achieve 19.1% efficiency on larger-area IBC cells applying low-cost methods like wet chemistry and screen-printing.[37] Another lower cost cell approach that has been published is the use of a screen-printed Al-alloyed emitter which also reached 19.1% on n-Cz wafers.[34]

On the front-side of IBC cells, the front surface field (FSF) serves not only to reduce recombination but the FSF (together with the bulk resistivity) also has to improve the lateral transport of majority carriers. The latter is important when the contact pitch on the rear becomes large, which can be the case if lower cost methods like screen printing are used to define the contact structure. Besides the FSF, the cell design requires the highest resolution patterning possible, within the patterning method used, to minimize lateral transport losses. On the rear side of IBC cells, the p1nn+ structure needs to be well passivated with appropriate dielectrics. Traditionally, high-quality silicon oxides have been used for this purpose which benefit from a low density of fixed charges and low interface state density. Lower cost methods like deposition of dielectric layers by for example PECVD are under investigation by several groups including ECN.

2.1.4.2 Opportunities for improvement of solar cell efficiency

While the standard approach to cell processing has been the dominant manufacturing strategy for quite some time, it is increasingly clear that it will become necessary to lower costs even further, in order to remain competitive within the future landscape of PV. For all steps within the c-Si supply chain as well as at the installed systems level, there is little choice but to call upon gains in efficiency in order to achieve these ends—and it appears that the standard cell processing approach will ultimately not be able to deliver the 20–25% power conversion efficiencies that other industrially-relevant

---

[33] P.J. Cousins et al. Generation 3: improved perfomance at lower cost. Proc. 35th IEEE PVSC, Honolulu, Hawaii, USA, 2010 p. 275-278

[34] C. Gong et al. High efficient n-type interdigitated back contact silicon solar cells with screen-printed AL-alloyed emitter. Proc. 35th IEEE PVSC, Honolulu, Hawaii, USA, 2010 p. 3145-3148

[35] R. Bock et al. Back-junction back-contact n-type silicon solar cells with screen-printed aluminium alloued emitter. Appl. Phys. Lett, 2010 Vol. 96, no. 263507

[36] F. Granek et al. Enhanced Lateral Current Transport Via the Front Np Diffused Layer of N-type High-efficiency Back-junction Back-contact Silicon Solar Cells. Prog. Photovolt: Res. Appl. 2009 Vol 17, p. 47-56

[37] F.J. Castano et al. Development towards 20% efficient n-type Si MWT solar cells for low cost industrial production. 1st internationa Conference on Silicon Prhotovoltaics, Freiburg, Geramny, 2011

manufacturing processes are capable of delivering. The efficiency of solar cell is one of the important parameter in order to establish this technology in the market. Presently, extensive research work is going for efficiency improvement of solar cells for commercial use. The efficiency of monocrystalline silicon solar cell has showed a very good improvement year by year. It starts with only 15% in 1950s and then increased to 17% in 1970s and continuously to increase up to 28% nowadays. According to Zhao et al.[38] research work, the role of light trapping in polycrystalline solar cell and improvement of contact and surface of solar cell help in increasing the efficiency. The polycrystalline solar cell also achieved 19.8% efficiency to this date but the commercial efficiency of polycrystalline is coming in between 12% and 15%. The work many research institutions in the field of high-efficiency silicon solar cells is strongly dedicated to the transfer of high-efficiency cell structures into industrial production.[39]

The hypothetical cells for each p-type (Figure 27) and n-type (Figure 28, Figure 29) technology approach capture several of the currently known opportunities for creating more efficient c-Si devices and, in principle, could be made with equipment that is currently available for industrial-scale manufacturing.

Figure 27: Front-side metallization on a p-type Cz wafer (20–22% cell efficiency). Source: NREL, 2012

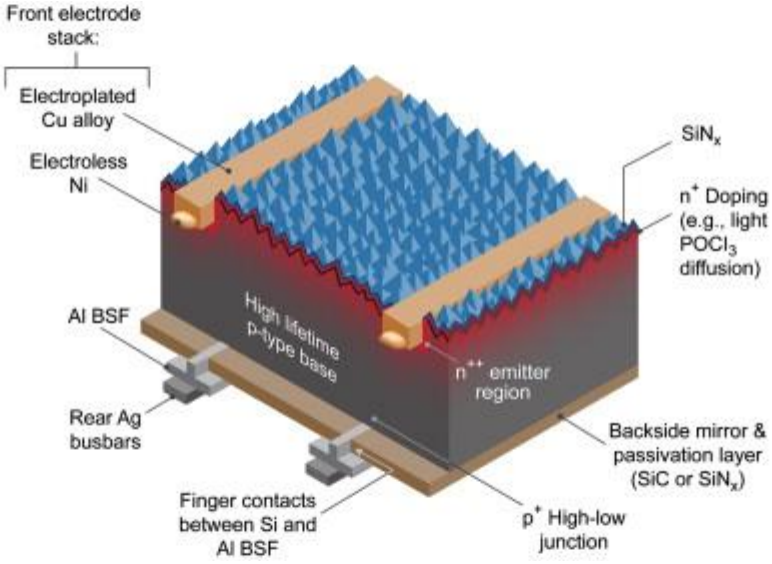

The highest efficiency c-Si solar cell to date, at 25%, is based upon an architecture called the Passivated Emitter Rear Locally-diffused (PERL) cell. The record efficiency mark for this cell has been in place since 1999, and, although it is cost-prohibitive to precisely replicate all aspects of the PERL cell, several of its underlying concepts are clearly appearing within many of the new equipment designs and industrial research and development programs. While not the only contributor to the high cell efficiency, the PERL concept incorporates the idea of a heavily doped emitter region that is narrowly focused at the point of contact between Si and the frontside metal, in addition to a lightly

---

[38] J Zhao, A Wang, P Campbell, MA Green. A 19.8% efficient honeycomb multicrystalline silicon solar cell with improved light trapping. IEEE Transactions on Electron Devices, 46 (1999), pp. 1978–1983

[39] SW Glunz. New concepts for high-efficiency silicon solar cells. Solar Energy Materials and Solar Cells, 90 (2006), pp. 3276–3284

doped region over the entire wafer front surface. Today this design is more commonly called a 'selective', rather than a 'locally diffused', emitter; and it possesses several advantages over the standard cell architecture—primarily in optimizing the electrical connection between the frontside metal and silicon without also creating unnecessarily high rates of recombination over the unmetallized regions of the wafer's front surface. There are numerous manufacturing processes currently under development that can deliver industrially scalable derivatives of the PERL cells. These include the industrially-relevant options of either screen-printing dopant pastes, or using the laser-assisted doping of a wafer from a stream of H_3PO_4, to form the n^+ region.

Figure 28: Interdigitated back contact (IBC) c-Si solar cell (≈25% cell efficiency). Source: NREL, 2012

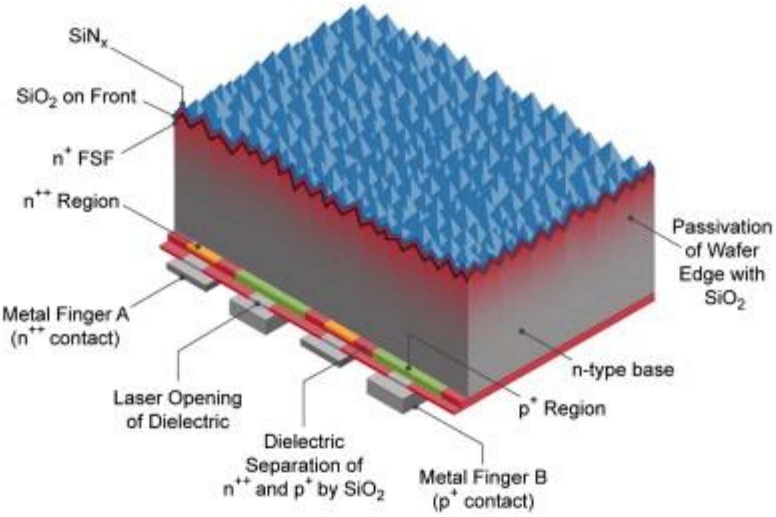

One of today's more esthetically pleasing PV modules has no obvious metal connections on top of or between the cells. Even to a layperson this design makes sense because there should be increased absorption in the solar cell by eliminating frontside metal grid shading—and indeed the relative gain in J_{sc} to be enjoyed by eliminating these optical shadowing losses is a noticeable 5–10% (depending upon the finger and busbar layout for the front-contacted cell). As another, not-so-obvious benefit of this design, by locating the metal contacts on the back there can also be a much greater emitter-to-metal area coverage. This helps mitigate FF losses, because there can be an overall lower series resistance without also increasing optical shading and reflection losses at the same time. But, in terms of enabling the full efficiency potential of c-Si in commercial-production, there are other advantages to this architecture that are just as hidden as the metal contacts.

A typical architecture for HIT cells is shown above, and a representative sequence for fabricating them is shown in Figure 29.

Figure 29: Heterojunction with intrinsic thin layer (HIT) cell (≈24% cell efficiency). Source: NREL, 2012

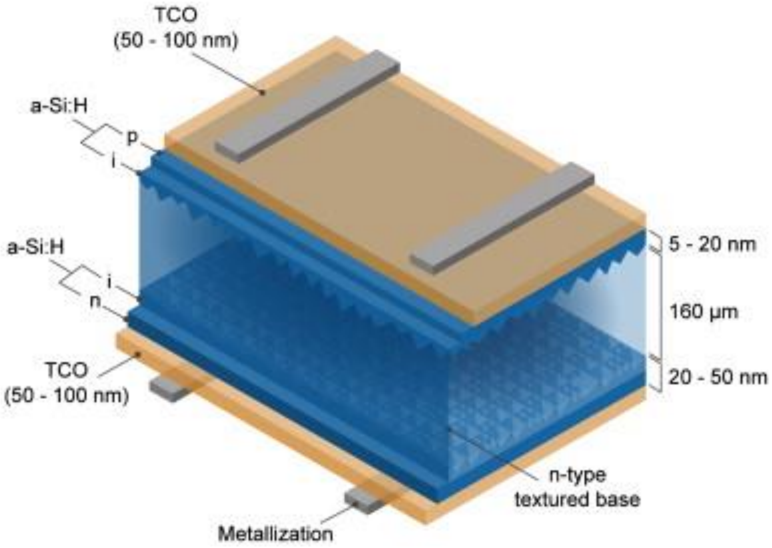

The cells utilize very thin a-Si:H layer stacks on *n*-type wafers to provide surface passivation, emitter formation, and a back surface field. Not only have these 'HIT' cells achieved commercial-production efficiencies that are a close second to the IBC cells, they can also offer some compelling benefits at the LCOE level as well. First, high V_{oc} HIT cells offer a temperature coefficient that can be slightly lower than the IBC cells, and almost half that of a standard c-Si cell. Second, HIT cells easily offer the possibility to realize bifacial structures, which can lead to greater total harvesting of solar power over a system's lifetime. HIT cells offer another potential benefit in that they can be fabricated using a very simple processing sequence that can be carried out—in its entirety—below 200 °C.

The forecast of the global market in future cell concepts is shown in Figure 30.

Figure 30: Expected market share of different c-Si cell concepts. Source: ITRPV, 2012

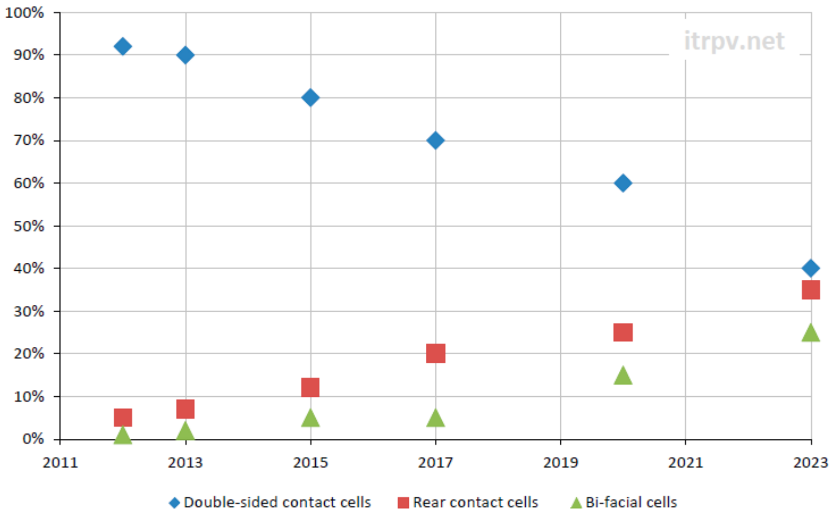

The overview of several technical improvement opportunities that are available to improve the efficiency of c-Si cells and modules is presented in Table 8. The assumed cell-to-module derate is 89% for the calculation of the module efficiencies shown in parentheses at the bottom of the table, although this value may be improved with changes to the assumed standard module design.

Table 8: Overview of several technical improvement opportunities. Source: NREL, 2012

Cell performance parameters	2011 Standard cell (*p*-type base)	Front-side metallization on a p-type Cz wafer (*p*-type base)	Interdigitated back contact (IBC) c-Si solar cell (*n*-type base)	Heterojunction with intrinsic thin layer (HIT) cell (*n*-type base)
Short-circuit current density:J_{SC}(mA/cm^2)	**35**	**38** • Backside optical mirror • Higher aspect ratio front gridlines • Buried front metal contacts • Selectively diffused emitter junctions	**41** • Reduce front-side shadowing losses by moving contacts to the back • Improved light trapping through novel surface texturing and higher internal light reflection • Lightly doped FSF • SiO_2 passivation	**40** • Develop a TCO with reduced free-carrier absorption • Develop a heterojunction window layer with reduced absorption
Open-circuit voltage:V_{OC}(V/cell)	**0.62**	**0.70** • Selectively diffused emitter junctions • Improve wafer quality: alternative dopants or magnetic CZ • Improve surface and bulk passivation	**0.74** • Ion implantation for precise control of dopant profiles • Use tightly focused metal-to-Si contacts in order to reduce contact recombination losses • Use *n*-type wafers with minority carrier lifetimes approaching 10 ms • Improve back, front, and edge surface passivation	**0.75** • Use *n*-type wafers with ms minority carrier lifetimes • a-Si:H/c-Si heterojunction surface passivation
Fill factor:*FF*(%)	**78**	**80** • Improve conductivity (σ) through electroplating • Develop and improve new metal and selective emitter paste chemistries • Selectively diffused emitter junctions	**82** • Reduce resistive (I^2R) losses, without compromising optical losses, by covering more solar cell area in a back-contact scheme	**80** • Use *n*-type wafers with ms minority carrier lifetimes • a-Si heterojunction surface passivation • Use a TCO for charge-carrier transport and anti-reflection coating, and develop a new one with a higher electrical

Cell performance parameters	2011 Standard cell (*p*-type base)	Front-side metallization on a p-type Cz wafer (*p*-type base)	Interdigitated back contact (IBC) c-Si solar cell (*n*-type base)	Heterojunction with intrinsic thin layer (HIT) cell (*n*-type base)
				conductivity
AM 1.5 power conversion efficiency (%):	**17% cells (14.5% modules)**	**20–22% (18.7%)**	**25% (22.4%)**	**24% (21.4%)**

2.1.4.3 Conclusions: c-Si solar cells

It is recognized in research and industry that n-type silicon offers advantages for creating very high efficiency cells, which is of high importance for reducing costs per Wp. Therefore, in addition to the very high-efficiency cells that Sunpower and Sanyo have been producing for a number of years, there are many new exciting developments and results of n-type cell technology, and it is very likely that n-type solar cells will rapidly gain a larger market share in the coming years. There are available technical improvement opportunities for moving standard c-Si solar cells toward higher sunlight power conversion efficiencies, however, the advanced cell architectures needed to achieve these higher efficiencies would likely require a greater initial capital equipment expenditure and higher materials costs on a piecemeal basis.

2.1.5 Module manufacturing

2.1.5.1 Current module manufacturing costs

In the final step of the c-Si supply chain, completed cells are incorporated into modules by first electrically connecting cells together into strings with conductive solder and tabbing ribbons. The ends of those strings are then soldered onto bussing ribbons. To protect this assembly from the elements, it is encased within a top-bottom stack of encapsulant films—typically ethyl vinyl acetate, or 'EVA'—that have been melted ($T_{melting}$≈145–160 °C) and vacuum-laminated onto the array. During this encapsulation step, the assembly is also bonded to a sheet of front glass and to a backside film or glass with a tape that is dispensed around the perimeter of the module. An aluminum frame is also oftentimes fit around the perimeter of the module—with the benefits that it can be used to protect the module edges, to provide a connection point for electrical grounding, to support snow and wind loads, and to make the module installation an overall easier process. (The frame is, however, a relatively expensive component, and there is still an open debate within the industry for how to realize those same benefits at a reduced cost.). The array of bussing ribbons connected to the ends of each series of strings is then crimped towards a through hole in the module backsheet film. The bussing ribbons are connected to bypass diodes, which are housed inside an electrical junction box, or 'J-box'. The purpose of these bypass diodes is to prevent excessive reverse current flow and power consumption in cells that may be receiving different amounts of sunlight, such as when the module might be partially covered with snow, dust, or leaves, or by some other obstruction. As a final step in module assembly, the 'J-box' is set in place with adhesive sealant on the bottom of the backside film.

Within the industry, an intensive effort is underway to identify lower cost module materials and processes. But the adoption of these new approaches is tempered by a very clear need to maintain product bankability. This makes it unlikely that these materials will be significantly changed for at least the foreseeable future. Over the long-term, however, it is possible that the movement to thin or ultrathin wafers may necessitate that the final module materials be modified or even incorporated into wafer handling and cell processing, as many of the ideas that have surfaced for reducing wafer thickness frequently hinge upon the need to use the final module materials as a mechanical support and/or electrical conduit for the more delicate wafers. For example, the front glass/encapsulation combination may need to serve as an adhesive support for wafer bonding and cleavage from an epitaxial substrate; or a conductive film, paste, or epoxy may be needed to electrically connect very thin cells, should the stresses of conventional tabbing and stringing prove to be devastating. Without knowing the exact characteristics and purposes of these next-generation module materials, it is correspondingly, difficult to speculate on what their associated costs might be. Thus, as things stand, there is little choice but to assume the same balance of module materials costs within the long-term module price projections shown in Figure 31. With the balance of module materials constant across all technologies, it is the difference in cell efficiencies that explains the final—very subtle—differences in costs in dollars-per-watt terms.

Figure 31: Top: Cost model results for completed modules: a compilation of estimated costs for manufacturing standard modules and advanced modules within the full c-Si supply chain, assuming all products are transferred at minimum sustainable prices. The numbers underneath each cell type indicate the assumed module efficiency and wafer thickness for each. The long-term scenario reflects the projected costs and prices for modules made with cells on 80-µm wire-sawn kerfless wafers at minimum sustainable polysilicon prices. Bottom: efficiency-adjusted module prices for the different cell types, in consideration of balance-of-systems savings (HIT and IBC) or costs. The BOS efficiency adjustments to the module prices are normalized against the 20% module efficiency targeted within the U. S. Department of Energy's SunShot Initiative. Source: NREL, 2012

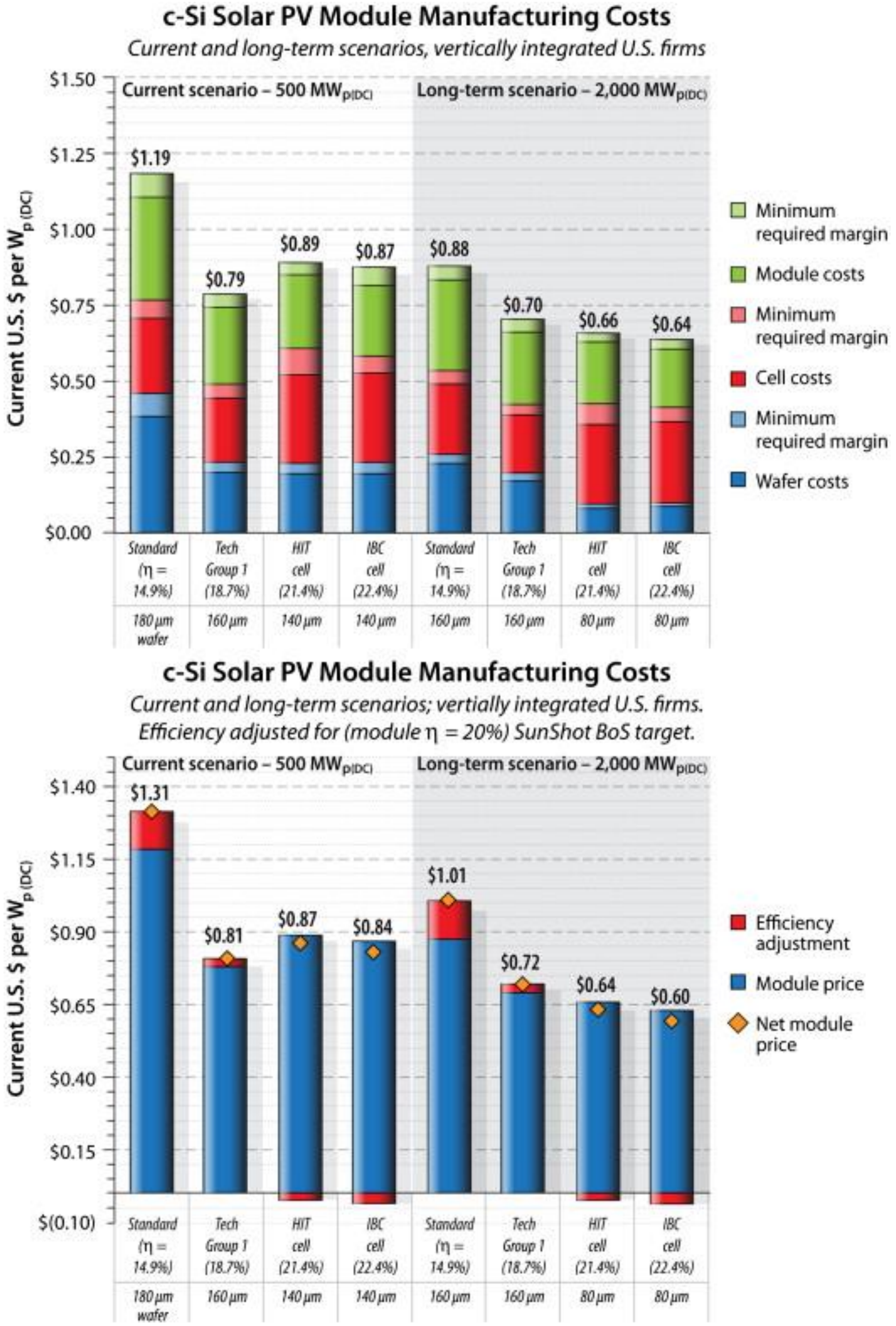

2.1.5.2 Automation in PV manufacturing

Good factory performance starting in the production of PV components and modules is a necessary prerequisite. Such factory performance is possible only by understanding the relevant processes, monitoring and controlling the process windows, ensuring stable processes, achieving the necessary product quality at all times, guaranteeing error-free production and promptly detecting any anomalies. Collecting and evaluating all of the applicable data and controlling the machinery require systems with the same order of complexity as the systems they control. Such systems are realized in the real world as integrated, intelligent automation systems. There are many names for the field that is generally known as 'automation': some companies refer to it as a manufacturing execution system (MES), and others as computer-integrated manufacturing (CIM) or automated material handling. No matter what it is called, the general purpose of automation is to move the right material to the right place at the right time and process it correctly - while controlling all of these steps in real time. The ability to do this reliably, predictably and flexibly has a direct impact on factory performance. In this article, automation is defined as a well-integrated system that manages and controls the flow of resources throughout the complete PV manufacturing process from crystal growing through to module manufacturing. FabEagle is such an integrated and intelligent automation system.

2.1.5.2.1 Benefit of automation: good factory performance

From the classical perspective, the process chain involved in producing PV modules and installing them in power stations comprises five areas: crystallization, wafering, cell production, module production and PV system installation. Each of these areas can be optimized in and of itself. Of course, this does not result in overall optimum conditions for the complete PV production system, since what may be optimum for one area might be far from optimum for another. The resulting conflicts between processes and dependencies are diverse.

Examples of such conflicts include:

- subsurface damages due to low-budget, aggressive wafering systems and the resulting lower cell efficiencies;
- ARC processes that are optimized for cell efficiency but not for potential-induced degradation (PID) effects, which reduce the module lifespan;
- high-efficiency solar cells need a lightly doped emitter which cannot be metallized;
- inhomogeneous and cheap lamination heating plates that are associated with uneven EVA gel content, exhibiting excessively large tolerances and causing reduced adhesion between glass cells and the backsheet such that the module lifespan is reduced, even though the IEC tests were passed.

All of these issues are related to conflicts of interest between the processes, but it is also vital to ensure appropriate quality at the level of each individual process. For example, incorrect thermal energy inputs due to soldering processes have a strongly negative impact on cell efficiency. This includes high tolerances during manual soldering in terms of the temperature and time, or high tolerances in the cooling sections of soldering machines.

The trend towards increasing professionalism in PV is making for less pronounced differences between the different cell technologies. Competitive advantages cannot be simply conjured up, which is something that was easier in the past. Additional improvements are possible only on the basis of a profound and highly detailed understanding of the actual process.This in turn will happen only if data are collected and evaluated in a sensible manner and feedback processes are introduced to improve productivity. Data evaluation must be carried out at all levels, which means at the process tool level ('in the box') and also between the processes ('between the boxes'). This is the only way to.guarantee good factory performance with the aim of achieving the ultimate goal in the field of PV, i.e. grid parity ('out of the box').

Figure 32 illustrates the target system that provides support - from the perspective of production technology - towards the aim of attaining grid parity. At the same time, Figure 32 provides a rough picture of the required basis for an MES automation system. Fig. 2 presents a somewhat more detailed listing of the factors that have considerable influence on, for example, the uptime. It makes clear that even the optimization of a single sub-objective, as represented by uptime, already involves a complex system. Actually optimizing the uptime involves preparing and interpreting the relevant data

Figure 32: The target system for state-of-the-art PV production (Technology leadership and integrated automation drives TCO). Source: Manufacturing the solar future, 2012

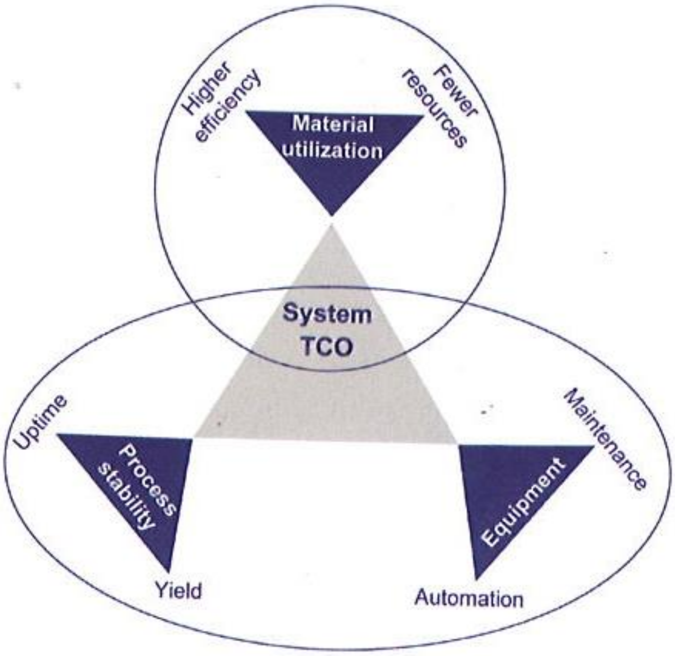

Figure 33: 6-M representation of the factors influencing uptime. Source: Manufacturing the solar future, 2012

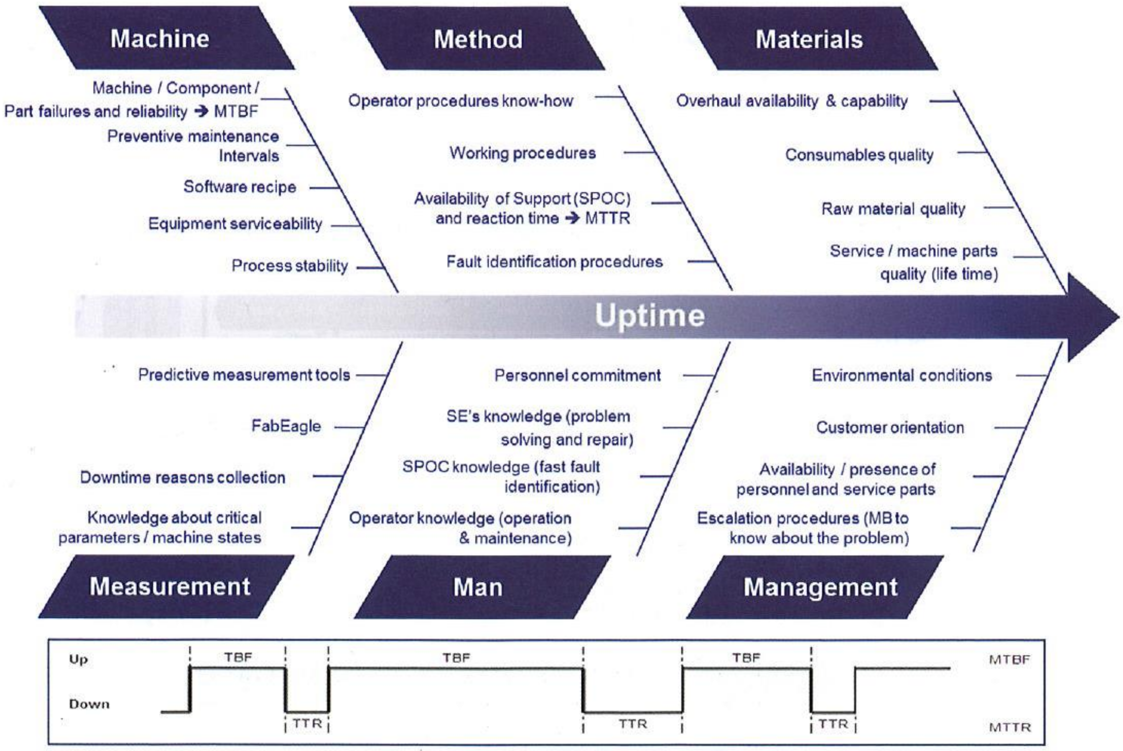

The purpose of an automated manufacturing execution system (MES) is to move the right material to the right place at the right time. Accordingly, the processes must be executed correctly, on the basis of systematic and integrated data acquisition, in the defined process window. This includes production data acquisition (PDA) processes necessary to ensure compliance with the process windows. Machine data acquisition (MDA) serves to guarantee high uptime and high throughput while representing the status of the machines and the material flow.

Data analysis steps between the processes must include indications of potential for continuous improvement (statistical process control, SPC) in such a manner that automatic control of the processes (advanced process control, APC) ultimately leads to the desired maximum factory performance. A material tracking system (MTS) integrates the entire system and ensures the existence of valuable feedback processes for improving productivity. The unique single wafer tracking system (brick slice code, BSC) developed by Meyer Burger Technology (MBT) should be mentioned in this context.

2.1.5.2.2 The price of non-conformance to quality is the price of quality

As a matter of principle, the objective of any production operation is to minimize costs while simultaneously achieving the required level of quality. The quality is based on the following four principles:

- Commitment of the management to quality;
- Prevention;
- Zero defects;

- Conformance to requirements.

In conclusion, the price of quality can be characterized by a simple formula: price of quality = price of non-conformance. Factory performance therefore means reducing the price of quality to zero, which in turn means simply that the target system as represented in Figure 32 must be implemented in a consistent manner. On the basis of an MES automation system of the type sold by AIS, it will now be demonstrated how this can be implemented in practical terms.

2.1.5.2.3 Integrated automation is key

The discussion above clearly shows that today's production environment is highly complex. Complex systems can only be managed by integration and interlinkage of all relevant elements including processes, equipment, material flow and maintenance. Integration leads to networks. Networked systems have the ability to provide supra-summative intelligence. If the problem space is complex, then the solution space must also be complex. A mathematical problem with five unknowns requires five equations in the solution space. "Intelligence in automation is required at every node in the process; intelligence that is integrated with other nodes".

The development of an MES automation system is thus based on an integral and systematic approach. It follows the principles of the input-process-output (IPO) model so that all of the elements are linked and integrated to form a network to take advantage of supra-summative intelligence. This leads to an increase in efficiency, effectiveness and flexibility, accompanied by continuous improvement. Of course, these are the key factors in achieving good factory performance.

With the growth of photovoltaics as a sustainable and successful industry, automation has become an important factor in securing and reaching grid parity. Due to the fast growth of PV, automation has been implemented highly selectively and in different ways with respect to integration and systems. Integration of such systems involves a very difficult, fragile and resource-intensive effort. Moreover, operators have had to manage the trade-offs between these different solutions. Such an approach is inefficient and expensive and leads to a high price for quality.

Figure 34: The P V system with elements in the box (1), between the boxes (2) and out of the box (3) is encompassed by the MES automation system (4), thus representing the second order of cybernetic feedback systems and fulfilling the requirements for an integrated, intelligent MES automation system. Source: Manufacturing the solar future, 2012

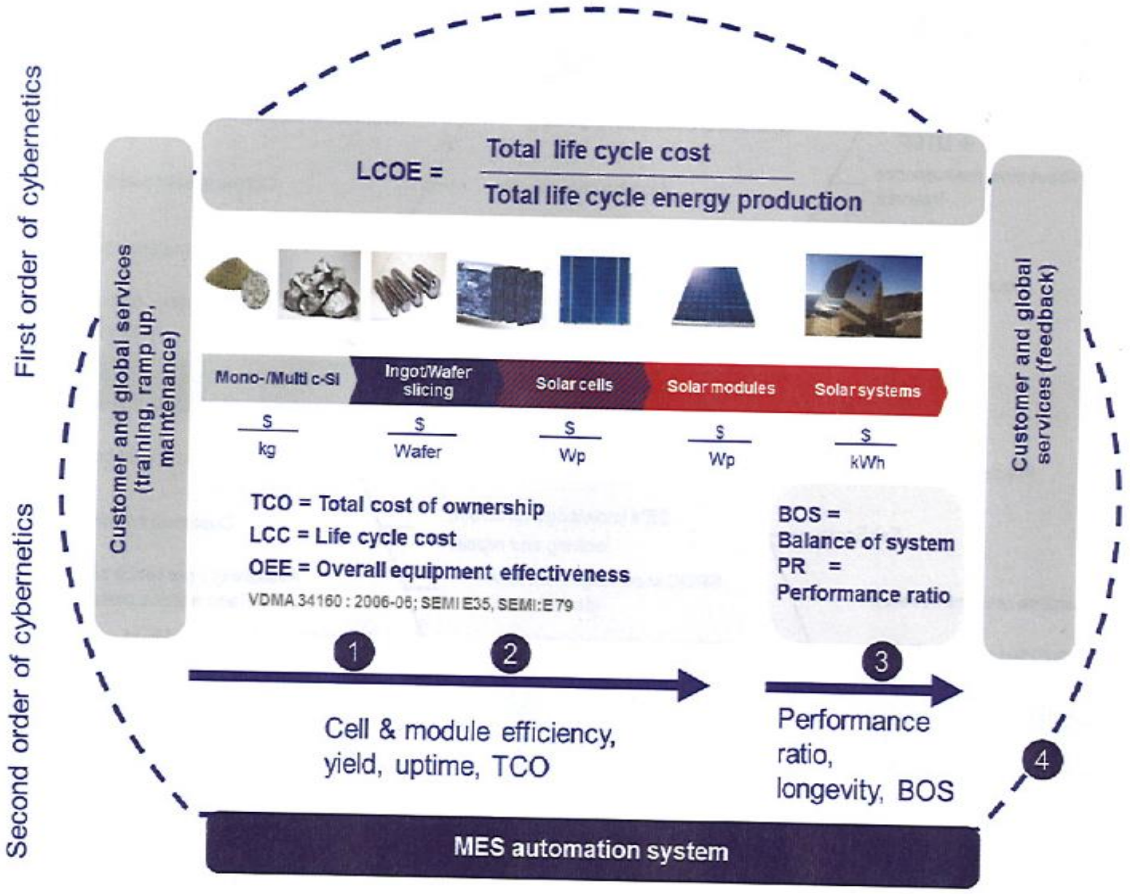

Meanwhile, PV production has matured, the processes are better understood, new standards have been defined in the area of interfaces such as PV2, and MES automation systems for PV applications have been adapted specifically to satisfy the needs encountered in PV production.

Figure 35 illustrates the benefits of integrated automation systems. If the processes are not accompanied by an MES automation system, production productivity creeps along the light grey curve. Disruptions are detected with a delay, problem sources are investigated using difficult and time- consuming trial and error methods, and the necessary responses are often implemented too late or even incorrectly. Using an integrated MES automation system shifts production to the blue curve. Disruptions are detected quickly.Thanks to the availability of insight into process relationships, necessary measures can be formulated and initiated very quickly. Moreover, production output is elevated to a level well above the benchmark thanks to the available feedback processes created using the MES automation system.

Figure 35: The blue curve shows the benefit of integrated systems with fast ramp-up and very short response times vs. the light grey curve which represents very low automation integration with a high risk of expensive trial and error processes. Manufacturing the solar future, 2012

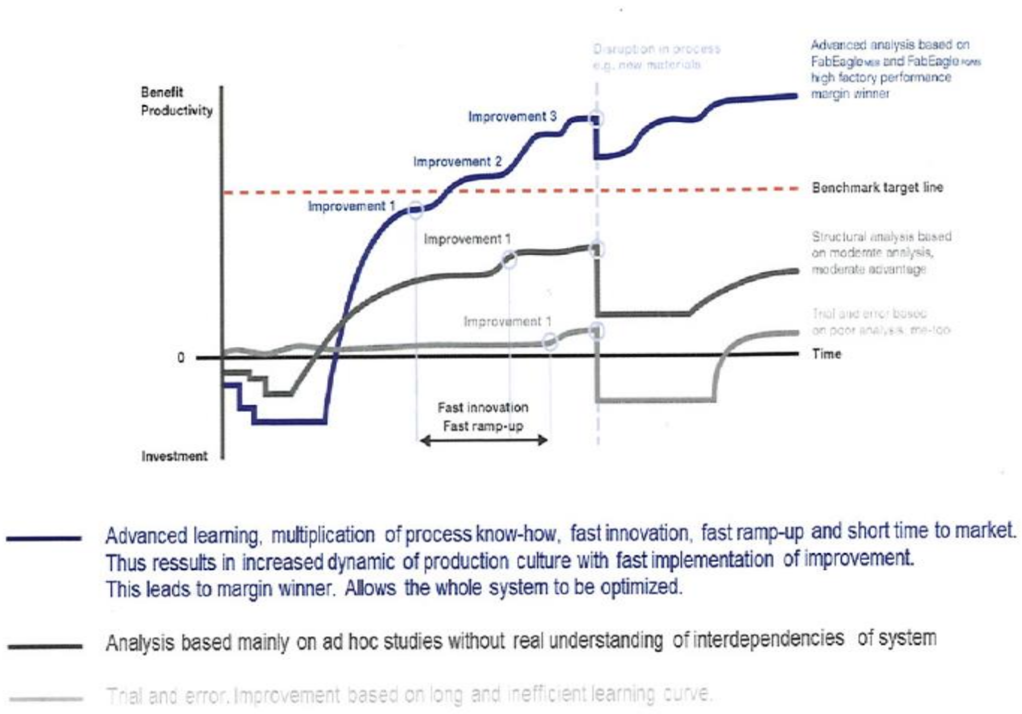

At the end of the day, the business drivers are arguably the most important. The potential of a PV manufacturer to make money depends on its ability to

- be the first to launch to market, when product profitability is greatest;
- drive the cost of manufacturing down, to remain competitive in the face of downward price pressure in order to stay on the cost curve (Figure 35).

Proven, well-integrated factory and tool automation solutions enable the PV manufacturer to reach volume production faster with a stable process and higher yield, while controlling cost through better resource and work-in- progress (WIP) tracking, as well as faster WIP turns

2.1.5.3 Potential for module cost reduction

Module cost can be further reduced through advanced manufacturing methods and module designs that (1) enable the use of thin high-efficiency cells with high manufacturing yield and throughput, (2) reduce labour content through enhanced automation and process simplicity, (3) reduce the capital expenditure required to construct a manufacturing facility, and (4) reduce input material costs.

Reducing wafer breakage and increasing the net yield of the manufacturing process has a cost impact comparable to increasing efficiency, but the potential savings provided by yield improvements is limited due to already high net manufacturing yields of approximately 90%. Current yields for wafering, cell processing, and module fabrication steps are above 95%, with best-in-class yields near 98%.[40] Large-scale, statistically meaningful experiments have provided insight into wafer handling and breakage modes. To reduce breakage, wafer surfaces must be devoid of microcracks of a critical length (which decreases with wafer thickness) and wafer-handling systems must apply a constant load instead of a constant deflection. [41] The interaction of bulk microdefects on internal stress can be quantified with infrared birefringence imaging[42] and Raman microspectroscopy.[43] One promising way to reduce breakage is to reduce the mechanical stress imparted on wafers by reducing the number of wafer handling steps, (e.g., the monolithic architecture presented below) or improving wafer handling processes (e.g., such as contactless, magnetically levitated silicon wafer transport systems). The expected yield trend in module manufacturing (ratio of good cells in good modules out to good cells in during the module assembly process), is shown in Figure 36. It implies continuous improvements, in parallel with the introduction of new wafer sawing technologies and module concepts. In order to process <150 µm cells with >99.3% yield from 2015/2016 onwards, a dramatically improved interconnection technology together with stress-relieving supporting structures is necessary.

Figure 36: Expected yield trend in module manufacturing (ratio of good cells in good modules out to good cells in) (Green Industrial solution exists and is being optimized in production. Yellow Industrial solution is known but not yet in mass production.Red Industrial solution is not known). Source: ITRPV, 2012

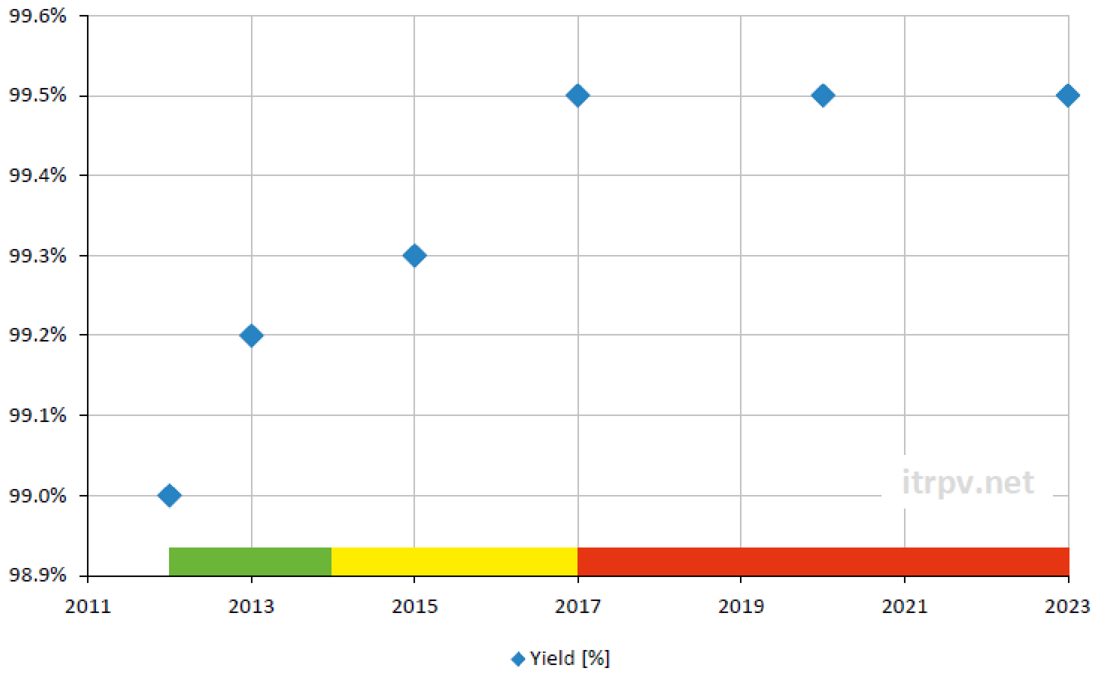

---

[40] Applied Materials, Wafer Wire Sawing Economics and Total Cost of Ownership Optimization, White paper, 2011

[41] P. A. Wang, Photovoltaic Energy Conversion, Conference Record of the 2006 IEEE 4th World Conference on, Waikoloa, HI, 2006, 1179–1182

[42] V. Ganapati, S. Schoenfelder, S. Castellanos, S. Oener, R. Koepge, A. Sampson, M. A. Marcus, B. Lai, H. Morhenn, G. Hahn, J. Bagdahn and T. Buonassisi, J. Appl. Phys., 2010

[43] J. Stopford, D. Allen, O. Aldrian, M. Morshed, J. Wittge, A. N. Danilewsky and P. J. McNally, Microelectron. Eng., 2011, 88, 64–71

To reduce the cost of floor space, module manufacturing equipment should occupy less floor space and achieve higher throughput. This is possible by combining continuous improvement with new developments, particularly for the interconnection and encapsulation processes. For the latter process new encapsulate materials with shorter processing times are desirable. For the interconnection process a significant improvement is expected after 2015 with the arrival of new interconnection technology and back-contacted cell concepts. As tool uptime and throughput in module production increase (Figure 37), the relative number of operators relative to line output will decrease.

Figure 37: Expected improvement in throughput for module manufacturing equipment (Green Industrial solution exists and is being optimized in production, Yellow Industrial solution is known but not yet in mass production, Orange Interim solution is known, but too expensive or not suitable for production). Source: ITRPV, 2012

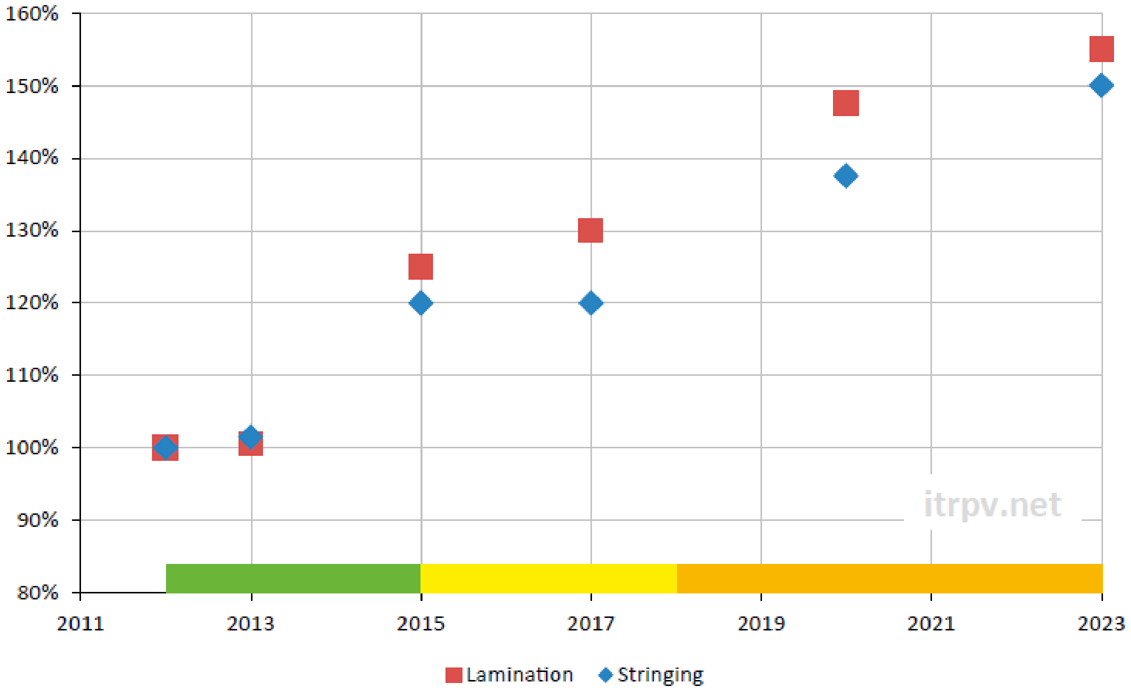

Yield and throughput can be improved by blurring the traditional lines between cell and module manufacturing. A monolithic module assembly, in which cells are fabricated while attached to the module glass, could greatly increase the ease of process automation as well as reduce wafer breakage through the inclusion of a supportive substrate. This would represent a fundamental shift in module fabrication, blending the traditionally discrete operations of cell fabrication and module fabrication. This method could also increase process simplicity and reduce labor content through the integration of interconnection and lamination into a single step. This approach is ideal for the back-contacted cell architecture discussed above, where a pre-metalized ‘printed circuit’ style back-sheet could be used for coplanar interconnection, eliminating the bottleneck of tabbing and stringing.[44] Such a process has already been demonstrated at a module assembly throughput of one cell per second.[45] On-laminate laser soldering is an alternative approach that avoids string handling by lasing through the module glass to solder the bottom side connections.[46]

Low-temperature processing is favored to support monolithic module manufacturing and more generally to reduce thermal stress in thin wafers. Additionally, wet bench steps should be eliminated to reduce breakage and improve yield. Laser-based processing provides these capabilities and has become more appealing based on cost and throughput over the past decade.[47] The combination of economical high-powered lasers and galvo mirrors enables a transition from 1D (laser edge isolation) to large-area 2D processing (surface texturing, emitter patterning). By exploiting the wide range of available wavelengths, pulse durations, repetition rates, and pulse energies, laser-techniques have been demonstrated for many cell fabrication steps including: doping, antireflective coating,[48] and contact firing.[49] Laser-techniques are uniquely capable of providing local energy application and heating, potentially reducing the electricity needed for thermal processes and enabling simultaneous processing of integrated components with significantly different thermal budgets. E.g., emitter diffusion and encapsulant cross-linking require thermal processing at significantly different temperatures; local energy application via laser processing might enable effective emitter diffusion without disturbing the encapsulant, a situation not possible with broad energy application (e.g., furnace anneal).

Automation levels must be increased in a cost-effective manner to reduce the labor cost (and related inflation risk) of the manufacturing operation. The PV industry has already begun to adopt very high levels of automation throughout the supply chain. Further improvements in automation could be enabled through the cell and module innovations outlined above. Additionally, an in-line kerfless wafering process could replace ingot crystallization and wafer slicing, the most manual steps in PV manufacturing. In addition to reducing labor content, process simplification enables reductions in the cost of constructing a manufacturing facility, (e.g., the replacement of crystallization furnaces, sawing stations, and ingot handling equipment with a single kerfless wafer machine). Input material costs for manufacturing can be reduced through a variety of methods. Frameless, laminated, modules can eliminate mechanical redundancies and reduce cost. The ITRPV identifies a differentiation in c-Si module types as well. Figure 38 shows the estimated market shares of frameless / glass-glass module types in relation to framed

---

[44] J. Löffler, L. A. Wipliez, W. J. Soppe, M. A.d. Keijzer, J. Bosman, M. W. P. E. Lamers, A. A. Mewe, A. W. Weeber, I. J. Bennett and P. C.d. Jong, 11th International Symposium on Laser Precision Microfabrication, Stuttgart, Germany, 2010

[45] M. Späth, P. C.d. Jong, I. J. Bennett, T. P. Visser and J. Bakker, 33rd IEEE PVSC, San Diego, CA, 2008, 1–6

[46] M. Gast, M. Köntges and R. Brendel, Progr. Photovolt.: Res. Appl., 2007, 16, 151–157

[47] D. Basting, K. Pippert and U. Stamm, RIKEN Review, 2002, 43, 14–22

[48] M. J. Sher, M. T. Winkler and E. Mazur, MRS Bull., 2011, 36, 439–445

[49] E. Schneiderlöchner, R. Preu, R. Lüdemann and S. W. Glunz, Progr. Photovolt.: Res. Appl., 2002, 10, 29–34

modules. We assume that framed modules retain a larger share, however, by 2023, frameless module types could reach a share of up to 40%.

Figure 38: Market share of different c-Si module types as fraction of worldwide production. Source: ITRPV, 2012

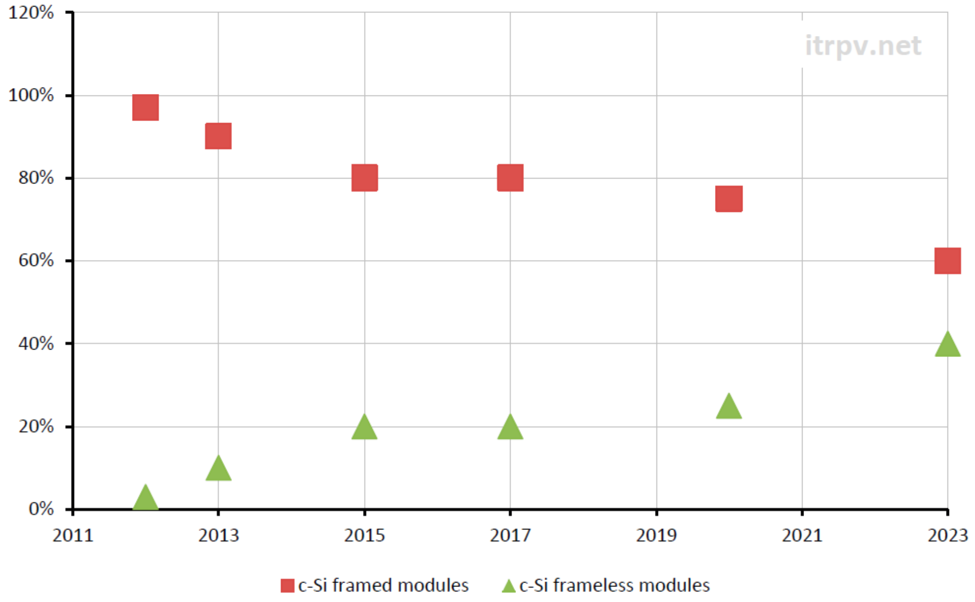

Looking at the module sizes it is becoming clear that the market will be split into different applications: 60 cell modules, large modules (72 cells) for utility scale applications with a market share >20% in 2023, and special sizes for niche markets (e.g. 36, 54, 80 cells) may account for up to 10% of the market share by 2023 (Figure 39). Today's mainstream modules (60 cells) are expected to retain a high market share of above 60% by 2023.

Figure 39: Market share of different module sizes. Source: ITRPV, 2012

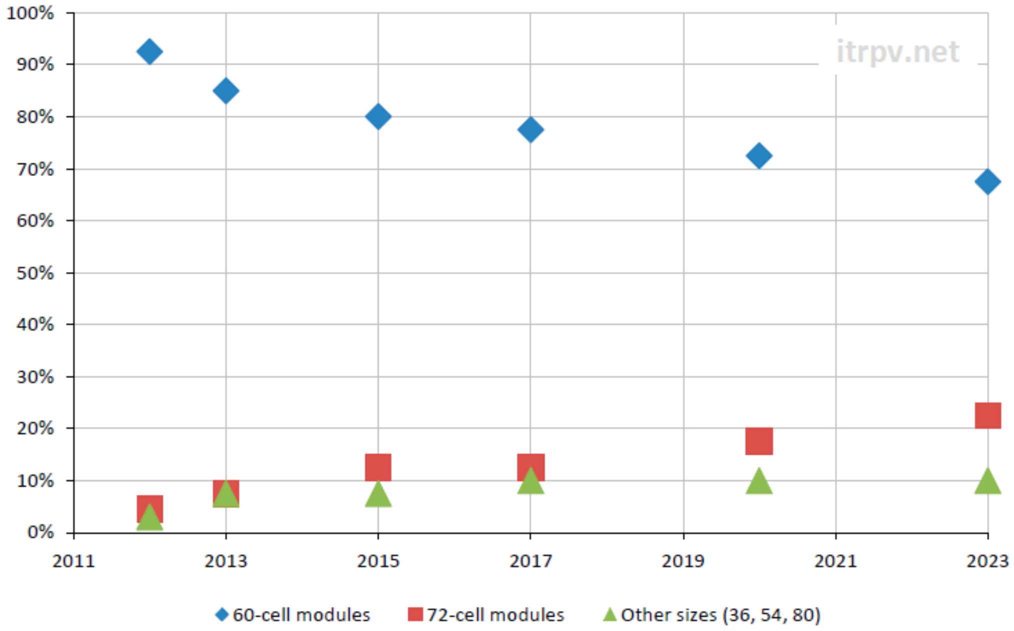

Likewise, high-strength encapsulants have the potential to enable thinner glass (1.1 mm) without compromising module strength. Lastly, the materials used to manufacture devices must be abundant and scalable. The PV industry currently uses approximately 10% of annual worldwide silver production. Low-cost, earth-abundant replacement metals currently explored include copper and nickel, both good electrical conductors but fast-diffusers in silicon. Low-temperature contact formation is a key challenge for these systems, both to prevent shunting and to reduce mechanical stress in thin wafers.

2.2 Thin Film

2.2.1 Overview of main trends

The photovoltaic (PV) market has grown continuously over the past years with a cumulated capacity installed worldwide reaching 100 gigawatt-peak to date. As a consequence, module sales prices have dropped tremendously. A trend that is expected to continue, driving module prices and production costs further down. The analysis by Rogol, Photon International, indicated that wafer cost constitutes about 85% of the cost of a crystalline Si, c-Si modules. Thin film modules do not require such wafers and hence they used to have a substantial cost advantage estimated at 50% over c-Si technologies, therefore are considered an alternative to reduce costs, energy pay-back time, and the consumption of raw materials. Thin film modules with conversion efficiencies of commercial modules being in the range of 8–13% as compared to 14–20% for c-Si based modules, however, these modules need lower production costs in order to compensate for higher PV system mounting costs. However, the current decline in the poly-silicon price has tended to reduce this cost advantage. Comparison of future commercial module performance levels[50] of a-Si:H, CdTe and CIGS thin film PV modules with the standard c-Si PV as well as the non-standard c-Si PV technologies such as SunPower rear-point contacted cells, Sanyo single crystal float zone and Czochralski c-Si/a-Si:H heterojunction with intrinsic thin layer (HIT) cells has shown that while the triple junction a-Si:H thin film technology is competitive, CIGS and CdTe thin film module technologies are highly competitive and presently offer the best approach for significantly exceeding the performance/cost levels of standard and non-standard c-Si PV technologies.

2.2.1.1 Market shares of thin film in PV

Since several years (from 2004 onwards) thin film (TF) materials have gained a first level of maturity at high volume manufacturing in a cost-competitive way. In the past 5 to 8 years the market share of thin film PV steadily increased by about 50% per year. While over the past decade crystalline and multicrystalline Silicon were the first and most advanced materials, thin films gained more and more maturity. Therefore the following estimation, depicted in Figure 40 was well received within the PV community.

---

[50] Neelkanth G. Dhere. Scale-up issues of CIGS thin film PV modules. Solar Energy Materials and Solar Cells. Volume 95, Issue 1, January 2011, Pages 277–280

This estimation was done in 2008 based on the technological status, cost and price and volume of the PV market worldwide.

Figure 40: Estimation of market shares of thin film materials CdTe, a-Si/uc-Si and CIGS in 2008[51]

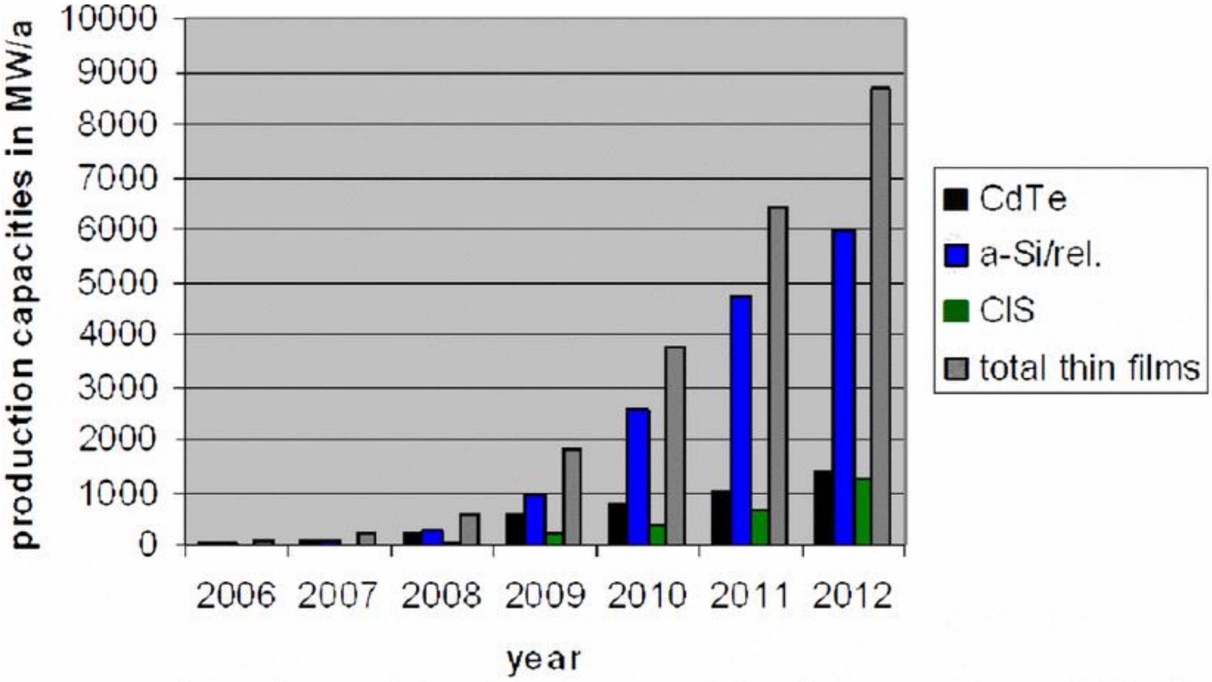

At that time it was predicted that TF PV was ready to speed up scaling to high volume manufacturing and rapidly gain market share. The window of opportunity was aided by the shortage of metallurgical silicon which hindered c-Si to follow the learning curve. Several companies developed and offered turn-key solutions for high volume production of a-Si/Ilc-Si. Within about two years time approximately 30 to 40 factories were constructed, each with a starting capacity between 30 and 60 MW_p/a. The scale-up was based on existing thin film equipment for the flat panel industry. Based on perceived synergies to the flat panel display business as well as the promised quality and cost targets for these factories the estimated installed capacity for this material in 2012 was to be in total about 6 GW_p/a. Unfortunately, none of the turnkey suppliers could fulfill their promised efficiency, productivity and cost targets. At the same time a rapid increase in metallurgical silicon supply made these factories non-competitive in a market of dramatically declining prices of c-Si modules. However, CdTe could meet and even surpass the estimation. This was realized by one company, First Solar, which had a solid technical and economic foundation coupled with the right strategic and economic decisions at that time. Back in 2009 First Solar already decided to rapidly scale to a capacity greater than 2 GW_p/a‘. At that time First Solar also had cost leadership over all competing PV technologies and continues to do so to this date. However, the margin has been eroded due to disadvantageous product attributes – low efficiency and small substrate size. CIGS as the most complex material to produce also gained maturity in the past decade, but so far has not been able to meet the cost expectations.

---

[51] B. Dimmler. CIGS and CdTe based thin film PV modules, an industrial r/evolution. Photovoltaic Specialists Conference (PVSC), 2012 38th IEEE, Issue Date: 3-8 June 2012

On the basis of current data and numbers collected and shared with the best experts worldwide and the background of fast c-Si growth and fast price drops a new market prognosis was done. The share of thin films was given as 17% (2009), 14% (2010) and 13% (2011) and was clearly decreasing.[52] One has to take in account that during this period the installations have risen from 7.9 GW in 2009, 17.4 GW in 2010 and 22.7 in 2011. Together the amount of thin films installed was 1.3 GW in 2009, 2.3 GW in 2010, and 3.2 GW in 2011. This represents a gain from year to year by +78% 2009, +72% in 2010 and +33% in 2011. According to these numbers and an updated estimation of a new market trend is shown in Figure 41.

Figure 41: Updated estimation of market shares of thin film materials CdTe, a-Si/f.lc-Si and CIGS, 2012, by B. Dimmler

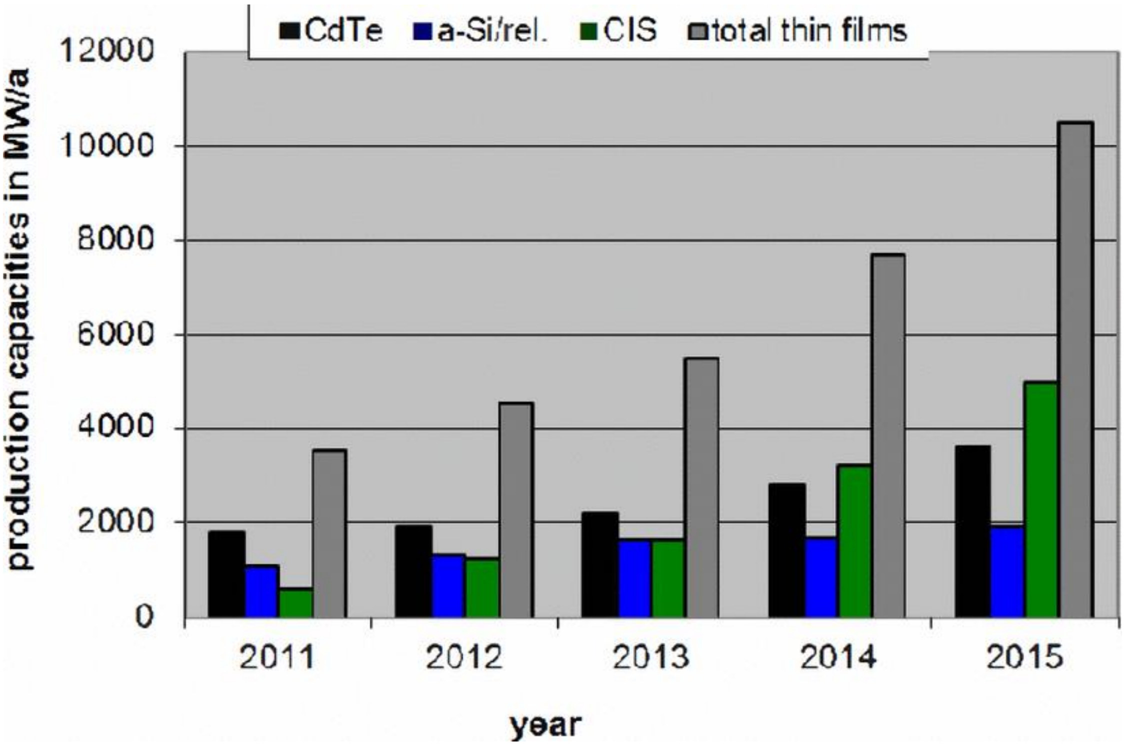

Due to the already existing and still operated capacities and newly announced capacities the a-Si/mc-Si share has drastically decreased and is estimated to be in the range of 2 GW$_p$/a operable capacity. CdTe module production is expected to increase steadily to roughly 4 GW$_p$/a whereas CIGS may increase most rapidly from about 700 MW$_p$/a in 2011 to about 5 GW$_p$/a in 2015. Thus the total installed thin film capacity is estimated to reach about 10 GW$_p$/a in 2015. One has to accept uncertainties in these estimations as the numbers depend on various and complex factors including market perspectives which are difficult to foresee.

In the following tables the main companies operating production volumes bigger than 30 MW$_p$/a are listed. Table 9 shows the worldwide situation of CIGS. Solar Frontier is the biggest producer in the CIGS field. It has reached about 1 capacity, a level which is necessary to reduce cost via scaling benefits. Other companies are already in the ten to

---

[52] P. Mints, Navigant Consulting Inc., Solar going Fonvard, presentation at EPIA ih Market Workshop, April 21st 2012, Brussels

hundred MW range, partially with new and innovative deposition techniques and materials. Würth Solar was the first company worldwide starting mass production in CIGS. Influenced by strategic reasons the capacity was halted at 30 in 2010. At that time manufacturing costs were already at a competitive level. Therefore Manz AG, a German equipment company and leading supplier worldwide, decided to take over the facility. The objective was to convert the line from manufacturing to innovation with the focus being qualification of process and equipment upgrades at the large scale level. These efforts are supported by ZSW Stuttgart, one of the leading research institutes in CIGS and the origin of Würth Solar technology. Manz is now offering turnkey lines based on Würth Solar's CIGS technology. This strong alliance with sound technology and equipment is thought to enable the proliferation of the CIGS technology to a wider manufacturing base.

Table 9: Overview of companies with operating capacities larger than 30 MW$_P$/a for CIGS modules worldwide[53]

Manufacturee	Deposition technology	Champion product % apa	Fab target % apa	Current nameplate capacity MW/a	Pro's	Con's	Comments
Manz (Wurth) Solibro	1-stage coevaporation	15.1 14.4	15.9 16	32 →8 (innoline) 120	Simpler, more advanced process	Sacrifices efficiency	Glass-glass Cd-buffer
Global Solar Energy	3-stage coevaporation		17..5		Highest known TF efficiency	Complex process	SS substrate glass/polymer
MiaSole	Reactive sputter	15.7	16.5%		Good efficiency potential, rel. small capaex exp.	Complex process	SS substrate glass-glass CdS-dry
Solar Forntier, Stion/TSMC	2-step Sputter+H2Se/S Selenization	14.1	15.5%	980 5 + 135 +300	Advanced process, potentially higher CapEx	Sacrifices efficiently Higher OpEx than evap.	Glass-grass CdS glass-glass Cd-free
Avancis, Hyundai	2-step Sputter+Se-evap.+RTP-cryst./H2S		30+100 +100				Glass-glass CdS Glass-glass Cd-free
Solo powe	2-step electoplatr-Selenization	13.4		30+400	Good metal utilization rel. low CapEx	Sacrifices efficiency	SS substrate polymer CdS

In Table 10 the currently biggest companies producing CdTe based modules are shown. First Solar is by far the most advanced and in the past had a maximum capacity of 2.7 GW$_p$/a spread over in several factories worldwide. Due in part to the large scale volume First Solar had the lowest manufacturing costs, but this advantage has been eroding fast due to increasing pressure from Chinese c-Si manufacturers. As a result, First Solar had to report losses for the first time in 2011 and is currently undergoing

---

[53] M. Beck, "High volume manufacturing of CJGS-based Photovoltaic modules,", presentation at PHOTON's 4th Thin Film Conference, San Francisco, Febr. 15th 2012

significant restructuring efforts aimed at return to profitability. Others listed Table 10 are trying to add production volume to be or stay competitive

Table 10: Overview of companies producing thin film modules based on CdTe worldwide[54]

Manufacturee	Deposition technology	Champion product % apa	Fab target % apa	Current nameplate capacity MW/a	Pro's	Con's	Comments
First solar	Medium vacuum thermal evaporation	14.4 (total area) Champion lab cell 17.3%	14.5 in 2014	2.700 closing severa lines	Simple and matured process, eff. potential	Global payer, Quality?	Glass-glass
Primestar	Thermal evaporation	12.8% Champion lab cell 12.8%		30 400		Techn. Status?	Glass-glass
Abound solar	Thermal evaporation	12.2%		Downturn, innoline for next gen		Techn. Status?	Glass-glass
Calyco	Atmospheric thermal evapotation	13.4% Champion lab cell 16.2%		80		Techn. Status?	Glass-glass

2.2.1.2 Module quality

Module quality is a combination of the absolute conversion efficiency of light to electricity and of product lifetime in the field. Currently the market expects a lifetime of 25 to 30 years and stable long term performance is a prerequisite for market entry alongside high conversion efficiencies. To achieve a longer lifetime, which is directly connected to the cost of electricity, further R&D focus is necessary.

To be competitive in the PV market module efficiency has to be high and comparable to c-Si. Thus, activities to transfer laboratory scale record efficiencies to high volume productions have to be intensified. In order to be competitive to c-Si there is no alternative to this requirement as lower efficiency entails an additional BOS penalty. The lab to manufacturing transition process has to be sped up and intensified. To this end more efforts have to be done in alliances with high-level fundamental R&D, equipment manufacturers as well as companies with a proven technological and manufacturing basis. In Figure 42 expert estimations for the prospects of lab cell efficiency and module production efficiencies for all thin film materials are shown.

---

[54] H.W. Schock, "Thin film solar cells - technology options and development trends,", presentation at SNEC 6th May 16th 2012, International Photovoltaic Power Generation Conference, Shanghai

Figure 42: Expectations of experts of the evolution of efficiencies on cell (dashed lines) and module level (solid lines) in the future[55]

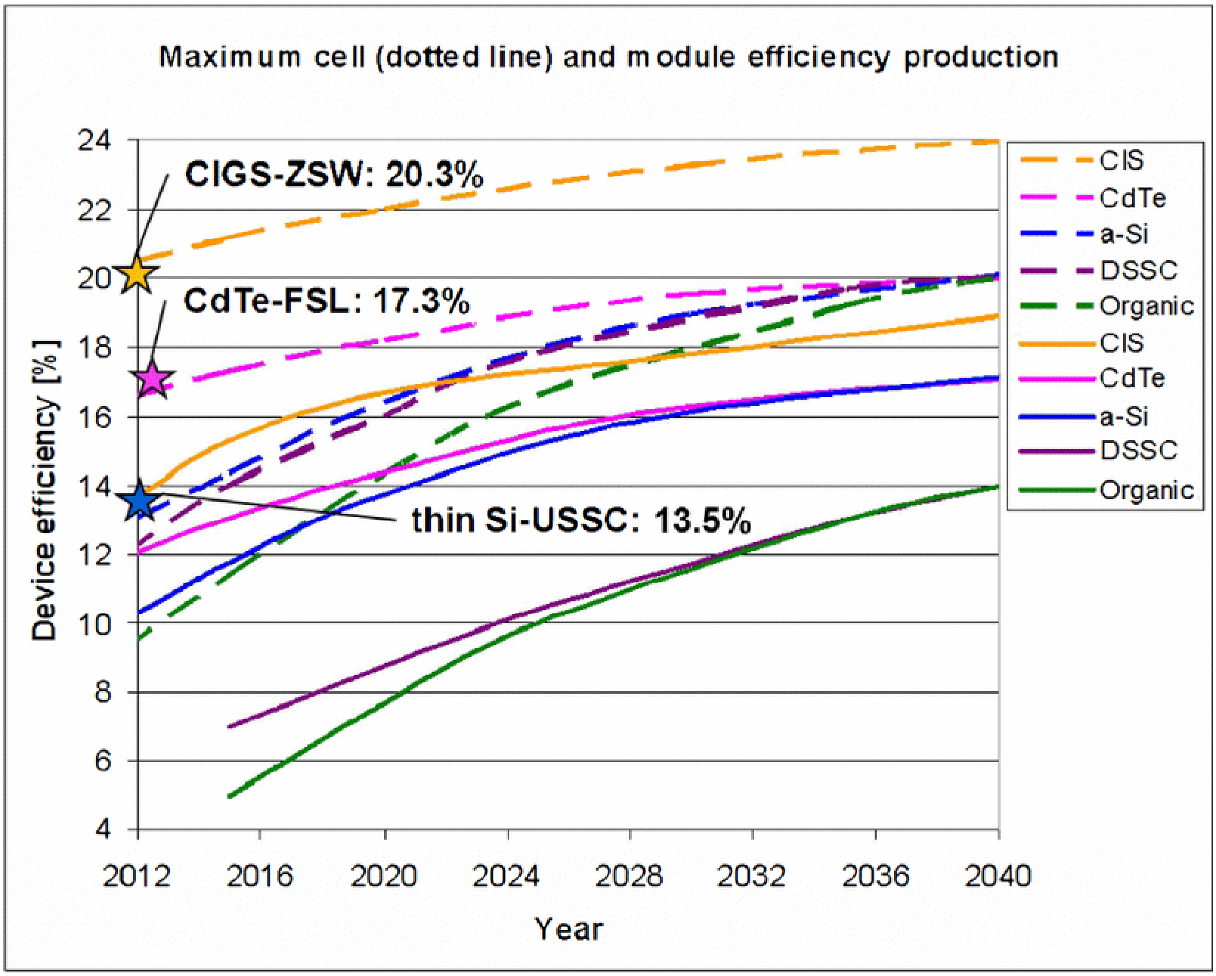

CIGS is currently the leading material and is estimated to remain the superior material system capable of reaching record efficiencies of 24% at the cell level while approaching an average of 20% at the module level within the next 30 years. The lab and module efficiency evolution for both CdTe and thin Si are forecast to reach about 4% less in record cell level performance as compared to CIGS whereas module efficiencies might approach 17%. Other and new materials not yet in the market place could also reach a two digit level module efficiency.

2.2.1.3 Cost and Innovations

Similar to the need of an accelerated efficiency and product reliability transfer from the laboratory to high volume manufacturing, the overall cost structure has to be improved. Innovations in this segment are also best accomplished via co-operations with leading industry partners and research institutes. Manufacturing cost is the key metric for successful business operation in a highly competitive market. The result of the cost structure analysis is shown in Figure 43.

---

[55] N. Pearsall et al., "A strategic Research Agenda for Photovoltaic Solar Energy Technology,", ed.2 2011, p.32, ISBN 978-92-79-20172-1

Figure 43: Cost structure according to detailed calculations of Manz AG for a CIGS module production of 200 MWp/a today[56]

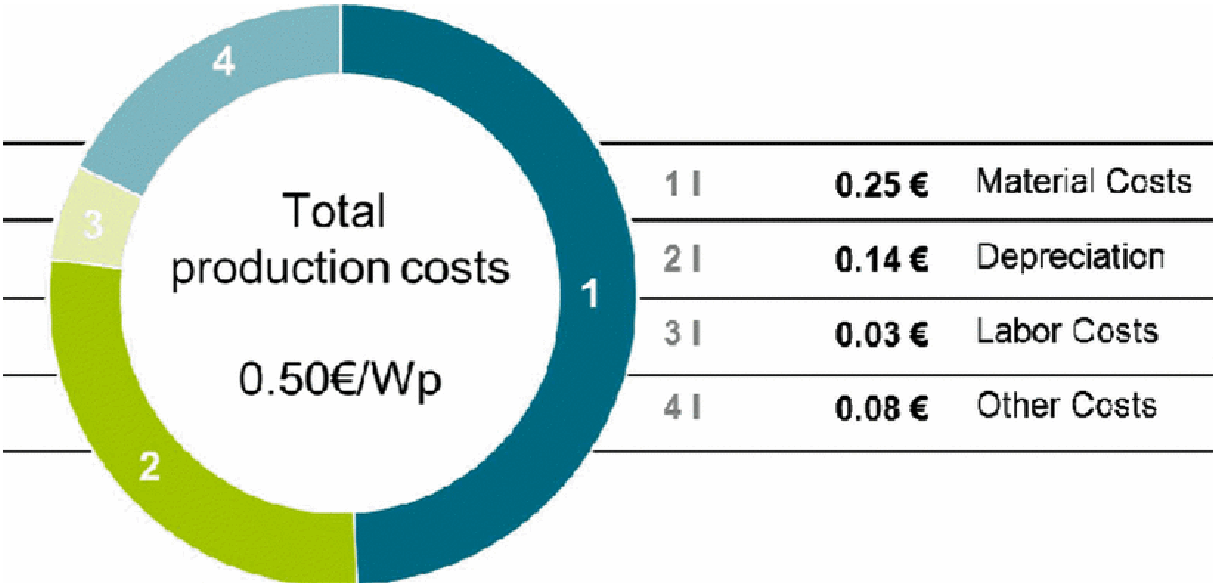

As evident from Figure 43, the material share of the total production cost is 50% and, hence, offers the highest cost reduction potential. Capital cost, i.e. depreciation in this case, is 28% of the total. Minor influences have labor with 6% due to the high automation level of thin film factories and others, which include energy, with 16%; nevertheless all cost factors should be reduced in the coming years substantially after qualification in the innovation line. Both CdTe and CIGS are in a similar level of cost today; nevertheless, mainly efficiency potentials see to be advantages for CTGS. Figure 44 attempts to show the qualitative influence of the various costs factors.

Figure 44: Main impacts on production cost for large-scale CIGS manufacturing

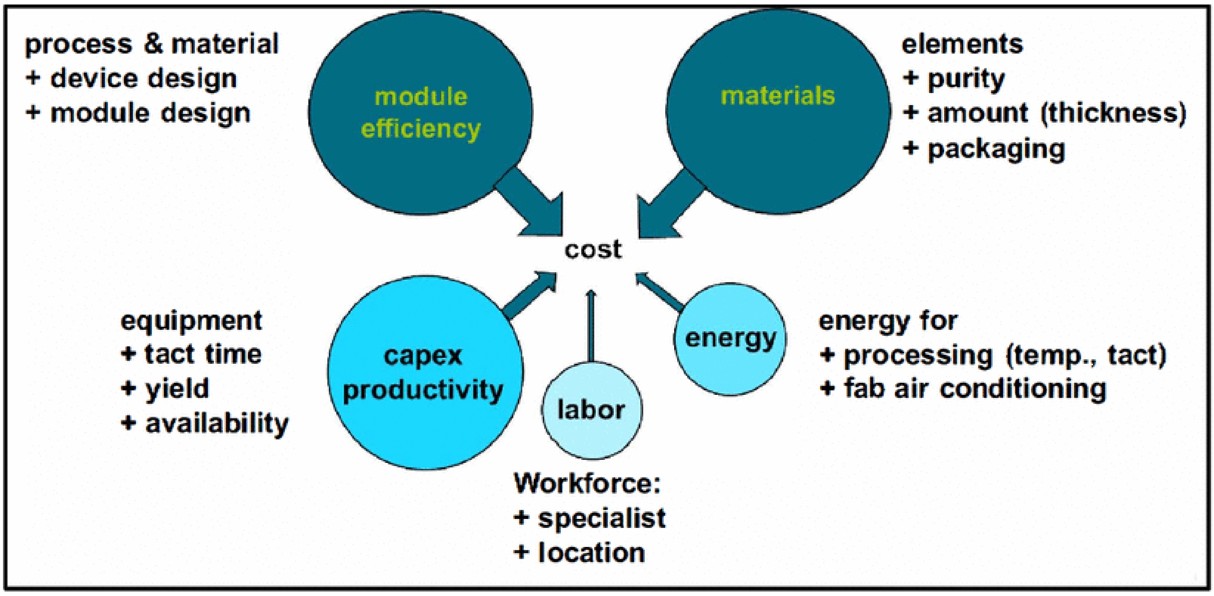

The size of the bubbles in the graph as well as the size of the arrows represents the respective influence on cost. Hence, total production costs are mostly influenced by module efficiencies and materials costs. While the aspect of module efficiency was

---

[56] D. Manz, "CJGS - take the short cut to success now,", presentation at SNEC 6th, May 16th 2012, International Photovoltaic Power Generation Conference, Shanghai

already discussed above, the materials cost aspect requires further assessment. A closer look at the various materials costs reveals packaging (two sheets of glass plus polymer filler sheet) accounts for about half the materials costs whereas high purity feedstock materials contribute to about 1/3rd of all materials costs. The latter is partially already being reduced via the following measures, listed in order of significance:

- Less pure feedstock materials
- Increasing material utilization during deposition
- Reduced active layer thicknesses
- Minimization of interconnect losses

As most of these points have not yet been realized in production they offer short-term cost reduction potential. Moreover, module packaging requires further efforts and new module designs as well as materials offer mid-term cost reduction potential. With depreciation accounting for only about 30% of the total cost of ownership it nevertheless is an important factor when planning investments into manufacturing capacity. The key aspects to be addressed are:

- Throughput/tact time per unit per equipment
- Process and manufacturing yield
- Equipment availability/uptime

All of the above aspects are currently being optimized. Therefore a good technology base coupled with manufacturing experience are prerequisites for CdTe and CIGS, especially as key IP is not in the public domain and equipment still not standardized.

The energy payback time is an additional advantage for TF PV in the comparison to c-Si and might become a decisive factor in the not too distant future. Already today all thin film PV technologies require a factor of 2 to 3 less energy in production than c-Si. Currently the share of energy in the cost analysis is too insignificant, but in the long term the cost of energy could gain importance.

Today CdTe and CIGS are the most advanced thin film materials already in high volume manufacturing. Among the two, CIGS is superior in device efficiency both at the lab and production scale. CdTe, on the other hand, seems to be less complex in manufacturing and, as shown by e.g. First Solar, can be competitive in today's market. Future success of CdTe appears to be mainly tied to advances in efficiency and long term stability. A further topic associated with CdTe is the uncertain acceptance of Cd-containing products in various markets. At the same time, CIGS is on the way to maturity and might well prove to be the only material to compete directly with c-Si. The outcome of this challenge is directly dependent on the successful transfer of laboratory scale results to the low cost, high volume manufacturing scale. A significant degree of innovation at the equipment and product design level is a key prerequisite to reach this goal. If the key aspects of each technology can be resolved both, CIGS as well as CdTe, should be able to approach production cost well below 30 € cents/W in the long term in particular as manufacturing energy costs become increasingly important in the PV industry. From a technology and physics point of view this is possible. At the same time the window of opportunity for thin films to gain a more significant market share is still open. Presently CdTe as well as CIGS are undergoing a technological and industrial evolution (described more in detail in next sections); whether it will be a revolution depends on the progress within the next two to three years.

2.2.2 Cadmium Telluride photovoltaic technology

A typical layer stack used in commercial-production CdTe modules is shown in Figure 45. Primarily driven by stability requirements enabling high temperature material growth, and the difficulty of achieving a low-resistance electrical contact to the CdTe interface, devices are typically fabricated in the ‘superstrate’ configuration. The layers are built on top of the heat-stabilized front glass and the module is then flipped over in deployment so that sunlight must first pass through the front glass, transparent conducting oxide (TCO, typically either Cd_2SnO_4, Cd_2SnO_4/Zn_2SnO_4, SnO_2:F, or SnO_2:F/SnO_2), and CdS before reaching the CdTe layer. The figure is shown starting from one edge of the module; the cell pattern is repeated until the other edge is reached. The cell width, relative to the scribe widths, is greatly reduced in the figure so that it may fit within the scale of the page. In actual modules the cell size is optimized to consider series resistance and dead zone losses (bigger cells suffer from greater series resistance losses, while opting for smaller cells leads to greater total module ‘dead zone’ current losses as the inactive areas of the module grow in proportion to the number of laser scribes). Other materials used in module assembly include an ethyl vinyl acetate (EVA) encapsulant, edge seals, tempered soda lime back glass, an array of metallic bus bars for connecting the module's cells, and a junction box for the purpose of connecting modules together into strings when they are installed.

Figure 45: A cross-sectional representation of a monolithically integrated layer stack used in commercial (single-junction, polycrystalline) CdTe cells. Source: NREL 2012

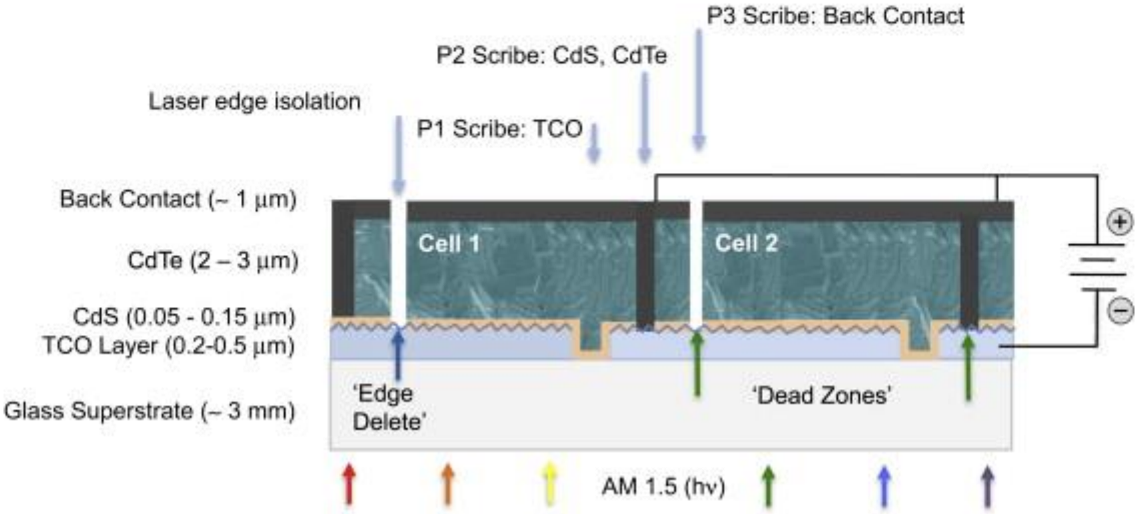

CdTe sales are growing rapidly, but there is concern about projecting hundredfold increases in power production relative to current production with CdTe PV modules. One reason is that Te, a humble non-metal that is actually abundant in the universe, is as rare as many of the precious metals recovered from Earth’s crust. Furthermore, current technology now uses Te at rates that are substantial fractions of its supply. For the present technology, generating 1 gigawatt (GW) of power requires 91,000 kg (91 metric tons, MT) of Te (a cost of about $20 million). If all of the PV delivered in 2009—7 GW—had been produced with CdTe, about 640 MT of Te would have been required, which is comparable to its present annual production.[57] If PV is to supply 10% of the projected demand of electricity worldwide in 2030, the per annum growth rate must be 18.5%; for 25% of world electricity, it must be 25%. In 2030, the annual production would require 200 GW/year (at 10% electricity supply) or 670 GW/year (at 25% supply). For the current CdTe modules, 19,000 or 61250 MT of Te per year, respectively, would be needed, equivalent to an increase in supply by a factor of about 40 to more than 100, respectively (Figure 46).

Figure 46: Projecting paths for CdTe photovoltaics. The concerns about Te availability limiting CdTe PV module production assume that the layer thickness will be maintained at 3 μm. Projections of maximum market share attainable are shown based on modest increases in Te production (from 1% growth per year in copper production, its main supply route) and module efficiency (15%), but substantial decreases in CdTe active-layer thickness. The blue and purple lines are market-share maxima if 10% of the world electricity is made from PV in 2030, with layer thicknesses of 0.67 and 0.2 μm, respectively. Similar projections (orange and green) are for 25% world electricity production by PV in 2030. In all cases, with thin enough CdTe, nearly 100% market share might be attained. The inset shows tellurium in its native form. Source: K. Zweibel, 2010

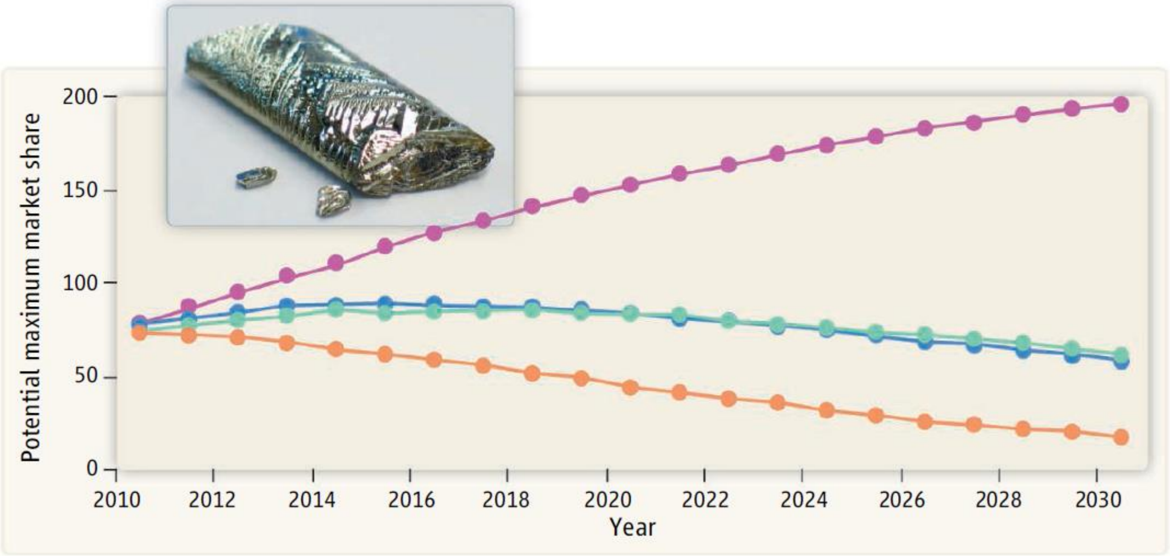

In 2011 a record high Tellurium price between $400 and $450/kg was reached, but this was still a very good bargain in light of the element's relative crustal abundance (for contrast, the *orders of magnitude* more abundant elements Ga, In, and Ag respectively traded for around $900, $750, and $1300/kg over the same year). Part of the reason for Tellurium's historically low trading price has been because the total demand from its known uses in steel alloying, thermoelectrics, etc. have been quite limited and because it is primarily extracted as a byproduct of much larger copper mining operations, where it

---

[57] K. Zweibel. The Impact of Tellurium Supply on Cadmium Telluride Photovoltaics. SCIENCE VOL 328 7 MAY 2010, 699-701

has always been considered more of a nuisance than a meaningful opportunity. However, a tipping point was reached in 2010 in that the annual demand for the element for PV applications significantly eclipsed the demand from any other category of competing uses for the first time. And there is every reason to expect this trend to continue as several new—as well as incumbent—CdTe module manufacturers have expressed ambitions to scale to greater production volumes (notwithstanding the 2012 temporary decrease in demand for PV modules).

The main aspects of Cadmium Telluride photovoltaic technology are very well analised in the recent study of The National Renewable Energy Lab (NREL, US) on perspectives for Cadmium Telluride Photovoltaics.[58] The indicated trends and main findings are summarised in the section below.

2.2.2.1 CdTe module manufacturing costs and potential reductions

The bulk volume price of Te is around $130/kg—with a major material supplier; however, the exact pricing terms for any contract, and the duration of delivery, are highly guarded and need to be considered on a case-by-case basis. The information is needed to estimate the Te intensity for module production is presented in Table 1.

Table 11: Snapshot of typical 2011 parameters for estimating the Te intensity of CdTe module production and the effect of the metalloid's price upon module costs. The typical, and publicly available, input parameters are cited and used for the calculations. Source NREL 2012

Parameters of Tellurium price sensitivities: 2011 baseline	
Weight % of Te in CdTe: 53%	CdTe layer thickness: 2.5 µm
Density of CdTe: 5.85 g/cm^3	
% Recovery of Te from ores or Cu anode slimes: 50–55%	% Utilization in manufacturing: 90.%
Purified Te Price: $280—$430/kg	Purified material requirements: 16 g CdTe/m^2 (8.6 g Te/m^2)
CdTe compound price (large volumes): $410–$560/kg	
Module efficiency: 11.7%	CdTe cost: $6.7–$9.1/m^2
CdTe compound contribution to module cost: $0.06–$0.08/Wp	Te material requirements (DC power):Purified (>99.9995%): 74 MT/GWUnrecovered: 60–74 MT/GW

Not all of the Tellurium that is present in an ore or Cu anode slime can be recovered into sufficiently pure material: estimates are that the current recovery efficiency is between 50 and 55%. Although it has been pointed out that the rate could be improved to up to 80%, this higher recovery rate is not implemented today because the associated costs of recovering the additional Tellurium are higher and its current price does not justify the added expense. Also, current refining operations are more focused on the much greater value proposition of recovering the actual copper and precious metals (Au, Ag, Pt, etc.) that naturally occur together with Te. Thus, until a sufficient price is offered, the recovery rate for Te is likely to stay at or near current levels.

---

[58] http://research.eeescience.utoledo.edu/lees/SEP/References/Papers/Woodhouseetal_TelluriumforPV_120911.pdf

In both manufacturing and balance-of-system, the need to call upon gains in efficiency in order to arrive at economically competitive solutions is certainly clear. With module efficiencies around 11–12% now routinely produced (remarkably, even at annual production levels in the gigawatts), the rapidly realized progress of CdTe manufactures has certainly been remarkable.

There are also many reasons to believe that tremendous upside exists for even further advancements:

- The direct bandgap of CdTe, at 1.45 eV, is very close to the Shockley–Quiesser ideal and so current losses due to spectral mismatching are relatively small. There also remains a tremendous amount of work that can be done to optimize the material properties of each layer that is used in the typical module that is produced today. While the maximum theoretical efficiency for any single-junction PV absorber is 32%, for any real PV cell material the actual efficiency that can be expected will be less than this value—due to the spectral mismatch between the light absorber and the solar spectrum, as well as electrical recombination losses within the various cell layers—and an even lower efficiency is to be expected for modules because of series resistance and cell current-matching losses. In the case of single-junction polycrystalline CdTe, after accounting for these factors the average commercial-scale module-area efficiency potential is expected to be reached at around 18%.
- Pure CdTe is a direct bandgap semiconductor and so the minimum thickness needed for this purpose can be quite small. Before consideration of texturized front or back surface structures, plasmonics, or metal back reflector layers (which can significantly enhance optical absorption), knowing the 'optical penetration depth' of the useful can serve as a useful starting point for estimating such a minimum thickness. In Figure 47 a, the absorption characteristics of CdTe are plotted: a reasonable first-order approximation is that the thickness needs to at least be around 1.0 μm in order to be near the absorption depth for photons in the red and Near Infrared (NIR) regions of the solar spectrum. Because these red and NIR photons are capable of producing quite a bit of photocurrent within CdTe devices, their full absorption is likely necessary in order to realize the 18% module efficiency target. In Figure 47 b the results are shown of a simulation intended to portray the percentage of possible current that could be generated as a function of CdTe thickness. In order to generate at least 95% of the total possible current that could be expected from such a CdTe device, a full 1.0 μm of active layer appears to be necessary; the thinner layers would result in unacceptable losses in device efficiency.

  Moreover, despite innumerable attempts, it has generally been observed that the Voc and FF can only be maintained even at the small-area laboratory cell level for thicknesses down to around 1.0 μm, after which they both decrease very rapidly.

Figure 47: Light absorption and current generation characteristics of CdTe solar cells. (a) The plot on the left displays the absorption coefficient of CdTe, and the curve on the right (b) portrays the relative amount of current that can be expected (normalized from the current density at the cell's maximum power point) as a function of the CdTe layer thickness. The curve is derived from the spectral output seen after AM 1.5 light has been attenuated by front glass reflection and absorption from 600 Å CdS on 1.0 μm SnO_2. Source NREL 2012

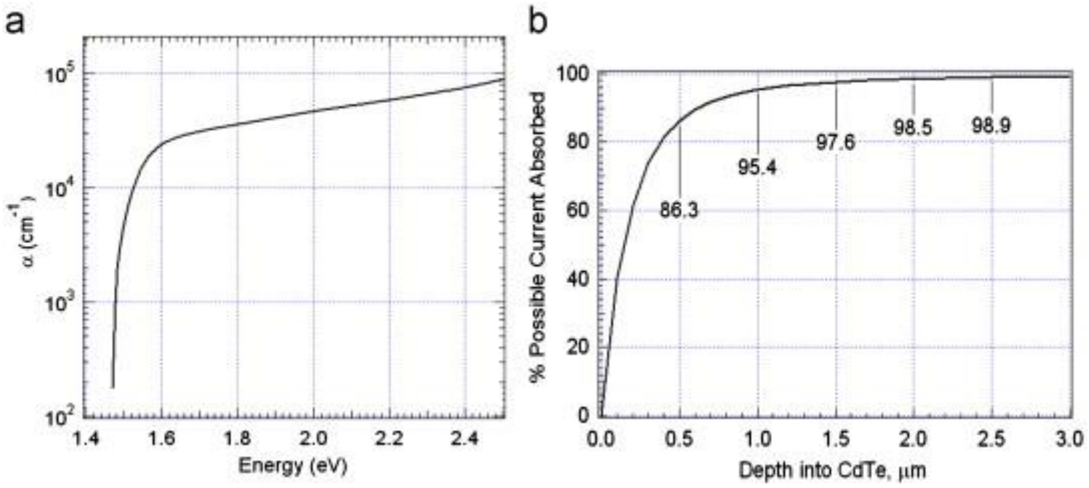

- With complete light absorption and charge carrier collection (i.e., a QE of unity for all wavelengths in the AM 1.5 profile that have energy greater than the bandgap), an ideal CdTe cell could produce close to 30 mA/cm2 of short-circuit current. However, what is actually delivered from the modules that are produced today is significantly less than this value. Approximately 5–10% of all incident light is reflected off of a normal, flat glass- air interface. In addition, the soda lime glass that is typically used in commercial modules noticeably reduces the transmission of light relative to several alternatives that have a lower internal concentration of parasitic light absorbers, principle among them being iron. By examining the current-voltage and quantum efficiency curves for devices prepared with the two different glass types, it appears that up to 1.5 mA/cm2 of current might be gained in devices that switched to the higher transmission glass. This would boost the overall efficiency by around 0.9%; however, 'ultra clear' grade low-iron glass currently costs around $6.50/m2 more than typical soda lime glass (even at large scale purchase volumes) and so such a proposed device would actually be around $0.06/Wp more expensive - even at the 12.6% efficiency. So while the efficiency gain is certainly significant, it will (1) be necessary to procure higher transmission glass at a lower cost in order to provide an overall impetus for the change (with concurrent requirement of having a high temperature tolerance, in the case of the superstrate architecture); or (2) carefully consider whether the increased cost can be offset by balance-of-systems level savings because of the higher efficiency.
- The TCO that is to be employed is a matter of on-going debate within the CdTe community. Presumably, Sn02: F (FTO) remains in place today because it enjoys a low-cost advantage - made possible by the fact that it can be deposited within a glass float line by relatively inexpensive chemical vapor deposition (CVD) techniques (which use little or no vacuum), and because of its ability to withstand

the typical processing temperatures that can approach 600 °C. In spite of its low cost, FTO is far from being the optimal choice in terms of both improving efficiencies and reducing the CdTe layer thickness. Its surface roughness necessitates thicker CdS and CdTe layers in order to overcome potential shunting between the very large SnO2 grains and the back contact. Alternatives do exist: sputtered CdSnO4 appears to be one promising candidate and indeed the former world-record CdTe cell efficiency of 16.7% was known to employ this TCO. Aluminum-doped zinc oxide is another promising alternative - provided the stability concerns surrounding this TCO are addressed and accepted - but may be limited to manufacturing methods with much lower processing temperatures (e.g., cells made in the substrate architecture or in sputtered cells). In total, up to 1.5 mA/cm2 may be gained by replacing today's FTO with an ‘ideal’ replacement - provided the alternative can withstand high temperature processing conditions if it is to be used in fabricating superstrate devices. While sputtered materials may seem to be the most immediate solution, it may still prove to be the lower-cost CVD option that retains its preferred status—especially in light of some recent, very promising results that show it is quite possible to address the problems mentioned above. If a complete replacement cannot be found, the use of TCO buffer layers could also help to reduce the effects of pinholes and weak diodes within CdS, and the transmission of light could possibly be improved by increasing the bandgap of CdS via partial oxidation.

The technical overview of some of the changes that might be implemented in order to arrive at the target of 18% commercial-production modules is given in Table 12.

Table 12: Overview of some technical improvement opportunities that are available to improve the efficiency of single-junction polycrystalline CdTe modules. Source NREL 2012

Cell performance parameters	Baseline 2011	Near term	Mid-term	Full potential
Short-circuit current density: J_{SC} (mA/cm^2)	23	24	25	26
	–	Improved light transmission through the front glass: thinner glass; lower Fe content, Sb doping	Improve TCO transmission (reduce NIR absorption from free carriers)	Reduce window layer absorption: - Thin or replace CdS - Substrate architecture
Open circuit voltage: V_{OC} (V/cell)	0.80	0.90	1.0	1.0
	–	Improve minority-carrier lifetimes in CdTe: grain size, crystallinity, grain boundary passivation	- Reduce CdS/CdTe junction recombination via doping - Resistive oxide TCO buffer layers	- Improve film uniformity - Electron back reflector
Fill factor: FF (%)	70	75	80	80
	–	- Improve ohmic contact to back electrode assembly - Improve minority-carrier lifetimes in CdTe	- Improve charge-carrier mobility in TCO - Resistive oxide TCO buffer layers	- Improve film uniformity - Electron back reflector
AM 1.5 Power Conversion	13% Cells (11.7%	16%	20%	21% Cells (18% Modules)

Cell performance parameters	Baseline 2011	Near term	Mid-term	Full potential
Efficiency (%):	Modules)			

If the CdTe thickness can be reduced with simultaneous improvements in module efficiency, there will be a very noticeable and important decline in the amount of Tellurium that is required for each GW of manufacturing capacity. The plot shown in Figure 48 depicts how the Te intensity might change over time by imposing the rates of improvement in commercial modules. Should such champion modules become qualified for commercial production, the minimum amount of Te required to assemble modules could progress to potentially be as low as 19 MT/GW$_p$ of DC power with the same material utilization (90%) in manufacturing. Improving the manufacturing utilization to 100% would reduce the material intensity by an additional 2 MT/GW$_p$.

Figure 48: Projected roadmap Te intensity for module production over time. The rates of improvement in efficiency and CdTe thickness were set at +0.4% per year and −75 nm per year, respectively. Source NREL 2012

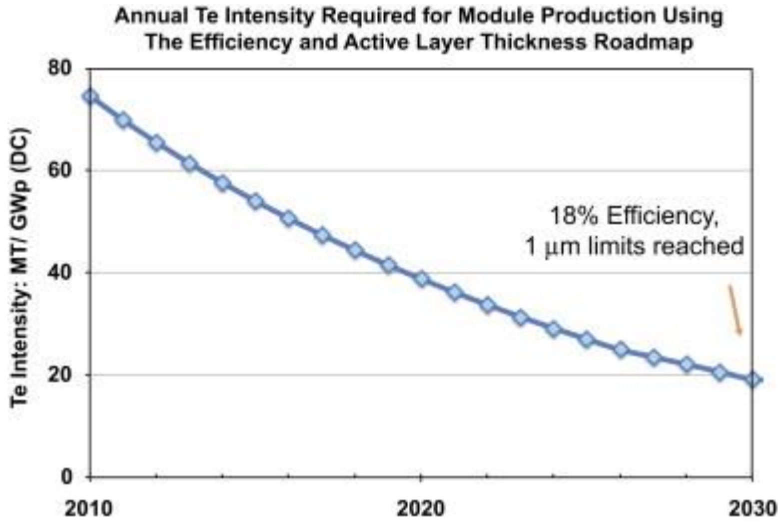

As efficiencies improve, the concurrent benefits of lowered manufacturing costs can be quite significant. Simulations run from the cost model developed in Figure 49 suggest that CdTe modules could perhaps be produced at a cost as low as $0.47/W and could be sustainably sold at a price as low as $0.57/W near the 18% efficiency and 1.0 μm CdTe targets (Figure 50). This result would approach the very ambitious module price goals.

Figure 49: Overview of module manufacturing cost model results for monolithically integrated CdTe in rigid glass. Source NREL 2012

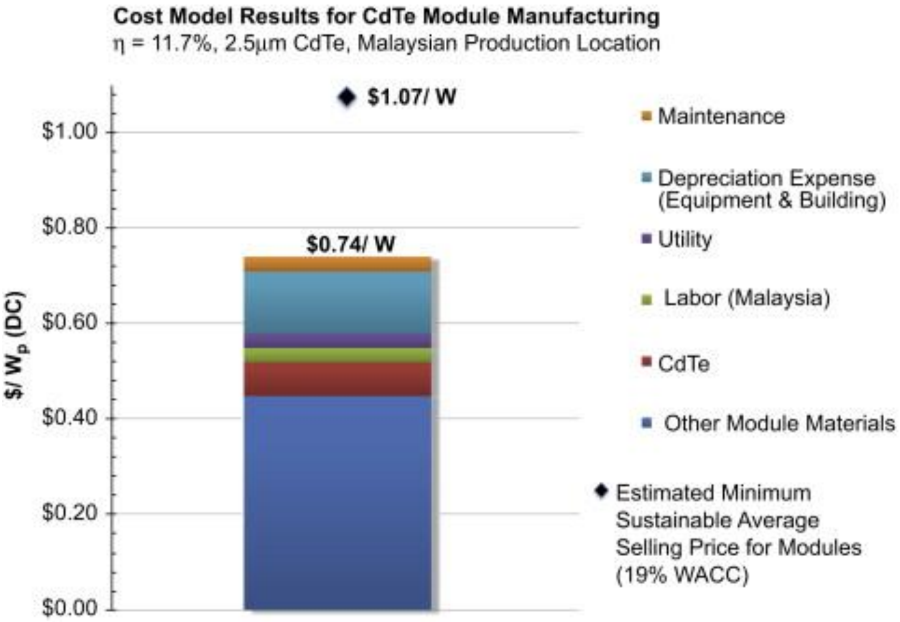

Figure 50: Simulated CdTe module manufacturing costs as a function of changing the input efficiency, WACC, and CdTe thickness. The simulation was run without changing the Te price or capital costs. Gradual reductions in the CdTe thickness are represented, as is the WACC in anticipation that the required rate of return for investments in PV companies will be lowered in the future as the industry matures and is given the expected benefit of a reduced risk profile. Some of the technical improvement opportunities that are available are shown within the figure captions. In coordination with Table 12, they have been put forth here as examples that may achieve the efficiency targets shown. Source NREL 2012

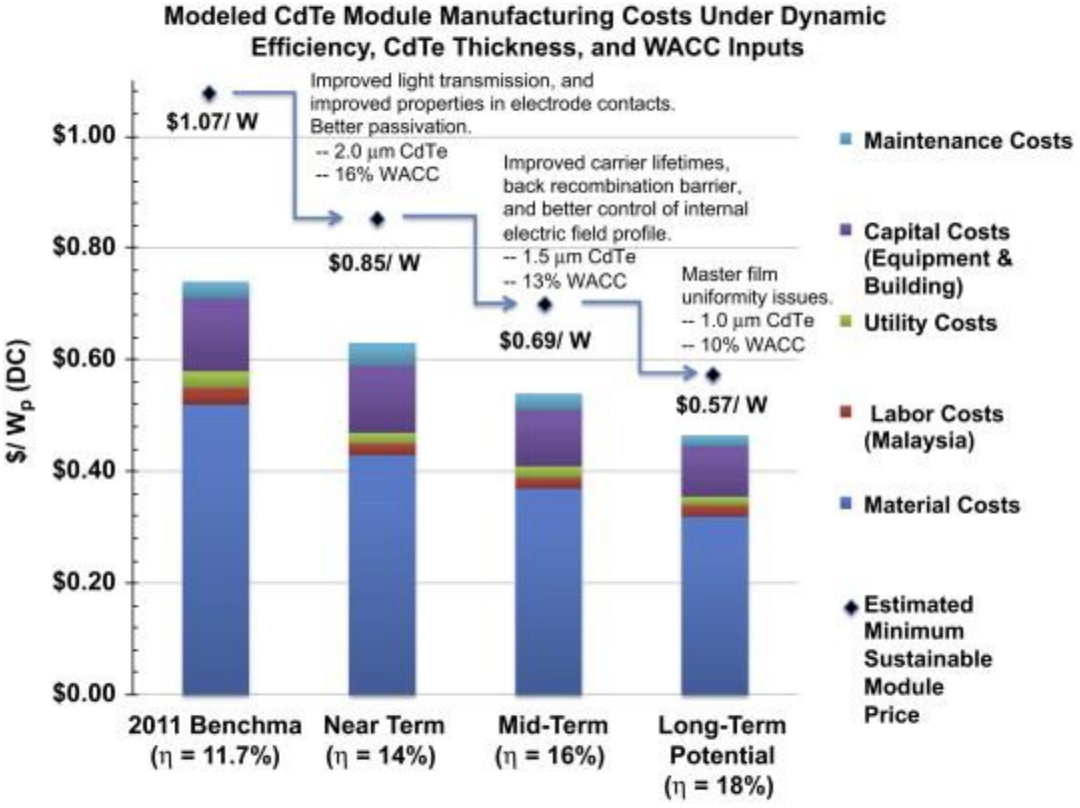

The results shown in are based upon an assumption that all material and capital costs are constant while the efficiency is improved, but there are at least two principle challenges to that assumption. First, many of the pathways to improved CdTe efficiencies - but certainly not all - involve replacing specific materials within certain layers (e.g., transparent conducting oxide (TCO), window layer, front glass, or back contact replacements). Such changes can oftentimes prove difficult to justify in manufacturing because of the added expense to manufacturing costs—whether it is in the materials themselves, in the additional equipment costs needed to deposit them, or in the costs and difficulties associated with potentially interrupting the manufacturing process flow (it does need to be stated that analogous cost-or-performance tradeoffs also exist for many of the materials and processes used within the other PV technologies as well). A second risk factor specific to CdTe is that a rise in Tellurium prices is to be expected should demand for it significantly increase, in which case it will become progressively more imperative that module manufacturers incorporate techniques that keep the cost of the photovoltaic layer to a manageable level. In Figure 51 a waterfall chart to capture an estimated rough limit in the price for Tellurium is provided. Reducing the CdTe layer thickness - in addition realizing gains in efficiency - can work together to accommodate much higher Te prices. Whatever the change in Te prices actually turns out to be, the value of reducing the CdTe thickness in order to accommodate a higher price is essentially just as significant as what would be expected from efficiency gains alone; moreover, module manufacturers could only absorb around a 5X increase in Te prices if they focused only upon gains in efficiency but neglected to make improvements in the thickness parameter.

Figure 51: Waterfall chart to represent how CdTe module manufacturers could conceivably address dramatic increases in the price for Te and still meet a module price target that may be competitive against the projected long-term price of c-Si. All other material and depreciation expenses are assumed to be constant. Source NREL 2012

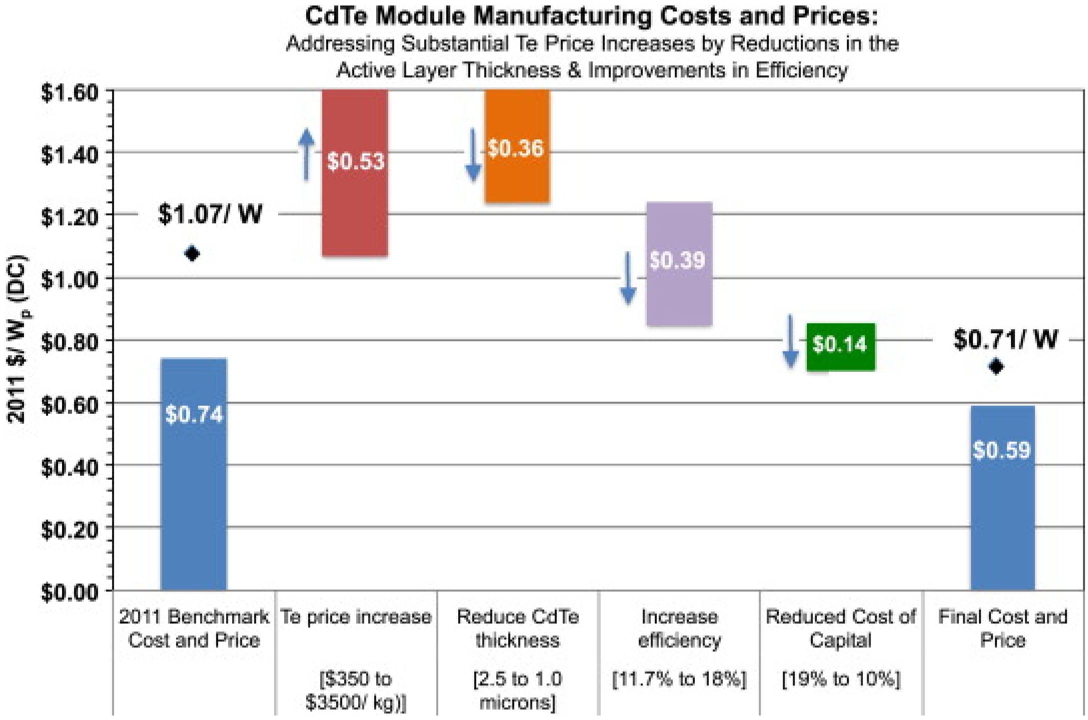

2.2.2.2 Conclusions: CdTe

Te prices made a significant contribution to module costs in 2011 (around \$0.07/W) and that the future price of this critical element could be a defining issue to the economic viability of this PV technology. The additional prospects of using recycled CdTe modules as a future source of Tellurium are expected to be significant especially because the recovery efficiency for the process is very high, and because the material intensity will have been so much greater in earlier vintage modules. Still, recycling programs will presumably not be utilized until the expected (and warranted) module lifetimes of 25 years have been reached. As it is only recently that CdTe PV has been deployed at a scale where the amount of Tellurium expected to be available from module recycling will be meaningful to future demands, these contributions will presumably not occur until after 2030.

As a direction of future research, it will become increasingly imperative to master techniques that enable the use of ultrathin active layers - while also improving efficiencies - in order to keep their cost to a manageable level. It would also be very advantageous if the efficiency of CdTe modules could be improved without introducing new materials or processes that may increase the total module cost. Fortunately, a multitude of opportunities are indeed available to achieve that end.

2.2.3 Copper–indium–gallium–diselenide (CIGS) photovoltaic technology

At first glance, cadmium telluride and CIGS technologies are basically similar and their production costs should be comparable (Figure 52 and Figure 53). Cadmium telluride has the advantages of a single binary compound, cadmium chloride treatment that brings the cadmium telluride precursor to a solar cell grade layer, commercially large-scale produced transparent and conducting oxide (TCO) layer of SnO_2:F and availability of very fast CdTe deposition techniques such as close-space sublimation (CSS) and vapor transport deposition (VTD). For the record, it may be noted that cadmium telluride technology also had its share of teething problems and false starts.

Figure 52: Monolithically interconnected CIGS solar cells

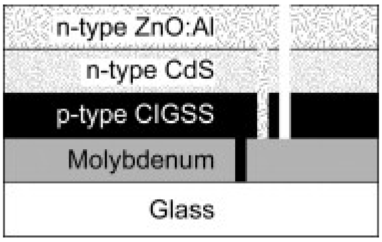

Figure 53: Monolithically interconnected CdTe solar cells

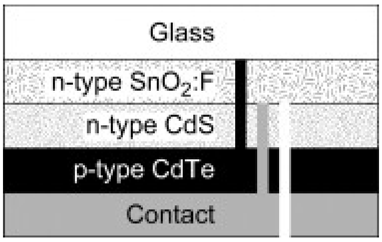

The production cost of cadmium telluride thin film solar cells has already been reduced to ~0.7€ peak watt (Wp). The production cost of CIGS thin film solar cell still hovers in the range 1.12–1.31€/Wp.

2.2.3.1 CIGS thin film deposition

The principal CIGS technologies are based on co-evaporation or reactive sputtering of Cu, In and Ga with selenium, selenization and/or sulfurization of sputter-deposited Cu–In–Ga precursor, and selenization and/or sulfurization of Cu–In–Ga precursor deposited by non-vacuum techniques such as electrodeposition, doctor-blade or ink-jet techniques.[59] The cell efficiency first increases with Ga alloying up to Ga/In+Ga>0.3 and then decreases.[60] Gallium profiling can be used for creating a back surface field as well as broadening of the band gap towards the front (the so-called notch effect). Gallium incorporation has advantages in terms of improving adhesion and broadening the range of the Cu/In+Ga ratio for the formation of the alpha phase.

Of the various CIGS thin film preparation processes, co-evaporation of Cu, In and Ga with selenium offers the most flexible and controllable approach.[61] CIGS preferred orientation is also known to influence the efficiency.[62] Here indium and gallium are co-evaporated in the presence of selenium vapor at a low temperature of ~350 °C to form a smooth indium–gallium selenide thin layer. Copper and selenium are then co-evaporated at a high temperature of ~550 °C to form a large grain, Cu-rich CIGS thin layer. This is followed by co-evaporation of indium, gallium and selenium to inform an optimally Cu-poor CIGS layer. In a slight variation to this process, gallium evaporation is suspended in the final, very thin layer. Maintaining the optimum (2–10*x*) selenium excess pressure especially on increasingly large areas becomes a challenge. Co-evaporation is used by several companies, e.g. Würtz Solar (current production 30 MW/year, efficiency 11.5%), Global Solar (75 MW/year) and Ascent Solar (Flexible).

Selenization and/or sulfurization of magnetron sputtered Cu–In–Ga precursor layers currently employed by Showa Shell (80 MW/year), Honda (27 MW/year), Sulfurcell (~5 MW/year), Avancis (20 MW/year) and other companies is amenable to large volume production. For example, in the low emissivity architectural glass coatings up to nine layers typically consisting of successive layers of antireflective (AR) oxide, infrared (IR) reflective metal, metal primer and AR metal oxide are all deposited by magnetron sputtering on soda lime glass or other substrates. Examples of AR reflective layers are zinc and tin metal oxide or aluminum, silicon nitride or oxynitride, IR reflective metals are silver or silver and copper, metal primer is titanium.

---

[59] N.G. Dhere, R.G. Dhere. Thin-film photovoltaics, J. Vac. Sci. Technol. (A), 23 (2005), pp. 1208–1214

[60] U. Rau, H.W. Schock. Electronic properties of Cu(In,Ga)Se2 heterojunction solar cells-recent achievements, current understanding, and future challenges, Appl. Phys. A, 69 (1999), pp. 131–147

[61] I. Repins, M.A. Contreras, B. Egaas, C. DeHart, J. Scharf, C.L. Perkins, B. To, R. Noufi. 19.9%-efficient ZnO/CdS/CuInGaSe2 solar cell with 81.2% fill factor, Prog. Photovoltaics: Res. Appl., 16 (2008), pp. 235–239

[62] M.A. Contreras, M.J. Romero, R. Noufi. Characterization of Cu(In,Ga)Se2 materials used in record performance solar cells, Thin Solid Films, 511–512 (2006), pp. 51–54

Cu–Ga alloy target pioneered by the FSEC PV Materials Lab is now used widely even on large industrial scale. Here the challenge consists of obtaining the optimally Cu-poor CIGS layer starting from a Cu-poor Cu–In–Ga precursor. Selenization and/or sulfurization are carried out in a conventional furnace in the batch process or rapid thermal process (RTP) in the in-line process. Showa Shell has achieved efficiencies of 15.7% on a 855 cm^2 and 13.1% on a 7108 cm^2 PV modules by selenization and sulfurization of magnetron sputtered Cu–In–Ga precursors.[63] Usually, selenization is carried out in diluted hydrogen selenide, metalorganic selenides such as $(C_2H_5)_2Se$, $(CH_3)_2Se$ or selenium vapor while sulfurization is carried out in sulfur vapor or diluted H_2S. Metalorganic selenides are preferred because of their lower toxicity and because they are liquids at room temperature and hence do not need storage of highly toxic H_2Se in a high pressure cylinder.[64]

The non-vacuum processes have potentially a very high material utilization. While considering non-vacuum techniques, it is important to distinguish between thin film and thick film technologies. Thin films are grown atom by atom or molecule by molecule as in vacuum evaporation, sputtering, chemical bath deposition, chemical vapor deposition, electrodeposition, etc. while thick films are grown by agglomeration of particles from slurry or a suspension as in screen printing, ink jet printing and doctor-blade techniques. In the doctor blade technique, a flat knife blade held slightly above is moved over the substrate onto which the material is to be deposited to prepare thick layers and sheets. For thin layers, the blade has periodic notches, the period and the openings are adjusted to obtain an average thickness depending on the rheology of the ink. Ink jet and doctor blade techniques employ an ink formed of nano-particle suspension of precursor metals or their oxides, nitrates or other compounds in the desired proportion. After drying, first any non-selenide compounds must be reduced prior to selenization and/or sulfurization. There are engineering challenges for coating on large area and for carrying out the reduction, selenization and/or sulfurization in a reproducible and speedy process.

2.2.3.2 Back contact, heterojunction and front TCO

The back-contact, heterojunction formation and front transparent and conducting coating steps that are usually common to several CIGS technologies are discussed in the following sections.

2.2.3.2.1 Molybdenum back contact

Molybdenum is the back contact of choice because it can tolerate the harsh reactive ambient of the selenization/sulfurization processes at elevated temperatures. A thin $MoSe_2$ molybdenum selenide/sulfide interfacial layer is known to assist in the formation

---

[63] K. Kushiya, Y. Tanaka, H. Hakuma, Y. Goushi, S. Kijima, T. Aramoto, Y. Fujiwara. Interface control to enhance the fill factor over 0.70 in a large-area CIS-based thin-film PV technology, Thin Solid Films, 517 (2009), pp. 2108–2110

[64] N.G. Dhere, A.A. Kadam, CuIn1-xGaxSe2-ySy (CIGSS) thin film solar cells prepared by selenization/sulfurization in a conventional furnace using a new precursor, U.S. Patent 7632701

of an Ohmic contact with a low resistance while a Schottky type contact is formed without $Mo(Se,S)_2$ layer.[65] It also promotes adhesion. Molybdenum layers deposited at low sputtering power and high argon gas pressure develop a residual tensile stress while those deposited at high sputtering power and low argon gas pressure develop a residual compressive stress. Therefore, the stress is minimized by carrying out the deposition either at an optimum intermediate sputtering power and argon pressure or by using alternative layers having tensile and compressive stresses. Molybdenum layers with more open structure can allow sodium to diffuse from soda lime glass substrate to the growing CIGS thin layer, it can also cause microononuniformities due to uneven sodium out-diffusion. Even though, a low residual stress, single Mo layer with an open structure that allows Na-diffusion is used for achieving the highest efficiency CIGS thin film solar cells, the production technique requires improved method of avoiding microononuniformities caused by uneven sodium out-diffusion. Therefore, a barrier layer is employed underneath the molybdenum coating to impede the sodium out-diffusion and controlled quantity of sodium is provided through a deposition of a sodium compound, such as sodium fluoride. The molybdenum layer deposited on glass, polyimide or other insulating substrates is scribed with a laser scriber, the so-called P1 scribe so as to separate the cell strips at the bottom contact level (Figure 52).

2.2.3.2.2 Heterojunction partner

The heterojunction partner, CdS layer is usually deposited by chemical bath deposition (CBD). In production, it is usually a batch process. Attempts have been made to achieve an in-line, all vacuum approach by developing CdS vacuum deposition process. However, it may be noted that a batch process can be more economical than an in-line process.

2.2.3.2.3 Transparent and contacting oxide

Usually a transparent and conducting oxide (TCO) window bilayer of undoped zinc oxide and zinc oxide doped with aluminum is deposited by RF magnetron sputtering. The deposition rates achievable with RF magnetron sputtering are low and hence limit the production speed. Therefore, reactive sputtering from Zn and Zn:Al metallic targets using dual targets or pulsed DC are being developed.[66] It is essential to optimize target poisoning (control the level of oxidation) to obtain highly transparent and conducting window layers. Chemical vapor deposition of boron-doped zinc oxide layers has also been developed and has been found to result in better quality window layers.

The second scribe (P2) is carried out usually by mechanical scribing after the deposition of undoped zinc oxide layer (Figure 52). It produce openings that allow the subsequently deposited top ZnO:Al contact layer to connect the top contact layer of the preceding cell to the bottom molybdenum contact layer of the succeeding cell. If the second scribe is

---

[65] T. Wada, S. Nishiwaki, T. Negami. Characterization of the Cu(In,Ga)Se2/Mo interface in CIGS solar cells, Thin Solid Films, 387 (2001), pp. 118–122

[66] M. Powalla, B. Dimmler, Pilot line production of CIGS modules: first experiences in processing and further developments, in: Proceedings of the 29th IEEE Photovoltaic Specialists' Conference, 2002, pp. 571–574

carried out after the heterojunction partner CdS layer deposition and prior to the deposition of undoped ZnO layer, the undoped zinc oxide layer can contribute additional series resistance as well as cause reliability problems. The third scribe (P3) usually carried out by mechanical scribing after the deposition of ZnO:Al layer serves to separate the cell strips at the top contact layer level (Figure 52). It is preferable to carry out the P2 and P3 squares by laser scribing especially in the case of cells deposited on insulating polymer sheets. Moreover, laser scribing can produce more closely spaced and finer scribe lines.

2.2.3.3 Volume, speed and yield

An excellent review by Ingrid Repins describes the various processes in CIGS thin film and cell preparation for achieving the maximum efficiency for small calls and PV modules.[67] The other equally important considerations, viz. volume, speed and yield of production are discussed in the following. It may be noted that a manufacturing plant is designed to produce a certain production volume, i.e. certain area of PV circuits and modules. The material and labor cost is also dictated by the production volume. Initial research and development is concentrated on optimizing the operational windows of various processing techniques to consistently achieve the desirable high efficiency of small area (~0.4 cm^2) CIGS solar cells within ±20% range. This laboratory process is then transferred to intermediate size equipment to achieve the high efficiencies within the acceptable range on a large number of small area cells or a PV circuit on a larger area (50–100 cm^2) in each run, day after day. This experience is then used to scale-up to a pilot plant (0.5–6 MW/year) to produce 0.1–1 m^2 CIGS cell circuits, minimodules and modules and later to production equipment for a large-scale manufacture (>20 MW/year) of large area (~1 m^2) PV circuits and modules. The yield determines the actual production volume in MW/year that is presented to the outside world, i.e. investors, funding agencies, consumers and general public. Most importantly, it determines the production cost in ¢/Wp. Therefore, it is important to achieve an overall yield of ~90% for the production process prior to embarking on a large-scale manufacture.

2.2.3.4 Sizing of production equipment

Optimal sizing of the production equipment is important for making an initial impact, gaining credibility and finally achieving viable production at competitive cost. It is desirable to demonstrate the highest efficiency, high average efficiency and yield in the production equipment. Too small a production volume will not create the initial impact, especially under the current circumstances when a number of large companies are manufacturing on a large scale. Usually the equipment cost is amortized in 7 years. As a result, choosing an excessively large production volume will hamper in attaining the low cost. Most of the production issues can be sorted out at a production scale of 0.5–

---

[67] I. Repins, S. Glynn, J. Duenow, T.J. Coutts, W.K. Metzger, M.A. Contreras, Required material properties for high-efficiency CIGS modules, in: Proceedings of Thin Film Solar Technology, SPIE vol. 7409, 2009, pp. 1–14

6 MW/year. Afterwards, the production equipments can be scaled to 20–30 MW/year. This manufacturing equipment is then duplicated with minor improvements in subsequent production plants. Initially, the speed is sacrificed for attaining the desirable efficiency and yield. In the final analysis, however, the speed determines the production volume in MW/year and thus the ultimate cost in 0.4€/Wp. The current low production cost of 0.7€/Wp for CdTe modules is certainly made possible by the high speed of production.

2.2.3.5 Conclusions: CIGS

At present, the production of CIGS PV modules lags considerably behind that of CdTe PV modules. This is mainly because of its complexity. Scale-up issues related to various CIGS preparation technologies such as co-evaporation, metallic precursor deposition by magnetron sputtering and non-vacuum techniques such as ink-jet printing, electroplating or doctor-blade technology followed by their selenization/sulfurization are needed to be introduced to assist the CIGS technology to attain its full potential. Besides the welcome announcements of large volume production, it is essential to achieve the production cost below 0.75€/Wp in the near term and attain production speeds comparable to CdTe production speeds. Comparable production speeds are expected to be achieved within the next decade. This will enable reduction of CIGS module production costs to ~0.48/Wp that would be comparable to the CdTe module projected production cost. Additionally CIGS will have a higher efficiency premium.

2.2.4 Thin film silicon modules

2.2.4.1 Amorphous silicon

With initial demonstrations stemming back to 1969 thin film silicon (TF-Si) developers have the longest history of commercial production among thin-film PV technologies on the market today. The firms offering TF-Si modules to the market have developed a wide range of technical variations on the commercial scale, including single-junction amorphous silicon (a-Si), dual-junction a-Si/a-Si, tandem-junction microcrystalline silicon-amorphous silicon (commonly named “micromorph”), and triple-junction germanium-doped amorphous silicon (a-Si/a-SiGe/a-SiGe). Representative schematics of these structures are shown in Figure 54.

Figure 54: Schematics of example commercial thin-film silicon PV module device structures. (a) A single-junction a-Si PV module with Al back contact (e.g. Applied Materials a-Si turn-key products) (b) Dual-junction a-Si/a-Si module, (c) Tandem-junction a-Si/μc-Si "micromorph" PV module with ZnO:Al backcontact and white paste reflector (e.g. Oerlikon micromorph turn-key products), and (d) Triple-junction a-Si/a-SiGe/a-SiGe PV cell built on stainless steel foil (e.g. Uni-Solar (Energy Conversion Devices)).[68]

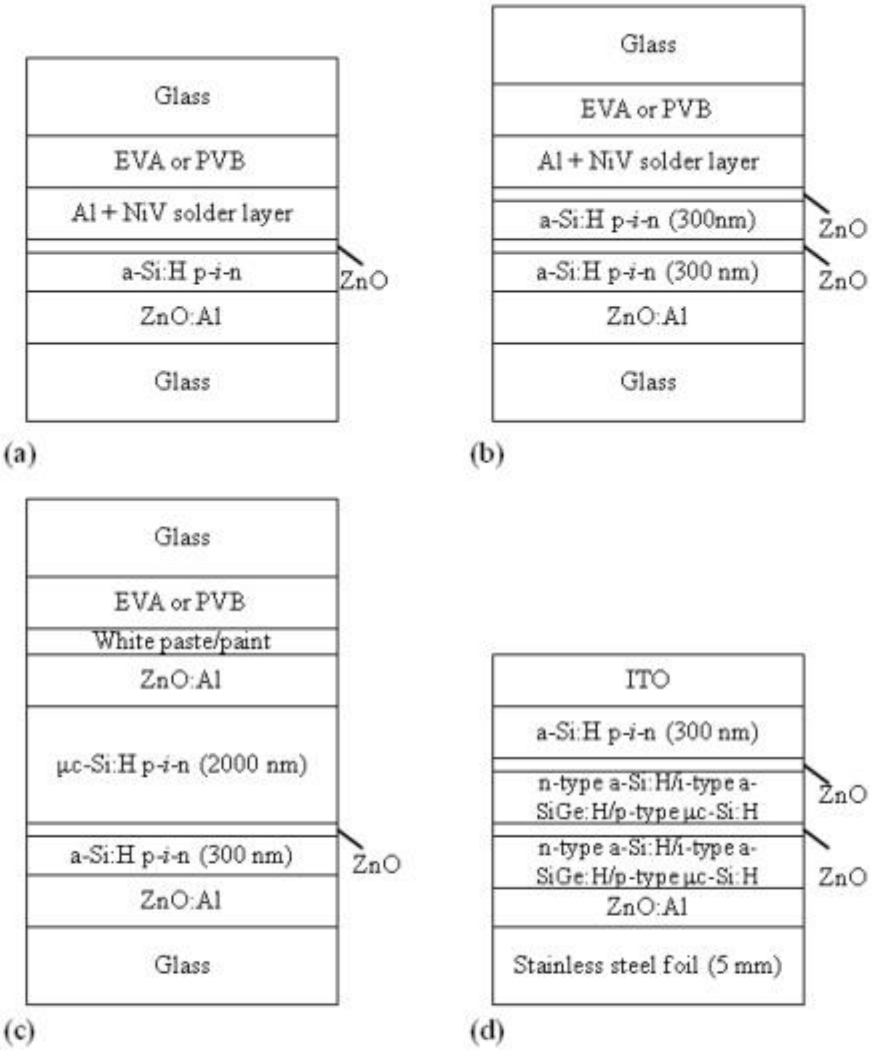

In each superstrate design, the transparent conducting oxide (TCO) – typically aluminum-doped zinc oxide (ZnO:Al) – is deposited by atmospheric-pressure CVD (APCVD), low-pressure CVD (LPCVD), or RF sputtering either at the module manufacturer or the glass supplier. The active TF-Si layers are then deposited via plasma-enhanced chemical vapor deposition (PECVD), followed by the deposition of a thin ZnO buffer layer and the backcontact of Al, Ag, or ZnO:Al. For glass/glass module assembly, the individual cells are defined via laser scribing and the module is encapsulated using either a polyvinyl butyral (PVB) (typical) or ethylene vinyl acetate (EVA) laminate and a top cover glass.

In thin film technology, amorphous silicon is very popular compared to other material such as CIS/CIGS and CdS/CdTe due to its higher efficiency. Amorphous silicon is a non-crystalline form of silicon in disordered structure and has 40 times higher rate of light

---

[68] J. Schmidtke. Commercial status of thin-film photovoltaic devices and materials. Optics Express, Vol. 18, Issue S3, pp. A477-A486 (2010)

absorptivity compared to monocrystalline silicon. The advantage of its random structure is it gives high band gap which is 1.7 eV. Amorphous (uncrystallized) silicon is the most popular thin-film technology with cell efficiencies of 5–7% and double- and triple-junction designs raising it to 8–10%. But it is prone to degradation. Some of the varieties of amorphous silicon are amorphous silicon carbide (a-SiC), amorphous silicon germanium (a-SiGe), microcrystalline silicon (μc-Si), and amorphous silicon-nitride (a-SiN). Thin-film silicon modules, such as amorphous silicon (a-Si:H) based modules, are considered as one of the best options for PV market.[69] a-Si:H modules are mostly targeted for application in large-scale power plants, preferably in hot regions. The lower mounting costs for such power plants are more favourable for modules with lower efficiency. For application in hot regions with higher module operating temperatures the energy output of a-Si:H based module is favourable with respect to c-Si based modules due to the lower temperature coefficient.[70] Additionally, the light-induced degradation of such modules is lower at elevated temperatures.[71] Moreover, thin film silicon modules are ideal candidates for building-integrated photovoltaics (BIPV) due to the homogeneous, dark appearance and the flexibility in module size up to 5.7 m^2. The low temperature coefficient favours high output in BIPV applications. The possibility in producing semi-transparent modules by laser scribing, and the use of non-toxic raw materials make thin film silicon attractive for BIPV.

After the first a-Si:H/μc-Si:H ("micromorph") solar cells were reported in 1996 by Meier et al.,[72] Kaneka was the first company developing high efficiency tandem and triple cells with currently up to 12.3% stable efficiency[73] and started large-scale module production around ten years ago. In the past few years many companies established production lines with module efficiencies continuously being increased to currently up to 9–10% in production average and module size up to 5.7 m^2.[74] Prototype modules on production scale reach stabilized efficiencies close to 11% based on a tandem junction or a triple junction. [75] These values are remarkably close to the best solar cell efficiencies of up to 12.3% obtained in laboratories with tandem junctions and, recently reported by LG

---

[69] A. Feltrin, A. Freundlich. Material considerations for terawatt level deployment of photovoltaics, Renewable Energy, 33 (2) (2008), pp. 180–185

[70] A.Virtuani, D. Pavanello, G. Friesen, Overview of temperature coefficient of different thin film photovoltaic technologies in: Proceedings of the 25th EU Photovoltaic Solar Energy Conference and Exhibition, 5th World Conference on Photovoltaic Energy Conversion, Valencia, Spain, 2010, pp. 4248–4252

[71] R. Ruther, J. del Cueto, G. Tamizh-Mani, A. Montenegro, S. Rummel, A. Anderberg, B. von Roedern, Proceedings of the 33rd IEEE Photovoltaic Specialists Conference, 2008, pp. 1–5

[72] J. Meier, P. Torres, R. Platz, S. Dubail, U. Kroll, J.A.A. Selvan, N. Pellaton-Vaucher, C. Hof, D. Fischer, H. Keppner, A. Shah, K.-D. Ufert, P. Giannoules, J. Köhler. On the way towards high efficiency thin film silicon solar cells by the "micromorph" concept, Proceedings of the Materials Research Society Symposium, 420 (1996), pp. 3–14

[73] K. Yamamoto, M. Yoshimi, Y. Tawada, Y. Okamoto, A. Nakajima. Cost effective and high-performance thin film Si solar cell towards the 21st century, Solar Energy Materials and Solar Cells, 66 (2001), pp. 117–125

[74] J. Springer, T. Dittkrist, D. Hrunski, J. Pantförder, S. Bönisch, T. Bergmann, F. Lindner, A. Katzung, J. Rittner, F. Schöne1, M. Vouters, R. Hesse, T. Liebschner, B. Stannowski, U. Klemm, T. Brammer, T. Hänel, B. Rech, Proceedings of the 25th European Photovoltaic Solar Energy Conference, Valencia, Spain, 2010, p. 2896.

[75] O. Kluth, J. Kalas, M. Fecioru-Morariu, P. A. Losio, J. Hoetzel, Proceedings of the 26th European Photovoltaic Solar Energy Conference, Hamburg, Germany, 2011, p. 2354.

Electronics, 13.4% with an a-Si:H/μc-Si:H/μc-Si:H triple junction.[76] It demonstrates the mature processes and production equipment benefitting from the flat panel display industry, on the one hand side, but also the urgent need to push up the laboratory efficiencies on the other hand side. The low module efficiency is the most severe restraint and a potential show stopper for this technology if no new concepts for higher efficiencies are developed.

To increase the stabilized tandem module efficiency well beyond 12% two major limitations need to be overcome: the weak light absorption in μc-Si:H due to its indirect band gap and the light induced degradation of a-Si:H (and a-SiGe:H) solar cells due to the Staebler–Wronski-Effect (SWE). To cope with both of these drawbacks advanced light-trapping schemes were developed and successfully implemented, resulting in total current densities (the sum of all junctions) almost reaching 30 mA/cm^2 for tandem junctions and triple junctions. [77] Even though it is remarkably high, this is still only 2/3 of the theoretical maximum of about 43.5 mA/cm^2 for crystalline silicon. The missing part is lost due to light reflection out of the cell and parasitic absorption, predominantly in the TCO front contact. The above mentioned record solar cells exhibit initial efficiencies reaching the highest reported value of 16.3% for a n-i-p type triple cell by the Uni Solar group.[78] This efficiency value, however, degrades due to the SWE. Unraveling the microscopic defect-creation mechanisms in a-Si:H and finding methods to circumvent this effect are subject of present work.[79] Unless the SWE can be solved or alternative, stable high and medium band gap materials are found, two scenarios—or a combination of both—are possible: Firstly, revolutionary new light trapping schemes facilitating total currents well above 30 mA/cm^2 for thin solar cells are developed.[80] As an example, attempts are being made to de-couple the light scattering from the TCO deposition, e.g. by nano-imprinting of scattering structures[81] or textured glass.[82] At PVcomB further improvement of the above discussed annealed AZO, combining a thin (<400 nm) annealed AZO with a scattering superstrate is the subject of current research.

---

[76] S. Kim, J. Park, H. Lee, H. Lee, S.-W. Ahn, H.-M. Lee. Microcrystalline silicon carbide p-layer with wide-bandgap and its application to single- and triple-junction silicon thin-film solar cells, Japanese Journal of Applied Physics, 51 (2012), pp. 1–4 10NB11

[77] M. Boccard, C. Battaglia, S. Hänni, K. Söderström, J. Escarré, S. Nicolay, F. Meillaud, M. Despeisse, C. Ballif. Multiscale transparent electrode architecture for efficient light management and carrier collection in solar cells, Nano Letters, 12 (2012), pp. 1344–1348

[78] B. Yan, G. Yue, L. Sivec, J. Yang, S. Guha, C.-S. Jiang. Innovative dual function nc-SiOx:H layer leading to a >16% efficient multijunction thin-film silicon solar cell, Applied Physics Letters, 99 (2011), p. 113512

[79] M. Fehr, A. Schnegg, B. Rech, K. Lips, O. Astakhov, F. Finger, G. Pfanner, C. Freysoldt, J. Neugebauer, R. Bittl, C. Teutloff. Combined multifrequency EPR and DFT study of dangling bonds in a-Si:H, Physical Review B, 84 (2011), pp. 1–10 245203

[80] M. Vanecek, O. Babchenko, A. Purkrt, J. Holovsky, N. Neykova, A. Poruba, Z. Remes, J. Meier, U. Kroll. Nanostructured three-dimensional thin film silicon solar cells with very high efficiency potential, Applied Physics Letters, 98 (16) (2010), p. 163503

[81] C. Battaglia, J. Escarre, K. Söderström, L. Erni, L. Ding, G. Bugnon, A. Billet, M. Boccard, L. Barraud, S. De Wolf, F.-J. Haug, M. Despeisse, C. Ballif. Nanoimprint lithography for high-efficiency thin-film silicon solar cells, Nano Letters, 11 (2) (2011), pp. 661–665

[82] J. Steinhauser, J.-F. Boucher, E. Omnes, D. Borrello, E. Vallat-Sauvain, G. Monteduro, M. Marmelo, J.-B. Orhan, B. Wolf, J. Bailat, S. Benagli, J. Meier, U. Kroll, Improving low pressure chemical vapor deposited zinc oxide contacts for thin film silicon solar cells by using rough glass substrates, Thin Solid Films 520 (4), 2011, 1218–1222

This could be the TCO substrate of choice for high efficiency with thin TCO and thin silicon layer thicknesses, hence, allowing for low production costs. For the second scenario, high-quality silicon layers in the range of 10 µm and more need to be employed. To date this is not a feasible, low-cost route for a-Si:H/µc-Si:H based solar cells due to the low deposition rate of 0.5–1 nm/s for high quality µc-Si:H layers on production-scale equipment that is available. Other, high rate thin-film Si material needs to be developed. As one of the largest producers of a-Si:H/µc-Si:H tandem modules, Masdar PV GmbH operates a sunfab-type production line from Applied Materials with a name plate capacity of 95 MW_p. With a-Si:H single junction based modules reaching stabilized efficiencies of 8% produced first, the production was changed to a-Si:H/µc-Si:H tandem modules in August 2011. As a cooperation partner of Masdar PV the Competence Center Thin-Film and Nanotechnology for Photovoltaics Berlin (PVcomB) offers a platform for technology development and process transfer for thin-film PV modules. For this purpose two R&D lines for a-Si:H/µc-Si:H and CIGS based modules on 30×30 cm^2 are operated.

2.2.4.2 Status of poly-Si thin-film solar cells

So far, polycrystalline silicon (poly-Si) thin films have not reached the maturity and performance required for market entrance. However, poly-Si layers exhibit distinct advantages since they could benefit from the advantages of the crystalline silicon wafer approach while maintaining the advantages of thin-film technologies: crystalline silicon is a non-toxic material with high stability and durability, and possesses an energy gap of 1.12 eV which is nearly perfectly suited for maximum single-junction solar cell efficiencies. Furthermore, silicon is an abundant material and therefore not subject to natural resource limitations in case of a strong rise of the solar electricity demands in the future. Fabricated as thin layers, polycrystalline silicon also features all advantages of thin-film technologies, namely low costs due to low material wastage with up to factor 100 less material compared to wafer-based solar cells, and the technically feasible monolithic fabrication of large area devices. With an appropriate light trapping concept crystalline silicon thin-film solar cells can principally reach single-junction efficiencies of more than 17% close to that of silicon wafer-based solar cells, as calculated by R. Brendel in 2003.[83] Despite all those promising properties, poly-Si thin films did not establish itself on the photovoltaic market so far. CSG Solar, the only company that produced poly-Si thin-film solar cells on glass on industrial scale, fell victim to the crisis in the photovoltaic sector in the year 2011. The technology of CSG Solar relied on thermally solid phase crystallized silicon thin films on glass substrate with a module efficiency of 10.4% demonstrated on an area of 10×10 cm^2—being up to now the world record of poly-Si thin-film submodules. In the past years, research in poly-Si thin-film solar cells has considerably moved forward, providing a roadmap to higher efficiencies at which poly-Si will compete with incumbent technologies.

---

[83] R. Brendel. Thin-Film Crystalline Silicon Solar Cells. Wiley-VCH, Berlin (2003)

Further, the four important approaches for the fabrication of poly-Si thin-film solar cells on foreign substrates, which have been subject to intensive research activities in the past years are sumarised. In all poly-Si fabrication approaches described here, silicon films are grown by vacuum deposition techniques onto a foreign substrate, such as glass, and are aiming at an electrical material quality as close as possible to crystalline silicon wafer material. The fundamental technological aspects, characteristic structural and electrical material properties as well as current record solar cell results in terms of efficiency and open circuit voltage are presented in detail.

2.2.4.2.1 Solid phase crystallization

Solid phase crystallization (SPC) of amorphous silicon thin films by thermal annealing is a popular technique for the fabrication of poly-Si layers due to its technological simplicity. As only moderate temperatures around 600 °C are required for the crystallization process in a time span of several hours, cheap substrates such as glass or metal can principally be used. According to Bergmann[84] the substrate has just to fulfill three requirements: (1) It has to be stable upon poly-Si processing temperatures; (2) Diffusion of impurities into the silicon bulk has to be prohibited either by the inclusion of barrier layers or by the use of high-quality substrates. Usually this requirement results in the integration of barrier layers as pure substrates are often very expensive; (3) The thermal expansion coefficient has to be adapted to that of crystalline silicon in order to avoid cracking and flaking during thermal treatment.

The typical microstructure of poly-Si thin films prepared by SPC is based on randomly oriented grains with a size of 1–3 μm if an amorphous substrate like glass is used. Nucleation, growth and resulting grain size can be influenced by experimental parameters, such as annealing time, temperature and substrate texture.[85] In the as-crystallized state, the quality of such SPC poly-Si material is not sufficient for photovoltaic applications as it contains many deep level intra-grain defects and grain-boundary defects, limiting the electrical performance. Post-crystallization treatments are necessary such as rapid thermal annealing (RTA) at temperatures above 900 °C for the activation of dopants and to heal out extended defects,[86] and hydrogen passivation in order to saturate silicon dangling bonds.[87] By a combination of both treatments the electrical material quality can be considerably enhanced. The open circuit voltage increases from about 150 mV up to about 500 mV and accordingly the density of

---

[84] R. Bergmann, J. Kohler, R. Dassow, C. Zaczek, J. Werner. Nucleation and growth of crystalline silicon films on glass for solar cells. Physica Status Solidi A—Applied Research, 166 (1998), pp. 587–602

[85] T. Sontheimer, S. Scherf, C. Klimm, C. Becker, B. Rech. Characterization and control of crystal nucleation in amorphous electron beam evaporated silicon for thin film solar cells. Journal of Applied Physics, 110 (2011), p. 063530

[86] B. Rau, T. Weber, B. Gorka, P. Dogan, F. Fenske, K.Y. Lee, S. Gall, B. Rech. Development of a rapid thermal annealing process for polycrystalline silicon thin-film solar cells on glass. Materials Science and Engineering B, 159–60 (2009), pp. 329–332

[87] B. Gorka, B. Rau, P. Dogan, C. Becker, F. Ruske, S. Gall, B. Rech. Influence of hydrogen plasma on the defect passivation of polycrystalline Si thin film solar cells. Plasma Processes and Polymers, 6 (2009), pp. S36–S40

paramagnetic defects which can be attributed to silicon dangling bonds decreases from about 1×10^{18} cm^{-3} to below 1×10^{16} cm^{-3} (Table 13).[88]

Table 13: Maximum open circuit voltages, efficiencies and grain sizes of poly-Si thin-film solar cells prepared by diverse methods. Source: Applied Physics Letters, 2012

Poly-Si fabrication method		V_{oc} (mV)	J_{sc} (mA/cm^2)	FF (%)	η (%)	Grain size (µm)
Solid phase crystallization	Max η	492	29.5	72.1	10.5	1-3□
	Max V_{oc}	553	25.0	66.4	9.2	up to 5
Seed layer approach	Max η	522	21.6	75.8	8.5	10□
	Max V_{oc}	534	20.7	73.0	8.0	10
Direct crystalline growth	Max η	504	14.3	68.8	5.0	0.2
	Max V_{oc}	536	4			0.2
Liquid phase crystallization	Max η	557	24.2	62.3	8.4	up to 10,000
	Max V_{oc}	582	13.5	53.1	4.3	up to 10,000

The record SPC poly-Si thin-film solar cell device has been developed by CSG Solar (formerly Pacific Solar) in Sydney with an efficiency of 10.4% demonstrated in the year 2007. Here, a textured borosilicate glass with a thermal expansion coefficient very close to that of silicon is used as a substrate, on which a silicon (oxi)nitride diffusion barrier and an 1–2 µm thick n^+pp^+-doped a-Si:H layer stack are grown by PECVD. This layer stack is subsequently exposed to SPC at around 600 °C and the above mentioned defect-healing processes RTA and hydrogen-passivation are applied. A sophisticated contacting scheme allows for carrier collection without transparent conductive oxide layers. The light trapping concept including an advanced textured glass substrate and an optimized back reflector leads to a striking short circuit current density j_{SC} of almost 30 mA/cm^2. However, despite strong efforts in the field of defect annealing and passivation processes in the past years the material quality of SPC poly-Si on glass could not be improved significantly, limiting the open circuit voltage V_{OC} to 500 mV.

In 2007 this SPC technology matured to industrial production and the company CSG Solar was founded in Thalheim, Germany. Unfortunately, due to the difficult situation on the photovoltaics market CSG Solar had to declare bankruptcy and to stop production in 2010 again. Although this insolvency might be mainly attributed to the global market situation, also technological drawbacks such as very slow and thus non-economic silicon deposition rates of the PECVD method, long annealing times of more than 10 h for SPC, and the above mentioned moderate material quality limiting the device efficiency could have been possible reasons.

---

[88] M. Fehr, P. Simon, T. Sontheimer, C. Leendertz, B. Gorka, A. Schnegg, B. Rech, K. Lips. Influence of deep defects on device performance of thin-film polycrystalline silicon solar cells. Applied Physics Letters, 101 (2012), p. 123904

2.2.4.2.2 Epitaxial thickening of large-grained seed layers

The idea of the so-called 'seed layer approach' is the growth of a very thin silicon seed layer with excellent crystallographic properties as a template, and the transfer of the structural information into the solar cell absorber material by epitaxial thickening. Whereas SPC grown poly-Si thin films are restricted to rather small grain sizes of several micrometres, poly-Si layers with substantially larger grains and a higher crystalline quality can be achieved by laser crystallization[89] or aluminium induced crystallization (AIC)[90] forming the seed layer for epitaxy. Particularly AIC has gained considerable interest in the photovoltaics community due to achievable grain sizes larger than 20 µm. Here, Al/a-Si double layers separated by a thin native oxide are thermally annealed at temperatures far below 600 °C for about 1–4 h,[91] inducing the crystallization of the silicon and a simultaneous layer exchange process of the Si and Al film. For epitaxial thickening, many different techniques have been developed, using various deposition methods at different temperatures.[92] The crystallographic quality of poly-Si seed layers compared to SPC material is higher and is much closer at the ideal monocrystalline value of 3.2 cm^{-1}. However, often the full potential of such seed layers with large grains cannot be fully exploited for poly-Si thin-film solar cell applications, as the structural characteristics and electrical performance of this material are limited by intragrain defects, i.e. by defects inside the grains, rather than by grain boundaries.[93]

The best poly-Si thin-film solar cells produced by the seed layer approach have been developed by IMEC, Belgium, and rely on aluminium-induced crystallization (AIC) of amorphous silicon in combination with thermal chemical vapor deposition (CVD) at elevated temperatures beyond 1100 °C. These very high temperatures disallow the use of common glass types. Alumina substrates which are covered with a spin-on oxide to reduce the surface roughness were found to be feasible for the deposition process. Other technological characteristics of this concept are the implementation of a-Si/poly-Si heterojunction emitters, enabling much higher V_{OC}-values than conventional diffused homojunction emitters, plasma texturing of the front surface in order to increase light trapping and current density, and interdigitated finger contacts (using ITO/Ti/Pd/Ag) yielding high fill factors. An efficiency of 8% with a maximum V_{OC} of 534 mV was achieved in 2007. By a further improvement of the hydrogen passivation process using a remote instead of a direct plasma and subsequent advanced surface texturing, an

---

[89] D. Van Gestel, M. Chahal, P.C. van der Wilt, Y. Qiu, I. Gordon, J.S. Im, J. Poortmans, Thin-film polycrystalline silicon solar cells with low intragrain defect density made via laser crystallization and epitaxial growth, in: Proceedings of the 35th IEEE Photovoltaic Specialists Conference, 2010, pp. 279–282

[90] A. Aberle, A. Straub, P. Widenborg, A. Sproul, Y. Huang, P. Campbell. Polycrystalline silicon thin-film solar cells on glass by aluminium-induced crystallisation and subsequent ion-assisted deposition (ALICIA). Progress in Photovoltaics: Research and Applications, 13 (1) (2005), pp. 37–47

[91] O. Nast, S. Brehme, S. Pritchard, A. Aberle, S. Wenham. Aluminium-induced crystallisation of silicon on glass for thin-film solar cells. Solar Energy Materials and Solar Cells, 65 (1–4) (2001), pp. 385–392

[92] D. Van Gestel, I. Gordon, J. Poortmans, Metal-induced crystallization for thin-film polycrystalline silicon solar cells: achievements and perspective, Solar Energy Materials and Solar Cells same issue.

[93] D. Van Gestel, M.J. Romero, I. Gordon, L. Carnel, J. D'Haen, G. Beaucarne, M. Al-Jassim, J. Poortmans. Electrical activity of intragrain defects in polycrystalline silicon layers obtained by aluminum-induced crystallization and epitaxy. Applied Physics Letters, 90 (9) (2007), p. 092103

efficiency of 8.5% was reached (Table 13). Up to now, the seed layer approach has not been scaled up to industrial scale due to the rather complex fabrication procedure and very high process temperatures that have to be applied.

2.2.4.2.3 Direct crystalline growth

In contrast to the seed layer approach, the direct growth of poly-Si thin films without further annealing steps is an appealing option with little technological intricacy. The poly-Si films are grown directly in the crystalline phase if the substrate is heated above a certain temperature. For electron–beam evaporation of silicon, a physical vapor deposition technique, this minimum temperature for crystalline growth has been reported to lie between 350 °C and 400 °C for a pressure around 1×10^{-7} mbar.[94] In general, the transition between amorphous and crystalline growth depends on various experimental parameters, such as the substrate temperature, pressure, and the composition and flow of precursor material. For atmospheric pressure CVD and low pressure CVD transition temperatures of 680 °C and 580 °C have been reported, being also compatible with the use of glass substrates. From a technological perspective, this approach strongly resembles microcrystalline/micromorph silicon thin-film concepts, relying on a one step deposition process of the final material. However, whilst microcrystalline silicon consists of a certain fraction of nanocrystallites embedded in an amorphous matrix, direct crystalline growth aims at the production of polycrystalline silicon films with 100% crystalline fraction.

Directly grown poly-Si thin films usually consist of columnar grains with a size ranging from 0.1 up to 10 µm. Very often a <1 1 0> orientation of the columnar grains has been reported,[95] which is assumed to affect the solar cell performance in a positive way.[96] Furthermore, such a columnar structure can be beneficial for photovoltaic applications, as the grain boundaries are aligned parallel to the current flow. Poly-Si thin-film solar cells by direct growth have been manufactured by IMEC, Belgium. The fabrication process of these directly grown poly-Si devices strongly resembles the procedure for solar cells prepared by the seed layer approach. The main difference is the use of a non-crystalline substrate such as oxidized Si-wafers instead of a large-grained poly-Si seed layer. No additional crystallization step is required. All other characteristic process steps are identical, such as plasma texturing of the poly-Si surface followed by hydrogenation and n^+ a-Si:H heteroemitter deposition, as well as contacting by an interdigitated pattern. The best directly grown poly-Si thin-film solar cell has an efficiency of 5.0%. By reduction of the poly-Si absorber thickness down to only 0.2 µm 536 mV was reached, however, at a significantly reduced short circuit current (see Table 13). Despite

---

[94] C. Becker, F. Ruske, T. Sontheimer, B. Gorka, U. Bloeck, S. Gall, B. Rech. Microstructure and photovoltaic performance of polycrystalline silicon thin films on temperature-stable ZnO:Al layers. Journal of Applied Physics, 106 (2009), p. 084506

[95] L. Carnel, I. Gordon, D. Van Gestel, G. Beaucarne, J. Poortmans. High open-circuit voltage values on fine-grained thin-film polysilicon solar cells. Journal of Applied Physics, 100 (2006), p. 063702

[96] T. Matsui, M. Tsukiji, H. Saika, T. Toyama, H. Okamoto. Correlation between microstructure and photovoltaic performance of polycrystalline silicon thin film solar cells. Japanese Journal of Applied Physics, 41 (1) (2002), pp. 20–27

technological simplicity, directly grown poly-Si thin-film solar cells have not been considered for industrial production due to limited efficiencies.

2.2.4.2.4 Liquid phase crystallization

In the past year, substantial progress has been made in the development of silicon liquid phase crystallization (LPC) processes. By focusing the energy mainly into the silicon layer the thermal budget inside the substrate is reduced. Poly-Si layers on glass with grain sizes up to the millimeter range were successfully realized by line-focussed energy sources such as laser,[97] electron–beam[98] or halogen-lamps.[99] In this technological approach, silicon of 5–15 µm thickness is deposited in amorphous or nanocrystalline phase by a high-rate deposition method, enabling the growth of thick layers in a reasonable time span, followed by a subsequent crystallization process by heating up the silicon above the melting point of 1414 °C. A major advantage of this approach is the fact that the deposition conditions are decoupled from the electronic quality of the absorber layers, since the total defect density is defined during the crystallization from molten silicon. In contrast to the formation of directly grown poly-Si or µc-Si:H, a precise control of the deposition process to maintain a well hydrogenated, defect free absorber is not mandatory. Consequently, the choice of an appropriate deposition technique relies on economic considerations. Simple processing and high deposition rates are important requirements for establishing a low-cost production process with high throughput. In contrast to concepts based on seed layers where the quality of the seed represents the best achievable quality of the epitaxial thickened absorber (grain boundaries and defects in the seed propagate and/or agglomerate into the absorber during epitaxial growth), LPC enhances the crystallographic properties of the absorber since grains are grown from silicon melt. However, due to the high temperature processing, special care has to be taken to select adequate interlayers as diffusion barrier, wetting agent or dopant sources during absorber crystallization. In addition, buffer layers such as SiC_x, SiO_x or SiN_x are necessary to reduce the thermo-mechanical mismatch between silicon and glass substrate. Liquid phase crystallized absorbers exhibit a morphology comparable to wafers fabricated using the edge defined film fed growth (EFG) or string ribbon technique.

The liquid phase crystallization approach has the potential to solve two major problems of conventional solid phase crystallization techniques for poly-Si thin film fabrication: First, grain size and electrical material quality of liquid phase crystallized silicon layers are significantly increased, enabling a clear break through the current pertinacious V_{OC}-limit of SPC material of around 500 mV. Second, the crystallization time is reduced from at least 10–15 h for SPC down to only some seconds, permitting a promising boost of

---

[97] G. Andra, J. Bergmann, F. Falk. Laser crystallized multicrystalline silicon thin films on glass. Thin Solid Films, 487 (1–2) (2005), pp. 77–80

[98] D. Amkreutz, J. Mueller, M. Schmidt, T. Haenel, T.F. Schulze. Electron–beam crystallized large grained silicon solar cell on glass substrate. Progress in Photovoltaics: Research and Applications, 19 (8) (2011), pp. 937–945

[99] T. Kieliba, Zone-melting Recrystallization for Crystalline Silicon Thin-film Solar Cells, Ph.D. Thesis, Universität Konstanz, 2006.

throughput in industrial production. As summarized in Table 13, record V_{OC} values well above 550 mV were achieved by two research groups. Within a time period of two years the short circuit current density was raised by more than a factor of two, resulting in an efficiency record of 8.4% embedding a laser crystallized absorber into a superstrate, rear-junction, rear-contacted cell architecture. An even higher V_{OC} of 582 mV was recently achieved in an electron–beam crystallized poly-Si thin-film solar cell device using a contact system allowing for both-sided illumination.

2.2.4.3 Prospective poly-Si thin-film solar cell technologies

The three emerging trends in poly-Si thin-film solar cells are based on the following technologies: the high-rate deposition of silicon by electron-beam evaporation as a high-throughput and low-cost alternative to conventional CVD; a poly-Si structuring technique based on nanoimprint-lithography aiming at an efficient light trapping in poly-Si thin-film absorbers and a liquid phase crystallization technique for silicon thin-film solar cells using a focussed line-shaped electron-beam for the high-throughput fabrication of large-grained poly-Si material with high electrical material quality.

2.2.4.3.1 High-rate electron–beam evaporation of silicon

In contrast to micromorph silicon (μc-Si:H) thin films which comprise a hydrogen content of approximately 10% and therefore rely on CVD techniques, poly-Si thin layers can be grown without hydrogen by physical vapor deposition methods. Physical vapor deposition techniques are desirable for silicon thin-film solar cell production, as these rather simple techniques enable the high-rate deposition of silicon at reduced fabrication costs, thereby increasing productivity and throughput. Deposition rates up to 4000 nm/min were demonstrated.[100] Hence, poly-Si thin-film solar cell concepts using more than about 10 μm thick films, e.g. in case of the liquid phase crystallization approach, become economically feasible.

Figure 55 illustrates the main components of an electron–beam evaporation (EBE) system for the high-rate physical vapor deposition of silicon. The main chamber is equipped with an electron gun, a water cooled copper crucible that encloses the silicon target, a boron effusion cell, a graphite heater, and a rotatable lift that holds the sample holder. A tungsten hot cathode generates the electron beam at a constant voltage of 10 kV. The energy input and therefore the deposition rate is controlled by the emission current. A magnetic field directs the electron beam towards the target where its kinetic energy induces the melting of silicon in its proximity. This resulting small area source evaporates Si with a certain emission characteristic towards the heated sample. The substrate temperature defines the structure of the evaporated Si: A deposition at temperatures well below the transfer regime around 350–400 °C, results in amorphous silicon thin films; at higher temperatures, directly poly-Si films are grown. A high-temperature effusion cell can be used for co-evaporation of high-purity elemental boron

---

[100] J.-P. Heinß, H. Morgner, K. Häfner, Crystallization of silicon layers with a scanned electron beam, in: Proceeding of the 24th European Photovoltaic Conference 2009, Hamburg, Germany, 2009, p. 2800

during silicon evaporation to accurately control the doping level between 1×10^{16} cm^{-3} and 1×10^{20} cm^{-3} in the Si films.

Figure 55: Schematic drawing of a silicon electron–beam evaporation chamber. Courtesy: Oerlikon Solar AG, 2012

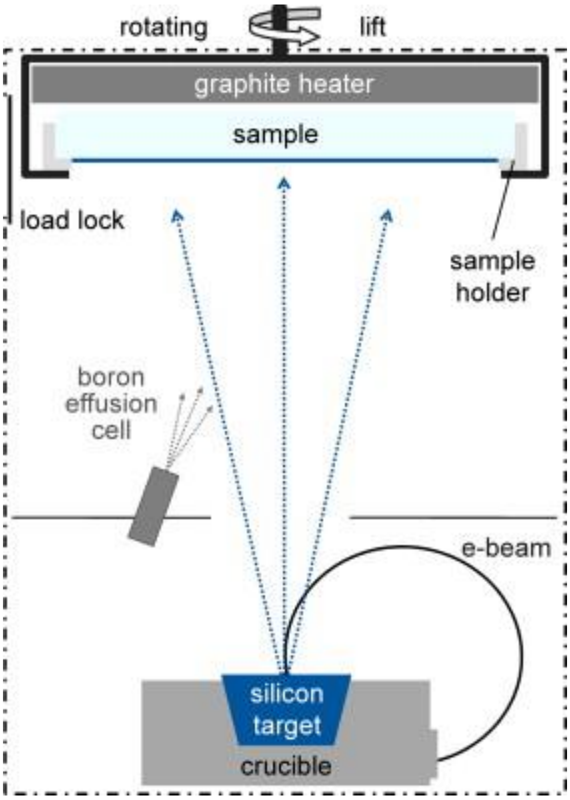

The deposited Si exhibits characteristics that are in conformity with the requirements of PV grade material. SIMS measurements on Si layers evaporated at a deposition rate of 300 nm/min and a pressure of 1×10^{-7} mbar confirm a low oxygen concentration of 3×10^{17} cm^{-3} for a-Si and 5×10^{16} cm^{-3} for directly grown poly-Si. The concentration of nitrogen in the deposited films was found to be $2(\pm1)\times10^{16}$ cm^{-3}. In photovoltaics, EBE was firstly used for the epitaxial thickening of silicon wafers.[101] In 2006, a first prototype of solid phase crystallized poly-Si thin-film solar cells grown by EBE on glass substrate was demonstrated.[102] By further improvements the efficiency was raised up to 6.8% without and 7.8% with back side texturing,[103] verifying that EBE-deposited silicon exhibits an equivalent material quality as PECVD-grown material. Further improvement of the short circuit current density of EBE solid phase crystallized Si thin-film solar cells failed so far due to the incompatibility of the EBE method with the use of textured substrates, which are indispensable for a satisfying light trapping in the thin poly-Si

---

[101] L. Oberbeck, R. Bergmann. Electronic properties of silicon epitaxial layers deposited by ion-assisted deposition at low temperatures. Journal of Applied Physics, 88 (5) (2000), pp. 3015–3021

[102] D. Song, D. Inns, A. Straub, M.L. Terry, P. Campbell, A.G. Aberle. Solid phase crystallized polycrystalline thin-films on glass from evaporated silicon for photovoltaic applications. Thin Solid Films, 513 (1–2) (2006), pp. 356–363

[103] T. Sontheimer, C. Becker, F. Ruske, C. Klimm, U. Bloeck, S. Gall, O. Kunz, T. Young, R. Egan, J. Hüpkes, B. Rech, Challenges and opportunities of electron beam evaporation in the preparation of poly-Si thin film solar cells, in: Proceedings of the 35th IEEE Photovoltaic Specialists Conference, 2010, pp. 614 –619.

absorber.[104] In contrast to CVD methods, providing a conformal coating of a textured substrate with silicon, e-beam evaporated silicon impinges the substrate with a certain flux direction. It has been shown that the poly-Si material quality deteriorates if substrate textures consist of steep flanks with inclination angles larger than 30°, leading to a strong incorporation of oxygen and even suppressing the SPC process for angles larger 40°. However, the specific growth characteristic of EBE on textured substrates is not necessarily a drawback, but can be an opportunity for the large-area fabrication of periodic crystalline silicon nanoarrays.

2.2.4.3.2 Light trapping in poly-Si thin films on periodic nanoimprinted substrates

A challenge that is inherent to all crystalline silicon thin-film solar cell technologies is light trapping. Due to the weak absorption of crystalline silicon near its bandgap energy and the typically low film thickness of a few micrometers, which is determined by the electrical material quality, efficient light management is a prerequisite to achieve high solar cell performance. Besides various statistical light trapping approaches such as SiO_2 bead coated, abrasion etch textured and aluminum induced textured glass substrates, backside texturing of the silicon film or metal nanoparticles on the rear side for surface plasmon enhanced light trapping have been applied. A novel approach towards high light trapping efficiencies is to replace the planar absorber layer by a periodically structured nanophotonic thin film. This opens up the possibility to surpass the so-called Yablonovitch limit, which states that the light path length enhancement that can be obtained by statistical light harvesting concepts is limited to $4n^2$, in which n denotes the refractive index of the absorber material.[105] A promising technology allowing for the design of arbitrarily structured subwavelength-sized light trapping textures on large areas is nanoimprint lithography (NIL).[106] NIL as high throughput structuring technique has already been successfully applied for nanotexturing of front electrodes in amorphous silicon thin-film solar cells and as surface texture in poly-Si thin-film solar cells. A special sol-gel is used as resist material[107] such that the final substrate textures are stable up to temperatures of 800 °C and are therefore compatible with subsequent high-temperature processes during the fabrication of poly-Si.

The combination of such temperature-stable nanoimprinted glass substrates with the unique growth characteristics of e-beam evaporated silicon on textured surfaces, allows the bottom-up fabrication of highly absorbing periodic poly-Si nano- and

---

[104] T. Sontheimer, E. Rudigier-Voigt, M. Bockmeyer, D. Lockau, C. Klimm, C. Becker, B. Rech. Light harvesting architectures for electron beam evaporated solid phase crystallized Si thin film solar cells: statistical and periodic approaches. Journal of Non-Crystalline Solids, 358 (2012), pp. 2303–2307

[105] Z. Yu, A. Raman, S. Fan. Fundamental limit of nanophotonic light trapping in solar cells. Proceedings of the National Academy of Sciences of the United States of America, 107 (41) (2010), pp. 17491–17496

[106] H. Schift. Nanoimprint lithography: an old story in modern times? A review. Journal of Vacuum Science and Technology B, 26 (2008), pp. 458–480

[107] E. Rudigier-Voigt, M. Bockmeyer, V. Hagemann, S. Bauer, Sol–gel based structuring of the front-electrode in Si-based thin film pv device, in: Proceedings of the 24th European Photovoltaic Conference 2009, Hamburg, Germany, 2009, p. 2884.

microarchitectures by SPC, etching and mechanical abrasion.[108] One strategy is to structure the absorber layer itself in nano- or microhole array geometry.[109] Here, a 2 µm square lattice periodic glass substrate was used yielding a large-area poly-Si microhole array (inset Figure 56). This structure exhibits a substantial increase of absorption in the entire spectral range compared to a reference film (thickness 2.1 µm) on a planar glass substrate, which was deposited in the same coating process (Figure 56). During the measurement the poly-Si samples without any antireflective coating have been placed inside the integrating sphere of the optical spectrometer in order to collect all scattered light. The absorption enhancement is particularly strong in the near infrared where the extinction coefficient of crystalline silicon is low. At a wavelength of 900 nm the silicon absorption is boosted from about 7% (planar) up to 41% (structured) although the effective layer thickness of the microhole array is lower (d_{eff}=1.5 µm) due to the removal of material in the holes. A solar cell device based on these poly-Si microhole arrays should be feasible if the increased surface area is well passivated. However, these structures might also be suitable for applications in other fields of optics such as photonic crystals.

Figure 56: Absorption spectra of a solid phase crystallized 2 µm-periodic poly-Si microhole array (black) and a planar poly-Si film (grey) with a nominal layer thickness of 2.1 µm. The microhole array (see inset) was fabricated via a bottom-up process on a nanoimprint-textured glass substrate. Courtesy: Oerlikon Solar AG, 2012

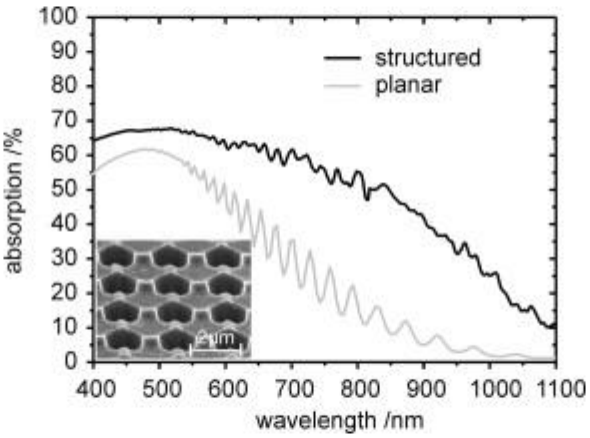

The use of nanoimprint-lithographically textured glass substrates as light trapping structures is an appealing option also for liquid phase crystallized poly-Si thin-film solar cells. The inset of Figure 57 shows a cross-sectional SEM micrograph of a 6 µm thick electron–beam crystallized poly-Si thin-film on nanoimprinted glass substrate with 2 µm periodicity.

---

[108] C. Becker, V. Preidel, T. Sontheimer, C. Klimm, E. Rudigier-Voigt, M. Bockmeyer, B. Rech. Direct growth of periodic silicon nanostructures on imprinted glass for photovoltaic and photonic applications. Physica Status Solidi C Current Topics in Solid State Physics, 9 (2012), pp. 2079–2082

[109] S.E. Han, G. Chen. Optical absorption enhancement in silicon nanohole arrays for solar photovoltaics. Nano Letters, 10 (3) (2010), pp. 1012–1015

Figure 57: Absorption spectra of a liquid phase crystallized poly-Si thin-film on a 2 µm-periodically structured glass substrate (black) and a reference film on a planar glass substrate, both with a nominal thickness of 6 µm. The inset shows a cross-sectional SEM micrograph of the LPC poly-Si thin-film on nanoimprint-textured glass substrate. Courtesy: Oerlikon Solar AG, 2012

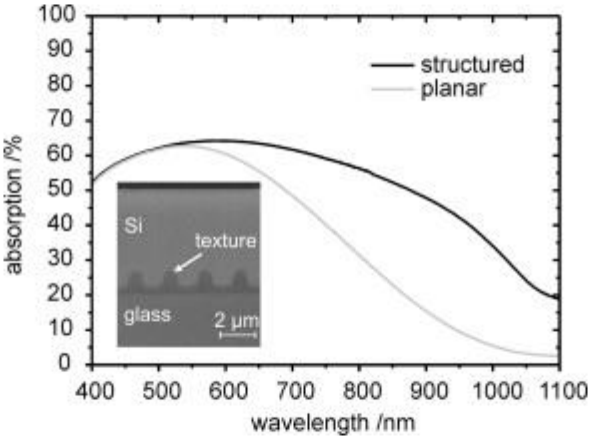

Here, the sol-gel was covered by a SiO_x(200 nm)/SiC_x(50 nm) barrier/wetting layer stack such that the texture is able to withstand the high temperatures present during the short-term LPC process. This demonstrates that LPC is not limited to planar interfaces. The absorption of this structured e-beam crystallized poly-Si thin-film on a 2 µm square lattice periodic glass substrate is significantly increased in the wavelength range above 600 nm compared to a planar poly-Si reference film with the same thickness (6 µm) as can be seen in Figure 57. The large absorption at the band edge at 1100 nm very likely arises from defect absorption multiplied by the light trapping effect. At 900 nm the backside grating realized by the nanoimprinted solgel texture leads to a strong increase of the absorption by a factor of three from about 15% to 48% although only the rear side of the poly-Si film is textured and the front side is completely planar. The surface reflectivity can be significantly reduced by front side texturing, e.g. by large area nanowire arrays fabricated from electron beam crystallized poly-Si by nanosphere lithography and reactive ion etching exhibiting a drastic gain in absorption.[110]

2.2.4.3.3 Liquid phase crystallization of silicon by electron–beam

Poly-Si thin films fabricated by liquid phase crystallization exhibit the largest grains and the best electrical material quality in terms of V_{OC}. The best LPC poly-Si thin-film solar cells were prepared by laser crystallization and exhibit an efficiency of 8.4%. Another possibility for the preparation of LPC poly-Si is the crystallization by a line-focused electron–beam yielding the highest V_{OC} of 582 mV in poly-Si thin-film solar cells up to date. Figure 58 shows the schematic of the electron beam crystallization setup employed at Helmholtz-Zentrum Berlin. Emerging from a constant current heated tungsten cathode, the electrons are focused electrostatically onto the substrate. The samples are placed on top of a heated graphite chuck in order to reduce the thermal gradient in the substrate, and are pulled underneath the line source with a constant scanning speed while the electron-gun is fixed in the tool. As LPC methods benefit from high-rate silicon

---

[110] S.W. Schmitt, F. Schechtel, D. Amkreutz, M. Bashouti, S.K. Srivastava, B. Hoffmann, C. Dieker, E. Spiecker, B. Rech, S.H. Christiansen. Nanowire arrays in multicrystalline silicon thin films on glass: a promising material for research and applications in nanotechnology. Nano Letters, 12 (8) (2012), pp. 4050–4054

evaporation processes, a combined evaporation and crystallization tool is feasible. From this point of view especially electron beam methods are the predominant choice, as deposition and crystallization can be combined in a single vacuum environment.

Figure 58: Schematic of the electron gun (top) and picture of the crystallization process (bottom). Courtesy: Helmholtz-Zentrum Berlin, 2012

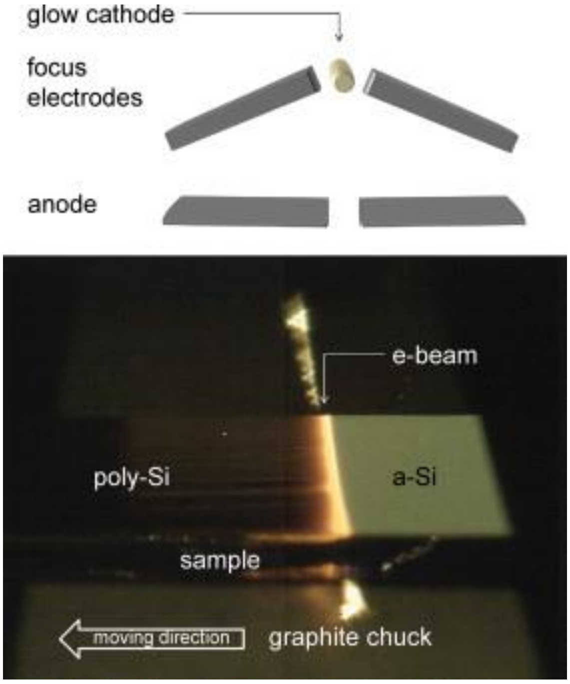

The experimental setup facilitates a large degree of freedom, such that the poly-Si microstructure can be varied systematically. Typical process parameters are a scanning speed of 6 mm/s to 20 mm/s and an energy density around 100 J/cm^2 for a 10 µm thick silicon layer on Corning Eagle XG glass substrates. Depending on the chosen speed and energy, different morphologies can be obtained. While grains in proximity to the air/Si interface exhibit a size of up to 10 µm (scanning speed of 12 mm/s in combination with an energy density around 65 J/cm^2), crystals close to the Si/diffusion barrier interface are considerably smaller. This peculiar vertical grain size distribution can be explained by a partial melting of approximately the upper 2/3 of the absorber's silicon layer. Increasing the energy density (72 J/cm^2) during crystallization and extending the duration of the liquid phase by a slightly reduced scanning speed of 10 mm/s, a homogeneously crystallized absorber is produced exhibiting grains of 2–10 µm in size. A further increase in energy density (75 J/cm^2) yields macroscopic grains throughout the entire absorber which extend up to centimeters in length along the scanning direction. Obviously the temperature gradient inside the absorber is too small to cause a high nucleation rate along the cross-section, hence the re-solidified regions (where the e-beam has passed) act as seed during grain growth.

All LPC techniques – using laser, electron–beam, halogen lamps or other alternatives – require a careful choice of appropriate interlayers between glass substrate and silicon during the high-temperature crystallization. In general, these layers must be deposited free of hydrogen, as rapid hydrogen effusion will occur during crystallization, causing partial or full delamination of the layers. Therefore sputter- or PECVD-processes at elevated temperatures are the deposition methods of choice for interlayer deposition. Using a line shaped electron beam, for instance, an a few hundred nanometer thick layer of amorphous SiC_x:B deposited by radio frequency (RF) magnetron sputtering on Corning Eagle XG substrates enables the liquid phase crystallization of an approximately 10 μm thick silicon absorber. SiC_x layers enable a wide process window with respect to the amount of heat introduced to the absorber until dewetting occurs, thus allowing a stable and homogeneous crystallization over the entire sample on large areas. Furthermore, a boron reservoir inside this layer can be used to provide an appropriate absorber dopant level about 10^{16} cm^{-3}.[111]

In recent publications[112] a-SiC_x was partially or fully replaced by SiO_x or SiN_x for different reasons: Comparably thick layers of amorphous SiC_x tend to crack during crystallization due to the brittleness of the material. This problem was tackled by reducing the SiC_x thickness significantly and adding a separate diffusion barrier such as SiO_x which is known as an effective barrier against the diffusion of impurities inside the glass substrates. As determined from secondary ion mass spectroscopy (SIMS) data, a combined interlayer of 200 nm SiO_x and 10 nm SiC_x is sufficient to suppress impurity diffusion from the substrate into the absorber. The impurity concentrations of Fe, Ni and Cr were found to be below the detection limit of SIMS ($<10^{13}$–10^{14} cm^{-3}), the Al concentration was below 10^{15} cm^{-3} and oxygen was found with a concentration of 7×10^{17} cm^{-3}. In addition, no cracks of the crystallized silicon layer were observed after electron-beam crystallization over the entire sample area.

By using these barriers, the short circuit current density of solar cells was increased by 33% compared to the previously achieved results. Further improvement of the cells electrical performance is expected to be achieved by optimized post-crystallization treatments such as hydrogen passivation as well as embedding a defined p^+ doped region at the glass/silicon interface to act as a back surface field. By an implementation of periodic light trapping structures a strong increase of the short circuit current density might be reached. If optical energy sources like lasers are used such a surface roughness would cause light scattering during crystallization giving rise to inhomogeneous energy doses over the sample's surface. Using an electron–beam for crystallization, however, might be advantageous to crystallize silicon on textured substrates, since scattering effects will not occur thus a homogeneous energy dose is maintained. The low fill-factor stems from poor adhesion of the front contact grid which can be improved by using additional adhesion layers. In conclusion: Electron–beam crystallization of silicon yields poly-Si thin-films with excellent electrical material quality yielding V_{OC} values up to 582 mV and a V_{OC} potential clearly above 600 mV. However, a good absorber material quality is only the first step towards a high-efficient poly-Si thin-film solar cell and more effort is required to optimize the device design. Recent work on laser crystallized poly-Si

---

[111] D. Amkreutz, J. Mueller, M. Schmidt, T. Haenel, T.F. Schulze. Electron–beam crystallized large grained silicon solar cell on glass substrate. Progress in Photovoltaics: Research and Applications, 19 (8) (2011), pp. 937–945

[112] J. Dore, R. Evans, B. Eggleston, S. Varlamov, M. Green, Intermediate layers for thin-film polycrystalline silicon solar cells on glass formed by diode laser crystallization, in: MRS Proceedings, vol. 1426, 2012

thin film solar cells have demonstrated that an improved device structure yields encouraging efficiencies up to 8.4%. The implementation of periodic light trapping structures is possible giving rise to a promising absorption enhancement. By combining these prospective elements with an innovative device concept, high conversion efficiencies are within the realms of possibility.

2.2.4.4 Conclusions: silicon thin-films

In the past, poly-Si thin-film solar cells were often classified by correlating the grain size with solar cell performance parameters V_{OC} and/or efficiency. As a general trend, cell efficiency was found to drop with decreasing grain size. With the extremely high V_{OC} demonstrated by Matsuyama et al. as an exception (Table 13) this trend is still visible. Diverse technologies have been developed in the past years for the fabrication of poly-Si thin film solar cells. The current poly-Si thin-film solar cell efficiency record is still held by an SPC device. However, due to the limited grain size accompanied by a moderate material quality (V_{OC}<500 mV) and long-lasting expensive fabrication processes the SPC technology was not competitive enough to survive on the global market. By the seed layer approach larger grains and V_{OC} values, but no improved efficiencies were demonstrated. For poly-Si thin-film solar cells by direct growth no improvement of efficiency or material quality was realized. Liquid phase crystallization approaches for poly-Si thin-film solar cells have the highest potential to achieve large grains, high V_{OC} values and therefore high solar cell efficiencies by fast and cost-effective fabrication processes. Although the efficiencies lie still below the SPC record, the material quality with maximum V_{OC} above 580 mV is striking and the learning curve is steep. With an optimized optical and electrical device design, LPC approaches are likely to surpass the benchmark of 10.4% efficiency in the near future. The emerging trends in the field of poly-Si thin-film solar cells on foreign substrates are based on four technological methods for the fabrication of poly-Si thin-film solar cells that have been intensively investigated in the past years: Solid phase crystallization, the seed layer approach, direct crystalline growth and liquid phase crystallization. With 10.4%, the current poly-Si thin-film solar cell efficiency record is held by a device fabricated by solid phase crystallization. However, due to a limited material quality in terms of open circuit voltage and due to time-consuming, expensive fabrication techniques the commercial success was limited so far.

2.3 Concentrator photovoltaics

Besides Si and II–V materials, single-junction solar cells have also been researched for and demonstrated by III–V materials, and GaAs (Gallium arsenide) stands out with high cell efficiency that can be attributed to its direct band gap with a value suitable for PV application. However, GaAs solar cells have not been considered for wide terrestrial application because the material is very expensive. This restriction has been recently alleviated by the noticeable progress of adopting ’lift-off‘ technology in GaAs cells.[113] This lift-off technology allows the expensive substrate to be re-used after the epitaxial film is removed, and therefore the material cost is greatly reduced. Although not many fabrication details have been released by Alta Device, the commercial company that has deployed R&D on this topic, the basic concept is considered similar to the ’layer transfer‘ for Si thin cells. With this technology, a cell efficiency of 28.3% has been achieved; this is not only a new record for GaAs cells but also a record for all types of single-junction cells.[114] Furthermore, the efficiency of the modules made of thin film GaAs cells by the same company has created a record of 23.5%, which for the first time surpassed the 22.9% single-junction solar module efficiency that had been maintained by Si modules. The new high cell and module efficiencies open another promising avenue for low cost high efficiency PV in terrestrial applications. Research priorities include: (1) maintaining the high efficiency of solar cells grown from the same substrate; (2) exploring the limit of substrate re-use; (3) raising the growth rate of metal organic chemical vapor deposition (MOCVD) currently being used for epitaxial layer growth, or exploring other high-speed growth techniques; (4) producing larger modules of good uniformity; and (5) developing manufacturing equipment and procedures for high volume production.

Although single-junction solar cells of different materials are being improved for higher efficiency, multi-junction solar cells have also demonstrated a great progress. III–V materials are extensively explored for this purpose because they provide wide options of band gap and lattice constant for system optimization. Because of the high cost related to expensive materials and complex fabrication steps, multi-junction solar cells are usually adopted in concentrating PV (CPV) configurations for terrestrial application. Solar cell efficiencies can be dramatically improved by dividing the broad solar spectrum up into smaller wavelength ranges, each of which can be converted more efficiently, through the use of multijunction cells. Multijunction CPV solar cells are the only third-generation photovoltaic technology - cells with double or triple the 15%–20% efficiencies targeted by first and second generation PV cells[115] and able to overcome the Shockley–Queisser efficiency limit for single-junction cells - that are now in commercial production. A large measure of success has been achieved with 3-junction GaInP/GaInAs/Ge concentrator solar cells operating on this principle, the first solar cell technology of any type to reach over 40% efficiency,[116] and which is now the baseline technology for 40% production CPV cells.[117] As efficient as they are, however, this

---

[113] Bolinger M, Wiser R. Understanding trends in wind turbine prices over the past decade. Lawrence Berkeley National Laboratory; 2011

[114] Earth Policy Institute from European Photovoltaic Industry Association (EPIA), Global Market Outlook for Photovoltaics Until 2013 (Brussels: April 2009), p. 3; EPIA, Global Market Outlook for Photovoltaics Until 2015 (Brussels: May 2011)

[115] Green MA. Third generation photovoltaics: ultra-high conversion efficiency at low cost. Progress in Photovoltaics: Research and Applications 2001; 9: 123

[116] King RR, Law DC, Edmondson KM, Fetzer CM, Kinsey GS, Yoon H, Sherif RA, Karam NH. 40% efficient metamorphic GaInP/GaInAs/Ge multijunction solar cells. Applied Physics Letters 2007; 90: 183516

[117] Ermer JH, Jones RK, Hebert P, Pien P, King RR, Bhusari D, Brandt R, Al-Taher O, Fetzer C, Kinsey GS, Karam N. Status of C3MJ + and C4MJ Production Concentrator Solar Cells at Spectrolab. 37th IEEE Photovoltaic Specialists Conf. (PVSC), Seattle, Washington 2011

baseline 3-junction design is still far from the optimum combination of subcell bandgaps, and far from its efficiency potential.

Efforts to incorporate concentrators into PV modules date back to the 1970s. The basic idea is to use low-cost optical concentrators to reduce the required area of solar cells, which are more expensive than optics. Using the ratio of a concentrator's active area to a solar cell's area as the standard, CPV can be categorized as low-X (1–10X), mid-X (10–100X), and high-X (100–1000X).[k] In this section, we review the current status and potential R8D opportunities for the currently dominant type, high-X CPV. The most commonly adopted III–V multi-junction solar cells have three sub-cells, and their cost is two orders higher than that of Si cells. High-X concentrators may therefore be necessary for these multi-junction solar cells to compete with Si cells. Moreover, high-X CPV depends upon high-accuracy tracking, which introduces a significant additional cost. To compensate for the high costs of both solar cells and trackers, the commercial CPV systems in the market are usually around 500X.

Because the efficiency range from 40% to 50% is so leveraging, spanning a tipping point for which vast geographic regions become available for economic CPV plant operation without government subsidies, it is important to examine the variety of multijunction cell configurations that can take us well beyond 40%, even though these structures are generally more complex and technologically challenging than today's 3-junction cells. A progression of sample high-efficiency concentrator solar cell structures is shown in Figure 59, beginning with 3-junction cells of today and the near future, and advancing through 4-junction, 5-junction, and 6-junction cells with a variety of technologies. These include upright metamorphic (MM) cells, inverted metamorphic (IMM) cells with single, double, and triple (MMX3) graded buffer layers, epitaxial Ge and SiGe subcells, semiconductor bonding technology, and dilute nitride GaInNAsSb subcells.

Figure 59: Progression of various terrestrial concentrator solar cell designs, beginning with today's 3-junction C3MJ+ and 40% C4MJ cells, and increasing efficiency to over 50% under the concentrated AM1.5D spectrum[118]

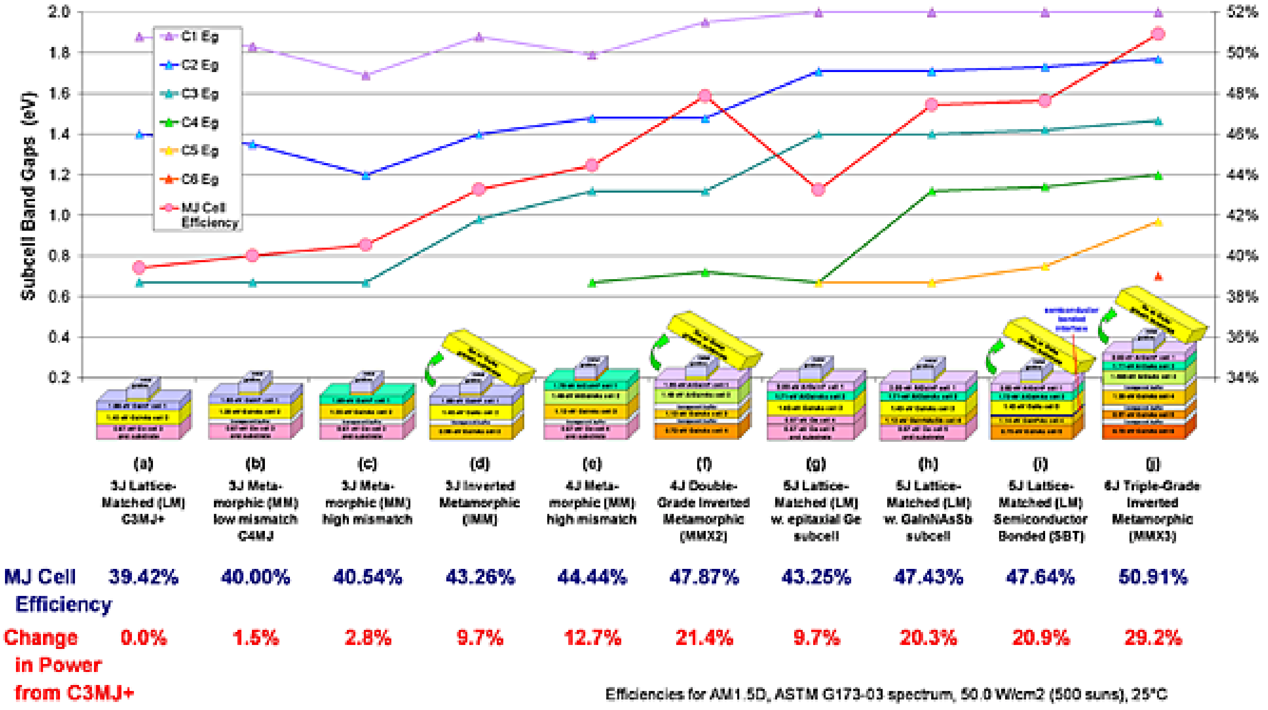

Projected average efficiencies in production are shown beneath each example cell type in Figure 59. Table 14 shows the best results for concentrator cells and concentrator modules (a smaller number of 'notable exceptions' for concentrator cells and modules additionally is included).

Table 14: Terrestrial concentrator cell and module efficiencies measured under the ASTM G-173-03 direct beam AM1.5 spectrum at a cell temperature of 25 °C[119]

Classification	Efficiency (%)[a]	Area[b] (cm2)	Intensity[c] (suns)	Test centre(and date)	Description
Single Cells					
GaAs	29.1 ± 1.3[d, e]	0.0505 (da)	117	FhG-ISE (3/10)	Fraunhofer ISE
Si	27.6 ± 1.0[f]	1.00 (da)	92	FhG-ISE (11/04)	Amonix back-contact
Multijunction cells (monolithic)					
GaInP/GaAs/GaInNAs	44.0 ± 3[g]	0.3104 (ap)	942	NREL (10/12)	Solar Junction
InGaP/GaAs/InGaAs	43.5 ± 2.6[h]	0.167 (da)	306	FhG-ISE (4/12)	Sharp, inverted metamorphic
GaInP/GaInAs/Ge	41.6 ± 2.5[e]	0.3174(da)	364	NREL (8/09)	Spectrolab, lattice-matched
Submodule					
GaInP/GaAs;	38.5 ± 1.9[i]	0.202 (ap)	20	NREL (8/08)	DuPont et al., split

---

[118] R. R. King, D. Bhusari, D. Larrabee, X.-Q. Liu, E. Rehder, K. Edmondson, H. Cotal, R. K. Jones, J. H. Ermer, C. M. Fetzer, D. C. Law, N. H. Karam. Solar cell generations over 40% efficiency. Progress in Photovoltaics: Research and Applications / Special Issue: 26th EU PVSEC, Hamburg, Germany 2011, Volume 20, Issue 6, pages 801–815, September 2012

[119] Martin A. Green et at. Solar cell efficiency tables (version 41). Progress in Photovoltaics: Research and Applications. Volume 21, Issue 1, pages 1–11, January 2013

Classification	Efficiency (%)[a]	Area[b] (cm2)	Intensity[c] (suns)	Test centre(and date)	Description
GaInAsP/GaInAs					spectrum
Modules					
Si	20.5 ± 0.8[d]	1875 (ap)	79	Sandia (4/89)[j]	Sandia/UNSW/ENTECH (12 cells)
Triple Junction	33.5 ± 0.5[k]	10,674.8 (ap)	N/A	NREL (5/12)	Amonix
'Notable Exceptions'					
Si (large area)	21.7 ± 0.7	20.0 (da)	11	Sandia (9/90)[j]	UNSW laser grooved

Any changes in the tables from those previously published are set in bold type.

1. [a] Effic., efficiency.
2. [b] (da), designated illumination area; (ap), aperture area.
3. [c] One sun corresponds to direct irradiance of 1000 Wm^{-2}.
4. [d] Not measured at an external laboratory.
5. [e] Spectral response reported in Version 36 of these Tables.
6. [f] Measured under a low aerosol optical depth spectrum similar to ASTM G-173-03 direct
7. [g] Current–voltage curve reported in the present version of these Tables.
8. [h] Spectral response and current–voltage curve reported in present version.
9. [i] Spectral response reported in Version 37 of these Tables.
10. [j] Recalibrated from original measurement.
11. [k] Based on ASTM E2527 rating, May 2012 (850 W/m^2 direct irradiance, 20 °C ambient, 4 m/s wind speed).

Triple-junction concentration solar cells have achieved a record efficiency of 43.5% at 418X.[114] Applying the principle of detailed balance, an ideal triple solar cell with band gaps of 0.94, 1.34, and 1.86eV that are optimized for current-match conditions can operate with an efficiency of 55.9% at the same concentration. The realized solar cell efficiency corresponds to 78% of the theoretical limit. Researchers continue to investigate even higher cell efficiency by applying alternative growth techniques to relax the restriction posed by lattice match so that the band gaps can further approach the theoretical optimal values. One example is the inverted lattice-mismatched GaInP/GaInAs/GaInAs solar cell that can tolerate more lattice mismatch by growing the epitaxial layers inversely and gradually increasing the order of lattice mismatch. This growth technique can realize band gaps closer to the theoretically optimal values and therefore higher solar cell efficiency. Efficiency (40.8%) at 326X has been achieved, and 45% efficiency is expected with continued development. Although noticeable progress has been observed on triple-junction concentration solar cells under standard measurement conditions, their performance in long-term operation needs more careful assessment. Triple-junction solar cells adopted in commercial CPV systems utilize a monolithic structure with the three sub-cells connected in series. The cell designs in Figure 60 represent only a few of the possible cell architectures leading to efficiencies from 40% to 50% but each serves as an example of the design considerations, some positive, some negative, that must be contended with on this path. Beginning toward the left, Figure 59 (b) shows a 3-junction upright MM cell structure. A larger schematic cross-section of this cell design, which corresponds to the 40% production average efficiency C4MJ cell, is shown in Figure 60 (a). Calculated light *I*–*V* curves for each subcell and the integrated 3 J cell are plotted in Figure 60 (b). Such 3-junction upright metamorphic GaInP/GaInAs/Ge concentrator cells have higher efficiency in principle than their lattice-matched (LM) counterparts, because the larger lattice constant in the metamorphic upper subcells (subcells 1 and 2) allows their bandgap to be lowered. For the wavelength distribution of the solar spectrum, the tradeoff between current and voltage is favorable for the lower bandgaps of the metamorphic upper subcells. This tradeoff results in maximum efficiency for an MM GaInAs subcell 2 composition of around 16%–17% indium in 3-junction GaInP/GaInAs/Ge cells, and with the composition of the MM GaInP subcell 1 at the same lattice constant. Figure 59 (c) shows a schematic cross-section of this cell type, with 40.5% projected production average efficiency under the AM1.5D solar spectrum. The lower lattice mismatch and subcell 2 composition of 5%-In GaInAs in 40%-efficient C4MJ cells represent a more robust, lower manufacturing cost approach than cells with higher indium content and lattice mismatch in the upper subcells, that still delivers substantial gain in cell efficiency, as well as providing the first step for commercial solar cells on the technology path to metamorphic cell architectures.

Figure 60: (a) Cross-sectional diagram and (b) illuminated *I*–*V* curves for subcells and the full multijunction cell for a 3-junction, upright metamorphic (MM) GaInP/GaInAs/Ge concentrator solar cell (C4MJ), with modeled production average efficiency of 40.0% at 500 suns (50.0 W/cm^2). Source: Source: Wiley Interdisciplinary Reviews, 2012

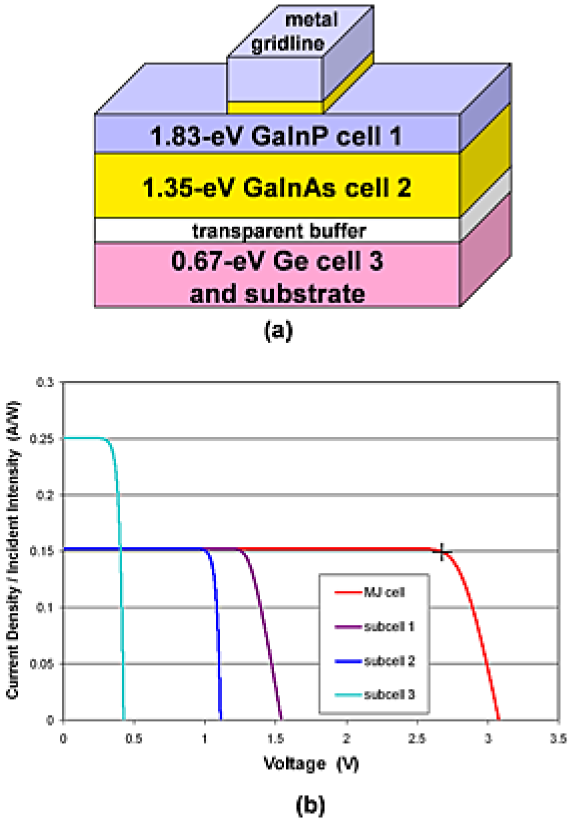

Both the design and measurement of these solar cells are based on a reference spectrum, usually ASTM G-173-03 Direct. However, the real spectrum can experience dynamic variation. The current match among the three sub-cells, or at least between the top and middle sub-cells, can be achieved under the reference spectrum, but it cannot be maintained constantly in real operation. Figure 61 shows the calculated efficiencies under different spectrum conditions for a triple-junction monolithic solar cell with band gaps optimized for current match.

Figure 61: Calculated efficiencies for ideal two-terminal triple-junction cells at 100X. The black dots are calculated using real spectrum at Golden, CO, USA in 2002. The red line is calculated under a simple assumption that air mass is the only factor that affects spectrum[120]

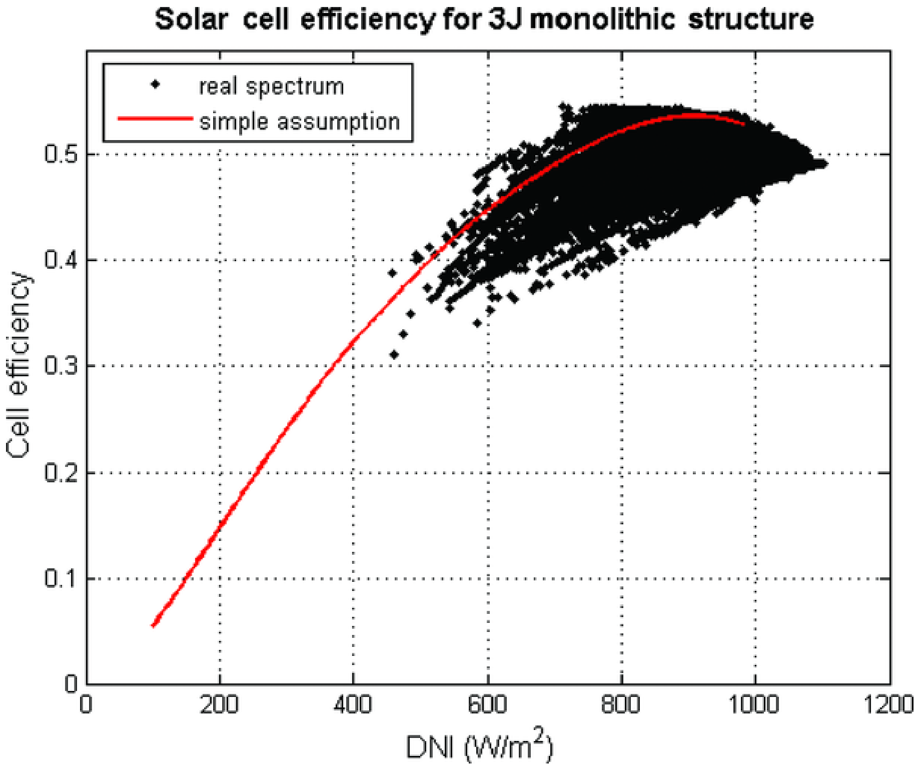

The purpose of Figure 61 is not to show the absolute value of the efficiency but to demonstrate the large efficiency deviation for a triple-junction monolithic solar cell; this great deviation is due to current mismatch caused by spectrum variation. The variation range can be greater than 20% even at high irradiation ranges. In Figure 61, efficiencies are not plotted in the low irradiation range because spectrum data are not available under those conditions. As CPV plays a more serious role in the PV market, the spectrum sensitivity issue has garnered more and more attention. Exploring research pertinent to this topic can be found in recent publications by academic institutes and commercial companies.[121,122,123,124,125,126] Considering the significant influence of spectrum variation

---

[120] X. Wang, J. Byrne, L. Kurdgelashvili, A. Barnett. High efficiency photovoltaics: on the way to becoming a major electricity source. Wiley Interdisciplinary Reviews: Energy and Environment, Volume 1, Issue 2, September/October 2012, Pages: 132–151

[121] Muller M, Marion B, Kurtz S, Rodriguez J. An investigation into spectral parameters as they impact CPV module performance. Proceedings of the 6th International Conference on Concentrating Photovoltaic Systems 2010, 307–311

[122] Peharz G, Siefer G, Araki K, Bett AW. Spectrometric outdoor characterization of CPV modules using isotype monitor cells. Proceedings of the 33rd IEEE PVSC 2008, 1–5

[123] Philipps S, Peharz G, Hoheisel R, Hornung T, Al-abbadi NM, Dimroth F, Bett AW. Energy harvesting efficiency of III-V triple-junction concentrator solar cells under realistic spectral conditions. Solar Energy Materials Solar Cells 2010, 94:869–877

[124] Chan N, Young T, Brindley H, Chaudhuri B, Ekins-Daukes NJ. Variation in spectral irradiance and the consequences for multi-junction concentrator photovoltaic systems. Proceedings of the 35th IEEE PVSC 2010, 003008–003012

[125] Kinsey G, Nayak A, Liu M, Garboushian V. Increasing power and energy in Amonix CPV solar power plants. Journal of Photovoltaics 2011, 1:213–218

on solar cell efficiency and the limited spectrum data resources, it would be valuable to deploy more R8D activities to quantify spectrum sensitivity. The research can indicate the proper locations for CPV installations, where dynamic spectrum variation is observed to be comparatively low. For those locations with relatively stable spectrum conditions, the band gaps of the three sub-cells may be tuned for optimal energy generation in long-term operation.

Ideal efficiencies of over 59% are possible for 4-junction cells, and for 5-junction and 6-junction terrestrial concentrator cells, efficiencies over 60% are achievable in principle. By providing a higher theoretical efficiency, solar cell architectures with 4-junction, 5-junction, and 6-junction offer a route to greater average efficiencies in high-volume manufacturing as well. Significantly, energy production modelling for 4-junction, 5-junction, and 6-junction CPV cells with the changing terrestrial spectrum that occurs with changing sun angle over the course of the day indicates that such cells have much greater energy production than 3-junction cells, retaining most of their advantage in efficiency at the design point for production of kilowatt hours in the field.

4-junction AlGaInP/AlGaInAs/GaInAs/Ge upright metamorphic cells as shown in Figure 59 (e) and Figure 62 are attractive candidates for the next generation of concentrator solar cells, because they have a projected average efficiency over 44%, well in excess of the nominal 40% production efficiency of present C4MJ cells; they require only a single growth run and a single metamorphic buffer; they utilize upright layer growth, avoiding thermal budget and dopant memory issues that can occur in inverted growth; and avoid the extra process complexity, cost, and yield loss associated with handle bonding and substrate removal for inverted metamorphic cells. However, questions remain about whether the highly lattice-mismatched AlGaInP and AlGaInAs subcells, at around 1.5% mismatch to the lattice constant of the Ge growth substrate, corresponding to 22%-In GaInAs, and with substantial Al content, can have the required minority-carrier lifetimes and mobilities.

---

[126] Dobbin A, Georghiou G, Lumb M, Norton M, Tibbits T. Energy Harvest Predictions for a Spectrally Tuned Multiple Quantum Well. 7th International CPV Conference; 2011

Figure 62: (a) Cross-sectional diagram and (b) illuminated *I–V* curves for subcells and the full multijunction cell for a 4-junction, upright metamorphic (MM) AlGaInP/AlGaInAs/GaInAs/Ge concentrator solar cell, with modeled production average efficiency of 44.4% at 500 suns (50.0 W/cm^2). Source: Wiley Interdisciplinary Reviews, 2012

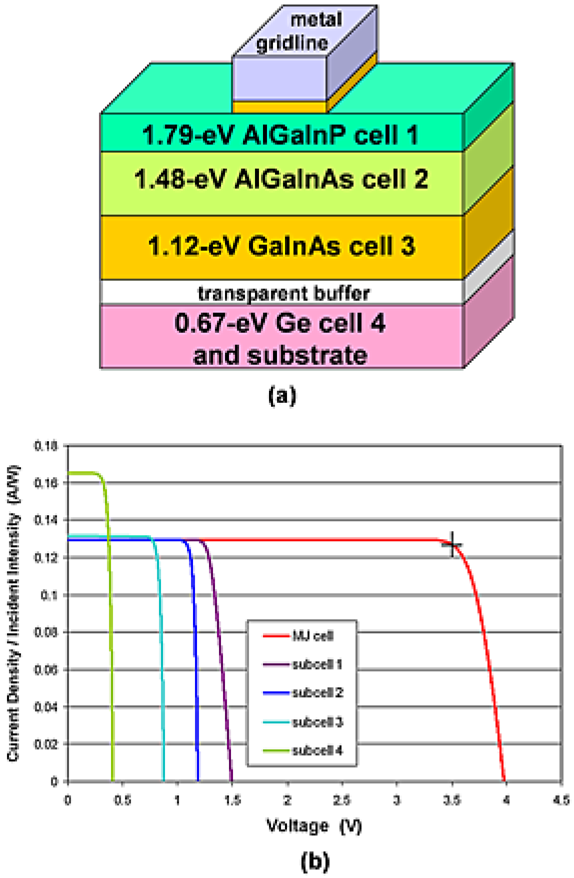

In another example, 5-junction cells with a dual-junction Ge/Ge subcell combination for the lower two subcells, using an epitaxially-grown Ge subcell 4, with an AlGaInP/AlGaInAs/GaInAs/Ge/Ge LM 5-junction structure as shown in Figure 59 (g) andFigure 63, also has an attractive projected 43.2% average efficiency. Other metamorphic variations using an epitaxial SiGe or SiGeSn subcell with higher bandgap than Ge can have still higher efficiency. The cell shown in Figure 64 is fully lattice-matched, simplifying manufacturing and avoiding the time and materials associated with growth of a metamorphic buffer. The upright structure of the 5-junction Ge/Ge cell also has the significant reduced thermal budget, reduced dopant memory, and reduced processing cost advantages described in the last paragraph, compared with inverted metamorphic structures. However, questions remain about the material quality, minority-carrier properties, and high degree of transparency needed for the epitaxial Ge, SiGe, or SiGeSn subcells.

Figure 63: (a) Cross-sectional diagram and (b) illuminated *I–V* curves for subcells and the full multijunction cell for a 5-junction, lattice-matched AlGaInP/AlGaInAs/GaInAs/epitaxial Ge/Ge concentrator solar cell, with modeled production average efficiency of 43.2% at 500 suns (50.0 W/cm²). Source: Wiley Interdisciplinary Reviews, 2012

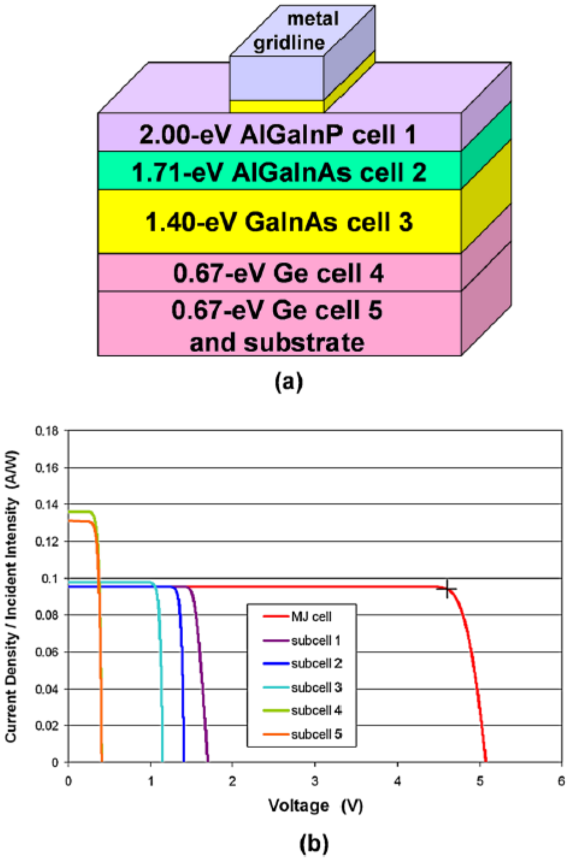

The need for a semiconductor with ~1-eV bandgap at or near the lattice constant of Ge or GaAs can be satisfied in principle using dilute nitride semiconductors such as GaInNAs or GaInNAsSb, with compositions around just 0.5% to 3% nitrogen. GaInNAs subcells grown by molecular beam epitaxy have demonstrated the necessary level of current density to be current matched in a 3-junction GaInP/GaAs/GaInNAs or 4-junction GaInP/GaAs/GaInNAs/Ge solar cell. Recently, a 3-junction cell using a dilute nitride bottom subcell was independently measured to have a record efficiency of 43.5%. Doping control and long minority-carrier diffusion lengths have historically been challenging to achieve in GaInNAs subcells grown by low cost, high throughput metal-organic vapor-phase epitaxy (MOVPE), though rich opportunities exist for growing these highly versatile ~1-eV GaInNAs(Sb) materials by low-cost growth methods.

Given the challenges in achieving high current densities in dilute nitride GaInNAs(Sb) materials, it can be advantageous to divide the solar spectrum more finely with the multijunction cell structure, such as a 5-junction or 6-junction cell, resulting in a high-voltage, lower-current multijunction cell for which the GaInNAs(Sb) cell can be current matched. GaInNAs cells with 1.168-eV bandgap have been grown at Spectrolab on 100-mm-diameter Ge wafers, in production-scale MOVPE reactors capable of growing 12 wafers per run at rates of 15–30 μm per hour, with open-circuit voltage V_{oc} of 684 mV at 1 sun. This bandgap-voltage offset $(E_g/q)-V_{oc}$ of 484 mV can be improved upon with further work and can already support many of the high-efficiency multijunction cell architectures envisioned with dilute nitride subcells. A 5-junction AlGaInP/AlGaInAs/GaInAs/GaInNAs(Sb)/Ge upright LM cell structure and projected average efficiency are shown in Figure 59(h) and Figure 64, with a projected production average efficiency of 47.4%. Again, the upright, LM structure of this design carries the formidable advantages of reduced thermal budget and dopant memory issues, and avoidance of the extra process complexity, cost, and yield loss associated with handle bonding and substrate removal, compared with inverted metamorphic cells. Integrated 4-junction cells with a similar subcell bandgap combination as the 5-junction cell, but with the dilute nitride subcell 4 absent, have been built and have reached measured efficiencies of 36.9% at 500 suns (50.0 W/cm^2) with relatively little optimization to date.

Figure 64: (a) Cross-sectional diagram and (b) illuminated *I–V* curves for subcells and the full multijunction cell for a 5-junction, lattice-matched AlGaInP/AlGaInAs/GaInAs/dilute nitride GaInNAs(Sb)/Ge concentrator solar cell, with modeled production average efficiency of 47.4% at 500 suns (50.0 W/cm^2). Source: Wiley Interdisciplinary Reviews, 2012

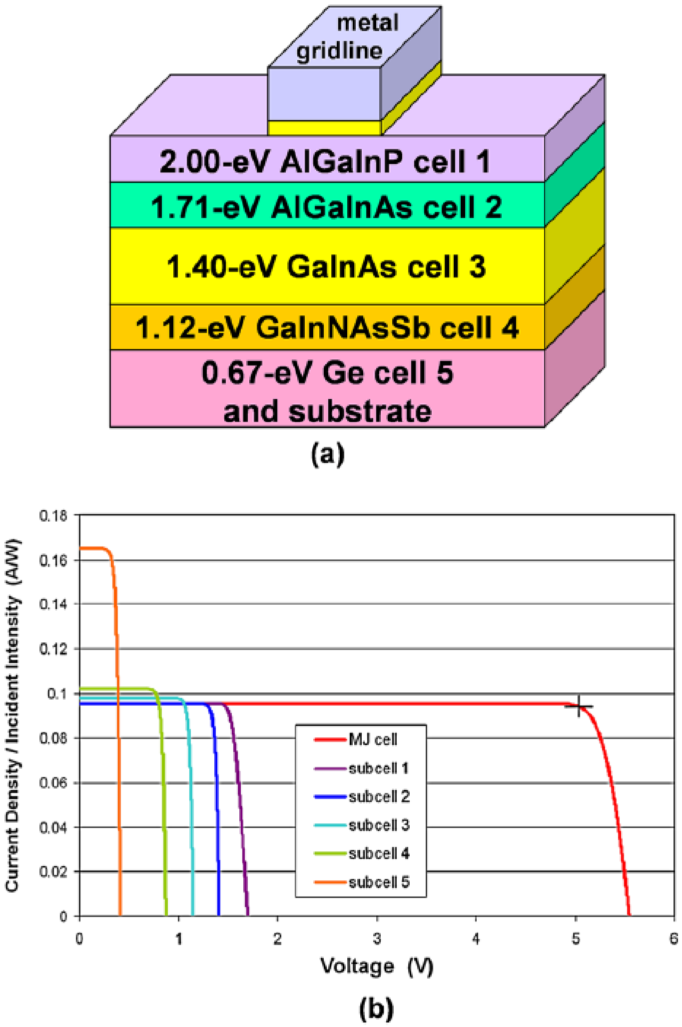

In spite of the greater expense and complexity associated with handle bonding and substrate removal for IMM cell structures, their ability to combine high bandgap, LM cells with low bandgap, metamorphic cells, with a high degree of bandgap flexibility, allows for very high efficiencies in practice. An example of a 6-junction

AlGaInP/AlGaAs/AlGaAs/GaInAs/GaInAs/GaInAs IMM cell with an MMX3 buffer structure is shown in Figure 59 (j) and Figure 65. The inverted metamorphic structure allows the bandgap combination needed for a projected 50.9% production average efficiency to be grown in a single growth run, albeit one with three metamorphic buffers. Questions about the achievable electronic properties of these new solar cell compositions and structures need to be answered experimentally, and these empirical studies will show which of the many promising theoretical solar cell designs are best suited to high-volume production.

Figure 65: (a) Cross-sectional diagram and (b) illuminated *I*–*V* curves for subcells and the full multijunction cell for a 6-junction, inverted metamorphic (IMM) cell and three transparent graded buffer regions (MMX3), with an AlGaInP/AlGaAs/AlGaAs/GaInAs/GaInAs/GaInAs structure, and with modeled production average efficiency of 50.9% at 500 suns (50.0 W/cm²). Source: Wiley Interdisciplinary Reviews, 2012

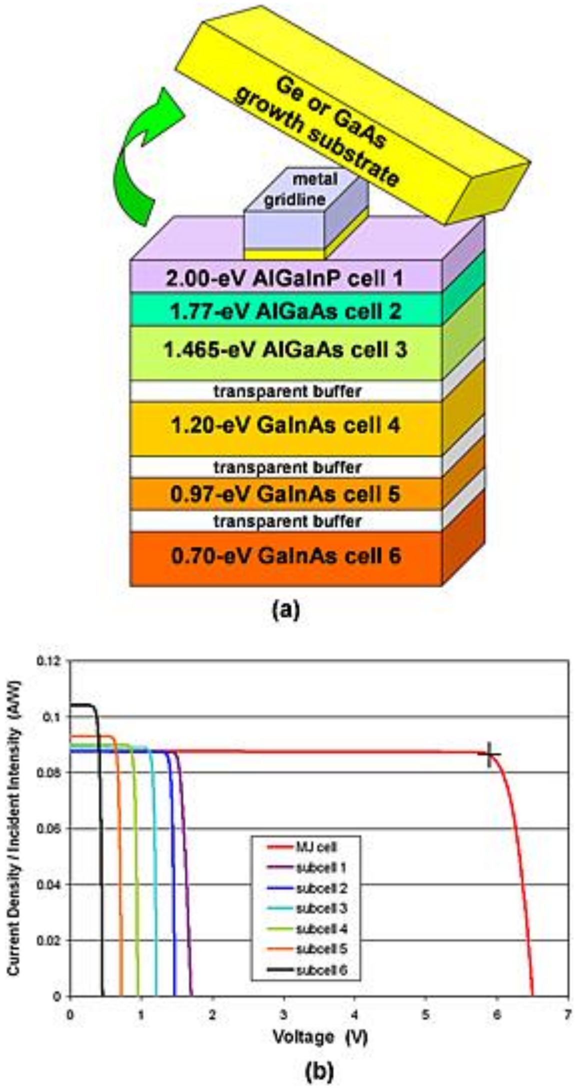

Another focus of CPV research is to further split the spectrum, using more junctions to absorb the broadband spectrum.[127] Combining this strategy with efforts to adjust band gaps to approach the optimal values can lead to future solar cell efficiency increases. However, actual operating conditions suggest that expanded spectrum splitting may

---

[127] International Energy Agency. Trends in photovoltaic applications survey report of selected IEA countries between 1992 and 2010. Report IEA-PVPS T1-20; 2011

create more problems than it solves. Highly dynamic spectrum variation raises doubt about the value of developing four-, five-, or six-junction solar cells, at least in a monolithic structure for terrestrial application. Figure 61 shows analyses only for triple-junction solar systems because they are the actual structures being adopted in the existing CPV market. It is predictable that, as the divisions of the spectrum increase, the solar cell efficiency will have a higher sensitivity to spectrum variation and therefore will experience more energy loss when the spectrum deviates from the standard. It remains to be seen if the efficiency gain by increasing the number of sub-cells predicted under the standard spectrum can be realized in field applications when dynamic spectrum variation occurs. For example, a switch from three to four sub-cells results in a theoretical efficiency gain of 8% (relative) under the standard spectrum.[128] However, in the field, a higher sensitivity to spectrum variation may make the energy production of the four-cell system close to or even lower than that of the three-cell system. Different from monolithic solar cells which split the spectrum in a vertical or a series way, another concept called 'lateral spectrum splitting' has recently been applied in some R8D projects. The basic principle is to split the spectrum using additional optics before the sunlight arrives at solar cells designed for different wavelength ranges. With the lateral spectrum splitting approach, the cells can be fabricated and optimized separately, and this can completely or partially release the restrictions of current match or lattice match. 36.7% and 38.5% record sub-module efficiencies have been demonstrated on prototypes of different structures. However, to prove the feasibility of this concept, more R8D efforts are required on the variation design of the electronic circuit because multiple outputs are present in the lateral structure compared with one output in the monolithic structure; also R8D efforts are required on module structure optimization because more components are present in the lateral structure than in the monolithic structure. Besides spectrum variation, another important issue that affects the performance of concentration triple-junction cells is the nonuniformity of illumination. In both the design and measurement phases of such a solar cell, it is assumed that the illumination is uniform across its surface. Although this condition is satisfied for flat plate PV, it cannot be guaranteed when a cell is assembled together with a concentrator and installed in the field. Although secondary optical components in high-X CPV are designed to homogenize the rays that pass through the primary concentrators, the designs are based on perfect tracking. When a tracking error occurs in field operations, the uniformity found in ideal tracking is not necessarily maintained. The nonuniformity of illumination directly causes voltage difference across a solar cell, which leads to lateral current flow and can be reflected as low FF on the I–V curve. This effect was analyzed as early as 1960 on a single p–n junction and discussed in the 1990s on a monolithic two-junction solar cell. The influence of nonuniform illumination on monolithic multi-junction solar cells necessitates three-dimensional analysis because the junctions are affecting each other when connected in series. Recent research suggests that in a CPV module utilizing secondary optics, the FF decreases by more than

---

[128] SEIA, GTM. US solar market insight Report, Q3 2011. Executive Summary; 2011

4%, whereas the short circuit current or Isc decreases by less than 2% at a tracking error of 0.5°. Considering the potential gain by improving the FF in real operating conditions, more R8D activities can be deployed to design secondary optics incorporating different tracking errors.

The above-mentioned issues concern CPV solar cell efficiency, but a large portion of energy is also lost on optics before it can even reach the cell. According to their working mechanisms, CPV concentrators can be categorized to two main types: reflective and refractive, as shown in Figure 66.

Figure 66: (a) A typical reflective CPV module structure; (b) a typical refractive CPV module structure. Source: Wiley Interdisciplinary Reviews, 2012

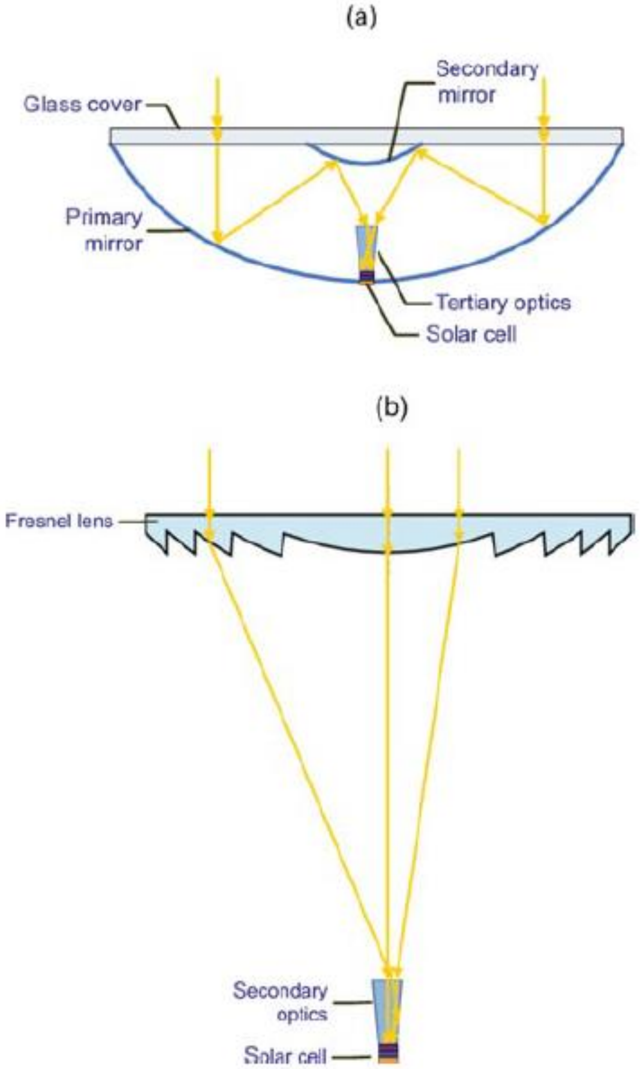

Compared with a refractive concentrator system (Figure 66 b), a reflective concentrator system (Figure 66 a) has the main advantage of compactness; the thickness of the module can be much smaller than the concentrator opening. This can potentially save material cost and facilitate fabrication, shipping, and installation. However, a reflective concentrator system has two more optical components where extra losses occur. One is the top glass cover, where an 8% optical loss occurs. The other is the secondary mirror, where another 8% optical loss occurs. Considering the higher optical efficiency, the following discussion is based on refractive concentrator systems. Refractive concentrators follow Snell's Law. A traditional smooth convex lens has a thickness proportional to the diameter of the lens. For lenses with diameters in the order of 10 cm, smooth lenses are too heavy and costly. To solve that problem, CPV modules usually adopt Fresnel lenses that have functioning grooves and dispose the chunk volume. The front side of a Fresnel lens is usually designed as a flat surface for cleaning convenience and to avoid dust accumulation. The Fresnel loss at the air–lens interface is 4%. At the rear surface of the lens, only rays passing through the optics axis have zero incidence angles at the lens–air interface; other rays are tilted and therefore have greater Fresnel losses. For a Fresnel lens with the *f*-number equal to 1, the loss is 5%. Compared with a smooth lens, extra losses on Fresnel lenses occur because of flaws at the non-ideal grooves, including non-zero draft angles and round corners. Sunlight striking flawed surfaces is scattered and cannot be guided to the target solar cell. For instance, a round corner of 5 μm radius and 3° draft angle can cause a 5% scattering loss. Considering the losses mentioned above, 87% of the direct normal irradiation (DNI) can pass through a Fresnel lens. However, these rays cannot be fully guided to the target solar cell because of the divergence angle of DNI, tracking errors, and chromatic aberration. The significant amount necessitates secondary optics. For an ideal solid secondary optics, the rays can either go through it without hitting the wall or strike the wall with an angle that satisfies TIR. Only considering the 4% Fresnel loss at the top surface and assuming zero absorption in the solid, the comprehensive optical efficiency is 83% at perfect system pointing. Although CPV trackers are still under development for more stable performance under diverse conditions, it is difficult to accurately quantify the frequency of tracking errors in field operation at this moment. For an optimistic estimation, we assume 5% efficiency loss due to pointing error, which can cause decline of both FF and Isc of the solar cells.

2.3.1 Conclusions: CPV

For future CPV modules of higher efficiency, there can be two major R&D directions: small units and low-mid X concentrations. The small unit concept means that each submodule has a small active area, creating several advantages. The first is at the optics level. The thickness of a smooth convex lens is proportional to its diameter, so a small dimension of the submodules of a CPV system allows smooth lenses to be adopted; therefore, the scattering loss at the non-ideal grooves of Fresnel lenses can be eliminated. The second advantage is at the electrical level. As the submodule area decreases, the resistive loss decreases. This is because the output power from a submodule is proportional to its operating current, or its active area, whereas its resistive loss is proportional to the square of its operating current. The third advantage is at the thermal level. For the same concentration, small submodules correspond to small solar cells and a smaller dimension of the cells is beneficial to heat dissipation. This is good because a cell's efficiency is inversely proportional to its operating temperature. The fourth advantage is at the material level. For the same concentration, small submodules correspond to thinner modules. Therefore, materials can be saved and lower cost is required for shipping and installation. Accompanying the advantages, there are two new problems. First, for the same active module area, small units mean a greater amount of the units, which may increase costs related to assembly. Currently, this problem has been solved by a technology called ’micro-printing‘. This technology can process many tiny solar cells at the same time. The other problem is the increased sensitivity to alignment error. Misalignment in actual manufacturing or assembling can cause higher losses for small submodules because a certain absolute value of the misalignment corresponds to a greater fraction of the operation dimension. It is yet to be proven that the high alignment accuracy can be maintained in both laboratory conditions and real operation.

Another R&D direction to achieve higher CPV module efficiency can be switching from high to low-mid concentration. Lower concentration can eliminate the use of secondary optics and/or reduce the sensitivity to system pointing. The success of this variation is intrinsically dependent on the cost decline of the multi-junction solar cells. Current technology used to fabricate III–V solar cells is MOCVD and most of the equipment is made by a commercial company named Veeco.[129] Veeco is developing new growth tools to realize fast growth of crystalline layers and reduce the fabrication cost of the solar cells. Another exploration direction is to adopt an innovation concept of ’lift-off‘ that allows multiple uses of expensive substrates for growth of thin epitaxial layers. For multi-junction cells, the micro-printing technology of the ’lift-off‘ concept allows the transfer of the tiny cells away from the growth substrate, indicating the potential of substrate re-use.

2.4 Emerging photovoltaics

It is widely accepted that solar cells can be broadly categorized into one of three technology “generations.” First generation cells are crystalline. Second generation cells are amorphous thin films of silicon and other materials meant to reduce costs normally associated with conventional semiconductor wafer production. The definition of third generation technology, however, is less clear, with the moniker “third generation” usually reserved for so-called emerging technologies.

The next generation photovoltaics are defined as high–efficiency, what is meant is energy conversion values double or triple the 15-20% range presently targeted, closer to the thermodynamic limit upon solar conversion of 93%[130,131] devices fabricated by using thin-film, second-generation deposition methods[132] or the other methods allowing large scale implementation.[133] The way to achieve these goals is to tackle one or both of

---

[129] http://www.veeco.com/

[130] M. A. Green. Third generation photovoltaics: Ultra-high conversion efficiency at low cost. Progress in Photovoltaics: Research and Applications. Volume 9, Issue 2, pages 123–135, March/April 2001

[131] Third Generation Photovoltaics: Advanced Solar Energy Conversion. Martin A. Green. Springer-Verlag Berlin Heidelberg 2003

[132] G. Conibeer. Third-generation photovoltaics (Review). MaterialsToday. Volume 10, Issue 11, November 2007, Pages 42–50

[133] G. Conibeer, S. Huang. Nanomaterials for third generation photovoltaics. International Journal of Nanoparticles. Volume 4, Number 2-3/2011, p. 200-215

the two major loss mechanisms in solar cells, that of non-absorption of below bandgap photons and thermalisation of carriers generated by photon energies exceeding the bandgap. This group is also sometimes described as any technology capable of overcoming the Shockley–Queisser limit of power conversion efficiency (33.7 percent) for a single junction device. Traditional c-Si or thin-film solar cells only harvest a fixed amount of energy from any given solar photon. However, the solar spectrum consists of photons with energies spanning 0.4 eV to 4.0 eV (Figure 67).

Figure 67: Spectral analysis of the minimum losses for a silicon solar cell (band-gap = 1.1 eV). These are the losses accounted for in the Shockley-Queisser limit and represent an upper limit for solar cells made from single-junction bulk semiconductors. Thermalization represents the largest loss in this analysis, and it increases for the higher energy portions of the solar spectrum. Courtesy by G. Conibeer and S. Huang

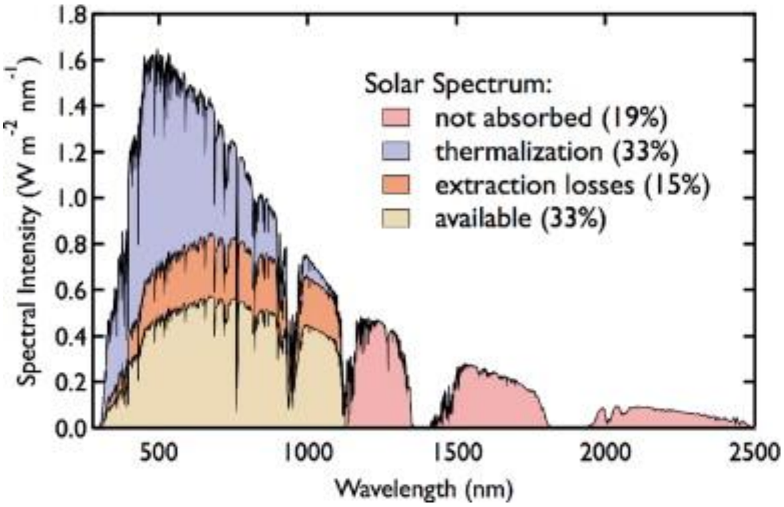

The band-gap of the semiconductor determines how much solar energy can be converted to electrical power: photons with energy less than the bandgap are not absorbed, while photons with energy greater than the bandgap lose excess energy unnecessarily via emission of phonons (thermalization). Figure 67 shows that the available free energy from an ideal present day single junction cell is about 33 %, while another 33 % is lost to thermalization and the remaining third is divided up between photons not absorbed and unavoidable thermodynamic losses. Those losses are associated with extracting photoexcited electrons at the contacts prior to radiative recombination. The analysis presented in Figure 67 was first introduced by Shockley and Queisser in 1961 and is for a solar cell of bandgap 1.1 eV operating under the AM1.5 global spectrum with 1000 W/m^2. First and second generation PV cells have best-cell power conversion efficiencies that are asymptotically approaching the Shockley-Queisser (SQ) limit; for example, the record for c-Si based solar cells is currently at 25 %, while for GaAs the record is 28.3 %. Next generation PV can have a higher limiting conversion efficiency by bypassing one of the assumptions of the SQ analysis and recovering either some of the energy lost via thermalization or providing pathways to harvest those photons not absorbed in a standard solar cell.

Most technologists would also include broad classes of other conversion devices including non-semiconductors such as polymer and dye-sensitized cells, tandem cells built from stacks of conventional materials (such as amorphous silicon or gallium arsenide), and nanotechnology. The new technologies and nanomaterials are expected to play important roles in solar cell technology in coming decade (Figure 68).

Figure 68: Basic research underway with the technology developments required to achieve the desired applications. Source: Nanotechnology for the energy Challenge, J. G. Martinez, 2010

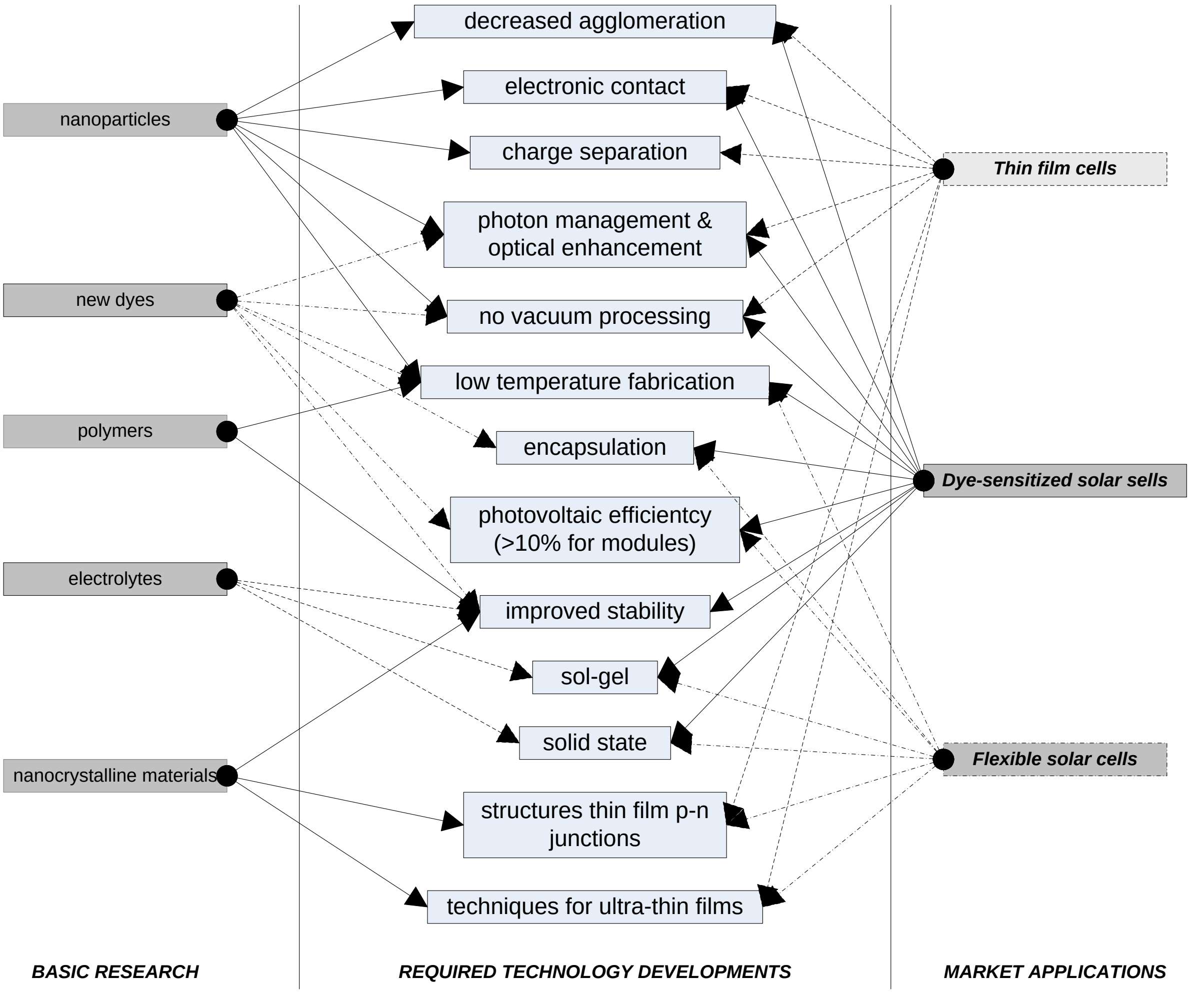

Emerging PV technologies, such as advanced organic solar cells and dye sensitized solar cells and solar cells based on novel concepts such as quantum and excitonic structures with their potential for cost reduction and performance improvement are forecasted to represent an increasing share of the PV deployment after 2020. However, significant R&D is still necessary to capture this potential.

2.4.1 Organic /Polymer solar cells

Organic /Polymer photovoltaic (OPV) research has been in an exponential growth phase since the early reports as witnessed by the number of papers produced yearly and the number of new scientists joining the field. This is naturally due to the pressing problem of finding sustainable energy solutions for the future, but perhaps also because the OPV technology is actually not very mature and possess a rich complexity offering many opportunities for research. This also has consequences for commercial exploitation, seemingly representing an uphill battle for an inferior PV technology having to compete with superior and established PV technologies that when taken together have to compete with many high performing renewable technologies such as wind energy and hydropower. The OPV technology is attracting because it promises to be very low cost, light weight, produced from abundant materials and easily manufactured at high speed in large scale on simple roll-to-roll printing machinery.[134,135] Calculations show that OPV technology is a potential technology, and cost-efficient power generation is achievable. A rough estimate from cost-model calculations shows that the low cost modules of OPV with lifetime between 5 and 10 years and efficiency between 8 and 10% can produce electricity at ~10 Euro cents/kWh.[136,137] On the other hand there are some evident hurdles to overcome: the present power conversion efficiency (PCE) is very low (≤10%) while optimistic projections have been made[138,] and the stability is also considered lacking.[139] Another problem that has not received much interest is the transition from square millimeter sized scientific devices arduously prepared in the laboratory to large scale technical production. In many ways it seems that the scientific pursuit of OPV has developed into a race for the best efficiency number through clever schemes of optimizing the chemistry and device fabrication rather than the more distant goal of producing practically useful solar cells. One of the reasons is perhaps that it is by no means settled which materials should be used and what the optimum construction of the OPV device is. It can thus be viewed as one of the attractions (and pitfalls) of OPV research that almost infinite variation is possible. Sometimes, it is argued that if polymer solar cells have such a huge potential, why are they still in the laboratories only? This question can be answered in this way that these devices still have to have many developments to be available in the market.

2.4.1.1 The state of the art of OPV

The progress of photovoltaic technologies is often summed up in a simple diagram of efficiency *versus* time and shows an impressive learning curve for OPV.[140] There has been steady progress in the performance; the polymer solar cell modules have been available for public demonstration, and the round robin studies have been started. There is a strong hope that, very soon, these devices will be capable enough to answer the critics. Along with the other solar cell technologies, year-wise progress in OPV has been

---

[134] R. Søndergaard, M. Hösel, D. Angmo, T.T. Larsen-Olsen, F.C. Krebs. Roll-to-roll fabrication ofpolymersolarcells,MaterialsToday15(2012)36–49.

[135] Y. Galagan, I.G. deVries, A.P. Langen, R. Andriessen, W.J.H. Verhees, S.C. Veenstra, J.M. Kroon. Technology development for roll-to-roll production of organic photovoltaics. Chemical Engineering and Processing 50 (2011) 454–461

[136] Dennler C, Scharber MC, Brabec CJ. Polymer fullerene bulk-heterojunction solar cells. Advanced Materials 2009; 21: 1323

[137] Dennler G, Brabec CJ. Organic Photovoltaics: Materials, Device Physics, and Manufacturing Technologies. Wiley-VCH: Weinheim, 2008

[138] M.C. Scharber, D. Wuhlbacher, M. Koppe, P. Denk, C. Waldauf, A.J. Heeger, C.L. Brabec. Design rules for donors in bulk-heterojunction solarcells – towards 10% energy-conversion efficiency. Advanced Materials 18 (2006) 789–794

[139] N. Grossiord, J.M. Kroon, R. Andriessen, P.W.M. Blom. Degradation mechanisms in organic photovoltaic devices. Organic Electronics 13 (2012) 432–456

[140] C.J. Brabec, S. Gowrisanker, J.J. Halls, D. Laird, S. Jia, S.P. Williams. Polymer-fullerene bulk-heterojunction solar cells. Advanced Materials 22 (2010) 3839–3856.

shown in Figure 69. The efficiencies of OPV are very low compared with other technologies, but still there are spaces where efficiencies can be improved further.

Figure 69: Year wise progress of different solar cell technologies. Source: National Renewable Energy Laboratory, 2012

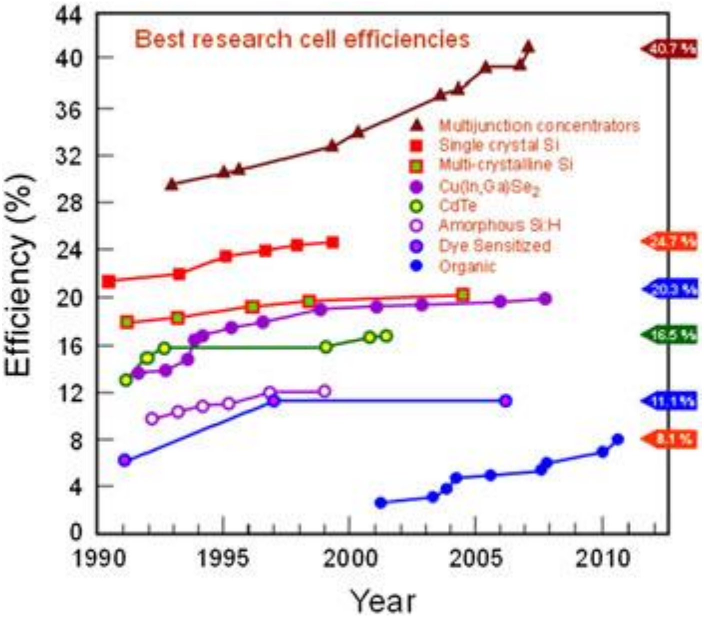

Since the first realization of photovoltaic effect in organic semiconductors[141] and then the introduction of donor-acceptor heterojunction concept in 1986,[142] there has been steady progress in the performance of OPV. The efficient photon harvesting via inter-mixing of donor–acceptor materials in a single layer (bulk heterojunctions – BHJ) revolutionized the technology and resulted into rather efficient devices.[143] These concepts stimulated the efforts to improve further the performance of OPV, and the number of publications on the research in OPV increased exponentially. The improved processing conditions, pre-fabrication and post-fabrication treatments, and the application of new advanced materials with new device designs have led these devices to high efficiencies. The best efficiency reported one decade earlier hardly reached beyond 1%, whereas efficiency more that 7% has been achieved today. Short life span of OPV is another important issue and needs serious attention. However, a few years back, OPV had a life span of only few hours, but today, the cells with outdoor life of more than 15 000 h have successfully been fabricated. By the use of advanced materials with high charge carrier mobilities and optimized nanoscale morphology, the efficiency of the devices is expected to increase further. From this point of view, research is also being carried out on organic–inorganic hybrid solar cells, which utilize the high charge carrier mobility of inorganic nanomaterials (ZnO, ZnS, CdSe, etc.) and wide-range absorption and solution processibility of conjugated polymers. Solar cells are prepared with both the small molecular and polymeric materials, and there is a head-to-head race going on

---

[141] Gosh AK, Feng T. Rectification, space-chargelimited current, photovoltaic and photoconductive properties of Al/tetracene/Au sandwich cell. Journal of Applied Physics 1973; 44: 2781–2788

[142] Tang CW. Two layer organic photovoltaic cell. Applied Physics Letters 1986; 48: 183–185

[143] P. Kumar, S. Chand. Recent progress and future aspects of organic solar cells. Prog. Photovolt: Res. Appl. 2012; 20:377–415

in between these materials towards being technologically more important. However, the device characteristics such as lifetime, efficiency, simplicity in fabrication process, and large-area device production may decide which one will rule the industry. However, it is expected that the tip may turn towards polymer devices.

For a quick comparison, the photovoltaic performance of some of the important solar cells are tabulated in Table 15.[143]

Table 15: Photovoltaic performance of some of the important organic solar cells by employing different device designs. Source: Wiley Interdisciplinary Reviews, 2012

Device	J_{sc} (mA/cm^2)	V_{oc} (V)	*FF* (%)	η (%)
Bilayer				
ITO/PEDOT:PSS/MDMO-PPV/PCBM/Al	0.96	0.78	0.5	0.5
ITO/CuPc (30 nm)/PTCBI (50 nm)/Ag	2.3	0.45	0.65	0.95
ITO/CuPc(18 nm)/SubPc(2 nm)/C_{60}(40 nm)/BPhen(8 nm)/Al	5.16	0.42	0.47	1.29
ITO/PPV (60 nm)/BBL (60 nm)/Al	2.15	1.1	0.50	1.5
ITO/MEH:PPV (60 nm)/BBL (60 nm)/Al	1.98	0.93	0.47	1.1
ITO/CuPc/PTCDA/In	2.0	0.55	0.35	1.8
ITO/SubPc (13 nm)/C_{60} (32.5 nm)/BCP (10 nm)/Al	3.36	0.97	0.57	2.1
ITO/NDP2 (1 nm)/ZnPc (14 nm)/C_{60} (1 nm)/ZnPc (3 nm)/C_{60} (2 nm)/ZnPc (2 nm)/C60 (3 nm)/ZnPc (1 nm)/C60 (34 nm)/BPhen (8 nm)/Al	10.13	0.49	0.51	2.2
ITO/PEDOT:PSS/tetracene (80 nm)/C_{60} (30 nm)/BCP (8 nm)/Al	7.0	0.58	0.57	2.3
ITO/pentacene (45 nm)/C60 (50 nm)/BCP (10 nm)/Al	15	0.36	0.50	2.7
ITO/Au (1 nm)/p-doped Di-NPB (30 nm)/Di-NPB (5 nm)/DCV5T (7 nm)/C60 (40 nm)/BPhen (6 nm)/	10.6	0.98	0.49	3.4
ITO/PEDOT:PSS/CuPc (20 nm)/C60 (40 nm)/BCP (12 nm)/Al	18.8	0.58	0.52	3.6
ITO/CuPc (20)/C60 (40 nm)/BCP (10 nm)/Ag	53.1	0.57	0.61	4.2
Bulk-heterojunction				
ITO/MEH-PPV:PCBM (1:4)/Ca	2.0	0.80	0.25	1.5
ITO/PEDOT:PSS/PFDTBT:PCBM (1:4)/LiF/Al	4.66	1.04	0.46	2.2
ITO/PEDOT:PSS/MDMO-PPV:PCBM (1:4)/LiF/Al	5.25	0.82	0.61	3.3
ITO/PEDOT:PSS/APFO-Green5:PCBM (1:3)/LiF/Al	8.88	0.59	0.49	2.2
ITO/CuPc:C60 (1:1, 33 nm)/C60 (10 nm)/BCP (7.5 nm)/Ag	15.4	0.50	0.46	3.5
ITO/CuPc(15 nm)/CuPc:C60 (1:1, 10 nm)/C60 (35 nm)/BCP (10 nm)/Ag	18.2	0.54	0.61	5.0
ITO/PEDOT:PSS/P3HT:PCBM (1:0.8)/Al	9.5	0.63	0.68	5.0
ITO/PEDOT:PSS/P3HT:PCBM/TiOx/Al	11.1	0.61	0.66	5.0
ITO/PEDOT:PSS/PCPDTBT:PCBM/Al	16.2	0.62	0.55	5.2
ITO/PEDOT:PSS/PTB7:PCBM/Al	14.5	0.72	0.69	7.4
Tandem				
ITO/p-MeO-TPD (30 nm)/ZnPc:C60 (1:2, 60 nm)/n-C60 (20 nm)/Au (0.5 nm)/p-Meo-TPD (125 nm)/ZnPc:C60 (1:2, 50 nm)/n-C60 (20 nm)/Al	10.8	0.99	0.47	3.8
ITO/CuPc (7.5 nm)/CuPc:C60 (12.5 nm)/C60 (8nm)/PTCBI (5nm)/Ag (0.5 nm)/ m-MTDATA:F4TCNQ (5 nm)/CuPc (6 nm)/CuPc:C60 (13nm)/C60 (16 nm)/BCP (7.5 nm)/Ag	9.7	1.03	0.59	5.7
ITO/PEDOT:PSS/PCPDTBT:PCBM/TiOx/PEDOT:PSS/P3HT:PCBM/TiOx/Al	7.8	1.24	0.67	6.5

In Figure 70 the power conversion efficiency (PCE) value of the individual 10533 solar cells are plotted against the year of submission for the paper.

Figure 70: The power conversion efficiency values obtained as a function of publication year, the inset shows the distribution of power conversion efficiency values. Courtesy by M. Jørgensen

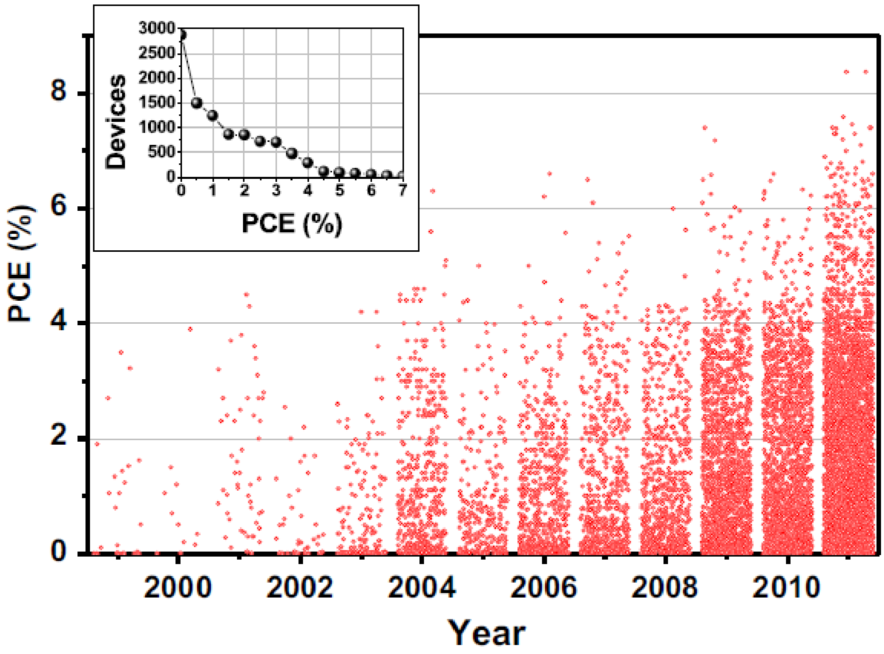

In most OPV papers the term "state of the art solar cells" are equated with the best or "hero" cells produced and these are normally used to indicate the status of the research field. It is clear that substantial progress is being made, but also that hero cells account for a very small part of the population and that they are not representative. Instead, the bulk of PCE values fall far below suggesting that these coveted results are actually rare exceptions. Remarkably, when the number of OPV devices is plotted as a function of PCE one does not get a normal distribution, but rather one that is skewed heavily toward zero PCE. One of the reasons is of course that the OPV field has become very complex with a huge number of possible variations in structure, chemical composition, fabrication history, interfacial layers *etc.*[144] As a consequence many less performing devices are reported describing non-ideal choices. Some are also due to comparative studies varying different factors and others may simply reflect less competent procedures. It must also be a testament to how poorly defined and documented OPV production is. Even skilled workers may have a hard time duplicating hero cells because it involves factors that are simply unknown or not made public.

The PCE is a function of the product of the open circuit voltage (V_{OC}), short circuit density (J_{SC}) and fill factor (FF) divided by the incident power of the light source (P_i):

$$PCE = \frac{V_{OC} J_{SC} FF}{P_i}$$

For bulk hetero-junction type OPV the upper limit for V_{OC} is believed to be determined by the energy difference between the LUMO energy level of the polymer/organic

---

[144] G. Li, R. Zhu, Y. Yang. Polymer solar cells. Nature Photonics 6 (2012) 153–161

molecule donor and the HOMO energy level of the acceptor material.[145] It is further reduced by the exciton binding energy and other factors. The fill factor of OPV devices vary greatly, but rarely exceeds 60%. It immediately follows that the factor of 0.55 is simply the product of VOC_{max} and FF_{max}. It is not a strict physical limit that cannot be overcome, but as the results show it seems very hard to do so. The VOC_{max} is also a linear function of the band gap which means that there is a trade-off in using low band gap polymers that harvest more low energy photons in that it reduces the possible VOC_{max}. The fill factor is a complex function of the electrical resistance elements in the device which in part depend on the sheet resistance of the electrodes. A common solution has been to decrease the cell size to less than 1 mm^2 to minimize these losses,[146] which would of course also limit their use in any practical application. The theoretical limits for the PCE of single cell OPV and estimated upper bounds fall in the range of 10–20%.[147] One of the main limiting parameters in organic solar cells is poor absorption. Large bandgap materials own a mismatch to the terrestrial solar spectrum. For example, poly(p-phenylene vinylenes) (PPVs) and polythiophenes, their bandgaps are ~1.85 and ~2.2 eV. The bandgap of 1.85 eV (absorb edge was at 670nm) only allowed 46% of photon was harvested. A bandgap of 1.1 eV (Si) allowed more than 90% of photon was harvested. The optical loss due to polymer bandgap mismatched with the solar spectrum is shown in Figure 71.

Figure 71: Optical losses due to polymer bandgap mismatch with solar spectrum. Source: W. Cai et al. Solar Energy Materials & Solar Cells, 2010

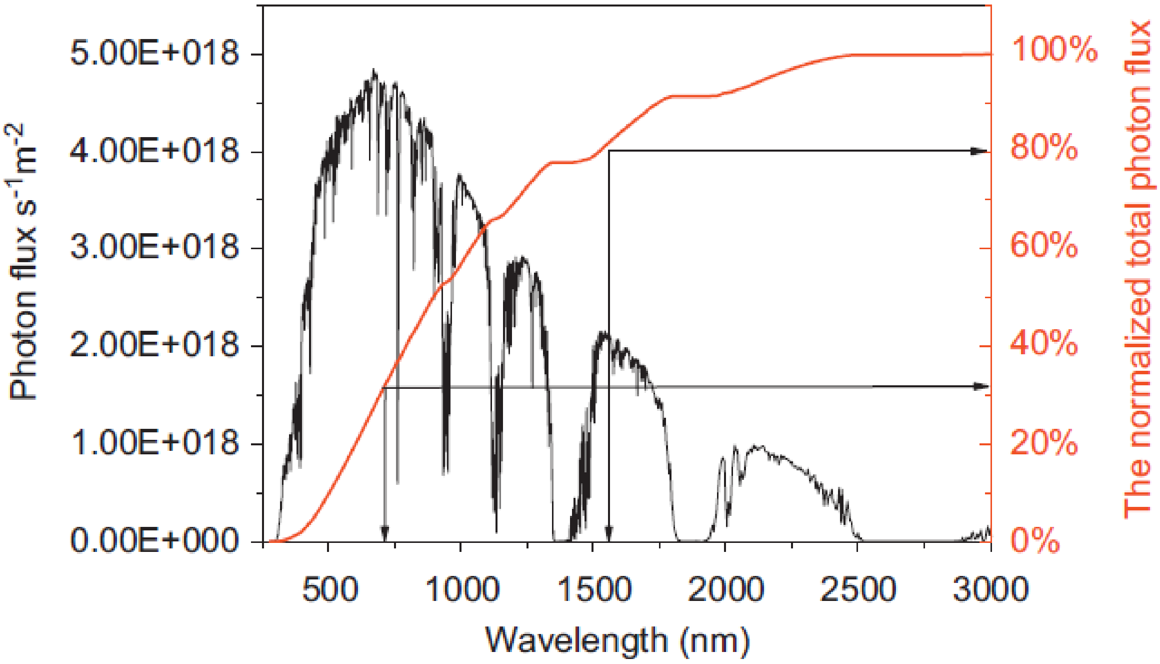

---

[145] T.M. Clarke, J.R. Durrant. Charge photogeneration in organic solar cells. Chemical Reviews 110 (2010) 6736–6767

[146] J.D. Servaites, S. Yeganeh, T.J. Marks, M.A. Ratner. Efficiency enhancement in organic photovoltaic cells: consequences of optimizing series resistance. Advanced Functional Materials 20 (2010) 97–104

[147] Z.M. Beiley, M.D. McGehee. Modeling low cost hybrid tandem photovoltaics with the potential for efficiencies exceeding20%. Energy and Environmental Science 5 (2012) 9173–9179

In order to exceed conversion efficiency over 10% from single layer polymer solar cells, the bandgap of donor polymers should be ~1.7eV and the LUMO of this donor polymers should be – ~3.9 eV if PCBM is used as the electron acceptor. The current state-of-art approaches to realize these low band gap donor polymers are based on donor–acceptor molecule structures. The strategy for synthesizing these polymers is often selecting donor unit with high ionization potential and acceptor unit with high electron affinity.

2.4.1.2 Outliers, polymers / acceptors and annealing / additives

An escape from the limitations of single cells is to construct tandem cell devices with two cells stacked on top of each other. The top and bottom cells should ideally harvest complementary regions of the spectrum and could at best double the V_{OC}.[148] The effect would be to increase the slope to obtain: $PCE_{max}=1.1\times J_{SC}$ doubling the possible efficiency. The number of papers describing tandem cells is still very small and the technical difficulties in the production of them seem to be very large.[149] Due to the limited spectral absorption range of the active components of OPV it has proven very hard to increase J_{SC} beyond 15 mA/cm^2.[150]. Chan et al. described two Copper Phthalocyanine/Rubrene based devices with staggering J_{SC}=22.9 mA/cm^2, PCE=4.72% and J_{SC}=30.1 mA/cm^2, PCE=5.58%.[151] Kim et al. used an optimized FTO electrode with the standard active layer mixture P3HT:PCBM to give four devices with J_{SC} 16.8–22.5 mA/cm^2.[152] A few of these high J_{SC} data points are due to devices with low band gap materials. Chen et al. described a silole-benzothiadiazole based copolymer (DTS-BDT) (J_{SC}=16.5 mA/cm^2).[153] Exchanging silicon for germanium Fei et al. obtained devices with J_{SC}=18.4 and 18.6 mA/cm^2.[154] In such cases experimental detail concerning the light source and illumination condition would enable more in depth analysis.

The polymers were subdivided into five categories: P3HT, MEH-PPV, MDMO-PPV, other polymers (mainly low band gap polymers) and none (usually molecular solar cells). In the case of acceptor materials solar cells incorporate C60, C70, PCBM Bis, ICBA and Bis-PCBM. The improvements in efficiency have been gained both in increased light harvesting resulting in a larger J_{SC}, but also by significantly increasing the V_{OC}. The main

---

[148] S. Sista, Z. Hong, L.M. Chen, Y. Yang. Tandem polymer photovoltaic cells - current status, challenges and future outlook. Energy and Environmental Science 4 (2011) 1606–1620.

[149] T.T. Larsen-Olsen, T.R. Andersen, B. Andreasen, A.P. Böttiger, E. Bundgaard, K. Norrman, J.W. Andreasen, M. Jørgensen, F.C. Krebs. Roll-to-roll processed polymer tandem solar cells partially processed from water. Solar Energy Materials and Solar Cells 97 (2012) 43–49.

[150] Y. Li. Molecular design of photovoltaic materials for polymer solar cells: toward suitable electronic energy levels and broad absorption. Accounts of Chemical Research 45 (2012) 723–733

[151] M.Y. Chan, S.L. Lai, M.K. Fung, C.S. Lee, S.T. Lee. Doping-induced efficiency enhancement in organic photovoltaic devices. Applied Physics Letters 90 (2007) 089902-1–089902-2

[152] H. Kim, G.P. Kushto, R.C.Y. Auyeung, A. Piqué. Optimization of F-doped SnO2 electrodes for organic photovoltaic devices. Applied Physics A 93 (2008) 521–526

[153] S. Chen, K.R. Choudhury, J. Subbiah, F. So, C.M. Amb, J.R. Reynolds. Photo-carrier recombination in polymer solar cells based on P3HT and silole-based copolymer. Advanced Energy Materials 1 (2011) 963–969

[154] Z. Fei, J.S. Kim, J. Smith, E.B. Domingo, T.D. Anthopoulos, N. Stingelin, S.E. Watkins, J.S. Kim, M. Heeney. A low bandgap co-polymer of dithienoger-mole and 2,1,3-benzothiadiazole by Suzuki polycondensation and its application in transistor and photovoltaic cells. Journal of Materials Chemistry 21 (2011) 16257–16263

factors are the shift from higher to lower band gap polymers and the choice of acceptors to match energy levels for maximizing the V_{OC}.[155]

In most OPV devices the active layer responsible for photon absorption and carrier generation is of the bulk heterojunction type where the donor (polymer) and acceptor microphase separate into a bi-continuous network with a high internal surface where electron hole separation can take place and act as channels for transport of the two carrier types.[156] The optimum morphology may require some post treatment procedures and the most common method is to anneal the devices by heating them for a short period of time.[157] An alternative option is to expose the devices to solvent vapors that have been proposed to dissolve selectively into one of the components of the active layer mobilizing it enough to help the morphology to change.[158] Both temperature and solvent annealing increases PCE, mainly through increases in J_{SC} and FF, while V_{OC} is negatively affected. Another popular stratagem is to use additives such as 1,8-diiodooctane or 1-chloronaphthalene to the active layer solution which increase the efficiency.[159] This time the better PCE is due to increases in all the parameters: V_{OC}, J_{SC} and FF. Quite significant part of molecular OPV devices are with the active layer composed of discrete molecules of compounds such as phthalocyanines (CuPc, ZnPc), pentacene, tetracene, oligothiophenes.[160] Typical devices are constructed using chemical vapor deposition of these compounds sometimes creating gradients or mixtures of several of these to obtain bulk heterojunction type structures. [161]

2.4.1.3 Normal versus *inverted geometry*

One of the important developments in OPV has been the shift from "normal" geometry of the OPV stack, where electrons exit from the top electrode (usually aluminum) and holes from the bottom (usually ITO), to the "inverted" geometry where electrons exit at the bottom and holes at the top.[162] This change allows (or determine) the use of other metals such as silver to be used as the top electrode which are much more resistant to

---

[155] J. Yuan, Z. Zhai, H. Dong, J.Li, Z. Jiang, Y. Li, W. Ma. Efficient polymer solar cells with ahighopen circuit voltage of 1 V. Advanced Functional Materials (2012) 885–892

[156] H. Hoppe, N.S. Sariciftci. Morphology of polymer/fullerene bulk-heterojunction solar cells. Journal of Materials Chemistry 16 (2006) 45–61

[157] W. Ma, C. Yang, X. Gong, K. Lee, A.J. Heeger. Thermally stable, efficient polymer solar cells with nanoscale control of the interpenetrating network morphology. Advanced Functional Materials 15 (2005) 1617–1622

[158] M. Campoy-Quiles, T. Ferenczi, T. Agostinelli, P.G. Etchegoin, Y. Kim, T.D. Anthopoulos, P.N. Stavrinou, D.D.C. Bradley, J. Nelson. Morphology evolution via self-organization and lateral and vertical diffusion in polymer: fullerene solar cell blends. Nature Materials 7 (2008) 158–164

[159] Y.Y. Liang, Z. Xu, J.B. Xia, S.T. Tsai, Y. Wu, G. Li, C. Ray, L.P. Yu. For the bright future-bulk heterojunction polymer solar cells with power conversion efficiency of 7.4%. Advanced Materials 22 (2010) E135–E138

[160] T.S. van der Poll, J.A. Love, T.Q. Nguyen, G.C. Bazan. Non-basic high-performance molecules for solution-processed organic solar cells. Advanced Materials 24 (2012) 3646–3649

[161] Y.Z. Lin, Y.F. Li, X.W. Zhan. Small molecule semiconductors for high-efficiency organic photovoltaics. Chemical Society Reviews 41 (2012) 4245–4272

[162] M.S. White, D.C. Olson, S.E. Shaheen, N. Kopidakis, D.S. Ginley. Inverted bulk-heterojunction organic photovoltaic device using a solution-derived ZnO under layer. Applied Physics Letters 89 (2006) 143517-1–143517-3

oxygen and water.[163] The result is usually far more stable OPV devices that with proper encapsulation may even last for years alleviating the operational stability challenge.[164] The normal geometry is still by far the most common accounting for 90% even in 2011. It also still has a slight edge over the inverted geometry in terms of PCE and J_{SC}.

2.4.1.4 Fabrication methods and environment

The standard method of fabricating OPV is still using spin coating to apply thin layers of solutions such as the polymer:acceptor and PEDOT:PSS. The reason for its widespread use is of course that it is a simple technology offering some control over the wet thickness of the film.[165] On the other hand it also constrains experiments to small individual rigid substrates which are far removed from any projected industrial production of OPV. Much of today's literature on OPV focuses on methods to optimize the efficiency and they may be hard to transfer from the laboratory to an industrial process.[166] So there is a real danger that much of this effort will have to be duplicated when a shift to roll-to-roll (R2R) fabrication methods occur. Most fabrication environments include a glovebox to minimize exposure to oxygen/water that are known to rapidly degrade devices.[167] Substrates are almost exclusively glass with a layer of ITO acting as one electrode. Finally nearly all fabrication methods involve a vacuum step such as evaporation of a metal electrode. R2R fabrication on flexible substrates only account for 0.5% of the solar cell devices listed in the literature (Usually for solar cell applications, the conjugated polymers are processed to make thin films via spin coating, dip coating, and doctor blading. These methods are used almost exclusively, but they are not suitable when we talk about high-volume production.

Table 16). Usually for solar cell applications, the conjugated polymers are processed to make thin films via spin coating, dip coating, and doctor blading. These methods are used almost exclusively, but they are not suitable when we talk about high-volume production.

Table 16: OPV fabrication methods and environment

Fabrication method	Environment	Substrate	Vaccum	ITP
Spin coating 86%	Glovebox 90%	Glass 99%	99%	95%
Roll to roll (R2R) 0.5%	Ambient air 10%	Flexible 0.5%	-	-
Unknown or other13%	-	-	-	-

---

[163] M. Hermenau, M. Riede, K. Leo, S.A. Gevorgyan, F.C. Krebs, K. Norrman. Water and oxygen induced degradation of small molecule organic solar cells. Solar Energy Materials and Sola rCells 95 (2011) 1268–1277

[164] S. Cros, R. deBettignies, S. Berson, S. Bailly, P. Maisse, N. Lemaitre, S. Guillerez. Definition of encapsulation barrier requirements: a method applied to organic solar cells. Solar Energy Materials and Solar Cells 95 (2011) 65–69

[165] K. Norrman, A. Ghanbari-Siahkali, N.B. Larsen. Studies of spin-coated polymer films, Annual Reports on the Progress of Chemistry Section C: Physical. Chemistr. 101 (2005) 174–201

[166] F.C. Krebs, J. Fyenbo, M. Jørgensen. Product integration of compact roll-to-roll processed polymer solar cell modules: methods and manufacture using flexographic printing, slot-die coating and rotary screen printing. Journal of Materials Chemistry 20 (2010) 8994–9001

[167] M. Jørgensen, K. Norrman, S.A. Gevorgyan, T. Tromholt, B. Andreasen, F.C. Krebs. Stability of polymer solar cells. Advanced Materials 24 (2012) 580–612

It must be mentioned, however, that at least one study has been carried out with R2R production of 10,000 solar cell modules (160,000 solar cells) made over a few days.[168] This demonstrates the huge difference in production speed between these two modes of fabrication.

From production point of view slot-die coating, gravure coating, knife over edge coating, offset coating, spray coating, and printing techniques such as ink jet printing, pad printing, and screen printing are the most suitable techniques (Figure 72 illustrated that organic solar cells can be manufactured using standard printing processes). Various printing and coating technologies have been proven their compatibility with semiconducting polymer processing.[169] However, these techniques are not explored much for polymer solar cells applications.

Figure 72: Schematic illustration of organic solar cells can be manufactured by standard printing processes. Source: R. Gaudiana et al. Nat. Photonics, 2008

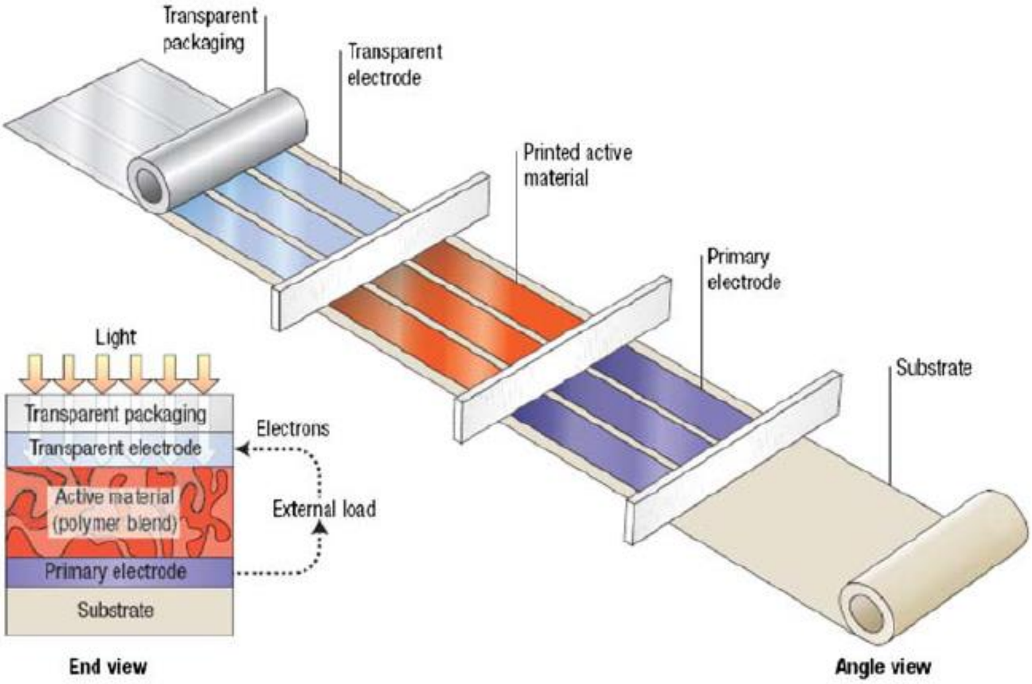

For R2R fabrication of polymer solar cells, ITO-coated flexible poly(ethyleneterephthalate) (PET) sheet is used as the base substrate where ITO is patterned using an R2R etching machine via printing a UV curable photoresist in desired pattern, stripping the photoresist by sodium hydroxide solution, developing and hardening the pattern, etching out undesired ITO in copper chloride (CuCl2) solution, washing with deionized water, and finally drying. Prior to any coating, the PET/ITO substrates are cleaned on both sides using isopropanol. For the coating of active layer, the solution of donor and acceptor materials in desired solvent are kept in separate

---

[168] F.C. Krebs, J. Fyenbo, D.M. Tanenbaum, S.A. Gevorgyan, R. Andriessen, B. van Remoortere, Y. Galagan, M. Jorgensen, The OE-AOPV demonstrator anno domini 2011, Energy & Environmental Science 4 (2011) 4116–4123

[169] Krebs FC. Fabrication and processing of polymer solar cells: A review of printing and coating techniques. Solar Energy Materials and Solar Cells 2009; 93: 394–412

vessels and are pumped via separate channels into the mixing head. The benefits of the R2R process are that the donor and acceptor materials are not mixed until they are used and one can use the same stock of solution with different materials by simply changing the source solution. In the context of operational stability and large-scale production without vacuum coating steps, the normal cell geometry is far from ideal, and the other device geometries are worth pursuing.

Development in roll to roll (R2R) processing would allow transferring the laboratory polymer solar cells to large-scale industrial production. There are a number of reports available in the literature on the fabrication and production of large-area polymer solar cells on a reasonable scale, but with power conversion efficiency (PCE) only beyond 6%, which is a value far away for daily applications.

2.4.1.5 The active area of OPV

Mature photovoltaic technologies usually measure the device area in many square centimeters and upwards. Most OPV devices on the other hand are less than 0.2 cm^2. One reason is the larger sheet resistivity of ITO compared to metals such as silver limiting the charge collection and thus also the efficiency. Although the data is limited for device areas above 1 cm^2 it seems the efficiency falls of exponentially with size at very small active areas and stabilize at higher active areas. How the sheet resistivity influences the maximum obtainable PCE depends on the geometry of the device and use of metal bus bars to help charge collection.[170] In a typical layout this would lead to a more linear dependence between PCE and the area which does not seem in accordance with the data. Another factor that must be considered is the uncertainty in measuring the area correctly.[171] Many authors advocate that exceptionally high efficiencies be checked by certified institutions such as NREL or Fraunhofer ISE and others. This is, however, a costly and time consuming practice that has not been widely adopted. It is also striking that while most researchers adhere to the promise of OPV as a low cost alternative to mature PV technologies the combined active area of all the laboratory scale OPV devices only cover 0.98 m^2 and the 86% of the devices which have an area of less than or equal to 0.2 cm^2 amount to only 0.04 m^2 in total.

2.4.1.6 Degradation and stability in organic solar cells

Along with the high efficiencies, reliability, stability, processibility, and cost are other important parameters, which all together will determine the success of OSCs. Although the early studies on stability and degradation of OSCs can be found in early 1990s, the issue has not been paid too much attention. Organic semiconductors are quite susceptible to chemical and physical degradation by oxygen and moisture, and OSCs degrade during both in dark and under illumination. Although reports can be found in the literature where stability of OSCs has been studied, the issue is not yet fully

---

[170] A. Manor, E.A. Katz, B. Hirsch, E.A. Katz, T.Tromholt, F.C. Krebs. Origin of size effect on efficiency of organic photovoltaics. Journal of Applied Physics 109 (2011) 074508-1–074508-9

[171] A. Cravino, P. Schilinsky, C.J. Brabec. Characterization of organic solar cells: the importance of device layout. Advanced Functional Materials 17 (2007) 3906–3910

understood.[172] A complete understanding and solutions to the degradation problems are urgently required. In the last decade, there have been consistent efforts on the improvement in efficiency of OSCs; however, the data available on their stability is very limited.

Figure 73: A graphical overview of the field of stability and degradation of polymer solar cells. Source: W. Cai et al. Solar Energy Materials & Solar Cells, 2010

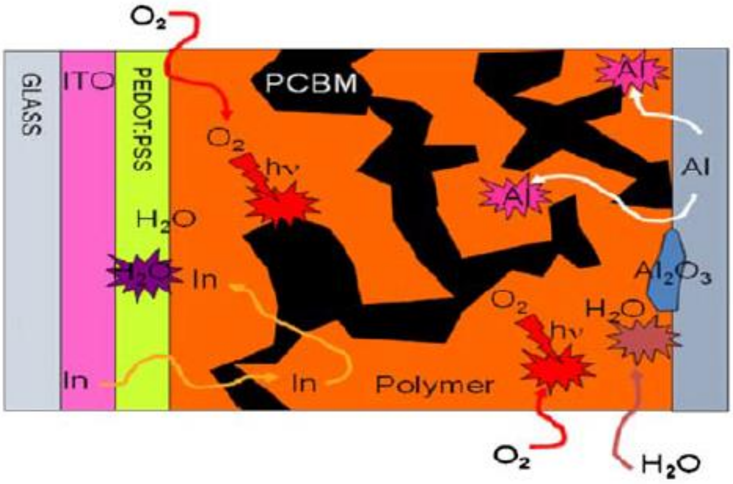

Chemical degradation includes the degradation due of interaction of organic molecules with oxygen, moisture, and electrode materials.[173] The degradation is also accelerated when the device was kept at higher temperatures. Oxygen and moisture may be introduced during the device preparation. Even after preparation, if the devices are exposed to oxygen and/or moisture, oxygen and moisture diffuse into the device and react with the active layer. The top electrode was found to be the main channel for oxygen/moisture diffusion, and diffusion through the sides was not significant. The diffusion through the metal top electrode is due to microscopic pin holes. Oxygen and moisture diffuse through the electrode pin holes regardless of whether the device is kept in dark or under illumination. However, under illumination, the device degrades faster. In the presence of UV illumination, oxygen is activated and becomes more attacking. It is therefore quite important to remove the microscopic pin holes, and detailed studies and investigations are urgently required. Alternately, new methods should be developed for the deposition of the top electrode.

2.4.1.7 Conclusions: OPV

It is clear that the field of OPV has drawn an enormous number of researchers to it and from the analysis above it is also evident that the furtherance of the field will require some mode of direction other than what is in operation today. Currently the research carried out in the field is self-justified with a few exponents defining research targets through achievement of extreme values for a single parameter which is most often the efficiency but also the operational stability has been used as a metric. In achieving those

---

[172] Jørgensen M, Norrman K, Krebs FC. Stability/degradation of polymer solar cells. Solar Energy Materials and Solar Cells 2008; 92: 686–714.

[173] W. Cai, X. Gong, Y. Cao. Polymer solar cells: Recent development and possible routes for improvement in the performance. Solar Energy Materials & Solar Cells 94 (2010) 114–127

values which serve as a firm ground for competition the field is in near contradiction with the original vision of OPV. To recite the advantages of OPV (and perhaps also its purposes) they are large area, flexible solar cells with a thin outline prepared under ambient conditions using fast modes of manufacture without the use of scarce elements such as indium, silver, gold or toxic solvents.[174] State-of-the-art OPV falls far from the vision in all these aspects. The clearest conclusion to draw is perhaps that the active area that one should as a minimum employ is 1 cm^2 and perhaps 4–5 cm^2 is a more conservative measure guaranteeing some level of scalability. It is, however, unreasonable to expect that scientists are willing to (or can) change the set of rules that are already in operation. It must also be borne in mind that this commonly practiced approach is linked to the questions of how good a value that can be achieved? but also to whom the result is addressed? The answer to the former question is still open. A second observation that might be partly linked to the active area imply that practical total area efficiencies for single junction carbon based PV will be around 5% (and perhaps 8% for tandem solar cells) when deployed over many square meters.

Under the assumption given above that single junction carbon based solar cells will maximally yield 5% power conversion efficiency on the total area (for square meter sized panels) in a form that can be mass produced, it is possible to pose the question of how an OPV power plant should be constituted to be useful? Firstly, the general view is that solar parks based on crystalline silicon solar cells are barely profitable due to the performance which is viewed as low for the purpose (12–20%) unless the geographic location provides favorable conditions in the form of a high degree of insolation or the local policy enables investment through favorable subsidy. It is thus clear that for a solar park based on OPV with the premise that the maximally achievable total area power conversion efficiency is 5% (8% on tandem architectures) will be unsuccessful if it is simply a deployment following the same methods as those currently employed for crystalline silicon solar cells.[175] This somber (but factual) view of the future of OPV will come true unless one takes specific advantage of the competitive edges that OPV does present while circumventing the distinct weaknesses that OPV admittedly also possess. To summarize, the weaknesses are linked solely to the power conversion efficiency and the operational stability and in the following we assume a total (large) area efficiency of 5% for single junctions and an operational lifetime under outdoor conditions of 5 years. The list of competitive edges of OPV compared to other solar cell technologies is long and even when compared to other renewable energy technologies OPV does have significant vantage points. The OPV technology is the only renewable energy technology that enables energy payback times of less than a few months, it is also the only technology that in spite of the relatively short service life potentially offer energy return factors in excess of 100. Finally, it is also the only energy technology that enables ultra-

---

[174] N. Espinosa, R. García-Valverde, A. Urbina, F. Lenzmann, M. Manceau, D. Angmo, F.C. Krebs. Life cycle assessment of ITO-free flexible polymer solar cells prepared by roll-to-roll coating and printing. SolarEnergy Materials and Solar Cells 97 (2012) 3–13

[175] N. Espinosa, M. Hösel, D. Angmo, F.C. Krebs. Solar cells with one-day energy payback for the factories of the future. Energy and Environmental Science 5 (2012) 5117–5132

fast manufacture of a given energy producing unit. This all implies that the OPV technology is already competitive and one can ask why it is not in use yet. The answer to this question is linked to the low performance and the consequent requirement for a large landmass. Also to make use of the advantages listed above the mode of deployment and the scaffold used for mounting the OPV has to be significantly different from traditional PV and clearly the landmass has to be available at very low cost. Arid regions that have no agricultural value are an obvious choice for PV and would be mandatory in the case of large scale deployment of OPV. Since insolation in such regions is usually high this would also be beneficial. One advantage of OPV is that it can be printed on flexible foil in near endless form and if this property was employed in the deployment such that for instance a roll of solar cells was installed by simply rolling it out along a long fixed scaffold the installation rates would exceed panel based PV by several orders of magnitude such that the installation rate ideally matches the manufacturing rate. This implies that the installation would have to be achieved in an automated fashion and would also have to enable simultaneous de-installation for potential re-use while reinstalling new OPV at the end of the service life. The scaffold would of course be a lasting and reusable structure. It can be outlined how OPV should be installed to be useful and also highlight that this can already be realized with the currently available version of OPV. In the ultimate vision OPV is deployed in conjunction with other large renewable energy harvesting parks such as solar farms on- or off-shore thus minimizing infrastructure requirements and thus exploiting the synergy inherent in the complementarity between the different renewable energy technologies such as wind and solar power.

Organic photovoltaics in principle offer to provide an eco-friendly, large-area flexible solar cell technology at low process cost. The following factors, which will help in the realization of the commercial viability of OPV and making the dream a reality could be point out:

- To break the efficiency limitations and get more than 10% efficiency, design, synthesis, and application of new materials with suitable bandgaps, appropriate HOMO and LUMO energy levels and high charge carrier mobilities are necessarily required.
- There are other areas as well like processibility, stability, and cost, which are also equally important and should be given sufficient attention to make OPV a sustainable technology. Although there has been significant progress to improve the performance of OPV, control of nanoscale morphology of the active layer is still very critical for efficient solar cells.
- The understanding of degradation phenomena is a prerequisite for successful implementation of the technology. Protection from ambient condition using suitable barrier materials may lead to longer life of OPV; however, there are various other factors as well, like purity of materials, diffusion of anode and cathode atoms into the organics, joule heating, and photo degradation, which are

responsible for the degradation of these devices and should be taken into account.

- For real development of OPV, the accuracy of measurements should seriously be taken into account. Polymer solar cells have been moving rapidly toward large-scale manufacture and demonstration, but there are still massive scientific challenges to overcome. The performance and especially the lifetime of polymer solar cells need to see significant developments before polymer solar cells will be competitive for production of on-grid electrical energy.
- Organic photovoltaic technology has developed remarkably and essentially come out from laboratories to the society with several commercial companies such as Konarka, Plextronics, Solarmer, and so on, and public demonstrations by laboratories. Although the business potential of polymer solar cells is large, the current performance leaves little room for competition with other thin film technologies. The power conversion efficiency, operational lifetime, and cost would all need to be much better before a significant market share can be anticipated.

2.4.2 Dye-sensitized solar cells

Dye-sensitized solar cells (DSCs) are attractive because they are made from cheap materials that do not need to be highly purified and can be printed at low cost. DSCs are unique compared with almost all other kinds of solar cells in that electron transport, light absorption and hole transport are each handled by different materials in the cell. The sensitizing dye in a DSC is anchored to a wide-bandgap semiconductor such as TiO_2, SnO_2 or ZnO. When the dye absorbs light, the photoexcited electron rapidly transfers to the conduction band of the semiconductor, which carries the electron to one of the electrodes. A redox couple, usually comprised of iodide/triiodide (I^-/I_3^-), then reduces the oxidized dye back to its neutral state and transports the positive charge to the platinized counter-electrode.

In terms of efficiency and easy fabrication, the dye-sensitized solar cell is stated to be one of the most promising alternatives to the silicon solar cells. In 1991, Oregan and Gratzel built the first dye sensitized nanocrystalline solar cells whose photoelectric energy conversion rate reached 7.1% and incident photon to electrical current conversion efficiency was approximately 80%.[176] This simple structure and low cost technology have further stimulated great research interest to improve the efficiency of dye-sensitized solar cells which has attained ca. 10%, a level deemed as necessary for commercial use. This approach dramatically improved light absorption and brought power-conversion efficiencies into a range that allowed the DSC to be viewed as a serious competitor to other solar cell technologies.[177] A schematic and energy level diagram showing the operation of a typical DSC is shown in Figure 74.

---

[176] Oregan B, Gratzel M. A low-cost, high-efficiency solar cell based on dye- sensitized colloidal TiO2 films. Nature1991; 353(6346): 737–40.

[177] Green, M. A., Emery, K., Hishikawa, Y., Warta, W. & Dunlop, E. D. Solar cell efficiency tables (version 38). Prog. Photovolt. Res. Appl. 19, 565–572 (2011)

Figure 74: Dye-sensitized solar cell device schematic and operation: a, **Liquid-based DSCs are comprised of a transparent conducting oxide (such as fluorine-doped tin oxide, FTO) on glass, a nanoparticle photoanode (such as titania) covered in a monolayer of sensitizing dye, a hole-conducting electrolyte and a platinum-coated, FTO-coated glass back-contact.** b, **Energy level and device operation of DSCs; the sensitizing dye absorbs a photon (energy *hv*), the electron is injected into the conduction band of the metal oxide (titania) and travels to the front electrode (not shown). The oxidized dye is reduced by the electrolyte, which is regenerated at the counter-electrode (not shown) to complete the circuit. *V*OC is determined by the Fermi level (*E*F) of titania and the redox potential (I_3^-/I^-) of the electrolyte. Source: Nature Photonics, 2012**

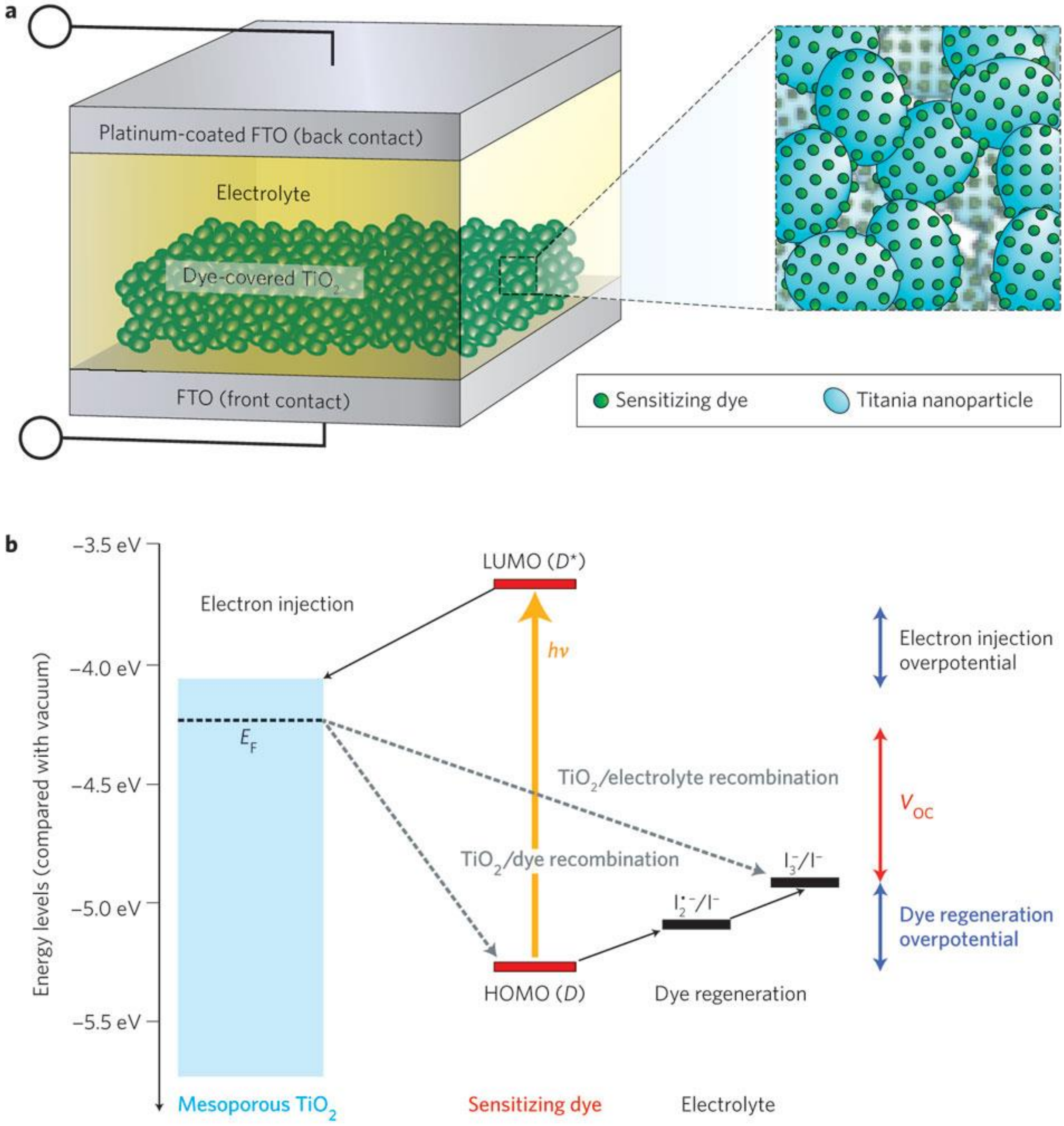

During the 1990s and the early 2000s, researchers found that organometallic complexes based on ruthenium provided the highest power-conversion efficiencies.[178] Figure 75shows a current–voltage curve under 1 Sun illumination, together with a plot of the external quantum efficiency as a function of photon wavelength.

---

[178] Mishra, A., Fischer, M. K. R. & Bäuerle, P. Metal-free organic dyes for dye-sensitized solar cells: From structure–property relationships to design rules. Angew. Chem. Int. Ed. 48, 2474–2499 (2009)

Figure 75: Best-in-class dye-sensitized solar cells: the external quantum efficiency versus wavelength (a) and photocurrent density versus voltage (b) for the ruthenium dye (CYC-B11)/iodide redox couple, the co-sensitized donor–pi–acceptor dye (YD2-o-C8 and Y123)/cobalt redox couple and a solid-state system comprised of the Y123 dye and the hole conductor spiro-OMeTAD. Absorbing into the NIR region of the spectrum increases the photocurrent density from 20 mA cm−2 to 30 mA cm−2. c, Chemical structures of the best-performing ruthenium-based complex CYC-B11, together with donor–pi–acceptor dyes YD2-o-C8 and Y123. d, Chemical structures of the iodide redox couple, a cobalt redox mediator and the solid-state hole conductor spiro-OMeTAD. Source: Nature Photonics, 2012

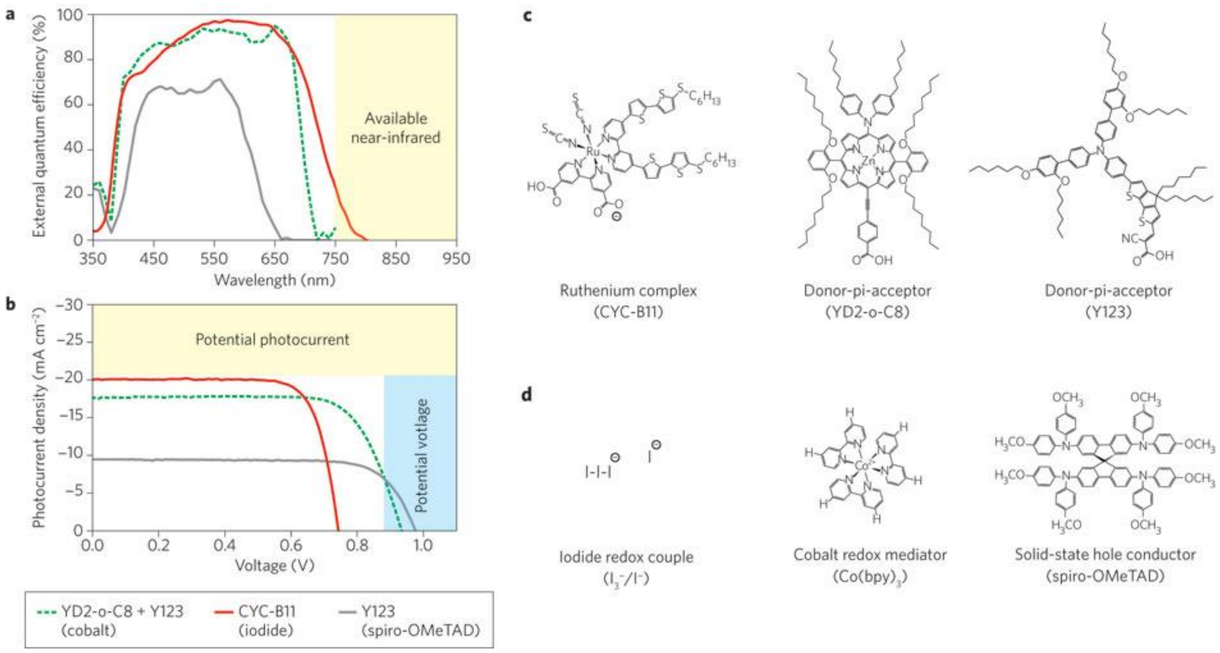

The iodide/triiodide system has been particularly successful in DSCs because of the slow recombination kinetics between electrons in the titania with the oxidized dye and the triiodide in the electrolyte, which leads to long-lived electron lifetimes (between 1 ms and 1 s).[179] Iodide reduces the oxidized dye to form an intermediate ionic species (such as $I^{\bullet}{}_2{}^-$) that then disproportionates to form triiodide and diffuses to the counter-electrode, providing two electrons per molecule, as shown in Figure 74 b. The slow recombination and relatively fast dye regeneration rates of the I^-/I_3^- redox couple have resulted in near-unity internal quantum efficiencies for a large number of dyes, providing the high external quantum efficiencies shown in Figure 75 a. The small size of the I^-/I_3^- redox components allows for relatively fast diffusion within the mesopores, and the two-electron system allows for a greater current to be passed for a given electrolyte concentration. Unfortunately, the I^-/I_3^- system is corrosive and dissolves many of the commonly used sealants and metal interconnects (such as silver, copper, aluminium and gold).

2.4.2.1 Obtaining maximum DSC power-conversion efficiencies

There are two main ways in which the efficiency of a DSC can be improved: extend the light-harvesting region into the near-infrared (NIR), and lowering the redox potential of the electrolyte to increase open-circuit voltage (V_{OC}). Using a dye that absorbs further

---

[179] Bisquert, J., Fabregat-Santiago, F., Mora-Seroó, I. N., Garcia-Belmonte, G. & Gimeónez, S. Electron lifetime in dye-sensitized solar cells: Theory and interpretation of measurements. J. Phys. Chem. C 113, 17278–17290

into the NIR, say to around 940 nm, while still managing to generate and collect the charge carriers efficiently, could increase the current by over 40%.[180] Further increasing the power-conversion efficiency beyond 14% will require improved dyes and electrolytes with smaller over-potentials to efficiently transfer charge. Single-electron redox mediators based on cobalt and ferrocene complexes have two advantages over iodide. First, they do not require an intermediary step during regeneration and can therefore reduce the loss-in-potential. Second, unlike iodide, which does not have an ideal redox potential (0.35–0.40 eV over the normal hydrogen electrode), alternative electrolyte couples can be tuned closer to the highest occupied molecular orbital (HOMO) level of the sensitizing dye to obtain a higher V_{OC}. Although efforts to solve these problems were stymied for many years,[181] new approaches have recently emerged and the world-record efficiency is climbing again.[182] Over the past 15 years, there has been a great deal of research and improved understanding of the associated chemistry and device physics of DSCs.

2.4.2.2 Strongly absorbing donor–pi–acceptor dyes

The sensitizing dye in a DSC is anchored to the n-type metal oxide surface. Light absorption is determined by the molar extinction coefficient of the sensitizing dye, the surface coverage of the dye and the total surface area of the oxide film.[183] Sensitizing dyes generally pack tightly on the titania surface, with a density of 0.5–1 dye molecules per square nanometre. Dyes typically contain a light-harvesting portion, acidic ligands (for example, carboxylic or phosphonic acid) to attach to the semiconductor surface, and ligands to increase the solubility in solution and reduce aggregation between dyes. Aggregation occurs when the dye molecules are packed so tightly that their wavefunction overlap is large enough to change their electronic character, which often causes the dyes to quench in the excited state before electron transfer can occur.

Sensitizing dyes have traditionally been made from ruthenium-based complexes such as N3, N719, C106 and CYC B11,[184] which have fairly broad absorption spectra ($\Delta\lambda \approx$ 350 nm) but low molar extinction coefficients (10,000–20,000 M^{-1} cm^{-1}).[185] These complexes also have extremely weak absorption at the band-edge (around 780 nm), which restricts NIR light harvesting. Although ruthenium-based complexes work well and have been the most widely used dyes over the past two decades, it seems that increased improvements in dye design and the promise of removing expensive metals

---

[180] naith, H. J. Estimating the maximum attainable efficiency in dye-sensitized solar cells. Adv. Funct. Mater. 20, 13–19, 2010

[181] Peter, L. M. The Gra¨tzel cell: Where next? J. Phys. Chem. Lett. 2, 1861–1867 (2011)

[182] ella, A. *et al*. Porphyrin-sensitized solar cells with cobalt(II/III)-based redox electrolyte exceed 12 percent efficiency. Science 334, 629–634,2011

[183] Grätzel, M. Conversion of sunlight to electric power by nanocrystalline dye-sensitized solar cells. J. Photochem. Photobiol. A 164, 3–14 (2004)

[184] Chen, C.-Y. *et al*. Highly efficient light-harvesting ruthenium sensitizer for thin-film dye-sensitized solar cells. ACS Nano 3, 3103–3109 (2009)

[185] Gao, F. *et al*. Enhance the optical absorptivity of nanocrystalline TiO_2 film with high molar extinction coefficient ruthenium sensitizers for high performance dye-sensitized solar cells. J. Am. Chem. Soc. 130, 10720–10728 (2008)

will result in not only increased power-conversion efficiencies but also greater potential to scale beyond 19 GW per year, which is the limit set by the availability of ruthenium.

Organic dyes generally have substantially higher molar extinction coefficients (50,000–200,000 M^{-1} cm^{-1}) than ruthenium-based complexes, but typically have narrower spectral bandwidths ($\Delta\lambda \approx$ 100–250 nm).[186] Over the past few years, great strides have been made in understanding and designing new dyes for use in DSCs. The best dyes contain both electron-rich (donor) and electron-poor (acceptor) sections connected through a conjugated (pi) bridge. The electron-poor section is functionalized with an acidic binding group that couples the molecule to the oxide surface. Photoexcitation causes a net electron transfer from the donor to acceptor sections such that the electron wavefunction couples to the titania conduction band states, while the hole wavefunction resides mostly away from the oxide surface where it is well-positioned to interact with the redox couple.[187] Alkyl chains are also often attached to the side of the dye to create a barrier between holes in the redox couple and electrons in the titania, thereby inhibiting recombination.

2.4.2.3 *The use of new redox couples to achieve higher voltages*

Although scientists have discovered several alternative redox couples that are less corrosive than iodide and whose potentials are more suited to achieving high V_{OC}, solar cells containing such complexes typically have unacceptably high recombination rates and consequently poor performance (efficiencies of <5%). However, recent success using Co^{2+}/Co^{3+}, ferrocene Fc/Fc^+, copper I/II and all-organic electrolytes have resulted in more promising power-conversion efficiencies. In the past, Co^{2+}/Co^{3+} electrolytes suffered from recombination rates that were at least an order of magnitude faster than iodide-based systems.[188] The I^-/I_3^- couple is an elemental system, whereas Co^{2+} and Co^{3+} ions are surrounded by ligands that can be modified to modulate the redox potential (Figure 75). Bulky groups on these ligands can function as insulating spacers, which slow down the recombination process between the electrolyte and the titania.[189] In 2010, Boschloo and co-workers demonstrated a significant improvement in the power-conversion efficiency of cobalt-based systems by adding bulky groups (such as insulating butoxyl chains) to an organic dye.[190] When the insulating ligands on the organic dye, which face away from the semiconductor, are used with the bulky cobalt redox couple, recombination in the system is reduced by at least one order of magnitude

---

[186] Campbell, W. M. *et al*. Highly efficient porphyrin sensitizers for dye-sensitized solar cells. J. Phys. Chem. C 111, 11760–11762 (2007)

[187] Lee, C.-W. *et al*. Novel zinc porphyrin sensitizers for dye-sensitized solar cells: Synthesis and spectral, electrochemical, and photovoltaic properties. Chem. Euro. J. 15, 1403–1412 (2009)

[188] Nusbaumer, H., Moser, J.-E., Zakeeruddin, S. M., Nazeeruddin, M. K. & Grätzel, M. $Co^{II}(dbbip)_2^{2+}$ complex rivals tri-iodide/iodide redox mediator in dye-sensitized photovoltaic cells. J. Phys. Chem. B 105, 10461–10464 (2001)

[189] Sapp, S. A., Elliott, C. M., Contado, C., Caramori, S. & Bignozzi, C. A. Substituted polypyridine complexes of cobalt(II/III) as efficient electron-transfer mediators in dye-sensitized solar cells. J. Am. Chem. Soc. 124, 11215–11222 (2002)

[190] Klahr, B. M. & Hamann, T. W. Performance enhancement and limitations of cobalt bipyridyl redox shuttles in dye-sensitized solar cells. J. Phys. Chem. C 113, 14040–14045 (2009).

without affecting the electron transfer rate. Grätzel and co-workers recently took this approach to the next level by applying the insulating ligand technique to a donor–pi–acceptor dye YD2-o-C8 (Figure 75 c), which has a broad absorption spectrum. In doing so, they achieved similarly low recombination rates and demonstrated DSCs with a laboratory-measured world record efficiency of 12.3% under 1 Sun illumination.[191] The improved performance was linked to a 16% increase in V_{OC} over cells containing an iodide-based redox couple, which demonstrates the importance of tuning the redox level to increase V_{OC}. The dye had an absorption onset at 725 nm and the cell had a total loss-in-potential of around 775 mV. In the short term, moving the dye absorption out to 830 nm could increase this efficiency to 13.6% without any further fundamental advances in technology. In recent work, an over-potential of only 390 mV was sufficient to regenerate the oxidized dye and achieve an external quantum efficiency of more than 80%.[192] Given a total loss-in-potential of 500 mV, and assuming a required over-potential of 100 mV on the electron-transfer side, it may be possible to increase the efficiency of the cobalt system to 19% by extending the absorption out to 920 nm.

One of the shortcomings of cobalt-based complexes is that their bulky groups significantly decrease the speed at which the ions can diffuse through the electrolyte - up to an order of magnitude less than conventional iodide ions.[193] Grätzel and co-workers found that reducing the illumination intensity increased the power-conversion efficiency to 13.1%, as it is less important for the ions to diffuse to the electrode quickly when the carrier density is lower. One could imagine obtaining this efficiency under 1 Sun illumination by using even thinner films to reduce the required diffusion distance. Later in this Review we will describe potential techniques for slowing recombination and attaining adequate light absorption in thin films.

Long-term stability studies have not yet been performed on cobalt complexes in dye-sensitized solar cells. It will be important to make sure that cobalt complexes do not undergo irreversible changes at the counter-electrode while providing stabilities similar to (or better than) iodide-based electrolytes.

2.4.2.4 Solid-state dye-sensitized solar cells

Solid-state DSCs (ss-DSCs), which use solid hole conductors instead of a liquid electrolyte, are also capable of delivering high voltages.[194] The hole conductor is typically made from either wide-bandgap small molecules (such as spiro-OMeTAD) or semiconducting polymers (such as PEDOT or P3HT). These DSCs are in principle more industrially compatible than standard DSCs because they do not contain a corrosive liquid electrolyte, which requires careful packaging. The highest values of V_{OC} (>1 V)

---

[191]

[192] Feldt, S. M., Wang, G., Boschloo, G. & Hagfeldt, A. Effects of driving forces for recombination and regeneration on the photovoltaic performance of dye-sensitized solar cells using cobalt polypyridine redox couples. J. Phys. Chem. C 115, 21500–21507 (2011).

[193] Nelson, J. J., Amick, T. J. & Elliott, C. M. Mass transport of polypyridyl cobalt complexes in dye-sensitized solar cells with mesoporous TiO_2 photoanodes. J. Phys. Chem. C 112, 18255–18263 (2008).

[194] Bach, U. *et al.* Solid-state dye-sensitized mesoporous TiO_2 solar cells with high photon-to-electron conversion efficiencies. Nature 395, 583–585 (1998)

achieved so far have been demonstrated in devices that exploit a small-molecule hole conductor.[195] In ss-DSCs, hole transfer occurs directly from the oxidized dye to the HOMO level of the hole conductor, which then transports the charge to the (typically silver) counter-electrode.[196] Dye regeneration occurs over a period of tens to hundreds of picoseconds — several orders of magnitude faster than regeneration with the I^-/I_3^- redox couple. Although the first ss-DSCs made with solution-processable small molecules achieved power-conversion efficiencies of less than 1%, researchers have recently increased this value to 7.1%.[197] Significant recombination rates, together with the difficulty in achieving high levels of pore-filling in thicker films, means that ss-DSCs currently work best at thicknesses of only a few micrometres. The greatest issues facing ss-DSCs are their incomplete light harvesting and lower internal quantum efficiency, which together result in current densities that are lower than liquid-based DSCs.

There are many factors that affect the recombination between conduction-band electrons in the titania layer and holes in the hole conductor layer. Under solar operating conditions, the hole density in ss-DSCs is highest near the dye-sensitized interface (the point of generation) and charge screening is not as effective as it is in cells containing liquid electrolytes, which typically leads to recombination rates that are an order of magnitude larger than those in the best I^-/I_3^- systems. Recombination in ss-DSCs can be significantly inhibited by interfacial engineering (discussed below) and having the correct mix of ionic additives in the hole transporter phase. Chemical p-dopants are often added to the hole transporter to increase the conductivity, resulting in increased values of V_{OC} and the fill factor.

Solid hole conductors are almost exclusively fabricated through solution-deposition techniques. However, pore-filling can never be complete through such procedures because space is left when the solvent evaporates[198]. The pore-filling fraction, which is defined as the fraction of porous volume taken by the hole conductor, can be as high as 60–80% with small-molecule hole conductors, and the pores are generally uniformly filled throughout the entire film thickness. Uniformly covering the dye/metal oxide surface is extremely important to ensure good charge separation and collection; as a rule of thumb, around 50% pore-filling is required in a mesoporous network to ensure monolayer surface coverage. Improving the pore-filling fraction is an important strategy for reducing recombination and might be achieved by infiltrating hole conductors from the melt.[199]

---

[195] Chen, P. *et al*. High open-circuit voltage solid-state dye-sensitized solar cells with organic dye. Nano Lett. 9, 2487–2492 (2009).

[196] Snaith, H. J. *et al*. Efficiency enhancements in solid-state hybrid solar cells via reduced charge recombination and increased light capture. Nano Lett. 7, 3372–3376 (2007)

[197] Burschka, J. *et al*. Tris(2-(1H-pyrazol-1-yl)pyridine)cobalt(III) as p-type dopant for organic semiconductors and its application in highly efficient solid-state dye-sensitized solar cells. J. Am. Chem. Soc. 133, 18042–18045 (2011).

[198] Ding, I. K. *et al*. Pore-filling of spiro-OMeTAD in solid-state dye-sensitized solar cells: Quantification, mechanism, and consequences for device performance. Adv. Func. Mater. 19, 2431–2436 (2009)

[199] Melas-Kyriazi, J. *et al*. The effect of hole transport material pore filling on photovoltaic performance in solid-state dye-sensitized solar cells. Adv. Eng. Mater. 1, 407–414 (2011).

Light-harvesting in ss-DSCs has benefited tremendously from donor–pi–acceptor dyes, which provide significantly enhanced light absorption in 2-μm-thick films. Careful control over the p-dopant, in combination with the use of a strongly absorbing donor–pi–acceptor dye, has recently led to efficiencies of over 7% in ss-DSCs that exploit small-molecule hole conductors. Another way of improving light absorption in ss-DSCs is to use light-absorbing polymers as the hole conductor. Polymer hole conductors, typically used in organic photovoltaic cells, have recently achieved power-conversion efficiencies of more than 5%[200]. Polymer hole conductors are also solution-processed, although the pore-filling fractions are much lower (<25%) than in small-molecule hole conductors. Despite this, however, the polymer can predominately wet the internal surface and carry holes efficiently out of devices of up to 7 μm in thickness.[201]

Compared with their liquid-electrolyte counterparts, ss-DSCs have been significantly underdeveloped. Relatively few hole conductors have been studied for DSCs, and there are still no clearly defined rules for hole conductor design, doping and additive requirements, and dye modifications. Although optical models[202] have been created for ss-DSCs, understanding why the internal quantum efficiency (for example, charge generation/separation or charge collection) is lower for ss-DSCs than liquid-based DSCs will require much better knowledge of the physics of these devices. We believe significant improvements could be made by improving pore-filling and developing new hole conductors with deeper HOMO levels, additives to further reduce recombination and dyes that could result in a loss-in-potential of 300 mV.

2.4.2.5 Engineering the interface to prevent recombination

In iodide-based DSCs, recombination is inherently slow and excessive electronic engineering of the interface is not entirely necessary. However, for both new electrolytes and solid-state hole conductor systems, fast recombination is a critical issue that must be reduced in order to realize maximum efficiency. It should be noted that a tenfold decrease in the recombination rate will result in a 50–60mV increase in V_{OC}. The oxide can be surface-treated through either organic modification or inorganic shell growth. For organic modification, co-adsorption of surface modifiers alongside the dye molecules can be used to help block direct contact of the hole conductor or electrolyte with the titania, or to modify the energetics of the interface by introducing a dipolar field.[203]

---

[200] Chang, J. A. *et al*. High-performance nanostructured inorganic–organic heterojunction solar cells. Nano Lett. 10, 2609–2612, 2010

[201] Abrusci, A. *et al*. Facile infiltration of semiconducting polymer into mesoporous electrodes for hybrid solar cells. Energ. Environ. Sci. 4, 3051–3058 (2011).

[202] Moulé, A. J. *et al*. Optical description of solid-state dye-sensitized solar cells. I. Measurement of layer optical properties. J. Appl. Phys. 106, 073111 (2009).

[203] Wang, M. *et al*. Surface design in solid-state dye sensitized solar cells: Effects of zwitterionic co-adsorbents on photovoltaic performance. Adv. Func. Mater. 19, 2163–2172 (2009)

For inorganic modification, thin shells of 'insulating' oxides can be deposited on the titania layer prior to dye loading.[204] The insulating shell must be thin enough to allow electron transfer from the photoexcited dye, but also thick enough to inhibit the recombination reaction. Because the fundamental mechanism for both forwards electron transfer and recombination is the same, we expect the same inhibition in both rates. This technique therefore requires the initial electron transfer process to be faster than is strictly necessary, and to inhibit recombination only to the point at which a drop in photocurrent occurs because electron transfer to the titania is not occurring fast enough. In practice, there is usually a slight drop in photocurrent accompanied by an increase in V_{OC}. Researchers often overlook the fact that coating the surface of an oxide such as titania with an insulating shell usually results in a shift in the surface potential of the oxide. This usually causes an increase in V_{OC} that can be mistakenly interpreted as being due to the inhibition of recombination.

Changing the ionic content in the hole conductor can be much more effective at slowing down recombination than introducing an inorganic shell.[205] This is most likely caused by holes in the hole conductor electrostatically screening the electrons in the titania layer. Because the dielectric constant for titania is extremely large ($\sim 100\varepsilon_0$), it is surprising that electrostatic screening is required once the electrons are transferred into the oxide. The fact that recombination is so sensitive to ionic additives suggests that the electrons undergoing recombination are in surface states and are not entirely screened by the bulk dielectric. Pacifying these surface states may therefore have a direct beneficial impact on charge recombination.[206]

2.4.2.6 Light trapping

In DSCs that do not contain the I^-/I_3^- redox couple, it is a challenge to make the cell thick enough to absorb almost all of the light while also thin enough to ensure all the charge carriers are collected, as many of the carriers recombine before travelling more than a few micrometres. This problem can be avoided by scattering light in the cell to increase its path length or using plasmonic effects to intensify the absorption near nanopatterned metal. The most commonly used light-trapping approach in cells containing liquid electrolytes is to deposit a film of titania particles measuring 200–400 nm in diameter on top of a layer of titania particles of normal size (20 nm, for example).[207] The larger titania particles scatter light and thereby increase the photon path length in the cell.[208]

---

[204] Palomares, E., Clifford, J. N., Haque, S. A., Lutz, T. & Durrant, J. R. Slow charge recombination in dye-sensitised solar cells (DSSC) using Al_2O_3 coated nanoporous TiO_2 films. Chem. Commun. 1464–1465 (2002)

[205] Kruger, J. *et al*. High efficiency solid-state photovoltaic device due to inhibition of interface charge recombination. Appl. Phys. Lett. 79, 2085–2087 (2001)

[206] Fabregat-Santiago, F. *et al*. The origin of slow electron recombination processes in dye-sensitized solar cells with alumina barrier coatings. J. Appl. Phys. 96, 6903–6907 (2004).

[207] Ito, S. *et al*. Fabrication of thin film dye sensitized solar cells with solar to electric power conversion efficiency over 10%. Thin Solid Films 516, 4613–4619 (2008)

[208] Palomares, E., Clifford, J. N., Haque, S. A., Lutz, T. & Durrant, J. R. Control of charge recombination dynamics in dye sensitized solar cells by the use of conformally deposited metal oxide blocking layers. J. Am. Chem. Soc. 125, 475–482 (2003)

In some cases, more well-ordered photonic crystals have been used to scatter light.[209] Alternative strategies are needed to trap light in ss-DSCs, whose thickness is limited to less than 3 μm. The use of plasmonic effects is particularly attractive for achieving this.[210] DSCs with plasmonic back-reflectors can be made by using nanoimprint lithography to press a hexagonal array of holes into a film of titania nanocrystals before the film is sintered. When the hole conductor infiltrates the film, it does not planarize the top surface. Consequently, when the silver electrode is deposited, it contains a patterned array of posts sticking into the solar cell that can scatter light very effectively and possibly couple it to plasmon–polariton modes. Plasmonic back-reflectors have been shown to improve the performance of cells containing weakly absorbing ruthenium-based dyes by 20%, and cells containing strongly absorbing donor–pi–acceptor dyes by 5%[211]. Another plasmonic approach is to incorporate metal nanoparticles covered with an insulator or n-type oxide directly into the solar cell.[212] Light excites the plasmon resonances of these particles and so significantly enhances the electric field (and therefore absorption) in the regions surrounding them.

Although light-trapping techniques are certainly helpful, the extent to which they can be used to solve absorption problems is limited because light-trapping also enhances parasitic absorption by the 'transparent' electrode and hole conductor.

2.4.2.7 Co-sensitization and energy relay dyes

One of the greatest opportunities for improving the efficiency of all types of DSC is to reduce the energy gap of the dyes so that more light in the spectral range of 650–940 nm can be absorbed (Figure 75 a). However, finding one dye that absorbs strongly all the way from 350–940 nm is extremely difficult. Typically, the peak absorption coefficient and spectral width of a dye are inversely related to each other. The most promising strategy for harvesting the whole spectrum is to use a combination of visible- and NIR-absorbing dyes. In the past, the co-sensitization of ruthenium metal complex dyes was considered to be problematic because their low molar extinction coefficient required full monolayer coverage on the titania of relatively thick films to absorb all the incident red photons. However, organic dyes have significantly higher molar extinction coefficients than ruthenium metal complex dyes and thus require smaller surface areas, making it possible to co-sensitize thinner DSC films without significantly reducing light-harvesting in any portion of the spectrum.[213] Today's record-efficiency DSC employs a co-sensitization strategy to boost absorption at a wavelength of 550 nm. Although co-sensitization for this device results in an overall increase in the power-conversion

---

[209] Nishimura, S. *et al*. Standing wave enhancement of red absorbance and photocurrent in dye-sensitized titanium dioxide photoelectrodes coupled to photonic crystals. J. Am. Chem. Soc. 125, 6306–6310 (2003)

[210] Brown, M. D. *et al*. Plasmonic dye-sensitized solar cells using core–shell metal–insulator nanoparticles. Nano Lett. 11, 438–445, 2010

[211] Ding, I. K. *et al*. Plasmonic dye-sensitized solar cells. Adv. Energ. Mater. 1, 52–57 (2011)

[212] Standridge, S. D., Schatz, G. C. & Hupp, J. T. Distance dependence of plasmon-enhanced photocurrent in dye-sensitized solar cells. J. Am. Chem. Soc. 131, 8407–8409 (2009)

[213] Cid, J.-J. *et al*. Molecular cosensitization for efficient panchromatic dye-sensitized solar cells. Angew. Chem. Int. Ed. 119, 8510–8514 (2007).

efficiency due to an increased short-circuit current density, V_{OC} is reduced slightly because the co-sensitized dye used to absorb light at 550 nm is not as good at blocking recombination as the YD2-o-c8 dye with which the device is co-sensitized.

Only a few NIR dyes (that is, peak absorption at >700 nm) have so far demonstrated good charge injection efficiencies in DSCs, although no NIR dye has yet independently achieved a V_{OC} greater than 460 mV in an electrolyte-based cell.[214] NIR-sensitizing dyes that do not require large over-potentials to regenerate and do not have high recombination rates will be required to push efficiencies towards 15%. The most significant challenge of co-sensitization using NIR dyes is maintaining a large V_{OC}, which requires that each dye adequately prevents recombination. The problem of V_{OC} reduction is likely to be even more pronounced with NIR dyes because they have small bandgaps. The resulting energy and hole transfer from neighbouring visible sensitizing dyes[215] can increase recombination and lower V_{OC}.[216]

Energy relay dyes (ERDs) decouple the light-harvesting and charge-transfer processes, and therefore have a range of potential advantages over co-sensitization techniques. In DSCs, ERDs absorb sunlight and then transfer energy non-radiatively to sensitizing dyes, which are responsible for charge separation (Figure 76). ERDs have been placed inside the electrolyte[217] and the semiconductor[218], co-sensitized[219] on the semiconductor surface, and tethered to sensitizing dyes. The use of ERDs has several important advantages over co-sensitization. Because ERDs do not participate in the charge-transfer process, they do not require precise energy levels for charge transfer, which allows for a wide range of dyes to be implemented in DSC systems. ERDs can be used to fill absorption gaps in the sensitizing dye for a liquid-based device, and also to increase the overall light-harvesting efficiency of solid-state systems.[220] ERDs do not need to attach to the semiconductor surface in order to contribute to light-harvesting, and thus their addition can both widen and strengthen the overall absorption spectrum for the same film thickness.

---

[214] Maeda, T. *et al*. Near-infrared absorbing squarylium dyes with linearly extended π-conjugated structure for dye-sensitized solar cell applications. Org. Lett. 13, 5994–5997 (2011)

[215] Sayama, K. *et al*. Efficient sensitization of nanocrystalline TiO_2 films with cyanine and merocyanine organic dyes. Sol. Energ. Mater. Sol. C. 80, 47–71 (2003).

[216] Hardin, B. E. *et al*. Energy and hole transfer between dyes attached to titania in cosensitized dye-sensitized solar cells. J. Am. Chem. Soc. 133, 10662–10667 (2011).

[217] Shankar, K., Feng, X. & Grimes, C. A. Enhanced harvesting of red photons in nanowire solar cells: Evidence of resonance energy transfer. ACS Nano 3, 788–794 (2009).

[218] Buhbut, S. *et al*. Built-in quantum dot antennas in dye-sensitized solar cells. ACS Nano 4, 1293–1298 (2010)

[219] Brown, M. D. *et al*. Surface energy relay between cosensitized molecules in solid-state dye-sensitized solar cells. J. Phys. Chem. C 115, 23204–23208 (2011).

[220] Yum, J. H. *et al*. Panchromatic response in solid-state dye-sensitized solar cells containing phosphorescent energy relay dyes. Angew. Chem. Int. Ed. 48, 9277–9280 (2009)

Figure 76: DSC containing ERDs: ERDs mixed inside the liquid electrolyte (a) and co-sensitized to the titania surface (b). Typical absorption process for lower energy (red) photons in DSCs: light is absorbed by the sensitizing dye (i), after which an electron is transferred to the titania and a hole is transported to the back contact through the electrolyte. The ERD process is similar except that higher energy (blue) photons are first absorbed by the ERD and then undergo Förster resonant energy transfer (FRET; ii) at rate k_{ET} to the sensitizing dye, which is responsible for charge separation (iii) involving electron injection (rate k_{inj}) and hole regeneration (rate k_{reg}). Source: Nature Photonics, 2012

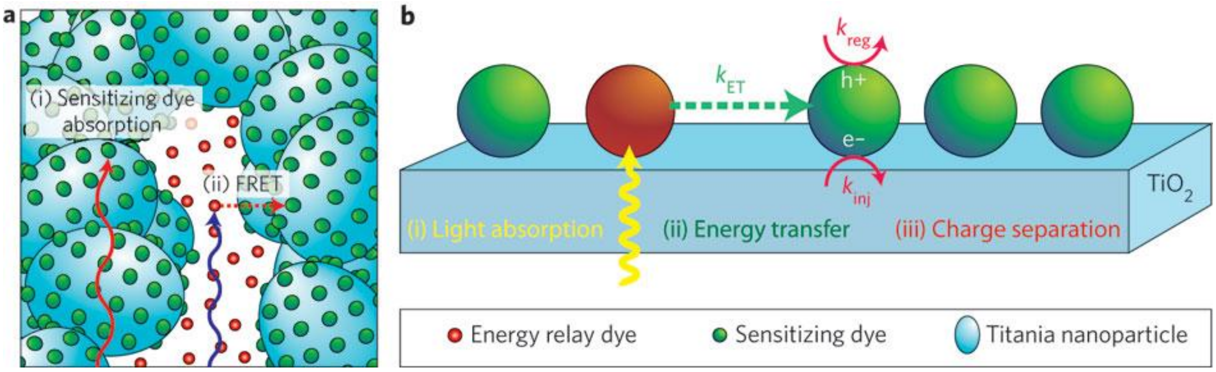

ERDs typically transfer energy via Förster resonant energy transfer, which involves dipole–dipole coupling between the ERD and the sensitizing dye. The distance over which energy transfer can occur efficiently is determined primarily by the molar extinction coefficient of the sensitizing dye and the overlap between the emission spectrum of the ERD and the absorption spectrum of the sensitizing dye. When designing ERDs, it is important to use dyes with relatively short photoluminescent lifetimes (<10 ns) because the rate of energy transfer depends on the rate of light emission and must therefore be faster than quenching by the electrolyte/hole conductor. It is possible to use multiple ERDs to expand the overall spectral coverage.[221]

Energy transfer may occur efficiently over fairly long distances (that is, >25 nm) for ERDs that have a strong emission overlap with the absorption spectrum of tightly packed organic dyes on the semiconductor surface.[222] This allows for high excitation transfer efficiencies of >90% for ERDs placed inside liquid-electrolyte systems[223] and >60% for ERDs placed in the hole conductor in ss-DSCs[224]. It has not yet been possible to dissolve enough ERDs into the electrolyte to absorb all of the light, although this should be possible to achieve by increasing the solubility and molar absorption coefficients of the ERDs. It is still possible for systems with weaker dipole–dipole coupling to efficiently transfer energy over short distances, although this requires the ERDs to be within 1–3 nm of the sensitizing dye requiring co-sensitization or tethering.

---

[221] Yum, J.-H. *et al.* Incorporating multiple energy relay dyes in liquid dye-sensitized solar cells. Chem. Phys. Chem. 12, 657–661 (2011).

[222] Hoke, E. T., Hardin, B. E. & McGehee, M. D. Modeling the efficiency of Förster resonant energy transfer from energy relay dyes in dye-sensitized solar cells. Opt. Express 18, 3893–3904 (2010)

[223] Hardin, B. E. *et al.* High excitation transfer efficiency from energy relay dyes in dye-sensitized solar cells. Nano Lett. 10, 3077–3083 (2010)

[224] Mor, G. K. *et al.* High-efficiency Fo¨rster resonance energy transfer in solid-state dye sensitized solar cells. Nano Lett. 10, 2387–2394 (2010).

2.4.2.8 Conclusions: DSC

The ultimate goal of any emerging solar cell technology is to achieve an installed cost-per-watt level that reaches grid parity versus conventional fossil fuel technologies and competes favourably against incumbent photovoltaic technologies. Silicon photovoltaic module costs have continued to reduce from 2.99€/W in 2008 to just 0.93€/W in 2011, with module efficiencies ranging from 15% to 20% and lifetimes guaranteed to 25 years. It is realistic to expect that silicon photovoltaic modules could continue to reduce in manufacturing costs to around 0.52€/W, with module efficiencies rising to 18–22%. Great strides have also been made in the commercialization of thin-film technologies, where CdTe has achieved module efficiencies of 10–12.5% at costs of 0.52€/W and current roadmaps expect to achieve module efficiencies of 14% at costs of 0.37€/W. Copper indium gallium selenide modules are now commercially available, with efficiencies of 12–15% and module costs expected to be less than 0.37€/W

How DSCs will compete in the future photovoltaic market depends not only on the ability to increase power-conversion efficiencies and develop ultralow-cost architectures that are stable over 20 years, but also on market factors such as the overall photovoltaic demand and the scarcity of rare elements. DCSs can be constructed from abundant non-toxic materials, which is a significant benefit over current thin-film technologies. Commercializing 10%-efficient modules may require ultralow-cost architectures that reduce inherent costs by removing at least one glass substrate, thereby pushing costs down to 15€/m^2. It is important to note there is an increased non-module 'balance-of-systems' cost associated with using less-efficient solar modules; for example, installing 10%-efficient modules costs 0.22€/W more than 15%-efficient modules. 10%-efficient DSC modules will therefore probably need to be priced at 0.15–0.22€/W and thus manufactured at 15–22€/m^2 to compete for utility-scale power generation. Substrates represent the largest module costs. At the gigawatt scale, glass covered with fluorine-doped tin oxide costs 6–9€/m^2, whereas uncoated glass costs 4€/m^2. The glass–glass laminate for DSCs would therefore cost at least 10€/m^2, leaving only US$7–17 m^{-2} for the remainder of manufacturing, which is possible but challenging.

Ultralow-cost DSCs could be built from cheap metal foils (such as stainless steel and aluminium) and plastic sheets to reduce glass costs. Although iodide is known to dissolve aluminium and stainless steel, there is significant opportunity to create pinhole-free protective coatings on foils and develop electrolytes that are less corrosive than iodide. Additional stability issues emerge when using plastics sheets instead of glass, which have significantly higher water vapour transport rates and thus allow moisture to ingress into the DSC. Researchers have yet to produce a plastic sheet that is cheaper than glass while also having an adequate water vapour transport rate. Developing water-tolerant DSCs is an interesting pathway that is unique to this technology. Furthermore, sputtered transparent conducting oxides on plastics are more expensive, less transparent and more resistive than when deposited on glass, which provides lower performance levels. Cheaper transparent conducting electrodes for DSCs must therefore be developed to match the efficiency of glass-based designs. Increasing the module efficiencies of DSCs to more than 14% would relax the ultralow-cost constraints, thus providing substantial incentive to create laboratory-scale devices with efficiencies greater than 15%. The relatively slow increase in record values for DSCs over the past ten years has left the impression of a performance ceiling, which is partially justified given that conventional iodide- and ruthenium-based DSCs have a realistic maximum possible efficiency of little more than 13%. The loss-in-potential can realistically be reduced to 500 mV by better matching the energy levels at the heterojunction, using more strongly absorbing dyes in thinner films and further inhibiting recombination losses, pushing efficiencies to 19% with a dye capable of absorbing out to 920 nm. Finally, although there have been a number of initial studies into the development of DSC modules, a thorough understanding of the overall lifetimes and degradation mechanisms of new DSC cell and module designs requires a great deal of further investigation.

2.4.3 New technologies for PV cell production

2.4.3.1 Concepts for nanostructured solar cells

Other than searching for new material to improve solar cell output, new technology in processing PV solar cell has been ascertained. Nanotechnology is used in order to help increase conversion efficiency of solar cell since energy band-gap can be controlled by nanoscale components. The potential advantages of using this technology are: (i) enhancement of material mechanical characteristic, (ii) low cost, (iii) lightweight and (iv) good electrical performances. A particular advantage of nanostructured materials is the tunability of their optical and electronic properties, which may enable the implementation of "third generation" approaches (i.e., strategies for reducing thermal losses) for improved PV power conversion efficiencies. Advancements in the field of nanostructured PVs (nano-PVs) have led to rapid improvements over the past decade in the power conversion efficiencies of this broad class of solar cells (Table 17).[225]

Table 17: Representative device performance of various single-junction nanostructured photovoltaic cells under 1-sun illumination. Source: Adv. Mater. 2011

Donor [a)]	Acceptor	E_G [eV]	V_{OC} [V]	J^{SC} [mA cm^{-2}]	FF	η_P [%]
Small Molecule						
NPD	C_{60}	3.0	0.86	2.5	051	1.1
Tetracene	C_{60}	2.3	0.58	7.0	0.57	2.3
PtOEP	C_{60}	2.3	0.66	5.6	0.57	2.1
DIP	C_{60}	2.1	0.93	8.4	0.74	3.9
Rubrene	C_{60}	2.1	0.91	3.2	0.53	1.5
DBP	C_{60}	1.9	0.92	6.3	0.65	3.6
PtTPBP	C_{60}	1.8	0.69	4.5	0.63	1.9
CuPc	C_{60}	1.7	0.50	15.5	0.56	4.5
SubNc	C_{60}	1.7	0.79	6.1	0.49	2.5
BP	Ind- C_{60}	1.7	0.75	10.5	0.65	5.2
DCV6T	C_{60}	1.7	0.9	6.5	0.64	3.8
SQ	$PC_{70}BM$	1.6	0.92	12.0	0.5	5.5
ZnPc	C_{60}	1.5	0.58	11.7	0.62	3.9

---

[225] R. R. Lunt, T. P. Osedach, P. R. Brown , J. A. Rowehl, V. Bulovic. Practical Roadmap and Limits to Nanostructured Photovoltaics. Adv. Mater. 2011, 23, 5712–5727

Donor a)	Acceptor	E_G [eV]	V_{OC} [V]	J^{SC} [mA cm^{-2}]	FF	η_P [%]
ClAlPc	C_{60}	1.5	0.82	6.5	0.58	3.0
SnPc	C_{60}	1.2	0.42	7.6	0.63	1.9
PT Psub	C_{60}	1.0	0.25	-	-	-
PT Pfused	C_{60}	0.9	0.2	-	-	-
CNT	C_{60}	0.9	0.25	-	0.51	0.6
DSSC						
D131	TiO_2, P3HT HTL	2.3	1.03	6.3	0.60	3.9
Zn5S	TiO_2	1.9	0.67	7.2	0.67	3.1
Cu-Complex 1	TiO_2	1.9	0.57	5.3	0.64	1.9
Ru-TPA-NCS	TiO_2 ,HTL	1.9	0.77	5.7	0.34	1.5
Ru-TPD-NCS	TiO_2,HTL	1.9	0.76	12.7	0.35	3.4
Ru Complex	TiO_2	1.8	0.68	15.3	0.69	7.1
K68	TiO_2	1.8	0.86	11.0	0.68	6.1
TCPP	TiO_2	1.8	0.46	-	0.62	3.5
Cu-Complex 1	TiO_2	1.8	0.56	5.9	0.70	2.3
C101	TiO_2, spiro-MeOTAD	1.8	0.80	8.2	0.69	4.5
D149	TiO_2, PEDOT HTL	1.8	0.86	9.3	0.75	6.1
Rul2(SCN)2	TiO_2	1.7	0.72	18.2	0.73	10.0
CYC-B6S	TiO_2	1.7	0.78	19.8	0.63	9.7
Ru-Complex	TiO_2	1.7	0.80	17.0	0.74	10.1
A6141	TiO_2	1.7	0.80	17.6	0.73	10.3
ZnPcTyr	TiO_2	1.6	0.36	2.3	0.67	0.5
Black Dye	TiO_2	1.5	0.74	20.9	0.72	11.1
RuL(NCS)3	TiO_2	1.4	0.72	20.5	0.70	10.4
Polymer						
P3HT	$PC_{70}BM$	1.9	0.64	12.4	0.51	4.1
P3HT	PCBM	1.9	0.64	11.3	0.69	5.2
APFO-3	$PC_{70}BM$	1.9	1.16	10.0	-	-
P3HT	Indene-C_{60}	1.9	0.84	10.6	0.73	6.5
F8TBT	P3HT	1.9	1.20	4.0	-	1.8
PCDTBT	$PC_{70}BM$	1.8	0.86	10.6	0.64	6.0
F8TBT	PCBM	1.8	1.10	4.0	-	1.3
PFDPP2T-c	PCBM	1.7	0.91	2.4	0.40	0.9
PBDTTT-CF	PCBM	1.6	0.76	-	0.66	6.8
MDMO-PPV	PCBM	1.6	0.92	3.0	-	-
PDPDTBT	$PC_{70}BM$	1.4	0.62	16.2	0.55	5.5
APFO-9	PCBM	1.4	0.81	6.5	0.44	2.3
PCPDTDPP2T-c	PCBM	1.3	0.61	5.7	0.49	1.7
P1TPQ	PCBM	1.2	0.71	0.8	0.58	0.3
P3TPQ	$PC_{70}BM$	1.2	0.52	7.3	0.54	2.1
PTBEHBQ	PCBM	1.2	0.72	0.6	0.53	0.2
P3	PCBM	1.1	0.41	5.2	0.29	0.6
LBPP1	PCBM	1.0	0.34	3.3	0.34	0.4
PBTTQ	PCBM	1.0	0.10	0.3	0.35	0.01
CQD						
PbS	-	2.2	1.32	-	0.42	2.9
CdSe	-	2.1	0.80	-	-	-
CdSe	-	1.9	0.53	6.2	0.53	1.8
CdSe	-	1.9	0.70	0.2	0.40	0.1
CdSe	-	1=9	0.63	4.8	0.52	1.5
CdSe	-	1.8	0.68	4.2	0.38	1.1
S_b2S_3	TiO_2P3HT	1.7	0.65	13.0	0.61	5.13
PbS	-	1.2	0.55	11.4	0.56	3.5
PbS	-	1.2	0.59	8.9	0.56	2.9
PbS	-	1.2	0.51	16.2	0.58	5.1
PbS	-	1.2	0.51	14.0	0.51	3.6
PbS	-	1.2	0.58	15	0.42	3.5
PbS	-	1.1	0.56	17.0	0.61	5.7

Donor a)	Acceptor	E_G [eV]	V_{OC} [V]	J^{SC} [mA cm^{-2}]	FF	η_P [%]
PbS	-	1.0	0.45	13.2	0.35	2.1
PbS	-	0.9	0.45	14.5	0.60	3.9
PbS	-	0.9	0.46	4.2	0.62	1.3
PbS	-	0.8	0.16	8.2	0.38	0.5
PbS	-	0.8	0.24	14.0	0.50	1.7
PbS	-	0.8	0.38	11.3	0.21	0.9
PbSe	-	0.7	0.18	27.0	0.35	1.7
PbS	-	0.7	0.33	-	-	-
PbS	-	0.7	0.32	12.3	0.44	1.8

a) Chemical abbreviations: NPD - N, N´-diphenyl-N,N’-bis(1-naphthyl)-1,1´biphenyl-4,4´´ diamine; PtOEP - 2,3,7,8,12,13,17,18-octaethyl-21H,23H-porphine platinum(II); DIP - di-indenoperylene; DBP - dibenzo{[f,f’] - 4,4′,7,7′-tetraphenyl}diindeno[1,2,3-cd:1′,2′,3′-lm]perylene; PtTPBP - platinum tetraphenylbenzoporphyrin; CuPc – copper phthalocyanine; SubPc - boron subphthalocyanine; BP - tetrabenzoporphyrin; DCV6T - bis-(dicyanovinylen)-sexithiophene; SQ - 2,4-bis[4-(N, N - diisobutylamino)-2,6-dihydroxyphenyl] squaraine; ZnPc - zinc phthalocyanine; ClAlPc - chloro-aluminum phthalocyanine; SnPc – tin phthalocyanine; PT Psub - diporphyrin–pyrene; PT Pfused - pyrene-fused diporphyrin; CNT - carbon nanotube; P3HT - poly(3-hexylthiophene); APFO-3 - poly[(9,9-dioctylfluorenyl-2,7-diyl)-alt-5,5-(40,70-di-2-thienyl-20,10,30-benzothiadiazole)]; F8TBT - poly((9,9-dioctylfluorene)-2,7-diyl-alt-[4,7-bis(3-hexylthien-5-yl)-2,1,3-benzothiadiazole]-2′,2″-diyl); PBDTTT-CF - poly[4,8-bis(2-ethylhexyloxy)-benzo[1,2-b:4,5-b′]dithiophene-2,6-diyl-alt-(4-octanoyl-5-fluoro-thieno[3,4-b]thiophene-2-carboxylate)-2,6-diyl]; MDMO-PPV - poly[2-methoxy-5-(3′,7′-dimethyloctyloxy)-1,4-phenylene vinylene]; PCPDTBT - poly[2,1,3-benzothiadiazole-4,7-diyl[4,4-bis(2-ethylhexyl)-4H-cyclopenta[2,1-b:3,4-b’]dithiophene-2,6-diyl]; P3 - 6,7-diphenyl-4,9-bis-(thiophen- 2-yl)-[1,2,5]thiadiazolo[3,4-g]quinoxaline/9-triarylamino-9H-carbazole; PCBM - [6,6]-phenyl-C61-butyric acid methyl ester; spiro-OMeTAD - (2,2(,7,7(-tetrakis-(N,N-dipmethoxyphenylamine) 9,9(-spirobifluorene); PEDOT - poly(3,4-ethylenedioxythiophene); HTL - hole transport layer.

2.4.3.1.1 Advantages of photovoltaics based on 1D nanostructure arrays

1D nanostructure arrays can be prepared by a variety of “bottom-up” and “top-down” approaches such as CVD, solution chemistry, photo- and electron-beam lithography, nanoimprinting, the vapor–liquid–solid (VLS) method, colloidal lithography, template-guided deposition and electrospinning etc.[226]

2.4.3.1.1.1 Improved anti-reflection and broadband absorption

The efficiency of a solar cell depends on the probability of an incident photon being absorbed, and the subsequent collection of the generated carriers, so solar cells surfaces with high absorbance and low reflectivity are often required. The current industrial standard of anti-reflection coating for thin-film solar cells is to use a quarter wavelength transparent layer with destructive interference. However, this technique only works for a narrow range of wavelengths.

Recently, reflection reduction and absorption enhancement have been widely observed in compound eyes of some nocturnal insects like moths, as well as 1D semiconductor nanostructure arrays.[227] As shown in

---

[226] Y. Z. Long, M. M. Li, C. Z. Gu, M. X. Wan, J. L. Duvail, Z. W. Liu and Z. Y. Fan, Prog. Polym. Sci., 2011, 36(10), 1415

[227] J. Zhu, Z. F. Yu, S. H. Fan and Y. Cui, Mater. Sci. Eng., R, 2010, 70, 330

Figure 77 a-b, between 400 and 650 nm, the absorption of nanocone arrays fabricated by the nanosphere lithography was maintained above 93%, which was much better than for either the nanowire array (75%) or thin film (64%). As shown in

Figure 77 c-d, these ordered dual-diameter pillar arrays with a thickness of only 2 µm showed an impressive absorbance of ~99% over a broad range of wavelengths of 300–900 nm.

Figure 77: (a) SEM image of amorphous Si:H nanocones prepared by nanosphere lithography. (b) Measured value of absorption on samples with a-Si:H thin film, nanowire arrays, and nanocone arrays as the top layer over a large range of wavelengths at normal incidence. (c) Schematic of a dual-diameter nanopillar array embedded in anodic aluminum oxide templates. (d) Experimental absorption spectra of a dual-diameter nanopillar array with D_1 = 60 nm and D_2 = 130 nm, and single-diameter nanopillar arrays with diameters of 60 and 130 nm. Source: Nanoscale , 2012, 4 M.Yu

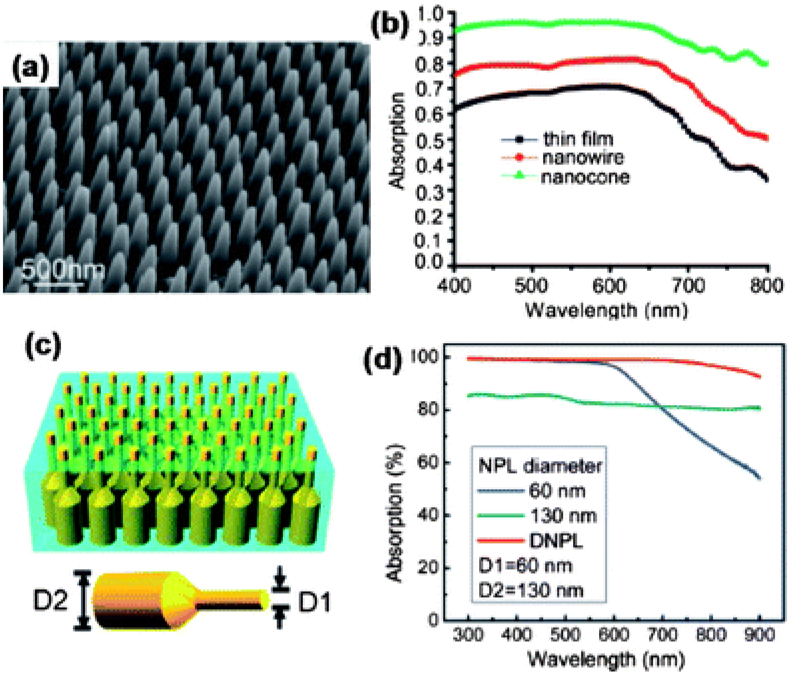

Power conversion efficiency has also been enhanced for solar cells coated with these 1D nanostructure arrays. For instance, Forberich et al.[228] fabricated a type of organic solar cells by using a nano-replicated moth eye anti-reflection coating as an effective medium at the air-substrate interface, and the efficiency can be improved approximately 2.5–3% compared with solar cells without this structure. It is well known that the Fresnel reflection at an interface of two media is equal to $[(n_1 - n_2)/(n_1 + n_2)]^2$, where n_1 and n_2 are the refractive indices of the two media. The mechanism of biomimetic 1D nanostructure arrays which may suppress the reflection losses and increase transmission of incident light can be understood easily in terms of a gradient change in refractive index from the top of the structure to the bulk materials. Namely, the anti-reflection effect is usually due to the tapered shape of nanostructures with better effective refractive index matching with air. However, through measuring maximum

---

[228] K. Forberich, G. Dennler, M. C. Scharber, K. Hingerl, T. Fromherz and C. J. Brabec, Thin Solid Films, 2008, 516, 7167

light trapping path length enhancement factors, Garnett and Yang[229] found that the light-trapping ability of Si nanowire solar cells was above the theoretical limit for a randomizing scheme, indicating that solar cells may show a photonic crystal enhancement effect. This result is consistent with the theoretical calculations. Due to the photonic crystal absorption enhancement effect in the presence of optical guided resonance modes,[230] vertical Si nanowire array solar cells with optimized photonic crystal architecture could lead to broad band solar-energy harvesting and offer conversion efficiency as high as 24% or more. In addition, for plasmonic solar cells,[231] quantum dot/nanoparticle arrays have also been incorporated for absorption enhancement in the region close to bandgap edge owing to the large resonant scattering cross-section of these particles or plasmonics.

2.4.3.1.1.2 Enhanced carrier collection efficiency

In additional to enhancing optical absorption, arrayed 1D nanostructures can also significantly enhance the photo-carrier collection efficiency if the structure is properly designed.[232] The rationale can be schematically shown in Figure 78 a-b. It is known that photo-carrier collection and light absorption are in competition for planar structured solar cells. Efficient carrier collection requires thin materials to shorten the minority carrier travel distance, and efficient light absorption requires thick materials for obvious reasons. This conflict may not be so severe in single crystalline Si as it has a minority carrier diffusion length in the hundreds of micrometers. However, the conflict is significant for poly-crystalline or even nanocrystalline materials which have relatively short carrier diffusion lengths. To greatly decrease the competition between carrier collection and light absorption, a 3D structure consisting of arrays of 1D nanomaterials for solar cells has been proposed. As shown in Figure 78 b, in such a structure, the p–n junction interface is parallel to light absorption direction, thus carrier collection occurs perpendicular to light absorption. An increase in the interface area of the p–n junction (compared with the planar structure) may significantly decrease the traveling distance for electron–hole pairs, and thus reduce the loss of electrons due to recombination. This mechanism works for both core/shell type p–n junction nanowire arrays and nanopillar/thin film hybrid devices. In fact, a comparison between nanorod arrays and planar Cd(Se,Te) photoelectrodes has been performed.[233] It was shown that the fill factors of the nanorod array photoelectrodes were superior to those of the planar junction devices. More importantly, the spectral response of the nanorod array photoelectrodes exhibited better quantum yields for collection of near-infrared photons relative to the collection of high-energy photons than the planar photoelectrodes, as shown in Figure 78 c.

---

[229] E. Garnett and P. D. Yang, Nano Lett., 2010, 10, 1082
[230] C. Lin and M. L. Povinelli, Opt. Express, 2009, 17, 19371
[231] O. L. Muskens, J. G. Rivas, R. E. Algra, E. P. A. M. Bakkers and A. Lagendijk, Nano Lett., 2008, 8(9), 2638
[232] B. M. Kayes, H. A. Atwater and N. S. Lewis, J. Appl. Phys., 2005, 97(11), 114302
[233] J. M. Spurgeon, H. A. Atwater and N. S. Lewis, J. Phys. Chem. C, 2008, 112(15), 6186

Figure 78: Schematic of carrier collection in a planar thin film single junction solar cell (a) and a 3D nanowire/pillar solar cell (b). (c) Spectral response of typical photo-etched planar and nanorod array photo-electrochemical cells with the external quantum yield normalized to its highest value. Source: Nanoscale , 2012, 4 M.Yu

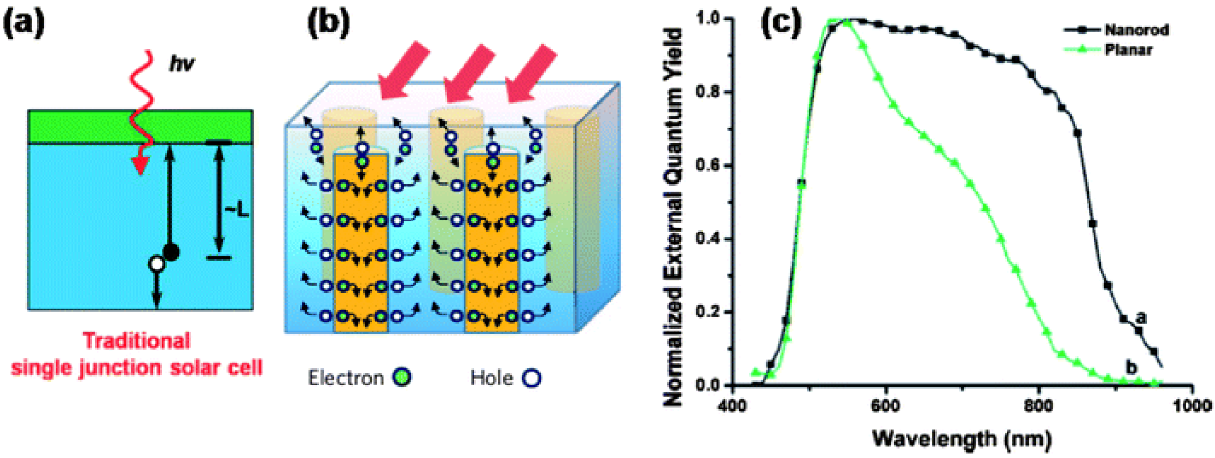

Furthermore, the performance benefit of orthogonalizing photon absorption and carrier collection was also demonstrated with the simulation of the CdS nanopillar/CdTe thin film hybrid solar cells.[234] In this work, the conversion efficiency of a device structure consisting of CdS nanopillar arrays embedded in a CdTe thin film were compared to that of a planar CdS/CdTe cell. The nanopillar structure showed improved conversion efficiency compared to its thin film counterpart, especially for small minority carrier diffusion lengths. This result provides an important guideline for solar cell design using low cost and low grade materials.

2.4.3.1.1.3 Improved self-cleaning capability

Besides their high performance optical properties, the antireflective structure (ARS) arrays with high aspect ratios also exhibit self-cleaning capabilities due to the high fraction of air trapped in the trough area between nanopillars.[235] This function may provide one approach to solve the problem of dust particles accumulating on the solar cell surface and blocking the sunlight and thus reducing the power efficiency. For example, Min et al.[236] reported a templating technique using non-close-packed silica or close-packed polystyrene nanospheres as etching masks for fabricating broadband self-cleaning ARS surfaces with high aspect ratios (up to ca. 10) on both Si and glass substrates. Such ARS surfaces exhibit high performance antireflective properties. In addition, both surfaces are superhydrophobic and the measured apparent water contact angle was 172° for Si pillar arrays and 160° for the glass pillar arrays, which is significantly enhanced from 108° and 105° on fluorinated flat Si and glass substrates. Li et al.[237] have successfully prepared high aspect ratio Si hollow-tip arrays for high performance antireflective surfaces (Figure 79 a). The surfaces can suppress surface

---

[234] . Y. Fan, H. Razavi, J. W. Do, A. Moriwaki, O. Ergen, Y. L. Chueh, P. W. Leu, J. C. Ho, T. Takahashi, L. A. Reichertz, S. Neale, K. Yu, M. Wu, J. W. Ager and A. Javey, Nat. Mater., 2009, 8, 648

[235] Y. F. Li, J. H. Zhang, S. J. Zhu, H. P. Dong, F. Jia, Z. H. Wang, Z. Q. Sun, L. Zhang, Y. Li, H. B. Li, W. Q. Xu and B. Yang, Adv. Mater., 2009, 21(46), 4731

[236] W. L. Min, B. Jiang and P. Jiang, Adv. Mater., 2008, 20(20), 3914

[237] Y. F. Li, J. H. Zhang, S. J. Zhu, H. P. Dong, Z. H. Wang, Z. Q. Sun, J. R. Guo and B. Yang, J. Mater. Chem., 2009, 19, 1806

reflection from ultraviolet, visible light, to the mid-infrared region, with specular reflectance lower than 1% in the 250–1600 nm range. In addition, the tip arrays possess perfect water-repellent properties (with a measured apparent water contact angle of 165° and a small sliding angle of 2°) due to their high aspect ratio, as shown in Figure 79 b.

Figure 79: (a) SEM image of the hollow-tip arrays, and (b) an optical image of the water droplet profile (5 mL) on the silicon hollow-tip array surface. Source: The Royal Society of Chemistry, 2009

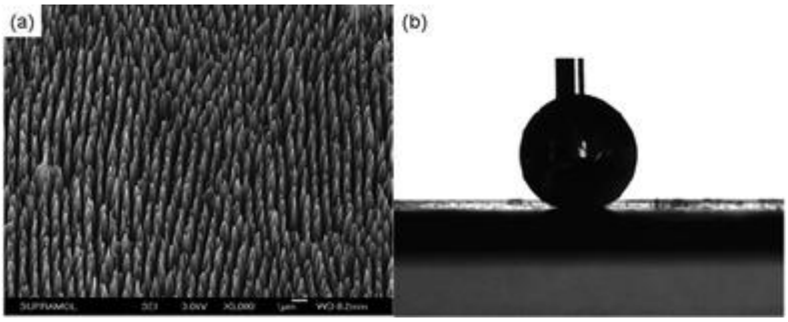

The ARS surfaces with water-repellent or antifogging properties enable the application of the devices in humid environments.

2.4.3.1.2 Three-dimensional nanostructured solar cells

2.4.3.1.2.1 Solar cells based on Si, Ge or GaAs nanowire/pillar arrays

Solar cells based on Si nanowires have drawn more and more interest in recent years for their strongly enhanced light trapping, high carrier collection efficiency and potential low cost, and a large number of promising works have been done on this series of materials. For instance, Tian et al.[238] have fabricated individual radial p–i–n coaxial Si nanowire structures consisting of a p-type Si nanowire core capped with i- and n-type Si shells. The open circuit voltages V_{oc}, short circuit current I_{sc} and fill factor FF are measured as 0.26 V, 0.503 nA and 0.55, respectively. The p–i–n Si nanowire elements yield a maximum power output of up to 200 pW per nanowire device and an apparent energy conversion efficiency of up to 3.4% after exclusion of the metal covered area. After that, large area arrays of Si nanowires with radial p–n junctions have been reported. For example, Garnett et al.[239] have demonstrated a simple and scalable method to fabricate large-area ordered Si nanowire radial p–n junction photovoltaics (Figure 80 a). The method requires dip coating a Si substrate to self-assemble SiO_2 spheres, followed by deep reactive-ion etching (DRIE) to form ordered nanowires and diffusion to form the p–n junction. A maximum light trapping path length enhancement factor, depending on the nanowire geometry, over the entire AM 1.5G spectrum between 1.7 and 73 were measured. This agrees well with enhancement factors between 2 and 62 extracted from optical transmission measurements. Their efficiencies are above 5%, with short circuit photocurrents higher than those of planar control samples. Bao et

---

[238] B. Z. Tian, X. L. Zheng, T. J. Kempa, Y. Fang, N. F. Yu, G. H. Yu, J. L. Huang and C. M. Lieber, Nature, 2007, 449(7164), 885

[239] E. Garnett and P. D. Yang, Nano Lett., 2010, 10, 1082

al.[240] have performed further research on such nanowires, and their investigation demonstrates that ordered nanowire arrays with random-diameters show significantly broadened and enhanced absorption, while random-length nanowire arrays show both significantly reduced reflection and enhanced absorption. The absorption enhancement can be attributed to the enhanced interwire multiple scattering and/or inner-wire resonance in the random array structure. In addition, Baek et al.[241] have observed the relationship between the wire length and cell performance. That is, the beneficial effects of the Si solar cells are derived from the better light trapping property with increasing wire length. Moreover, high-efficiency (up to 10.8%) solar cells have been achieved using a new large-area ordered Si nano-conical-frustum (NCF) array (Figure 80 b) by self-powered parallel electron lithography (SPEL).[242] The NCF array structure exhibits an impressive absorbance of ~99% (upper bound) over the wavelengths 400–1100 nm with a thickness of only 5 µm. The solar cells with ordered Si NCF arrays (800 nm lattice constant) had a short circuit current density (J_{sc}) of 26.4 mA/cm^2, V_{oc} of 0.59 V, FF of 0.69, and an efficiency of 10.8%. Although these NCF structure arrays have high light absorption efficiency, the solar cell efficiency is still less than half of that for bulk crystalline Si solar cells and the V_{oc} and FF are lower too. This is probably due to the high surface recombination losses, which are introduced by the highly enhanced surface area from the nanostructures, although a thin passivation oxide layer was used.

Figure 80: (a) Tilted cross-sectional SEM image of the Si nanowire solar cell. (b) The side view (45°) SEM image of the ordered Si NCF arrays, with scale bar 800 nm. (c) Cross-sectional schematic of ZnO-nanorod/a-Si:H solar cells. Source American Institute of Physics, 2011

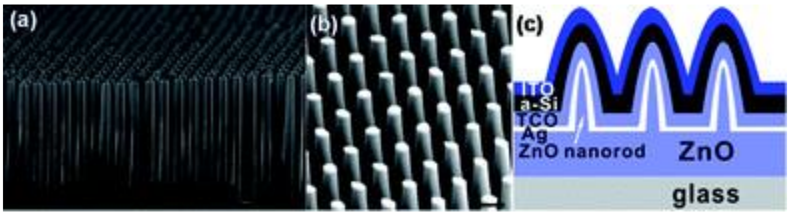

In addition, Kuang et al.[243] have employed an ultrathin hydrogenated amorphous Si (a-Si:H) n-i-p junction deposited on ZnO nanorod arrays, and the cross-sectional structure schematic is shown in Figure 80 c. In this case, an efficiency of 3.6% and a short-circuit current density of 8.3 mA cm^{-2} were obtained, significantly higher than values achieved from planar or even textured counterparts with a-Si:H absorber layers thickness of 75 nm.

Ge is an excellent light absorption material due to its small band-gap. For example, self-organized anodic Al_2O_3 membranes were used as templates for the vapour–liquid–solid growth of ordered, single-crystalline Ge nanopillar arrays on Al foil with controlled shape and dimensions. A dual-diameter Ge nanopillar structure is demonstrated by Fan

---

[240] H. Bao and X. L. Ruan, Opt. Lett., 2010, 35(20), 3378
[241] S. H. Baek, H. S. Jang and J. H. Kim, Curr. Appl. Phys., 2011, 11, S30
[242] R. Y. Lu and A. Lal, Nano Lett., 2010, 10, 4651
[243] Y. H. Kuang, K. H. M. van der Werf, Z. S. Houweling and R. E. I. Schropp, Appl. Phys. Lett., 2011, 98, 113111

et al.,[244] as shown in Figure 81 a-b. It enables fine control over geometry and shape of nanopillar arrays, without the use of complex epitaxial and/or lithographic processes. Here, a small diameter tip for minimal reflectance and a large diameter base for maximal effective absorption coefficient are required. The Ge NPL arrays exhibit an impressive absorbance of ~99% for λ = 300–900 nm. Peköz et al.[245] have analyzed the properties of the designed Ge/Si and Si/Ge core/shell and Si–Ge layered nanowires using a mathematical method. Both core/shell and layered nanowires have a strong charge-carrier separation, with electron states mainly on Si atoms and hole states on Ge atoms. This charge separation also potentially makes it easier to design and deposit effective contacts, either by the selective etching technique for the Si/Ge (Ge/Si) core/shell nanowires, or by direct connection in the case of the triangularly shaped, layered Si/Ge nanowires. It is believed that they all show promising features for use in photovoltaic applications by overcoming some of the existing problems.

Figure 81: (a) Cross-sectional SEM image of Ge dual-diameter nanopillars after the growth in anodic aluminum oxide (AAO) membranes. (b) SEM of a single Ge dual-diameter nanopillar. (c) SEM image of the GaAs core/shell nanowires. Source: American Chemical Society, 2010

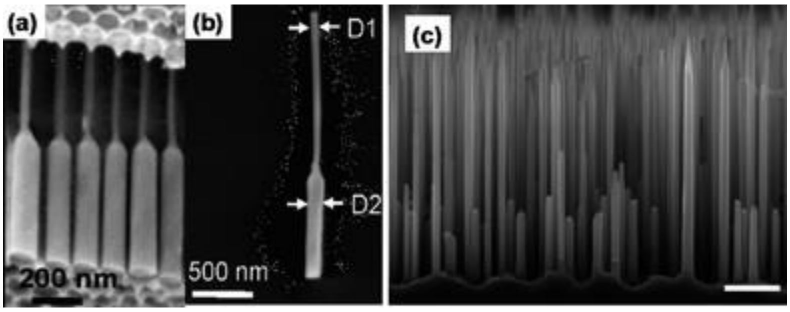

Si (or Ge) has many advantages for conventional planar solar cells, but due to its low optical absorption coefficient and small band gap, it may not be the only ideal material for nanowire solar cells. In comparison, GaAs has a larger optical absorption coefficient and nearly ideal band gap (E_g = 1.45 eV), although it still suffers from high surface recombination velocities. With efficiency η = 4.5% and fill factor FF = 0.65 under AM 1.5G illumination, Colombo et al.[246] have reported radial p–i–n diode nanowire solar cell devices based on GaAs. At the same time, LaPierre et al.[247] fabricated GaAs radial p–n nanowires with the single nanowire devices (Figure 81 c), and they exhibit η = 0.8% and FF = 0.26. Further research on GaAs nanowire solar cells has been continued by the same team. Also a numerical simulation of current–voltage characteristics of III–V nanowire core/shell p–n junction diodes under illuminated conditions is presented with an emphasis on optimizing the nanowire design for photoconversion efficiency. The calculation shows that the detailed balance efficiency of ~30% can be nearly achieved in a radial p–n junction with top contact geometry and minimal tip height, assuming that ohmic contacts and effective surface passivation can be implemented.

---

[244] Z. Y. Fan, R. Kapadia, P. W. Leu, X. B. Zhang, Y. L. Chueh, K. Takei, K. Yu, A. Jamshidi, A. A. Rathore, D. J. Ruebusch, M. Wu and A. Javey, Nano Lett., 2010, 10, 3823

[245] R. Peköz, O. B. Malcıoğlu and J. Y. Raty, Phys. Rev. B: Condens. Matter Mater. Phys., 2011, 83, 035317

[246] C. Colombo, M. Heiss, M. Gratzel and A. F. I. Morral, Appl. Phys. Lett., 2009, 94, 173108

[247] R. R. LaPierre, J. Appl. Phys., 2011, 109, 034311

2.4.3.1.2.2 CdS/CdTe nanopillar based solar cells

Since the 1.45 eV band gap of CdTe is nearly optimal for absorbing sunlight and CdS/CdTe compound semiconductors have much lower surface recombination velocities as compared to that of Si, this material system has been typically fabricated as polycrystalline films for solar cell applications. Several studies have focused on improving the efficiency of CdTe/CdS-based solar cells. For example, the Ready group has used vertically aligned periodic arrays of carbon nanotubes (CNTs) to create topographically enhanced light-trapping CdS/CdTe solar cells.[248] As shown in Figure 82 a, these 3D cells were composed of regularly spaced towers consisting of vertically aligned CNTs grown by CVD, which formed the back contact of the cell and served as a scaffold to support the photoactive hetero-junction. Then CdTe and CdS were deposited as the p/n-type materials by molecular beam epitaxy (Figure 82 b), and a conformal coating of indium tin oxide (ITO) was deposited as the transparent collection electrode. Due to multiple scattering process, the 3D cells exhibited a high current density (44.4 mA cm^{-2}) and increased power production at off-normal angles. Efficiency was shown to double from 3.5% at an orthogonal "high noon" azimuthal angle to 7% at a 45° solar incidence (Figure 82 c). Simulated modeling also showed that by optimization of geometrical parameters, such a 3D cell could obtain up to a 300% increase in power production over traditional cells.[249]

Figure 82: (a) SEM image of as grown array of vertically aligned CNT towers. (b) Cutaway view of individual CNT tower (black) coated with CdTe (gray) and CdS. (c) The corresponding increase in efficiency for CNT-cell with respect to azimuthal angle. Source: Springer-Verlag, 2007

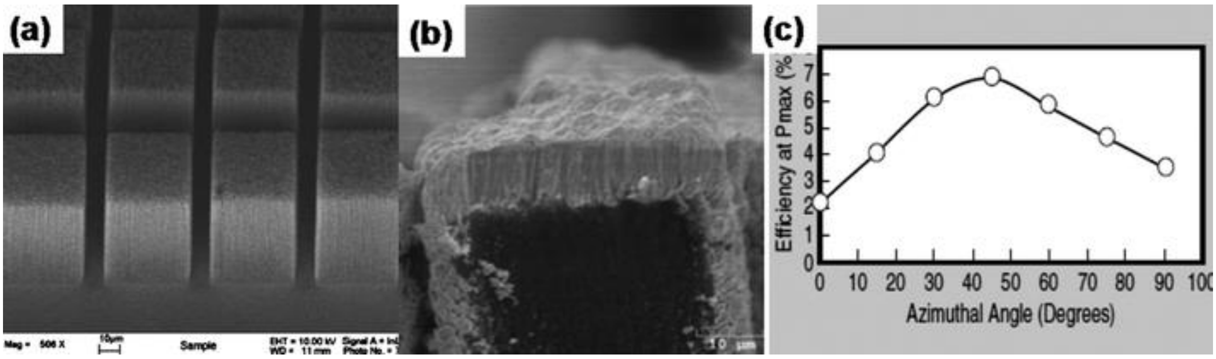

In particular, Fan et al.[250] have demonstrated a low cost nanopillar solar cell consisting of an array of CdS nanopillars partially embedded in a CdTe thin film (Figure 83 a). The nanopillar solar cells are fabricated as follows: first, n-type CdS nanopillars were grown by CVD in a porous anodic alumina membrane (AAM) with Au seeds as catalysts, which were electrochemically deposited at the bottom of the pores. Then the processed AAM was partially and controllably etched in a sodium hydroxide solution to expose the upper portion of the pillars to form the 3D structures. After that, a p-type CdTe thin film was deposited by CVD to serve as the photo-absorption layer. The top Cu/Au electrode

---

[248] R. E. Camacho, A. R. Morgan, M. C. Flores, T. A. McLeod, V. S. Kumsomboone, B. J. Mordecai, R. Bhattacharjea, W. Tong, B. K. Wagner, J. D. Flicker, S. P. Turano and W. J. Ready, JOM, 2007, 59(3), 39

[249] J. Flicker and J. Ready, J. Appl. Phys., 2008, 103(11), 113110

[250] Z. Y. Fan, H. Razavi, J. W. Do, A. Moriwaki, O. Ergen, Y. L. Chueh, P. W. Leu, J. C. Ho, T. Takahashi, L. A. Reichertz, S. Neale, K. Yu, M. Wu, J. W. Ager and A. Javey, Nat. Mater., 2009, 8, 648

was finally deposited by the thermal evaporation. In such a configuration, the backside electrical contact to the n-type CdS nanopillars was simply the Al support substrate. The cell performance was characterized under different illumination condition from 17 to 100 mW cm^{-2}. Under AM 1.5G illumination, the cell produced a short circuit current density of ~21 mA cm^{-2}, an open circuit voltage of ~0.62 V and a fill factor of ~43%, yielding an efficiency of ~6% (Figure 83 b). Besides using rigid substrates, nanopillar solar cell fabrication was also performed on plastics such as polydimethylsiloxane (PDMS) for flexible and high performance photovoltaics (Figure 83 c). It was found that the flexible nanopillar solar cell module exhibited negligible change in the cell performance, such as the energy conversion efficiency, under different bending conditions. In addition, further studies indicated that the conversion efficiency of CdS/CdTe solar nanopillar cells could be improved to over 20% through materials and device optimization.[251]

Figure 83: (a) Schematic of a solar nanopillar cell consisting of an array of CdS nanopillars partially embedded in a CdTe thin film. (b) The open-circuit voltage slightly increases with the intensity and the solar energy conversion efficiency is nearly independent of the illumination intensity for 17–100 mW cm^{-2}. (c) Schematic diagram of a bendable solar nanopillar cell module embedded in PDMS. Source: American Institute of Physics, 2010

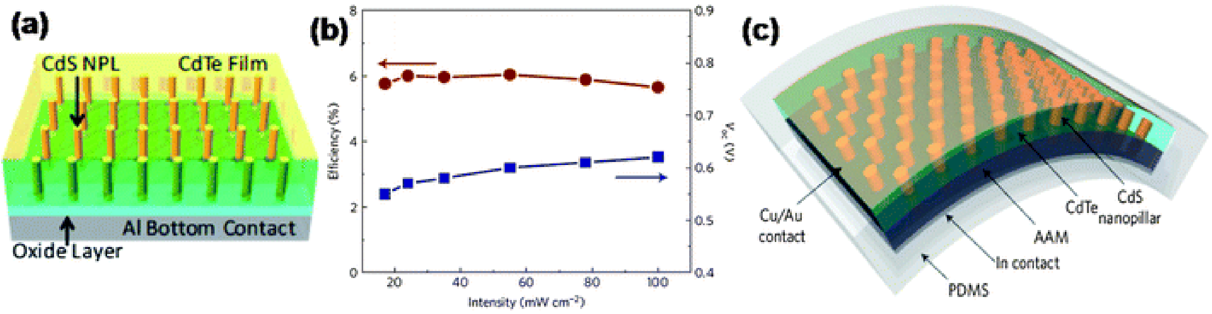

2.4.3.1.2.3 *DSSCs based on TiO_2 and ZnO nanowire/tube arrays*

4.3.1 ZnO and TiO_2 nanowires/rods. As shown in Figure 84 a, a ZnO nanowire dye-sensitized solar cell (DSSC) reported by Law et al.[252] in 2005 catalyzed research on 1D nanomaterial-based photovoltaics. The report demonstrated that 1D nanostructures might provide direct pathways for electron transport, longer diffusion length and higher charge collection efficiencies. In their work, vertical arrays of ZnO nanowires with diameters of ~130 nm were grown on F:SnO_2 (FTO) glass substrates by immersing seeded substrates in aqueous solutions. Photovoltaic measurements showed device characteristics of a short circuit current of 5.3–5.85 mA cm^{-2}, an open circuit voltage of 0.61–0.71 V, and a conversion efficiency of 1.2–1.5%. It was found that the ZnO nanowires had high electron diffusivity, 0.05–0.5 cm^2 s^{-1}, several hundred times larger than that typically used in ZnO nanoparticle films. The charge collection efficiency of ZnO nanowire photoanodes, ~55–75%, was also much higher than that of electrodes made of ZnO nanoparticles. In addition, flexible DSSCs based on vertical ZnO nanowire arrays on ITO-coated poly(ethylene terephthalate) substrates were demonstrated

---

[251] R. Kapadia, Z. Y. Fan and A. Javey, Appl. Phys. Lett., 2010, 96(10), 103116

[252] M. Law, L. E. Greene, J. C. Johnson, R. Saykally and P. D. Yang, Nat. Mater., 2005, 4(6), 455

(Figure 84 b).[253] Besides ZnO nanowire arrays, TiO_2 nanowire DSSCs were also recently reported.[254] For example, an overall conversion efficiency of 5–6% was obtained, which is obviously much higher than that of ZnO nanowire DSSC (1.2–1.5%). The improvement is attributed to a higher electron injection efficiency from excited dye molecules into the TiO_2 conduction band and/or a higher dye regeneration efficiency than that in ZnO.[255]

Figure 84: (a) Schematic diagram of a ZnO nanowire array DSSC. (b) Schematic view of a flexible ZnO nanowire array DSSC. (c) Schematic architecture of planar waveguide-nanowire integrated 3D DSSC. (d) Detailed structure of a unit waveguide-nanowire 3D DSSC. Source: Springer Group, 2011

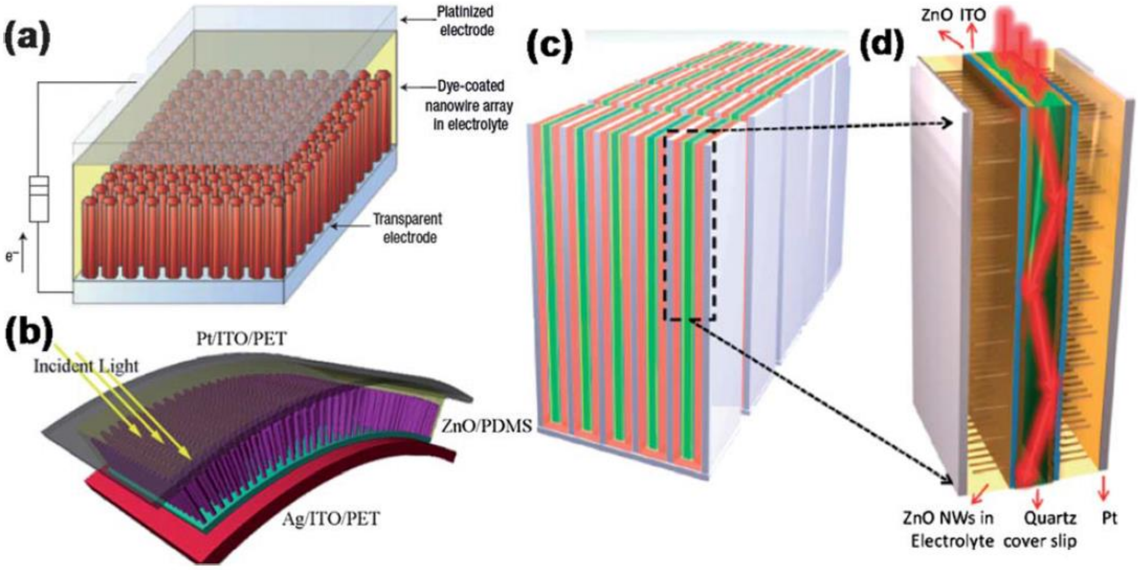

Here it should be noted that in order to improve device performance, an interesting new approach to fabricate high-efficiency 3D DSSCs by integrating planar waveguides and aligned ZnO nanowire arrays was recently presented.[256] The ZnO nanowires were grown normally on both surfaces of the quartz slide, which served as a planar waveguide for light propagation. As shown in Figure 84 c, the 3D DSSC is constructed by alternatively sandwiching the quartz slides and the planar Pt electrodes. The 3D cell can effectively increase the light absorbing surface area due to internal multiple reflections without increasing electron path length to the collecting electrode. On average an enhancement of energy conversion efficiency by a factor of 5.8 has been achieved when light propagating inside the slide is compared to the case of light illumination normal to the surface of the slide from outside. Moreover, full sun efficiencies have been achieved up to 2.4% for ZnO nanowires.

Since hollow structured nanotubes may provide a larger surface area than that of nanowires and nanorods, DSSCs based on TiO_2[257] and ZnO nanotubes[258] have drawn

---

[253] S. Chu, D. D. Li, P. C. Chang and J. G. Lu, Nanoscale Res. Lett., 2011, 6(1), 38
[254] F. shao, J. Sun, L. Gao, S. W. Yang and J. Q. Luo, J. Phys. Chem. C, 2011, 115, 1819
[255] M. Quintana, T. Edvinsson, A. Hagfeldt and G. Boschloo, J. Phys. Chem. C, 2007, 111(2), 1035
[256] Y. G. Wei, C. Xu, S. Xu, C. Li, W. Z. Wu and Z. L. Wang, Nano Lett., 2010, 10, 2092
[257] J. Bandara, K. Shankar, J. Basham, H. Wietasch, M. Paulose, O. K. Varghese, C. A. Grimes and M. Thelakkat, Eur. Phys. J.: Appl. Phys., 2011, 53, 20601
[258] J. B. Han, F. R. Fan, C. Xu, S. S. Lin, M. Wei, X. Duan and Z. L. Wang, Nanotechnology, 2010, 21(40), 405203

attention in the past years. Macák et al. reported for the first time in 2005 that TiO_2 nanotubes prepared by a simple anodic oxidation of titanium foil might have a DSSC application.[259] For back-side illumination of the DSSCs (the light comes from the counter electrode), a maximum of 4.24% efficiency has been obtained for a photoelectrode film that is comprised of ~6 μm long TiO_2 nanotubes. For front-side illumination (the light comes from the photoelectrode) with a 35 μm-thick TiO_2 nanotube photoelectrode film, a conversion efficiency as high as 7% has been reported.[260] In addition, $TiCl_4$ treatment of the TiO_2 nanotubes can also improve the conversion efficiency. However, for ZnO nanotube DSSCs,[261] the conversion efficiencies so far achieved were generally low (~1.2–1.6%). A possible reason is that the length and surface area of the ZnO nanotubes are limited by the fabrication methods such as etching ZnO nanorods or template growth.[262]

The power conversion efficiency of the nanowire/tube DSSC can be further improved by increasing the internal surface area of the photoelectrode via filling the interstices of nanowire/tube array films with nanoparticles,[263] or reducing the interfacial recombination rate via applying surface coatings on the nanowire array films.[264] For DSSCs based on hybrid nanostructures of nanowires/tubes (serving as a direct pathway for fast electron transport) mixed with nanoparticles (offering a high specific surface area for sufficient dye adsorption), most of the studies were carried out on array films of ZnO or TiO_2 nanowires, or TiO_2 nanotubes filled with ZnO or TiO_2 nanoparticles. For example, a significant increase in the conversion efficiency from 0.5–0.8% to 2.2–3.2% has been achieved in a DSSC based on ZnO nanowire arrays filled with ZnO nanoparticles.[265] The efficiency of a ZnO nanowire– nanoparticle hybrid DSSC could be further improved to ~4.2% (Figure 85).[266] Alivov et al.[267] also demonstrated that a photoelectrode made of TiO_2 nanotube array film filled with ~10 nm TiO_2 nanoparticles could increase the cell efficiency from 3.81% to 5.94%.

---

[259] J. M. Macák, H. Tsuchiya, Ghicov and P. Schmuki, Electrochem. Commun., 2005, 7(11), 1133

[260] J. H. Park, T. W. Lee and M. G. Kang,
Growth, detachment and transfer of highly-ordered TiO2 nanotube arrays: use in dye-sensitized solar cells. Chem. Commun., 2008, 2867

[261] A. B. F. Martinson, J. W. Elam, J. T. Hupp and M. J. Pellin, Nano Lett., 2007, 7(8), 2183

[262] A. B. F. Martinson, M. S. Goes, F. Fabregat-Santiago, J. Bisquert, M. J. Pellin and J. T. Hupp, J. Phys. Chem. A, 2009, 113(16), 4015

[263] S. Yodyingyong, Q. F. Zhang, K. Park, C. S. Dandeneau, X. Y. Zhou, D. Triampo and G. Z. Cao, Appl. Phys. Lett., 2010, 96(07), 073115

[264] J. Chung, J. Myoung, J. Oh and S. Lim, J. Phys. Chem. C, 2010, 114(49), 21360

[265] C. H. Ku and J. J. Wu, Appl. Phys. Lett., 2007, 91(09), 093117

[266] S. Yodyingyong, Q. F. Zhang, K. Park, C. S. Dandeneau, X. Y. Zhou, D. Triampo and G. Z. Cao, Appl. Phys. Lett., 2010, 96(07), 073115

[267] Y. Alivov and Z. Y. Fan, Appl. Phys. Lett., 2009, 95(06), 063504

Figure 85: (a) SEM image of ZnO nanoparticles on the surface of ZnO nanowires in the hybrid ZnO nanowire–nanoparticle photoanode, scale bars 100 nm. (b) Schematic representation of the possible electron path way (along the nanowire) in the hybrid nanowire–nanoparticle photoanode. Source: American Institute of Physics, 2010

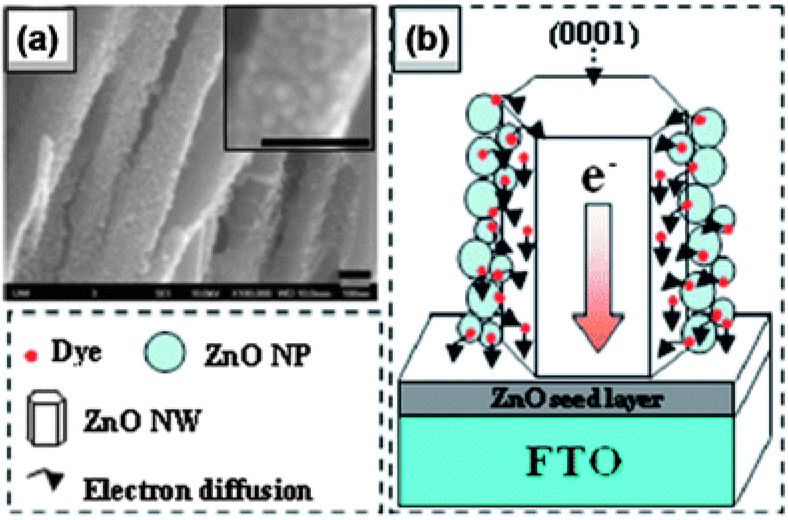

Since a surface barrier can reduce the charge recombination, core/shell structure with a coating layer on nanowire array film is also effective in enhancing photovoltaic performance. For instance, Law et al.[268] reported that ZnO nanowires coated by 10–25 nm-thick TiO_2 could increase the open circuit voltage of the DSSC and lead to an enhancement in the conversion efficiency from 0.85% to 1.7–2.1%. An improved efficiency from 2.1% for bare SnO_2 nanowires to 4.1% for TiO_2-coated SnO_2 nanowire photoelectrode was also achieved.[269] In another work, the cell performance of the ZnO nanowire-based DSSCs was greatly improved by the deposition of a thin ZnS shell onto the ZnO nanowires. The conversion efficiency was increased from 0.11% to 2.72%, which was resulted from the reduced visible absorption of the anode semiconductor and the reduced defect sites on the surface (which suppresses recombination of injected electrons). Furthermore, electrochemical deposition of CdSe onto TiO_2 nanorod arrays can also extend absorption into the visible light region and improve the photovoltaic performance.[270] The $ZnO/Zn_xCd_{1-x}Se$ ($0 \le x \le 1$) core/shell nanocable arrays were demonstrated to be promising photoelectrodes for photoelectronchemical solar cells, giving a maximum conversion efficiency up to 4.74%.[271]

Recently, three-dimensional (3D) hierarchical or aggregate nanostructure photoelectrodes in DSSC applications have drawn much attention due to the relatively large surface area, effective light harvesting, charge transport and charge collection. As shown in Figure 86, a variety of 3D nanostructures such as ZnO nanotetrapods,[272] branched ZnO nanowires,[273] ZnO or TiO_2 nanoforests,[274] dendritic ZnO nanowires,[275]

---

[268] M. Law, L. E. Greene, A. Radenovic, T. Kuykendall, J. Liphardt and P. D. Yang, J. Phys. Chem. B, 2006, 110(45), 22652
[269] S. Gubbala, V. Chakrapani, V. Kumar and M. K. Sunkara, Adv. Funct. Mater., 2008, 18(16), 2411
[270] J. H. Bang and P. V. Kamat, Adv. Funct. Mater., 2010, 20(12), 1970
[271] J. Xu, X. Yang, H. K. Wang, X. Chen, C. Y. Luan, Z. X. Xu, Z. Z. Lu, V. A. L. Roy, W. J. Zhang and C. S. Lee, Nano Lett., 2011, 11(10), 4138
[272] W. Chen and S. H. Yang, Front. Optoelectron. China, 2011, 4(1), 24
[273] H. M. Cheng, W. H. Chiu, C. H. Lee, S. Y. Tsai and W. F. Hsieh, J. Phys. Chem. C, 2008, 112(42), 16359

ZnO nanoflowers,[276] ZnO aggregates,[277] TiO_2 nanotubes on titanium mesh,[278] nanoporous TiO_2 spheres,[279] and hollow TiO_2 hemispheres[280] have been reported. It was found that these 3D nanostructure photoelectrodes can indeed improve photovoltaic performance. For example, an efficiency of 3.27% was reported for a photoanode film consisting of ZnO nanotetrapods, which was much higher than those obtained for ZnO nanowire/rod/tube arrays (~1.2–2.0%). Particularly, DSSCs based on ZnO or TiO_2 nanoparticle aggregates exhibited very high conversion efficiency of 5.4% and 10.5%, respectively, possibly due to very the high surface area, strong light scattering and short diffusion distance. Furthermore, recent investigations demonstrated that hybrid structures of ZnO nanotetrapods/SnO_2 nanoparticles,[281] hierarchical ZnO[282] or TiO_2 nanodendrites/nanoparticles[283] may be promising photoelectrodes for high-efficiency DSSCs.

Figure 86: SEM images of (a) ZnO nanotetrapods. (b) Branched ZnO nanowires, (c) ZnO nanotrees and, and (d) ZnO aggregates consisting of nanocrystallites for DSSC applications. Source: WILEY-VCH Verlag GmbH & Co. KGaA, 2008

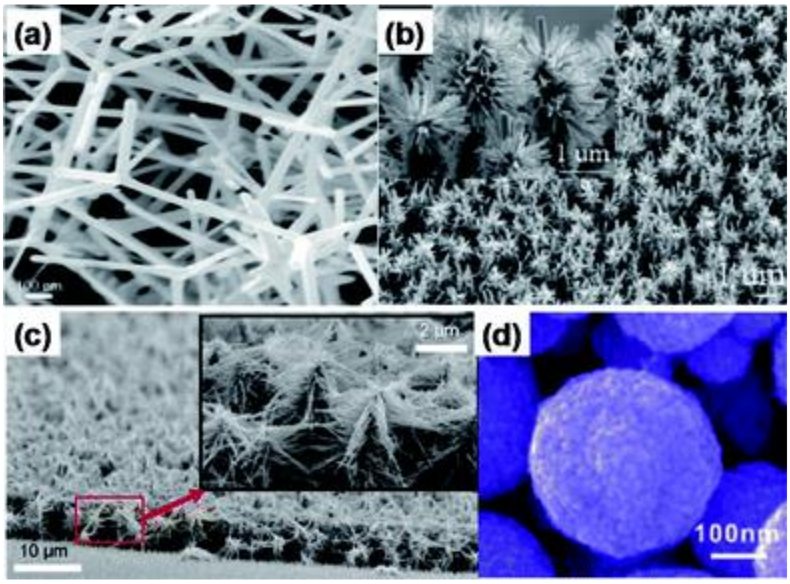

2.4.3.1.3 Solar cells based on electrospun nanofibers

2.4.3.1.3.1 Electrospun nanofibers as DSSC photoelectrodes

Electrospinning is a simple, low cost and versatile production method to prepare various continuous 1D fibers on a large scale, including polymers, ceramics and

---

[274] S. H. Ko, D. Lee, H. W. Kang, K. H. Nam, J. Y. Yeo, S. J. Hong, C. P. Grigoropoulos and H. J. Sung, Nano Lett., 2011, 11, 666

[275] J. B. Baxter and E. S. Aydil, Sol. Energy Mater. Sol. Cells, 2006, 90(5), 607

[276] C. Y. Jiang, X. W. Sun, G. Q. Lo, D. L. Kwong and J. X. Wang, Appl. Phys. Lett., 2007, 90(26), 263501

[277] Q. F. Zhang, T. R. Chou, B. Russo, S. A. Jenekhe and G. Z. Cao, Angew. Chem., Int. Ed., 2008, 47(13), 2402

[278] C. S. Rustomji, C. J. Frandsen, S. Jin and M. J. Tauber, J. Phys. Chem. B, 2010, 114(45), 14537

[279] Y. J. Kim, M. H. Lee, H. J. Kim, G. Lim, Y. S. Choi, N. G. Park, K. Kim and W. I. Lee, Adv. Mater., 2009, 21(36), 3668

[280] S. C. Yang, D. J. Yang, J. Kim, J. M. Hong, H. G. Kim and I. D. Kim, Adv. Mater., 2008, 20, 1059

[281] W. Chen, Y. C. Qiu, Y. C. Zhong, K. S. Wong and S. H. Yang, J. Phys. Chem. A, 2010, 114(9), 3127

[282] C. T. Wu, W. P. Liao and J. J. Wu, J. Mater. Chem., 2011, 21(9), 2871

[283] W. P. Liao and J. J. Wu, J. Mater. Chem., 2011, 21(25), 9255

composites. Since electrospun nanofibers can offer high specific surface areas (10^2–10^3 m^2 g^{-1}) and bigger pore sizes, much effort has been invested in the past a few years toward their application in dye-sensitized solar cells such as photoanodes and electrolytes.[284] Furthermore, compared with nanoparticle film-based DSSCs whose high efficiencies are often limited due to their disordered geometrical structures and interfacial interference in electron transport, nanofiber-based photoelectrods can offer direct pathways for electron transport, give larger electron diffusion length, and therefore provide enhanced energy conversion efficiencies in DSSCs. The highest efficiency for electrospun DSSCs reported to date has reached 10.3%.[285] Several electrospun materials such as TiO_2 and ZnO nanofibers have been utilized in DSSCs. For example, Song et al.[286] reported electrospun TiO_2 single-crystalline nanorods which were composed of nanofibrils with an islands-in-a-sea morphology (Figure 87 a). The nanorod electrode (Figure 87 b) provided efficient photocurrent generation in a quasi-solid-state DSSC, which showed overall conversion efficiency of 6.2% under AM 1.5G illumination. In addition, multiple networks of ZnO nanofibers were prepared using electrospinning followed by hot pressing and calcination steps. They were composed of a twisted structure of 200–500 nm diameter cores with ~30 nm single grains (Figure 87 c). The DSSCs based on these ZnO nanofiber mats exhibited a conversion efficiency of 1.34% under 100 mW cm^{-2} illumination.

Figure 87: (a) SEM image of a TiO_2 fiber showing an islands-in-a-sea morphology with nanofibrils. (b) SEM image of TiO_2 nanorod electrode. (c) SEM image of ZnO nanofiber mats hot pressed at 120 °C and calcined at 450 °C. The inset exhibits the networks of twisted nanofibers composed of individual grains of ~30 nm. Source: American Institute of Physics, 2007

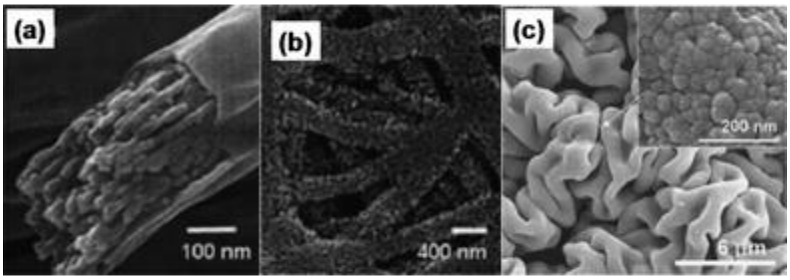

In an effort to maintain both a high surface area and efficient charge transport, a combination of electrospun nanorods/nanofibers and nanoparticles has been proposed. For example, Fujihara et al.[287] reported a solar cell with two TiO_2 layers: a ground electrospun TiO_2 nanoparticle layer on a glass plate and then a TiO_2 nanorod layer. It was found that the devices with a combination of electrospun nanorods and nanoparticles showed improved conversion efficiencies over the entirely nanorod devices. Chuangchote et al.[288] also suggested that nanofiber-modified nanoparticles are very promising materials for the electrode structure of DSSCs. In their work, TiO_2 nanofibers were fabricated directly onto thick nanoparticle electrodes by using

---

[284] M. J. Laudenslager, R. H. Scheffler and W. M. Sigmund, Pure Appl. Chem., 2010, 82(11), 2137
[285] S. Chuangchote, T. Sagawa and S. Yoshikawa, Appl. Phys. Lett., 2008, 93(03), 033310
[286] M. Y. Song, Y. R. Ahn, S. M. Jo, D. Y. Kim and J. P. Ahn, Appl. Phys. Lett., 2005, 87(11), 113113
[287] K. Fujihara, A. Kumar, R. Jose, S. Ramakrishna and S. Uchida, Nanotechnology, 2007, 18(36), 365709
[288] S. Chuangchote, T. Sagawa and S. Yoshikawa, Appl. Phys. Lett., 2008, 93(03), 033310

electrospinning and sol–gel techniques. The DSSCs comprised of a nanoparticle/nanofiber electrode showed an incident photon-to-current conversion efficiency (IPCE) of 85% at 540 nm with conversion efficiencies of 8.14% and 10.3% for areas of 0.25 and 0.052 cm^2, respectively. Here it is noted that the conversion efficiency of 10.3% is the highest reported efficiency for electrospun DSSCs. More recently, a composite photoanode made of electrospun TiO_2 nanofibers and conventional TiO_2 nanoparticles (15% nanofibers and 85% nanoparticles by weight) was reported.[289]

Figure 88 shows schematic illustration of the nanofiber/nanoparticle solar cell, which noticeably improved the light harvesting through the enhancement of Mie scattering without substantially sacrificing the dye uptake in DSSCs. With the same fabrication conditions and film thickness, the DSSCs demonstrated 44% higher device efficiency than those made from TiO_2 nanoparticles alone. In addition, the photovoltaic performance of electrospun DSSCs can be improved by creating hollow microtubes within the TiO_2 layer (these tubes act as light-scattering centers and thus increase the optical path length)[290] or improving the adhesion of electrospun fibers to the substrate.[291]

Figure 88: Schematic illustration of a nanofiber-nanoparticle composite solar cell Source: Royal Society of Chemistry, 2010

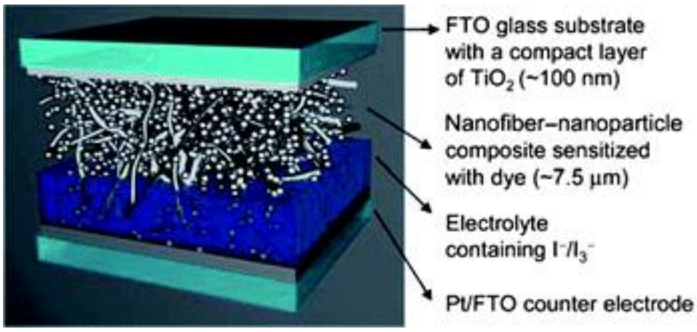

2.4.3.1.3.2 *Quasi-solid-state DSSCs with electrospun membrane electrolytes*

Besides the photoelectrodes, electrospun polymer nanofiber films can be also used as solid or semi-solid electrolytes instead of the traditional liquid electrolytes within DSSCs in order to improve durability and stability. This is because the electrospun polymer fiber films have lots of inter-connected pores that help to encapsulate electrolyte solution. For instance, Priya et al.[292] reported a quasi-solid-state solar cell with an electrospun poly(vinylidenefluoride-co-hexafuoropropylene) (PVDF-HFP) membrane electrolyte. As shown in Figure 89 a, the cell was fabricated by sandwiching a slice of the PVDF-HFP membrane electrolyte between a dye-sensitized TiO_2 electrode and a Pt counter electrode. The cell showed an open-circuit voltage of 0.76 V, a fill factor of 0.62,

---

[289] P. Joshi, L. F. Zhang, D. Davoux, Z. T. Zhu, D. Galipeau, H. Fong and Q. Q. Qiao. A first report on the fabrication of vertically aligned anatase TiO2 nanowires by electrospinning: Preferred architecture for nanostructured solar cells Energy Environ. Sci., 2010, 3(10), 1507

[290] . Zhao, J. Zhai, T. Wei, L. Jiang and D. B. Zhu, J. Enhanced photoelectrical performance of TiO2 electrodes integrated with microtube-network structures. Mater. Chem., 2007, 17, 5084

[291] I. D. Kim, J. M. Hong, B. H. Lee, D. Y. Kim, E. K. Jeon, D. K. Choi and D. J. Yang, Appl. Phys. Lett., 2007, 91(16), 163109

[292] A. R. S. Priya, A. Subramania, Y. S. Jung and K. J. Kim, Langmuir, 2008, 24(17), 9816

and a short-circuit current density of 15.57 mA cm^{-2} at an incident light intensity of 100 mW cm^{-2}. Although this cell showed a slightly lower solar energy-to-electricity conversion efficiency (7.3%) than the conventional liquid electrolyte solar cells (7.8%), the cell exhibited better long-term durability by preventing electrolyte leakage. Figure 89 b shows the conversion efficiency variation over time for a liquid electrolyte and an electrospun PVDF-HFP membrane electrolyte, respectively. It is evident that the quasi-solid-state solar cells remain at 96% of its initial value after 13 days. In addition, Kim et al.[293] also found that the photovoltaic performance of DSSC devices was improved by using electrospun PVDF-HFP nanofiber membranes.

Figure 89: (a) Schematic diagram of a quasi-solid-state DSSC with electrospun PVDF-HFP membrane electrolyte. (b) Normalized light-to-electricity conversion efficiency variation of the DSSCs with liquid electrolyte and electrospun PVDF-HFP membrane electrolyte Source: American Chemical Society, 2008

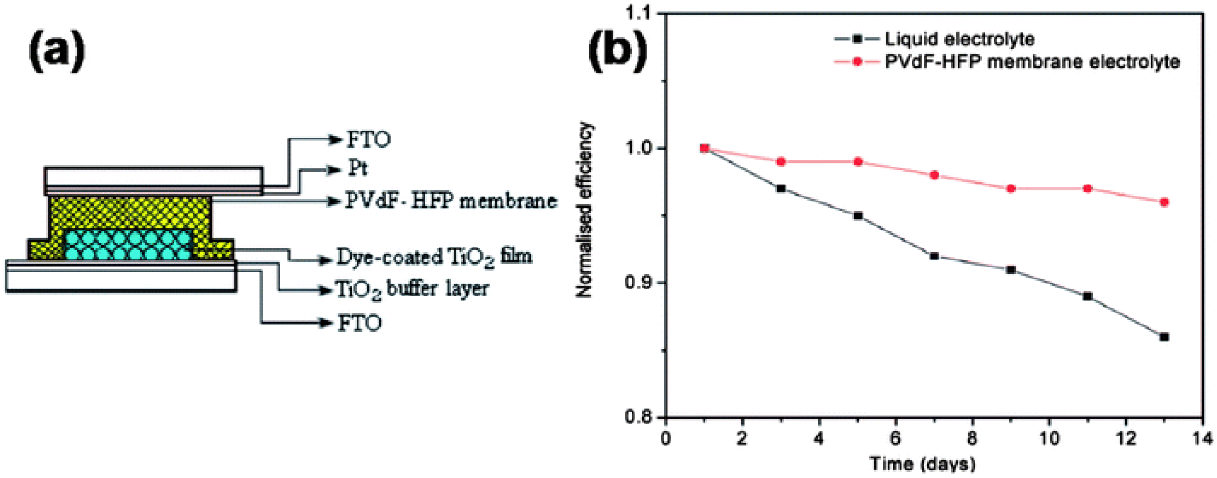

2.4.3.2 *Carbon nanotubes (CNT)*

Carbon nanotubes (CNT) are formed by hexagonal lattice carbon. CNTs offer a potentially cheaper and easier alternative to “dye” materials such as metal-free organic dyes through highly efficient Ru-based organic dyes such as ‘N3 dye’ and ‘black dye’ to engineered semiconductor quantum dots with a very high extinction coefficient. C_{60} has been shown to work as a ‘dye’ as well being photo active, highly conductive, strong, and chemically inert. Carbon nanotubes can be synthesized in multiple ways such as chemical vapor deposition or laser ablation. The natural ratio of as-synthesized carbon nanotubes is 2/3 semiconducting to 1/3 metallic. One research team has invented photodiode solar cell from CNT and successfully improves efficiency and current output from that solar cell.[294] The proof-of-concept solar cells that are entirely made of carbon nanotubes, carbon-nanotube-based solar cells is presented in Figure 90.

---

[293] J. U. Kim, S. H. Park, H. J. Choi, W. K. Lee and M. R. Kim, Sol. Energy Mater. Sol. Cells, 2009, 93, 803

[294] Klinger C, Patel Y, Postma HWC (2012) Carbon Nanotube Solar Cells. PLoS ONE 7(5): e37806

Figure 90: Carbon nanotube solar cells; comparison to Dye-Sensitized Solar Cells (DSSC), construction, and energetitcs. a) DSSC. b) Carbon Nanotube Solar Cell, CNSC. c) Layout of a CNSC. The top and bottom glass slides (light blue) are covered in carbon nanotube films which are electrically connected by the iodide-triiodide electrolyte (light red) that is contained by the silicone separator (white). The top film (green) is the photoactive electrode, while the bottom electrode (grey) is the counter electrode. The inset is an Atomic Force Micrograph of the height of a 2×2 m section of a carbon nanotube film. d) Band diagram of the CNSC. Source: PLoS ONE 7(5): e37806

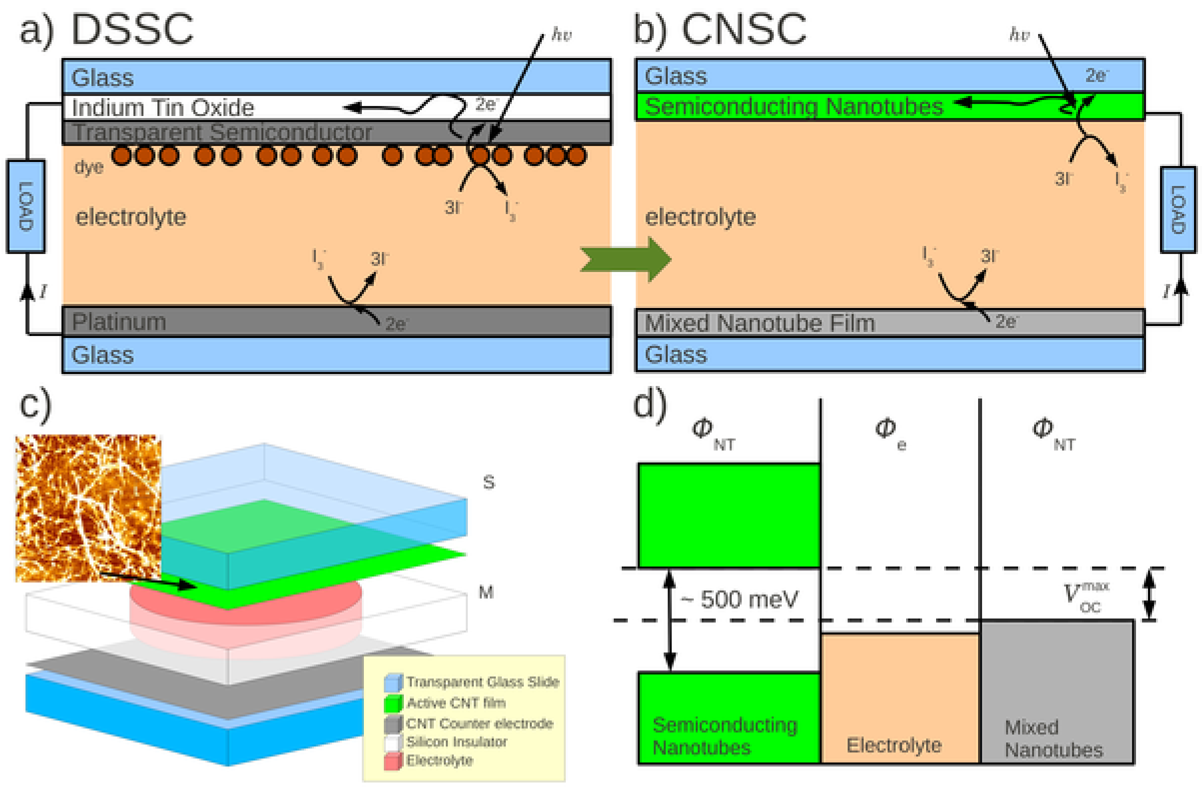

Although the efficiency for solar cell is still low (3–4%), many research will be carried out in this technology to improve the electrical output.

2.4.3.3 Quantum dots

Quantum dots (QD) can be described as a material that is built with many forms of material thus makes it a special semiconductor system with an ability to control band-gap of energy. Voltage output can be increased as band-gap energy size increases but on the other hand, smaller band-gap can also increase current output. As a solution, QDs are used since they can vary light absorption and emission spectra of light.[295] The two fundamental pathways for enhancing the conversion efficiency (increased photovoltage or increased photocurrent131,186) can be accessed, in principle, in three different QD solar cell configurations; these configurations are shown in Figure 91.

Figure 91: Three different generic QD Solar Cell Configurations: Photoelectrodes Composed of Quantum Dot Arrays (top), Quantum Dot-Sensitized Nanocrystalline TiO2 Solar Cells (middle) and Quantum Dots Dispersed in Organic Semiconductor Polymer Matrices (bottom). Source: Chemical Reviews, 2010

---

[295] P Kumar, A Deep, SC Sharma, LM Bharadwaj. Bioconjugation of InGaP quantum dots for molecular sensing. Analytical Biochemistry, 421 (2012), pp. 285–290

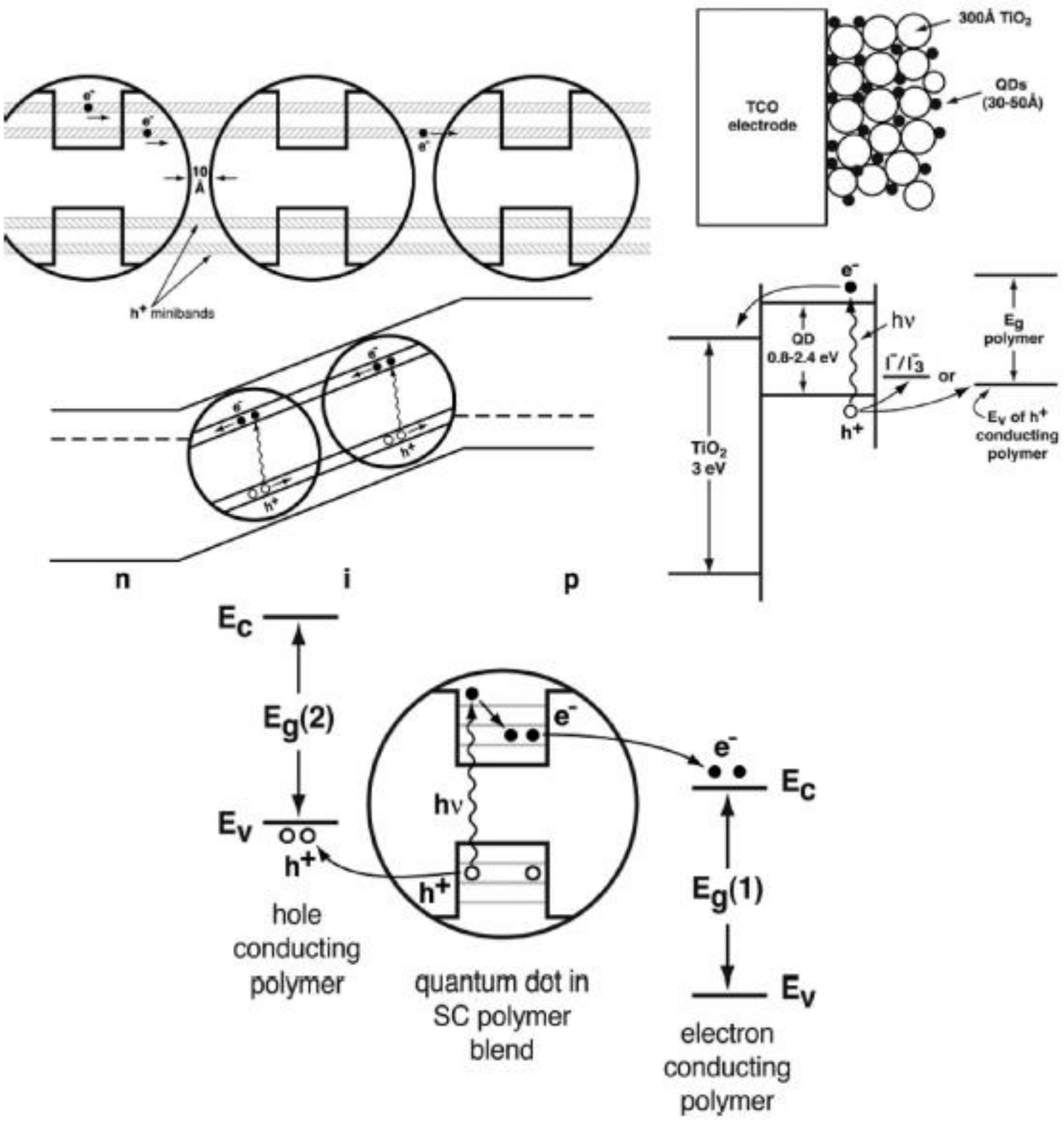

However, it is emphasized that these potential high efficiency configurations are theoretical and there are no experimental results yet that demonstrate actual enhanced power conversion efficiencies in QD solar cells over present-day solar cells in any of these systems. Aroutiounian et al.[296] developed a mathematical model to calculate photocurrent for the solar cell that is QD based. The model developed is based on two assumptions where (1) QDs are located in subsequent layers, which are periodically stacked M times together at a distance of d (2) $d \geqslant 0 \mathrm{d} \geqslant 0$, where a_0 is typical size of QDs. Efficiency of solar cells based on QD are easily influence by the defects on them.[297] Chen et al.[298] in their experiment had successfully increased the efficiency of quantum dot sensitized solar cell by applying mercaptopropionic acid (MPA)-capped CdSe QDs on

---

[296] V Aroutiounian, S Petrosyan, A Khachatryan. Studies of the photocurrent in quantum dot solar cells by the application of a new theoretical model. Solar Energy Materials and Solar Cells, 89 (2005), pp. 165–173

[297] NE Gorji. A theoretical approach on the strain-induced dislocation effects in the quantum dot solar cells. Solar Energy, 86 (2012), pp. 935–940

[298] J Chen, DW Zhao, JL Song, XW Sun, WQ Deng, XW Liu et al. Directly assembled CdSe quantum dots on TiO2 in aqueous solution by adjusting pH value for quantum dot sensitized solar cells. Electrochemistry Communications, 11 (2009), pp. 2265–2267

TiO_2 film in aqueous solution and concluded that pH value 7.0 is a suitable value to add maximum amount of CdSe QDs on TiO_2 film.

2.4.3.4 Hot carrier solar cell

Hot carrier (HC) is a challenging method compared to CNT and QD because it needs selective energy contacts to convert light into electrical energy without producing heat. Its efficiency reaches 66% which is three times higher than existing cell made from silicon.[299] But to this date, due to lack of suitable material that can decrease carrier cooling rates, HC has never been commercialized but remain an experimented technology.[300] Figure 92 shows the schematic of HC solar cell. Konig et al.[301] in their research discussed about principles, material and design of HC solar cell and concluded that materials like BBi, BiN, AlBi, BiP, Bi_2S_3, SiSn, BSb and InP are good as a hot carrier absorber material.

Figure 92: HC schematic diagram. Source: Physica E, 42, 2010

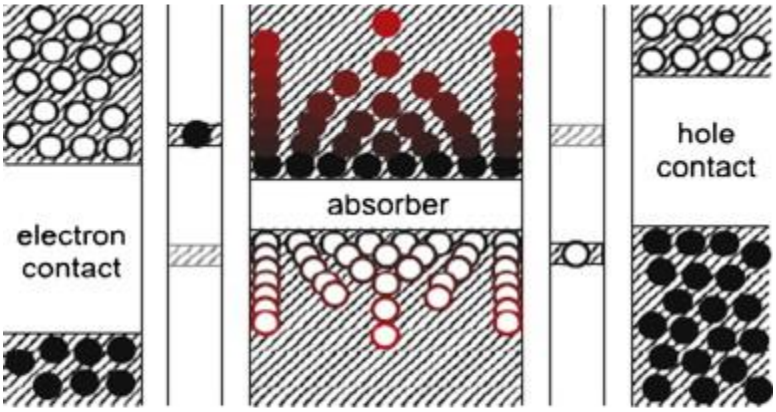

2.4.4 Conclusions: emerging photovoltaics

While emerging PV technologies have so far delivered power conversion efficiencies that are inferior to those of the best Si and III–V devices, the study of new materials does not necessitate inferior performance. The study of very different device concepts generates more thorough understanding of the fundamental mechanisms of PV devices and enables lateral thinking regarding common issues. Ideas stimulated by the need to improve emerging technologies may often also be applied to conventional solar technologies. The use of molecular and nanoparticulate materials is especially interesting in these respects. Quantum confinement of charges and excitations in nanoscale absorbers influences the rates at which charge and energy transfer processes occur. This means, first, that the dynamics and yield of these processes can be explicitly studied, for example, using spectroscopic techniques and taking advantage of the spectroscopic fingerprint of excited states in such nanoscale systems. Such studies

---

[299] RT Ross, AJ Nozik. Efficiency of hot carrier solar energy converters. Journal of Applied Physics, 53 (1982), pp. 3813–3818

[300] Hosenberg CB, Barnett AM, Kirkpatrick D Nanostructured solar cells for high efficiency photovoltaics. IEEE fourth world conference on photovoltaic energy conversion, WCPEC-4 2007; 2:2565–8.

[301] D. Konig, K Casalenuovo, Y Takeda, G Conibeer, JF Guillemoles, R Patterson et al. Hot carrier solar cells: principles, materials and design. Physica E, 42 (2010), pp. 2862–2866

enable a detailed analysis of the energy and charge losses at each stage between initial photoexcitation and charge collection in a way that would not be possible in classical semiconductors. Moreover, the potential to *control* the rates of relaxation and transfer by controlling chemical structure opens up the possibility to improve energy efficiency over conventional devices by reducing the fraction of absorbed solar energy that is lost during thermalization. That is essentially the goal behind the efforts to enhance multiple exciton generation in nanoparticle-based solar cells. The more recent observation of singlet fission in organic and hybrid heterojunctions is an alternative approach to reduce thermalization losses by exploiting the particular properties of excitations in molecular systems.

The study of novel technologies can provide innovations that benefit established PV technologies. For example, light-harvesting techniques developed to improve light absorption in thin devices of novel materials, e.g. using nanoparticle-based plasmonic effects or patterned electrodes, can be applied to improve light harvesting in more established PV device types when thicknesses are reduced. Similarly, the development of new electrode materials to enable selective contacts in undoped novel PV devices may enable improved function or lower cost fabrication of devices from established PV technologies. Although conventional PV technology, largely based on Si, is making impressive and growing contributions to energy supply, there are still compelling reasons to address new material technologies. Abundant and mass processable materials have the potential to offer cheaper module manufacture, while the particular properties of new materials (weight, colour, flexibility) open up routes to reduced BOS costs, further reducing electricity costs. New technologies with the potential for rapid growth in production capacity can help make early contributions to carbon emission mitigation. Ultimately, the maturing of these emerging PV technologies will act to accelerate reductions in system and electricity costs within the context of a growing industry, as has already been demonstrated in the case of silicon.

3 COMPLEMENTARY TECHNOLOGY: ENERGY STORAGE

3.1 Needs for electric energy storage

Energy storage is stated to be the currently missing link that will enable the intermittent renewable energy sources like wind and solar to play a much greater part in the future grid mix. In the representative study performed for Deutsche Bank AG in 2012 the main technological challenges of shifting in energy policy to renewable resources were formulated.[302] Generating power from renewable energy sources is subject to extreme fluctuations and cannot be controlled since the period during which power is generated (when the wind is blowing or the sun shining) only coincides by chance with power consumption. Already, today, not all the green energy generated can be fed into the grid all the time. Electricity generation from PV systems and wind power changes over the year with a certain regularity. Also, in the case of PV, relatively uniform changes can be observed during the day. Power consumption, too, follows a characteristic pattern, changing over the year, week or day and also fluctuating due to other factors which occur less regularly (Figure 93). In any grid network, the amount of energy used must correspond to the electricity producedat any point of time. If the very small tolerance threshold is violated, blackouts are the result. Traditionally, supply adjusts to fluctuating demand in two different ways - through energy storage and flexible excess capacity. The energy generation from renewable sources such as wind and PV power is creating an additional challenge as it is intermittent: output fluctuates according to a combination of different normal and random patterns between zero and full capacity. Their “must-take loads” have to be integrated by law as well as due to plain economics, once systems are already installed: their variable operating costs are lower than the ones of conventional power plants while initial fixed capital investment costs are high. The use of their output thus saves fuel expenses and other operating and maintenance (O&M) costs associated with thermal plants. Loads from renewable sources behave very differently.

---

[302] J. Auer et al. State-of-the-art electricity storage systems. Deutsche Bank AG DB Research, 2012

Figure 93: Total Load, Wind and Solar Power Output in Germany, September 2011. Source: The German Energy Transition – Issues and Perspectives, J. Keil, 2012

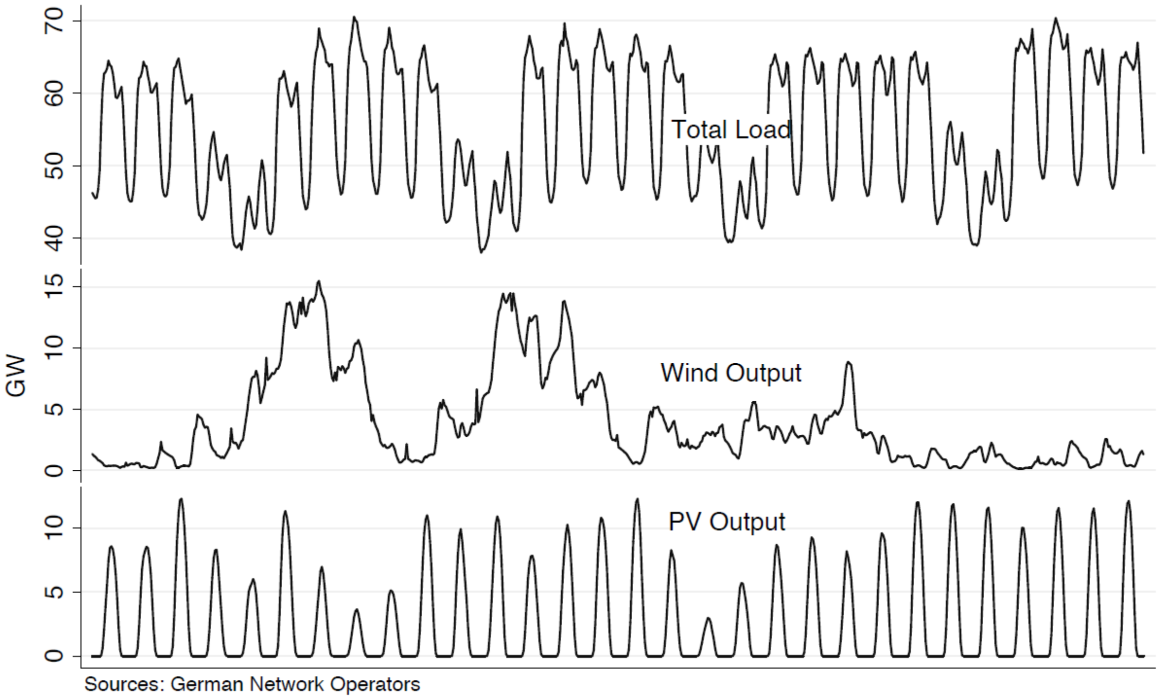

The Figure 94 shows that PV can be used very well as a source that serves expensive peak load.

Figure 94: Daily and Annual Patterns. Source: The German Energy Transition – Issues and Perspectives, J. Keil, 2012

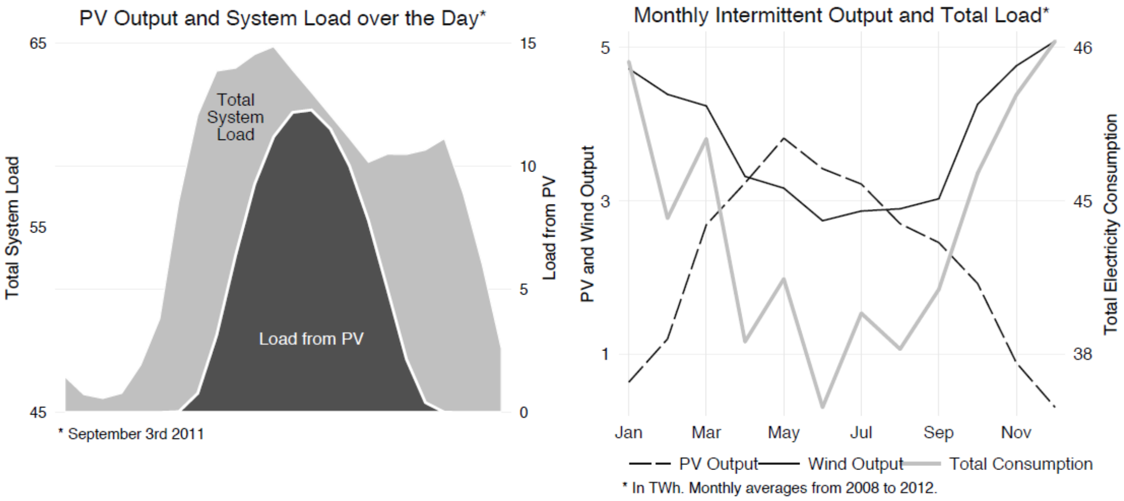

However, it is clear that PV cannot serve all of the peak load directly as peaking kicks in before dawn and spikes up again after dark. The intermittent character of PV and wind combined with the growth of installed capacities and shrinking consumption will lead to potential output losses due to temporary overproduction. While losses can be due to overload of the grid at certain points of the network or too strong winds that force wind farms to shut down temporarily, such losses are hard to estimate and are likely to be limited if the network extension is accomplished successfully. On a more basic level, overproduction will result if total load is below the output of PV, wind and power plants that cannot be regulated or lowered below a certain capacity factor. Shortages can occur if there is not sufficient flexible load available on demand from conventional plants, storage units or imports.

Now that more homes and businesses are installing photovoltaic systems, a new trend for combining these with battery backup is emerging. The volatility of the increasing volumes of solar energy needs to be evened out and matched to consumption in order to enjoy a stable power supply and avoid blackouts. Storing electrical energy is a proven means of absorbing any immediate surplus power and then making it available when required. Previously, battery storage systems were only thought necessary with solar PV and wind in stand-alone systems, separate from any grid connection, but as the grid supports more and more PV and wind systems, which can supply power only at certain times, the need for storage backup is becoming more apparent. For large commercial installations this is especially attractive because, although they may have negotiated contracts with utilities that bring down their overall electricity rates, the fees that they are charged for the times when they do draw power, which can be based on their highest peak energy use during a month, have been rising as much as 10-12% per year. By 2025, the requirement for short-term power storage could well double at the very least and increase still further thereafter. The end of production from ageing fossil-fuel power stations and the abandonment of nuclear energy require new capacity available on demand (in addition to the options of more imports, renewables and greater capacity utilisation) in order to avoid bottlenecks.

3.2 Electricity Storage: technology overview

Storage of electric energy is a way to ease the integration of intermittent sources from wind and solar power by storing output in excess of current consumption and reusing it to to meet demand when their output falls below demand. This potentially solves their most fundamental technical problem and is in most countries the only way to enable a renewable share of 100%. The basis of an energy system is the capacity of this system to generate sufficient energy to attend demand at accessible prices and to provide clean, safe and reliable electricity. Therefore, electrical energy storage has always been a challenge since various electrical energy generation technologies are subject to non-linear supply based on factors such as season (hydroelectricity and wind) and intermittence (solar), without considering load changes. Energy storage technologies cover a wide spectrum of power system applications (Figure 95). These applications require energy discharges ranging from fractions of a second in high power applications to hours in high energy applications.

Figure 95: Classification of energy storage applications in electric power systems.303

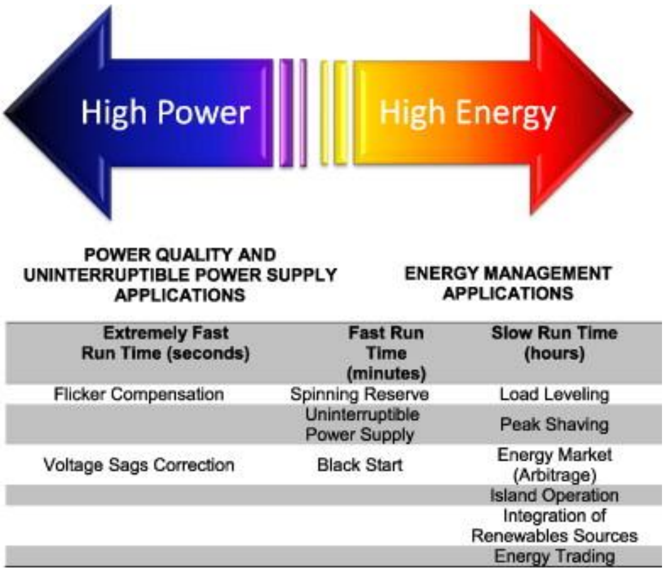

Extremely Fast Run Time (seconds)	Fast Run Time (minutes)	Slow Run Time (hours)
Flicker Compensation	Spinning Reserve	Load Leveling
	Uninterruptible Power Supply	Peak Shaving
Voltage Sags Correction	Black Start	Energy Market (Arbitrage)
		Island Operation
		Integration of Renewables Sources
		Energy Trading

Currently there exist various technologies for the application of energy storage systems. A. Nourai,[304] compared different technologies for energy storage applications, such as supercapacitors (electrochemical capacitors), flow batteries (ZnBr, VRB and PSB), sodium–sulfur batteries (NaS), lithium–ion batteries (Li–ion), nickel–cadmium batteries (Ni–Cd), lead–acid batteries, metal–air batteries, pumped hydro, compressed air energy storage (CAES) and flywheels. Figure 96 shows a comparison between diverse energy storage technologies in terms of efficiency and durability in charge–discharge cycles with an 80% depth of discharge.

Figure 96: Efficiency and reliability in discharge cycles for diverse energy storage technologies. Source: A. Nourai, 2002

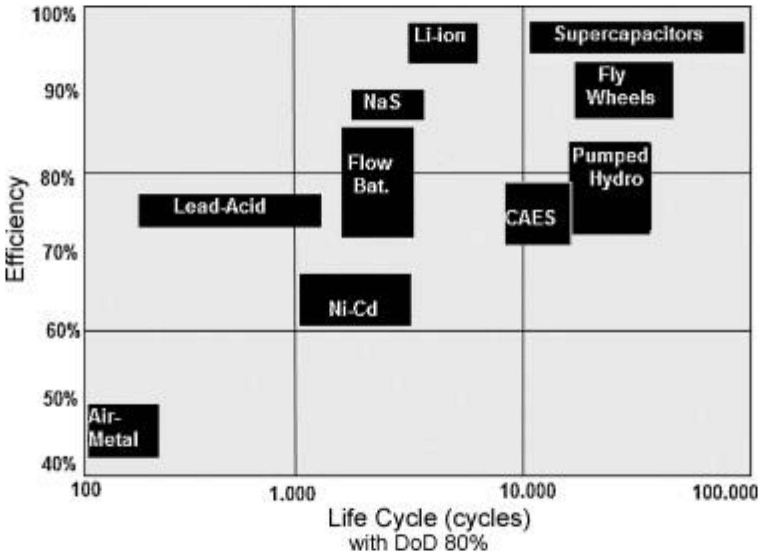

Energy storage systems for high power applications which includes maintenance of energy quality and continual supply of demand requires storage technologies such as

---

[303] O.M. Toledo et al. Distributed photovoltaic generation and energy storage systems: A review. Renewable and Sustainable Energy Reviews. Volume 14, Issue 1, January 2010, Pages 506–511

[304] A. Nourai. Large-scale electricity storage technologies for energy management. Power Engineering Society Summer Meeting, 2002, IEEE (2002)

supercapacitors, flywheels and others which are utilized in fractions of a second to guarantee reliability of the system. In high energy applications which includes energy management (supply and demand side management (SSM/DMS), balancing of the load curves and peak-shaving) storage technologies which utilize daily charge–discharge cycles to insure economic gains, such as fuel cells and sodium–sulfur (NaS) batteries are better suited. Figure 97 shows applications of energy storage systems in accordance with discharge time and rated power.

Figure 97: Application of energy storage systems in terms of discharge time and rated power. Source: A. Nourai, 2002

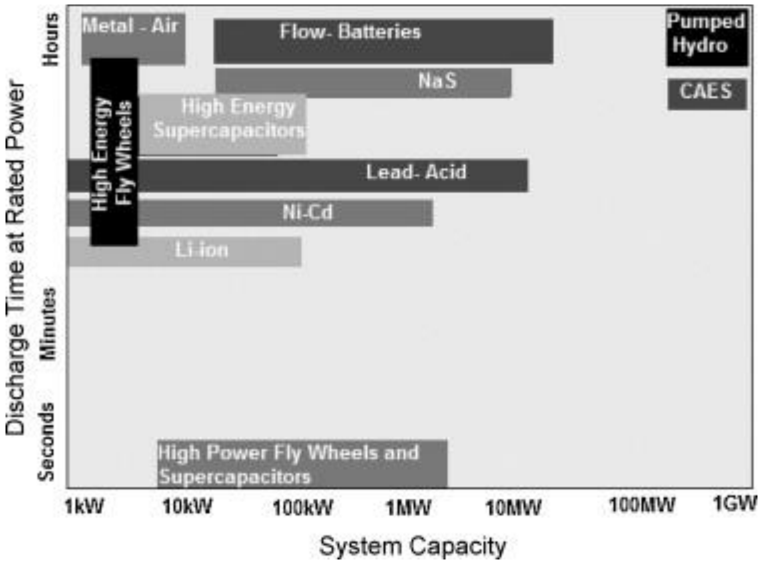

Although, due to their cost, batteries traditionally have not widely been used for large scale energy storage, they are now used for energy and power applications. Energy applications involve the storage system discharge over periods of hours (typically one discharge cycle per day) with correspondingly long charging periods. Power applications involve comparatively short periods of discharge (seconds to minutes), short recharging periods and often require many cycles per day. Secondary batteries, such as lead–acid and lithium-ion batteries can be deployed for energy storage, but require some re-engineering for grid applications.

3.2.1 Larger energy storage systems: comparison of technical features

The technical comparison between the different types of batteries, as well as with other types of large energy storage systems is tabulated in Table 18, whereas their technical characteristics[305] are tabulated in Table 19.[306] It is observed that lithium-ion batteries and sodium–sulfur batteries have high power and energy densities and high efficiency, but they have high production costs. Also, pumped hydro energy storage systems and compressed air energy storage systems have high capacity, but they have special site requirements. Furthermore, it is observed that with the exception of pumped hydro

---

[305] D. Connolly, H. Lund, B.V. Mathiesen, M. Leahy. The first step towards a 100% renewable energy-system for Ireland. Applied Energy, 88 (2011), pp. 502–507

[306] T.U. Daim, X. Li, J. Kim, S. Simms. Evaluation of energy storage technologies for integration with renewable electricity: quantifying expert opinions. Environmental Innovation and Societal Transitions, 3 (2012), pp. 29–49

energy storage systems and compressed air energy storage systems, all the other energy storage systems are fully capable and suitable for providing power very quickly in the power system. Regarding the energy applications, sodium–sulfur batteries, flow batteries, pumped hydro energy storage systems and compressed air energy storage systems are fully capable and suitable for providing energy very quickly in the power system, whereas the rest of the energy storage systems are feasible but not quite practical or economical.

Table 18: Comparison of large scale energy storage systems. Source: Applied Energy, 2011

Energy storage technology	Advantages	Disadvantages	Power applications	Energy applications
Lead–acid batteries	Low power density and capital cost	Limited life cycle when deeply discharged	Fully capable and suitable	Feasible but not quite practical or economical
Lithium-ion batteries	High power and energy densities, high efficiency	High production cost, requires special charging circuit	Fully capable and suitable	Feasible but not quite practical or economical
Sodium–sulfur batteries	High power and energy densities, high efficiency	Production cost, safety concerns (addressed in design)	Fully capable and suitable	Fully capable and suitable
Flow batteries	High energy density, independent power and energy ratings	Low capacity	Suitable for this application	Fully capable and suitable
Flywheels	High efficiency and power density	Low energy density	Fully capable and suitable	Feasible but not quite practical or economical
Pumped hydro-energy storage systems	High capacity	Special site requirement	Not feasible or economical	Fully capable and suitable
Compressed air energy storage systems	High capacity, low cost	Special site requirement, needs gas fuel	Not feasible or economical	Fully capable and suitable

Table 19: Technical characteristics of large scale energy storage systems. Source: Environmental Innovation and Societal Transitions, 2012

Technology	Power rating (MW)	Discharge duration	Response time	Efficiency (%)	Lifetime
Lead–acid batteries	<50	1 min–8 h	<1/4 cycle	85	3–12 years
Nickel–cadmium batteries	<50	1 min–8 h	N/A	60–70	15–20 years
Sodium–sulfur batteries	<350	<8 h	N/A	75–86	5 years
Vanadium redox flow batteries	<3	<10 h	N/A	70–85	10 years
Zinc–bromine flow batteries	<1	<4 h	<1/4 cycle	75	2000 cycles
Flywheels	<1.65	3–120 s	<1 cycle	90	20 years
Pumped hydro energy storage systems	100–4000	4–12 h	s–min	70–85	30–50 years
Compressed air energy storage systems	100–300	6–20 h	s–min	64	30 years

In Table 20, the technical suitability of the large scale energy storage systems to different applications is provided. It is observed that lead–acid and flow batteries are suitable for all applications. Pumped hydro energy storage systems and compressed air energy storage systems, are suitable for load levelling, peak generation, conventional spinning reserve, renewable integration and renewables back-up applications. The compressed air energy storage systems are also suitable for emergency back-up applications. Finally, flywheels are suitable for transit and end-use ride-through, uninterruptible power supply, peak generation, fast response spinning reserve and renewable integration applications.

Table 20: Technical suitability of large scale energy storage systems.

Storage application	Lead-acid patteries	Flow batteries	Flywheels	Pumped hydri energy storage systems	Compressed air energy storage systems
Transit and end-use ride-through	✓	✓	✓		
Uninterruptible power supply	✓	✓	✓		
Emergency back-up	✓	✓			✓
Transmission and distribution stabilization and regulation	✓	✓			
Load leveling[a]	✓	✓		✓	✓
Load following[b]	✓	✓			
Peak generation	✓	✓	✓	✓	✓
Fast response spinning reserve	✓	✓	✓		
Conventional spinning reserve	✓	✓	✓	✓	✓
Allow for renewable integration	✓	✓	✓	✓	✓
Suitable for renewables back-up	✓	✓		✓	✓

[a] Reducing the large fluctuations that occur in electricity demand.
[b] Adjusting power output as demand for electricity fluctuates throughout the day.

3.2.2 Operational and planned large scale battery energy systems

The operational and planned large scale battery energy systems around the world are tabulated in Table 21 and Table 22, respectively. It is observed that the largest battery energy storage systems use sodium–sulfur batteries, whereas the flow batteries and especially the vanadium redox flow batteries are used for smaller battery energy storage systems. The battery energy storage systems are mainly used as ancillary services or for supporting the large scale solar and wind integration in the existing power system, by providing grid stabilization, frequency regulation and wind and solar energy smoothing.

Table 21: Worldwide operational large scale battery systems

Project	Location	System size		Battery type	Services	Application
		MWe	MWh			
Amplex Group	United Arab Emirates	350	N/A	Sodium–sulfur	Ancillary services	Grid stabilization, frequency regulation, voltage support, power quality, load shifting and energy arbitrage
Tokyo Electric Power Company	Japan	200	N/A	Sodium–sulfur	N/A	N/A
Other Japanese Electric Companies	Japan	60	N/A	Sodium–sulfur	N/A	N/A
Abu Dhabi Water and Electricity Authority	United Arab Emirates	48	N/A	Sodium–sulfur	N/A	N/A
Japan Wind Development Co.	Japan	34	238	Sodium–sulfur	Wind integration	N/A
Laurel Mountain	West Virginia, USA	32	8	Lithium-ion	Wind integration	Frequency regulation and wind energy smoothing
Golden Valley Electric Association	Alaska, USA	27	14.6	Nickel–Cadmium	Ancillary services	Spinning reserve and power system stabilization
Zhangbei	China	20	36	Lithium-ion	Solar and wind integration	Grid stabilization, increased reliability, wind and solar energy smoothing
AES Westcover coal fired power station	New York, USA	20	N/A	N/A	Ancillary services	Frequency regulation
AES Gener new power plant installation	Northern Chile	20	N/A	N/A	Ancillary services	N/A
Puerto Rico Electric Power Authority Battery System	Puerto Rico	20	14	Lead–acid	Ancillary services	Frequency control and spinning reserve
Kahuku-kahuku wind power project	Hawaii, USA	15	10	N/A	Wind integration	Ramp control and curtailment mitigation
Southern California Edison Chino Battery Storage Project	California, USA	14	40	Lead–acid	Ancillary services	Load leveling, transmission line stability, local VAR control and black start
AES Gener Los Andes substation	Chile	12	N/A	Lithium-ion	Ancillary services	Frequency regulation and spinning reserve
American Electric Power	West Virginia, USA	11	N/A	Sodium–sulfur	N/A	N/A
KWP II Kaheawa wind power II project	Hawaii, USA	10	20	N/A	Wind integration	Uninterruptible power service
Berliner Kraft und Licht Battery System	Germany	8.5	14	Lead–acid	Ancillary services	Frequency regulation and spinning reserve
Pacific Gas and Electric Company	California, USA	6	N/A	Sodium–sulfur	N/A	N/A
Sumitomo Densetsu Office Battery System	Japan	3	0.8	Vanadium redox	Ancillary services	Peak shaving

Project	Location	System size		Battery type	Services	Application
		MWe	MWh			
				flow		
Project Sano	California, USA	2	N/A	N/A	Ancillary services	Frequency regulation
Project Carina	Indiana, USA	2	N/A	N/A	Ancillary services	Frequency regulation
Brockway Standard Lithography Plant	Georgia, USA	2	0.055	Lead-acid	Ancillary services	Power quality and uninterruptible power supply
Kauai Island utility Co-op	Hawaii, USA	1.5	1	N/A	Solar integration	Utility owned
Maui Kaheawa wind power project	Hawaii, USA	1.5	1	N/A	Wind integration	Ramp control and curtailment mitigation
Xcel solar technology acceleration center	Colorado, USA	1.5	1	N/A	Solar integration	Ramp control, curtailment mitigation and grid services
UPS system	Japan	1.5	N/A	Vanadium redox flow	Ancillary services	N/A
Hokkaidou Electric Power Company	Japan	1.5	N/A	Sodium-sulfur	N/A	N/A
Long Island, New York Bus Terminal Energy Storage System	New York, USA	1.2	6.5	Sodium-sulfur	Ancillary services	Load shifting
Lanai la Ola solar farm project	Hawaii, USA	1.125	0.5	N/A	Solar integration	Ramp control and grid services
Project Barbados	Pennsylvania, USA	1	N/A	N/A	Ancillary services	Frequency regulation
Project Redstone	Texas, USA	1	N/A	N/A	Ancillary services	Grid stabilization
New York Power Company	New York, USA	1	N/A	Sodium-sulfur	N/A	N/A
Xcel	Minnesota, USA	1	N/A	Sodium-sulfur	N/A	N/A
Younicos	Germany	1	N/A	Sodium-sulfur	N/A	N/A
Matlakatla Power and Light Battery System	Alaska, USA	1	1.4	Lead-acid	Ancillary services	Voltage regulation and displacing diesel generation

Table 22: Planned large scale battery systems in the world.

Project	Location	System size		Battery type	Services	Application
		MWe	MWh			
Rubenius	California, USA	1000	N/A	1,416,400	Sodium–sulfur	Solar and wind integration
Long Island Power Authority	New York, USA	400	N/A	N/A	N/A	Ancillary services
Power Sound Energy	Washington, USA	200	N/A	N/A	N/A	Ancillary services
Tres Amigas	New Mexico, USA	100	200	N/A	N/A	Ancillary services

3.2.3 Comparison of economic features

Economic comparison between the different types of batteries, as well as between other types of large energy storage systems is tabulated in Table 23. It is observed that a range of values exists for each system regarding power and energy related costs, due to various capacity sizes of the operational large scale energy storage systems around the world. Specifically, lead–acid batteries, sodium–sulfur batteries, flywheels and compressed air energy storage systems, have the lowest range of values regarding power related costs. Conversely, nickel–cadmium batteries, the two types of flow batteries, vanadium redox and zinc–bromine, as well as pumped hydro energy storage systems, have higher range of values regarding power related costs.

Table 23: Economical and environmental characteristics of large scale energy storage systems

Technology	Capiltal costs (€/KWh)	Environmental issues
Lead–acid batteries	37–232	Lead disposal
Nickel–cadmium batteries	299–1793	Toxic cadmium
Sodium–sulfur batteries	134–374	Chemical handling
Vanadium redox flow batteries	131–747	Chemical handling
Zinc–bromine flow batteries	149–448	Chemical handling
Flywheels	299–598	Slight
Pumped hydro-energy storage systems	6–75	Reservoir
Compressed air energy storage systems	1–75	Gas emissions

Regarding the energy related cost, pumped hydro and compressed air energy storage systems have the lowest range of values, followed by the lead–acid, sodium–sulfur, zinc–bromine flow batteries and flywheels.[307] The nickel–cadmium and vanadium redox flow batteries have the highest range of values regarding energy related costs. Regarding the environmental issues of each large scale energy storage system, the different types of batteries have to handle chemical disposal, specifically lead–acid and nickel–cadmium batteries which dispose lead and toxic cadmium. The effect of pumped hydro energy storage systems in the environment is the pollution during the construction of the two

---

[307] D. Steward, G. Saur, M. Penev, T. Ramsden. Lifecycle cost analysis of hydrogen versus other technologies for electrical energy storage. National Renewable Energy Laboratory, Golden, Colorado, U.S. Department of Energy, Washington, DC (2009)

reservoirs, whereas for the compressed air energy storage systems are the emission of gas into atmosphere. Finally, flywheels have only a slight effect in the environment.

3.2.4 Short-term storage: nanomaterial supercapacitors

Supercapacitors have been used to complement or replace batteries in energy storage and/or load-levelling applications including portable electronic devices, plug-in hybrid electric vehicles, solar plants, wind farms and long time constant circuits. Although supercapacitors offer high power density, market penetration has been limited because of high cost and a low energy density compared with batteries.[308] The speciality carbon material generally used in supercapacitor electrodes is presently expensive in terms of the resulting energy-power characteristics, and a reduction in the cost for supercapacitors (7–15€Wh^{-1} and 19–37€ kW^{-1} compared with 0.7–1.5€Wh^{-1} and US$75–150 kW^{-1} for batteries) is the main barrier to wider commercialization. A more detailed comparison of the important parameters of electrostatic capacitors, supercapacitors and batteries is presented in Table 24.

Table 24: A comparison of electrostatic capacitors, supercapacitors and batteries[309]

Parameters	Electrostatic Capacitor	Supercapacitor	Battery
Charge Time	10^{-6}–10^{-3} s	1–30 s	0.3–3 h
Discharge Time	10^{-6}–10^{-3} s	1–30 s	1–5 h
Energy Density (Wh kg^{-1})	<0.1	1–10	20–100
Power Density (W kg^{-1})	>10 000	1000–2000	50–200
Cycle Life	>500 000	>100 000	500–2000
Charge/Discharge Efficiency	1.0	0.90–0.95	0.7–0.85

Additional electrode material and supercapacitor aspects that must also be considered in the commercial context include environmental compatibility of the manufacturing, use and disposal cycle, the weight/volume topology (laminated, curved, spiral, flexible, etc.) and lifetime. The fastest growing and largest energy storage market is mobile energy storage, and where an improved supercapacitor energy capacity can be cost-effectively combined with their intrinsic high power capability and almost unlimited cycle life, significant market penetration can be expected.[310]

Based upon current R&D trends, supercapacitors can be divided into three general classes: electrochemical double-layer capacitors, pseudocapacitors, and hybrid capacitors. Each class is characterized by its unique mechanism for storing charge. These are, respectively, non-Faradaic, Faradaic, and a combination of the two. A graphical taxonomy of the different classes and subclasses of supercapacitors is presented in Figure 98.

---

[308] J. R. Miller and P. Simon, Science, 2008, 321, 651

[309] X. Zhao, B. Mendoza Sánchez, P.J. Dobson, P. S. Grant. The role of nanomaterials in redox -based supercapacitors for next generation energy storage devices. (Review Article) Nanoscale , 2011, 3, 839-855

[310] T. Ryhänen, M. A. Uusitalo, O. Ikkala and A. Kärkkäinen, Nanotechnologies for Future Mobile Devices, Cambridge University Press, 2010

Figure 98: Clasification of supercapacitors.[311]

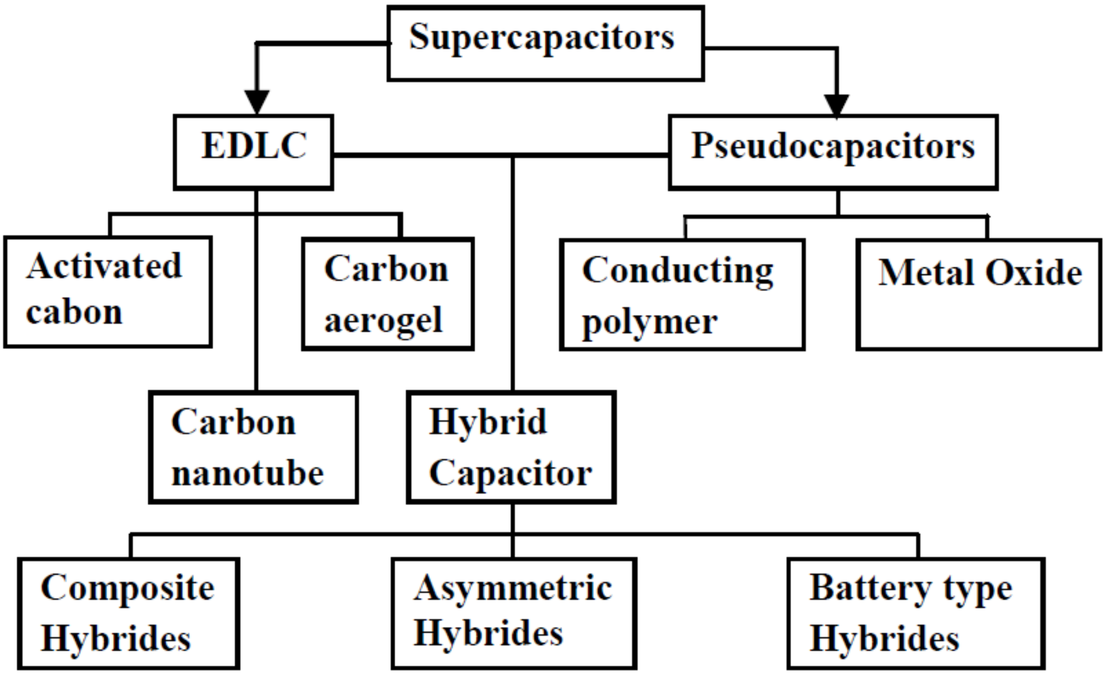

The typical advantages that can be conferred by nanostructured electrode materials include:

1. Reduced dimensions of the electrode materials can enlarge the electrode /electrolyte contact area per unit mass significantly, providing more ion adsorption sites for double-layer formation and charge-transfer reactions. In some cases, micropore (<2 nm) dimensions and their distribution may be tailored to optimize the areal or volumetric density of pseudo-capacitive (and EDLC) electrolyte/electrode interactions.

2. The tortuous ionic and electronic diffusion distance through porous electrodes may be reduced, resulting in shorter diffusion times, improved high rate charge/discharge capability, and energy densities that approach those of conventional lead-acid and Ni–MH batteries. Contiguous ion channels of mesoporosity ensure that the accessible electrode area is maximized and that the kinetics of electrolyte/electrode reactions are sufficiently fast at all points over the electrode surface. In particular, three-dimensional (3-D) nano/meso-architectures can be exploited without increasing the overall areal footprint of the electrochemical device.

3. The confinement of material dimensions to the nanoscale in the electrodes may cause deviations from their equilibrium structure, modifying phase transformations upon ion insertion /extraction and other reactions and engineering an improved tolerance to the otherwise pulverizing volumetric changes. Nanostructured electrodes in supercapacitors that show enhanced tolerance to strain and structural distortion can then be cycled many times at high rates.

---

[311] S. Mohapatra, A. Acharya, G. S. Roy. The role of nanomaterial for the design of supercapacitor. Lat. Am. J. Phys. Educ. Vol. 6, No. 3, Sept. 2012

4. Nanoscale electrode materials can offer exciting combinations of properties that will allow supercapacitors to address new markets. For example, supercapacitors that combine low weight, transparency, flexibility and biodegradability.

3.2.5 Conclusions: energy storage

The largest battery energy storage systems use sodium–sulfur batteries, whereas the flow batteries and especially the vanadium redox flow batteries are used for smaller battery energy storage systems. The battery energy storage systems are mainly used as ancillary services or for supporting the large scale solar and wind integration in the existing power system, by providing grid stabilization, frequency regulation and wind and solar energy smoothing.

By comparing the different types of batteries, as well as other types of large scale energy storage systems, it was observed that lithium-ion batteries and sodium–sulfur batteries have high power and energy densities and high efficiency, but they have high production costs. Also, pumped hydro energy storage systems and compressed air energy storage systems have high capacity, but they have special site requirements. Furthermore, it was observed that with the exception of pumped hydro energy storage systems and compressed air energy storage systems, all the other energy storage systems are fully capable and suitable for providing power very quickly in the power system. Regarding the energy applications, sodium–sulfur batteries, flow batteries, pumped hydro energy storage systems and compressed air energy storage systems are fully capable and suitable for providing energy very quickly in the power system, whereas the rest of the energy storage systems are feasible but not quite practical or economical.

Concerning the technical suitability of the large scale energy storage systems to different applications, it was observed that lead–acid and flow batteries are suitable for all applications. Pumped hydro energy storage systems and compressed air energy storage systems are suitable for load levelling, peak generation, conventional spinning reserve, renewable integration and renewables back-up applications. The compressed air energy storage systems are also suitable for emergency back-up applications. Flywheels are suitable for transit and end-use ride-through, uninterruptible power supply, peak generation, fast response spinning reserve and renewable integration applications.

Concerning the economic comparison of the large scale energy storage systems it was observed that a range of values exists for each system regarding power and energy related costs, due to various capacity sizes of the operational large scale energy storage systems around the world. Specifically, lead–acid batteries, sodium–sulfur batteries, flywheels and compressed air energy storage systems, have the lowest range of values regarding power related costs. Conversely, nickel–cadmium batteries, the two types of flow batteries, vanadium redox and zinc–bromine, as well as pumped hydro energy storage systems, have higher range of values regarding power related costs.

Regarding the energy related cost, pumped hydro and compressed air energy storage systems have the lowest range of values, followed by the lead–acid, sodium–sulfur, zinc–

bromine flow batteries and flywheels. The nickel–cadmium and vanadium redox flow batteries have the highest range of values regarding energy related costs. Regarding the environmental issues of each large scale energy storage system, the different types of batteries have to handle chemical disposal, specifically lead–acid and nickel–cadmium batteries which dispose lead and toxic cadmium. The effect of pumped hydro energy storage systems in the environment is the pollution of the construction of the two reservoirs, whereas for the compressed air energy storage systems is the emission of gas into atmosphere. Finally, flywheels have only a slight effect in the environment.

The recent advances in pseudo-capacitive nanomaterials for electrochemical supercapacitor applications had shown that nanoscale approaches are playing a key role in the progression of the technology. Nanoscale engineering is being applied to achieve elegant material and device configurations that offer a hitherto unachievable balance of energy and power characteristics at the laboratory scale. The beneficial use of nanoscale effects in electrochemical energy storage include: (1) a reduction in the dimensions of electrode materials that increases the electrode /electrolyte contact area per unit mass significantly, providing more ion adsorption sites for double-layer formation and charge-transfer reactions; (2) a reduction in ionic diffusion distances that improves high rate charge/discharge capability, including the use of three-dimensional nano/meso-architectures; (3) a greater tolerance to the otherwise pulverizing volumetric changes upon ion insertion /extraction and other reactions; and (4) the potential to achieve unusual multi-functionality such as low weight, transparency and flexibility.

Amongst pseudo-capacitive redox active materials, metal oxides are predominant. Technologies for well-controlled growth of metal oxide nanostructures have been established and provide the building blocks to construct nanoscale electrode configurations with optimized morphology, porosity, crystallinity and wetting characteristics. In particular, interpenetrated or vertically aligned 1-D wire-like, tubular and 3-D mesoporous topologies offer a low diffusion barrier, a high areal density of active surface sites and a high strain tolerance. Carbon-based materials are anticipated to continue to be an important component of commercial supercapacitors because they are efficient stabilizers and substrates for pseudo-capacitive materials and are available in a rich variety of morphologies and surface conditions. The technological use of CNTs or even graphene in supercapacitors is likely to first occur as a minority, low volume fraction additive to composite electrodes. Free-standing CNT electrodes can also be envisaged if manufacturing costs can be reduced significantly. The many device configurations afforded by nanostructured hybrid supercapacitors involving asymmetric and/or organic electrolyte configurations provides a wide scope to develop devices that can compete with commercial supercapacitors and batteries for particular energy density-power density combinations. The incumbent, industrialized supercapacitor technology based on activated carbon electrodes provides a stiff test for any emerging supercapacitor technology in terms of cost, cyclability and ease of manufacture. Cost-effective processing, assembly and packaging remains a major barrier for practical implementation of nanostructured materials. Therefore, increasing emphasis should be placed on nanoscale material-process combinations that offer the potential for cost-effective mass production if market penetration is to be achieved.

The main findings and recommendations of THINK Report on energy storage[312] summarised below:

- The core of the business model for electricity storage is how the storage facility's functionalities (regarding up- and down-ward adjustment and accumulation) are matched with the services to be provided. Numerous studies have shown that by focusing on only one specific application, electricity storage typically cannot reach profitability in the current market context.
- Electricity storage has been identified as one key technology priority in the transition of the European power system towards decarbonization in the 2020/2050 context, but the majority of possible technologies are not yet commercially available. Market failures and high risks at stake encourage private inventors and investors to focus on projects that pay off in the near-term, whereas the optimal portfolio of solutions providing flexibility has a considerably longer time horizon – certainly looking ahead to the 2050 target. Public support is needed to reduce the risks of investment in RD&D and boost the level and timing of private investment. The report confirms the importance of EU involvement in RD&D. Financial support to RD&D already takes place, however, support programs are hardly coordinated – neither between different Member States, nor between them and the EU. The European energy technology policy instrument in place (SET-Plan, launched in 2008) does not elaborate any comprehensive strategy for electricity storage development taking into account the whole set of technologies and their possible applications. There is no clear vision on the future role of electricity storage in the European power system. A renewed European energy technology policy, going beyond the SET-Plan horizon of 2020, should include a technology roadmap for electricity storage. Coordination among Member State and EU support policies have to be improved and public support should target a balanced portfolio of identified key technologies, including both centralized and decentralized energy storage technologies. Areas where European players already have a strong position in RD&D and/ or manufacturing and which have potential for future growth should be of particular interest.

---

[312] J. Vasconcelos et al. Topic 8: Electricity Storage: How to Facilitate its Deployment and Operation in the EU. Final Report, June 2012

4 FORECAST OF RELATED RTD ACTIVITIES AND SCIENTIFIC POTENTIAL DEVELOPMENT

4.1 Specific technology goals and R&D issues

With the aim of achieving further significant cost reductions and efficiency improvements, R&D is predicted to continuously progress in improving existing technologies and developing new technologies. It is expected that a broad variety of technologies will continue to characterise the PV technology portfolio, depending on the specific requirements and economics of the various applications. Figure 99 gives an overview of the different PV technologies and concepts under development.

Figure 99: Photovoltaic technology status and prospects[313]

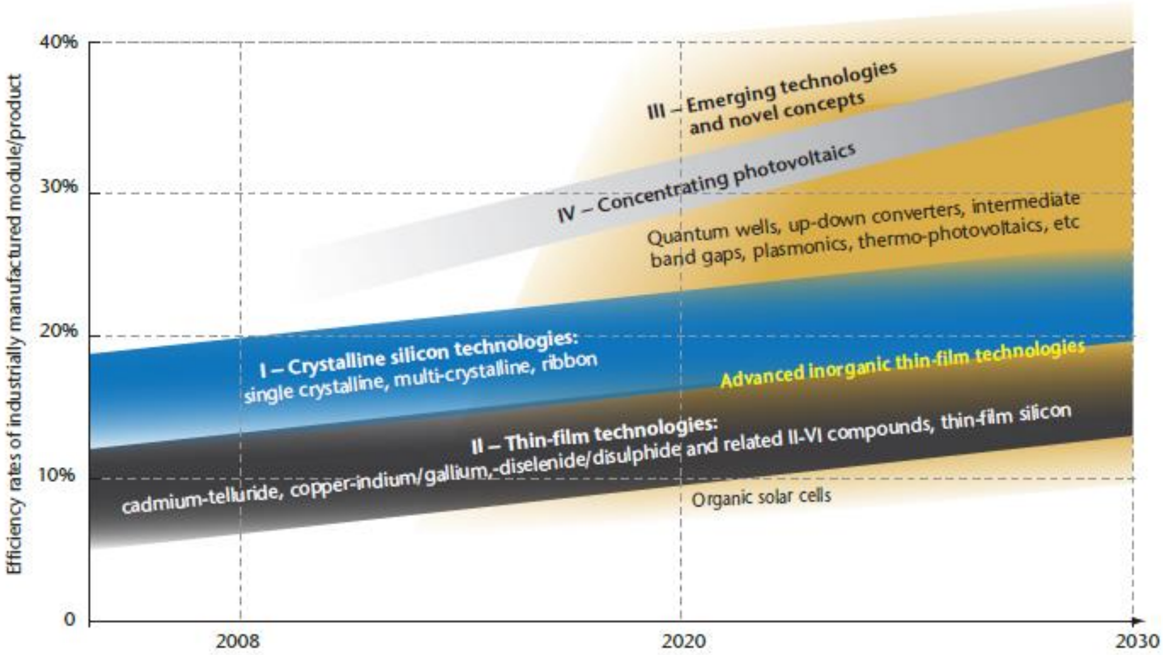

It is important to note that current mature technologies do and will co-exist with emerging technologies and novel concepts.

Quite a few PV technology roadmaps and research agendas are prepared on the basis of consultations with representatives of research, industry and other stakeholders.[14,314,315,316,317,318] setting the targets for PV technology with the parallel initiatives are undergoing in EU, US and Japan. All the initiatives are aimed at the same goal – to make the cost of solar energy competitive with the cost of other energy sources, paving the way for rapid, large-scale adoption of solar electricity. The SunShot Initiative aims to reduce the price of solar energy systems by about 75% between 2010 and 2020.

---

[313] Technology Roadmap: Solar photovoltaic energy. International Energy Agency. 2010

[314] A Strategic Research Agenda for Photovoltaic Solar Energy Technology. European Photovoltaic Technology Platform. Edition 2. 2011

[315] International Technology Roadmap for Photovoltaics (ITRPV). SEMI Europe. March 2012 (full edition)

[316] European Industrial Initiative on solar energy - Photovoltaic energy.

[317] PV2030+ (PV roadmap towards 2030 and beyond). NEDO Jan 2009

[318] SunShot Vision Study. US Department of Energy (Feb 2012)

Achieving this target is expected to make the cost of solar energy competitive with the cost of other energy sources, paving the way for rapid, large-scale adoption of solar electricity across the United States.

Table 25 summarises a set of general technology targets for PV systems, expressed in terms of (maximum) conversion efficiency, energy-payback time, and operational lifetime.

Table 25: General technology target

Target (rounded figures)	2008	2020	2030	2050
Typical flat-plate module efficiencies	Up to 16%	Up to 23%	Up to 25%	Up to 40%
Typical maximum system energy pay-back time (in years) in 1500 kWh/kWp regime	2 years	1 year	0.75 year	0.5 year
Operational lifetime	25 years	30 years	35 years	40 years

Typical commercial flat-plate module efficiencies are expected to increase from 16% in 2010 to 25% in 2030 with the potential of increasing up to 40% in 2050. Concurrently, the use of energy and materials in the manufacturing process will become significantly more efficient, leading to considerably shortened PV system energy pay-back times.[319] The latter is expected to be reduced from maximum two years in 2010 to 0.75 year in 2030 and below 0.5 year in the long-term. Finally, the operational lifetime is expected to increase from 25 to 40 years.

PV efficiency can refer to many components of a system, all of which affect energy conversion. Although the most straightforward metric is system energy conversion efficiency over the life cycle of the system, the sunlight-to-electricity (AC) process needs be broken down to several parts where specific R8D activities can be focused. Accordingly, R&D opportunities can be found at different levels: solar cell efficiency, PV module efficiency and long-term operational reliability.[320]

4.1.1 Crystalline silicon

Today, the vast majority of PV modules (85% to 90% of the global annual market) are based on wafer-based c-Si. Crystalline silicon PV modules are expected to remain a dominant PV technology until at least 2020, with a forecasted market share of about 50% by that time (Energy Technology Perspectives 2008). This is due to their proven and reliable technology, long lifetimes, and abundant primary resources. The main challenge for c-Si modules is to improve the efficiency and effectiveness of resource consumption through materials reduction, improved cell concepts and automation of manufacturing. The manufacturing of c-Si modules typically involves growing ingots of silicon, slicing the ingots into wafers to make solar cells, electrically interconnecting the

---

[319] The energy pay-back time is defined as the time needed for the PV system to repay the energy spent for its manufacturing.

[320] X. Wang et al. High efficiency photovoltaics: on the way to becoming a major electricity source. Wiley Interdisciplinary Reviews: Energy and Environment. Volume 1, Issue 2, pages 132–151, September/October 2012

cells, and encapsulating the strings of cells to form a module. Modules currently use silicon in one of two main forms: single- sc-Si or mc-Si. Current commercial single sc-Si modules have a higher conversion efficiency of around 14 to 20%. Their efficiency is expected to increase up to 23% by 2020 and up to 25% in the longer term. Multi-crystalline silicon modules have a more disordered atomic structure leading to lower efficiencies, but they are less expensive. Their efficiency is expected to increase up to 21% in the long term. Continuous targeted R&D on sc-Si technologies in public and industrial research with a near-term focus can result in a substantial cost reduction and an associated volume effect, both of which are needed to enhance the competiveness and accelerate the scaling-up of PV in the next decade. The major required R&D efforts for crystalline solar cells are summarised in Table 26.

Table 26: Technology goals and key R&D issues for crystalline silicon technologies

Crystalline silicon technologies	2012-2015	2015-2020	2020-2030 / 2050
Efficiency targets in % (commercial modules)	• Single-crystalline: 21% • Multi-crystalline: 17%	• Single-crystalline: 23% • Multi-crystalline: 19%	• Single-crystalline: 21% • Multi-crystalline: 21%
Industry manufacturing aspects	• Si consumption < 5 grams / Watt (g/W)	• Si consumption <3 g/W	• Si consumption < 2 g/W
Selected R&D areas	• New silicon materials and processing • Cell contacts, emitters and passivation	• Improved device structures • Productivity and cost optimization in production	• Wafer equivalent technologies • New device structures with novel concepts

As the dominant solar cell material in PV industry, crystalline Si has achieved 25% and 22.9% cell and module efficiencies, respectively. The record cell efficiency is at 84% of its theoretical efficiency limit of 29.8%, and the record module efficiency is 92% of the record solar cell efficiency. These great efficiencies require very high material quality that provides long initial carrier lifetimes, a well-controlled pure growth environment that maintains the long lifetimes during cell fabrication, and delicate cell structures. All of these factors can greatly increase cost and are not compatible with high volume manufacturing, given fabrication technologies that have already been developed for use by the microelectronics industry. As a relatively new field, the PV industry evolved mostly by adopting the available techniques and equipment of microelectronics. Thus, goals to increase efficiency largely avoid designs, which would depend upon radical alternations of microelectronics manufacturing methods and/or equipment. Despite the achievement of high efficiencies at both the cell and the module levels during the 1990s, the current PV market is dominated by Si-based modules[j] with efficiencies in the range of 13–17%. With the current practical constraint on efficiency, the PV industry has still experienced impressive growth in the volume of production, with 38% yearly market expansions on average during the past two decades. Having opened the door of the market, attention is now focused on increasing performance to lower the cost of PV energy supply and thereby widen its market. Si materials for PV fabrication can be generally divided into two categories: crystalline and amorphous. According to the grain size of the crystal, further sub-categories are as follows: single-crystalline (>10 cm), multi-crystalline (1–100 mm), poly-crystalline (1–1000 μm), and nano-crystalline (81 μm). From an engineering point of view, each type has potential to achieve higher efficiency at both the cell and module level. The limit of achievable efficiency, however, is intrinsically set by material quality. The current record efficiencies for mc-Si cells and modules are 20.4% and 18.2%, respectively. Although most commercial companies manufacture c-Si modules of efficiency in the range of 13–16%, one exception is SunPower, whose commercial products (e.g., E20/327) realize 22.5% efficient solar cells and have achieved module efficiency of more than 20%.The high module efficiency is mainly attributed to long lifetimes of the carriers and back contact cell design, which avoids the 7% shading loss for cells with screen-printed contacts. This achievement indicates another more radical R&D approach: instead of applying modifications while maintaining the main frame of the manufacturing line, newly designed lines can be developed for new concepts. Rather than improving the growth conditions and modifying the structure for the traditional thick Si cells, another more radical R&D approach is thin film Si cells. The most apparent advantage of thin film cells is the cost saving on material; moreover, high cell efficiency is another great attraction. The principle of the high efficiency resides in less bulk recombination due to a reduced distance; the minority carriers need to travel before they arrive at the depletion region. The realization of this concept, however, enhances the necessity of two other improvements: surface passivation and light trapping. As the thickness is reduced, the density of minority carriers generated close to the surface increases; therefore, cell efficiency is more dependent on the surface passivation. Si oxide and Si nitride have been used for that purpose. Another improvement related to thin film Si cells concerns light capturing. Si has an indirect band gap and the resultant low absorption coefficients require a longer path for sunlight to be highly utilized. As the physical thickness of a Si cell decreases, cell structure needs to be adjusted to increase the effective path length, and this is the basic concept of light trapping. One option of light trapping is to utilize interference in a Si oxide–metal structure on the bottom. Another option is texturing the front surface. Pyramids on the surface can alter the propagation direction of the sun's rays in the solar cell and therefore lengthen the optical path. When texturing on the front side is available, the rear side reflector can be adjusted such that total internal reflection (TIR) can occur for multiple passes. Another function of texturing is that the reflected rays at one pyramid strike a neighboring pyramid, allowing additional light to be captured. Although the high efficiency feature of thin film Si cells necessitates improvements on surface passivation and light trapping, the realization of its low cost requires innovations in wafer or epitaxy layer processing. To achieve thin Si cells, a straightforward approach is to reduce the thickness of the wafer. Currently, the thickness of commercial crystalline Si wafers is in the range of 180–210 μm; future improvements are likely to lead to wafer thickness below 100 μm. This change enhances the requirement of wafers‘ mechanical strength, and caution must be exercised in subsequent processing steps. For instance, sawing technologies need to be improved, as well as new screen printing techniques (or alternatives to fabricate the contacts) and better handling and shipping. The thin wafer approach is based on the assumption that the wafer is one functioning component of the solar cell. Overthrowing that assumption, there is a second approach that adopts the concept of ’layer transfer‘. This approach allows the thin solar cells to be lifted off the substrate wafer, which can be used multiple times. A mesoporous double layer between the substrate wafer and the thin solar cell is the innovative component that allows the layer transfer. Currently, a record efficiency of 19.1% has been achieved on thin Si solar cells fabricated with this technology. This achievement is a demonstration of realizing high efficiency in thin Si cells, and further improvement on performance is expected. However, the current laboratory fabrication steps are complex, and continuous R8D activities are required to simplify manufacturing steps for high volume production.

4.1.2 Thin films

Thin films are made by depositing extremely thin layers of photosensitive materials in the micrometre (μm) range on a low-cost backing such as glass, stainless steel or plastic. The first thin film solar cell produced was a-Si. Based on early a-Si single junction cells, amorphous tandem and triple cell configuration have been developed. To reach higher efficiencies, thin amorphous and microcrystalline silicon cells have been combined to form micromorph cells (also called thin hybrid silicon cells). In the area of II-VI semiconductor compounds, other thin film technologies have been developed, including Cadmium Telluride (CdTe) and Copper-Indium-Gallium-Diselenide (CIGS). Another option currently being researched is the combination of single-crystalline and amorphous PV cell technology. The HIT (Heterojunction with Intrinsic Thin layer cells) technology is based on a crystalline silicon cell coated with a supplementary amorphous PV cell to increase the efficiency. The main advantages of thin films are their relatively low conumption of raw materials, high automation and production efficiency, ease of building integration and improved appearance, good performance at high ambient temperature, and reduced sensitivity to overheating. The current drawbacks are lower efficiency and the industry’s limited experience with lifetime performances. Increased R&D is needed to bring thin film technologies to market and to create the necessary experience in industrial manufacturing and longterm reliability. The most promising R&D areas include improved device structures and substrates, large area deposition techniques, interconnection, roll-to-roll manufacturing and packaging. Table 27 summarises the prospects and key R&D issues for thin film technologies until 2030. Thin film technologies are in the process of rapid growth. In the last years, thin film production units have increased from pilot scale to 50 MW lines, with some manufacturing units in the GW range recently announced. As a result, thin films are expected to increase their market share significantly by 2020. CdTe cells are a type of II-VI semiconductor thin film and have a relatively simple production process, allowing for lower production costs. CdTe technology has achieved the highest production level of all the thin film technologies. It also has an energy payback time of eight months, the shortest time among all existing PV technologies. For CIGS cells, the fabrication process is more demanding and results in higher costs and efficiencies compared to CdTe cells. Today, CdTe has achieved a dominant position amongst thin film in terms of market share and has a market-leading cost-per watt. However, it is difficult to predict which of the thin film technologies will reach higher market shares in a mid- and long-term perspectives.

Table 27 Technology goals and key R&D issues for thin film technologies

Thin film technologies	2010-2015	2015-2020	2020-2030
Efficiency targets in % (commercial modules)	• Thin film Si: 10% • Copper indium gallium (di)selenide (CIGS): 14% • Cadmium-telluride (CdTe): 12%	• Thin film Si: 12% • CIGS: 15% • CdTe: 14%	• Thin film Si: 15% • CIGS: 18% • CdTe: 15%
Industry manufacturing aspects	• High rate deposition • Roll-to-roll manufacturing • Packaging	• Simplified production processes • Low cost packaging • Management of toxic materials	• Large high-efficiency production units • Availability of manufacturing materials • Recycling of modules
Selected R&D areas	• Large area deposition processes • Improved substrates and transparent conductive oxides	• Improved cell structures • Improved deposition techniques	• Advanced materials and concepts

With properties that are advantageous for PV applications, CIGS cells have been researched since the early 1970s. This research has led to improved material deposition methods, better device structure designs, and more cost-effective manufacturing procedures. The current record efficiencies for CIGS are 19.6% and 15.7% at the solar cell and module levels, respectively. These achievements, however, have been partially based on empirical improvements, and the underlying principles are not yet fully understood. Reproducibility of large volume manufacturing with current achieved performance and further efficiency improvement will depend upon a more solid understanding of the working mechanisms. For instance, it is empirically known that the presence of Na in CIGS is beneficial for PV performance. However, the principle underlying the effect of Na has not been fully understood, although a tentative explanation that Na helps passivation on grain surface is being investigated. Another puzzle concerns the influence of grain size on CIGS cell performance. Different from c-Si solar cells, whose performance is directly related to grain size (due to the correlated recombination), CIGS solar cells display insensitivity to grain size. Although tentative explanations are given, the underlying principles are not yet known. As with other solar cells, reducing recombination by improving material quality should be a fundamental R&D direction for CIGS solar cells. For that purpose, modeling of the grain boundary behaviours based on a detailed understanding of the phenomenon is necessary. Another R&D focus is to develop a better substrate. Because CIGS film growth occurs on top of a substrate made of a different material, the thermal expansion coefficients of the substrate and the CIGS film should be the same in order to avoid stress. A good match of this parameter has been found with soda-lime glass. However, this glass begins to soften at 500°C, whereas ideal solar cell fabrication needs an operating temperature above that point. This conflict does not greatly affect the record cell performance because the cell has a small area and its performance is not very sensitive to glass deformation. However, a glass with higher temperature resistance will be necessary for high efficiency large volume production. Compared with c-Si solar cells, CIGS involve multiple types of materials in the fabrication. This diversity necessitates more sophisticated control of material deposition parameters and diagnostic tools to identify problems. Developing a comprehensive design of deposition equipment, manufacturing and diagnostic tools could greatly improve large volume production, in which reproducibility and uniformity are desired.

A second type of extensively investigated thin film solar cells is based on CdTe. The record efficiencies of CdTe are 16.7% and 12.8% at solar cell and module levels, respectively, both of which are 2.9% (absolute), lower than that for CIGS. Notwithstanding its lower efficiency, CdTe experienced greater market penetration and developed more mature manufacturing techniques. The biggest CdTe commercial company, First Solar, has achieved a total manufacturing capacity of 2.4 GW. This company claimed that its FS-390 series has a module efficiency of 12.5%, very close to laboratory record. The current CdTe solar cell structure and fabrication conditions are based on empirical learning to a great extent, together with a basic understanding of this material. Although the band gap property of CdTe allows its theoretical solar cell efficiency to be above 30%, cell efficiency in the laboratory has hovered at 16.7% for a decade. The barrier has been commonly attributed to low open-circuit voltage (V_{oc}) and fill factor (FF). To raise this cell efficiency, a promising approach is to improve the quality of the CdS/CdTe junction to achieve lower forward-current recombination. An equally promising direction is to focus on reducing recombination states at the grain boundaries as well as in bulk. Besides recombination problems, another challenge is to overcome self-compensation in p-type CdTe doping to achieve the desired doping concentration. Each of these problems requires basic research in order to realize a deeper understanding of the material's properties. Another significant focus for CdTe solar cells is to stabilize long-term performance. A widely observed reliability issue for CdTe solar cells concerns the barrier at the back contact. Although tentative explanations attribute the problem to copper used in the back contact, a better understanding is needed.

4.1.3 Emerging technologies and novel concepts

The approach of emerging photovoltaics is mostly build on progress in nanotechnology and nano-materials. Quantum wells, quantum wires and quantum dots are examples of structures introduced in the active layer. Further approaches deal with the collection of excited charge carriers (hot carrier cells) and the formation of intermediate band gaps. These novel concepts are currently the subject of basic research. Their market relevance will depend on whether they can be combined with existing technologies or whether they lead to entirely new cell structures and processes. Large market deployment of such concepts – if proven successful – is expected in the medium to long term. Considerable basic and applied R&D efforts aimed at the mid- to long-term are required in order to further develop these approaches and to ultimately bring them to market in end use applications.

4.1.4 Concentrator technologies (CPV)

All PV technologies described so far are so-called flat-plate technologies which use the naturally available sunlight. As an alternative, direct solar radiation can be concentrated by optical means and used in concentrator solar cell technologies. Considerable research has been undertaken in this high-efficiency approach because of the attractive feature of the much smaller solar cell area required. Low and medium concentration systems (up to 100 suns) work with high-efficiency silicon solar cells. For the highest concentration levels beyond 500 suns, III-V compound semiconductors are being used for the CPV solar cells and efficiencies beyond 40% have been achieved in the laboratory. The CPV technology is presently moving from pilot facilities to commercial-scale applications. Further R&D efforts are required in optical systems, module assembly, tracking systems, high-efficiency devices, manufacturing and installation. The prospects and key R&D issues for CPV as well as emerging and novel technologies are summarized in Table 28.

Table 28 Prospects and key R&D issues for concentrating PV, emerging and novel technologies

Technology	Concentrating PV	Emerging technologies	Novel technologies
Type of cell	High cost, super high efficiency	Low cost, moderate performance	Very high efficiency Full spectrum utilization
Status and potential	23% alternating-current (AC) system efficiency demonstrated Potential to reach over 30% in the medium-term	Emerging technologies at demonstration level (e.g. polymer PV, dye PV, printed CIGS) First applications expected in niche market applications	Wide variety of new conversation principle and device concepts at lab level Family of potential breakthrough technologies
Selected R&D areas	Reach super high efficiency over 45% Achieve low cost, high-performance solutions for optical concentration and tracking	Improvement of efficiency and stability to the level needed for first commercial applications Encapsulation of organic-based concepts	Proof-of-principle of new conversion concepts Processing, characterization and modeling of specially nano-structured materials and devices

4.2 Expected impact of roadmaps and research agendas

In previous years the PV supply chain has been plagued by mismatched supply and demand. How can manufacturing supply chain stakeholders address these imbalances collectively? One approach, proven time and again in the semiconductor and other high-tech industries, is through working together on technology roadmaps and standardization. Technology roadmaps are a systematic way for a supply chain to chart its own future, agree on targets and milestones and identify change drivers together, leaving room for innovation and differentiation along the way (Figure 100). Collaborating on standards and technology development has never been more important in PV. One example of PV technology roadmap development is the ITRPV, International Roadmap for Photovoltaics.[321]

Figure 100: Application of international standards in Photovoltaic industry

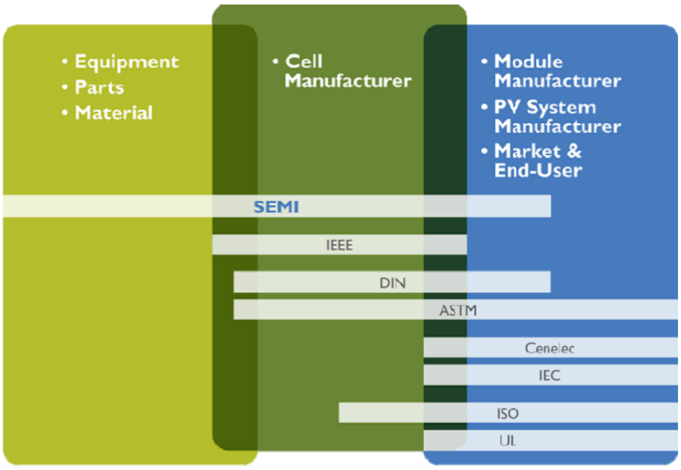

One of the c-Si manufacturers contributing to the ITRPV also spearheaded a Standards effort in the area of process automation. The semiconductor industry has long used a SEMI Standard for semiconductor equipment communication – generic equipment model (SECS-GEM), which is also applicable to the PV manufacturing process. The cell manufacturer actively contributed to a task force activity working on this issue, which finally resulted in SEMI PV2 Guide for PV Equipment Communication Interfaces (PVECI), now widely adopted in the industry. By participating in a collective public forum and influencing the direction the specification was taking, the manufacturer ensured manufacturability and subsequent cost reduction through a standardized approach to how individual pieces of equipment “talk” to one another, including standardized diagnostics data from multiple tools. This standards effort and others currently being developed set the competitive benchmark for the industry. Companies participating in the standards development process have an edge over those who don't, because they influence the direction a new standard is taking. The difference between redesigning a tool to be in compliance compared to taking existing design and making it standard can directly affect the bottom line. In the U.S., through the DOE SunShot Initiative, the College of Nanoscale Science and Engineering (CNSE) along with Sematech was awarded funding to form a CIGS (Copper Indium Gallium Diselenide) PV Manufacturing Consortium (PVMC) which includes collective R&D and piloting, as well as the development of a CIGS technology roadmap. Standards are a natural result of Roadmap activity. First, some history of successes is in order. Understanding the success of the

---

[321] http://www.itrpv.net/

standards making effort over the last forty years is key to one's understanding of how collaborating to make industry standards is in the best interest of one's own company. The SEMI International Standards Program founded in 1972, provides a global platform for expert volunteers from industry, academia and R&D to address cost drivers, safety concerns, process efficiency improvements and other issues collectively and globally. The Global PV Technical Committee, formed in 2008, has now grown to a 500 strong effort, spanning activities from silicon feedstock specifications to module vibration testing. 33 PV Standards have so far been developed by the international PV community, with dozens more in the works. SEMI's full portfolio of more than 800 Standards and Safety Guidelines contains dozens of other documents that are applicable to PV, and SEMI is putting great effort into communicating the cost reduction benefits when applying them in the field. Standards provide a global support system of specifications, test methods and safety guidelines needed to reduce manufacturing cost, ensure worker and equipment safety, enhance process efficiency through automation – and bring the global supply chain together around the issues that matter most to the industry, thus allowing time to focus on innovation and technology development in-house. These benefits accrue through the cycle but especially when investment dollars in research and development are spread thin in the down-cycle. Participants the standards making process find that they are able to leverage their in-house efforts in ways that protect and enhance their proprietary activities in good t in bad while promoting the best practices that are adopted by the industry at large risk of investment spending and technology choice grows larger disproportionately by comparison. This key differentiation may play a critica maturation of the PV industry as it did in semiconductors again creating positive opportunities for the industry to collaborate in ways that have proven benefits. The global PV market will continue to grow, and countries with balanced incentive schemes, a healthy domestic supply chain and the vision to collaborate internationally on pre- and non-competitive issues will lead. Roadmaps and Standards are proven means to counteract cyclicality and supply/demand imbalances and are a vital piece to increasing the level of public adoption of solar energy and its deployment everywhere.

5 CONCLUSIONS

The main conclusions that can be drawn from this study are detailed below.

Conclusion 1: c-Si currently is and will remain a dominant photovoltaic technology in the foreseeable future, however, it will lose its place of dominance in the total growing photovoltaic technology portfolio

Conclusion 1 is based on the following:

Growing c-Si photovoltaic production	Reducing share of c-Si photovoltaic technologies
(1) Mono- and polycrystalline PV technology have more than 80% market share with 15–18% efficiency; (2) c-Si PV is mature technology with well eactablised industrial infrastructure throughout the whole value chain (3) Higher learning rate in comparison with other PV technologies; (4) The element silicon is the second most abundant element on the earth's surface	(1) Thin film technologies (CdTe, CIGS) with 8-13% efficiency, are gaining first level of maturity at high volume manufacturing in a cost-competitive way (2) c-Si efficiency is close to the theoretical limit, for thin films there is still much room for improvements; (3) Polymer based solar cells and emerging solar cells are in development stage and extensive research work is going for efficiency and stability improvement for commercial use

Note: These points are drawn from Chaper 2 and 4 primarily.

Conclusion 2: Technology innovations are the main drivers for the cost reductions throughout the photovoltaic supply chain

Conclusion 2 is based on the following:

Crystalline Silicon photovoltaics

Main technology trends	Challenges to be solved
Wafer	
(1) The alternatives for common Czochralski process, such as the Magnetic-confined Czochralski and Gallium doped Czochralski (Ga Cz) growth technologies enabling the enhanced cell-efficiency.	(1) Aditional capital expense for each Cz-puller for implementation of the Magnetic-confined Czochralski (M-Cz) process. (2) Alternative dopants, such as Gallium greatly reduce the recombination within a wafer, but add production challenges: difficult management of doping during ingot formation – potentially limiting the usable as-grown length of ingots. (3) To avoid cross-contamination, silicon materials from ingot and wafer lines running boron-doped feedstock would have to be run entirely separate from gallium-doped silicon lines. (4) High lifetime materials produced using alternative dopants, such as Gallium, currently are not cost effective due to the negative impact on the Czochralski process yields
(2) Quasi-monocrystalline – emerging technology that enables solar cell efficiency of monocsyrstalline and the costs close to multicystaliine silicon	(5) The colour difference on the grains with different orientation after alkali texturing causes aesthetic concerns in residential applications. (6) The endurance and attenuation of the electrical properties (7) A consensus on the quality of the quasi-mono wafers is still missing.

Main technology trends	Challenges to be solved
(3) Reduced wafer thickness and low/zero kerf-loss	(8) Cost-effective and practical kerf-free wafering substitute to the present sawing technology (9) Solutions for mitigation of yield losses due to microcracks and throughput challenges. (10) development of wafer equivalent technologies
(4) n-type wafers that generally reaches (much) higher lifetimes than p-type silicon for solar cell production	(11) Solving the differences between n-type and p-type cell processing (12) The complexity and cost of managing multiple material streams in high volume operations
Solar cell	
(5) Efficiency improvement of solar cells introducing advanced and industrially-relevant architectures	(13) Use *n*-type wafers with ms minority carrier lifetimes (14) Selectively diffused emitter junctions (15) Improved light trapping through novel surface texturing and higher internal light reflection (16) Improve back, front, and edge surface passivation (17) Development of new laser-based manufacturing processes
(6) Reduced silver metallization	(18) Development of technologies for use of alternative materials such as Ni and Cu.
Module	
(7) Advanced manufacturing methods for higer yield and throughput	(19) Significant improvement of interconnection technology together with stress-relieving supporting structures (20) Integration of cell and module manufacturing (21) Laser-based and low-temperature processing for monolithic module manufacturing needed to reduce thermal stress in thin wafers (22) Automation levels must be increased in a cost-effective manner to reduce the labor cost (and related inflation risk), to reach volume production faster with a stable process and higher yield of the manufacturing operation (23) The movement to thin or ultrathin wafers necessitates the modification or even incorporation of module materials into wafer handling and cell processing
(8) New concepts and flexible design of PV modules, enabling diversification of application areas	(24) Development of solutions for: - Frameless, thin glass/glass modules, icluding new high-strenght encapsulants - Plastic-framed module designs - Flexible sizes of the modules for utility scale and niche applications

Note: These points are drawn from Chaper 2.1 and 4 primarily.

Thinfilm photovoltaics

Main technology trends	Challenges to be solved
(1) CdTe and CIGS are the most advanced thin film materials already in high volume manufacturing, however further cost reduction of manufacturing	(1) The key aspects to be addressed are: - Less pure feedstock materials - Increasing material utilization during deposition - Reduced active layer thicknesses - Minimization of interconnect losses - Throughput/tact time per unit per equipment - Process and manufacturing yield - Equipment availability/uptime
CdTe	
(2) The use of ultrathin active layers - while also improving efficiencies	(2) Technical improvement opportunities: - Improved light transmission through the front glass and thinner thinner glass - Reduce window layer absorption by thin or replace CdS, substrate architecture - Improve minority-carrier lifetimes in CdTe: grain size, crystallinity, grain boundary passivation; - Improve film uniformity - Reduce CdS/CdTe junction recombination via doping - Electron back reflector - Te price is significant contribution to module costs and is a critical element in evaluation of economic viability of this PV technology - Uncertain acceptance of Cd-containing products in various markets
CIGS	
(3) CIGS technology is on the way to maturity and overtake of CdTe PV modules, due to superior device efficiency both at the lab and production scale	(3) The following technological aspects of complex manufacturing are solved: scale-up issues related to various CIGS preparation technologies such as co-evaporation, metallic precursor deposition by magnetron sputtering and non-vacuum techniques such as ink-jet printing, electroplating or doctor-blade technology followed by their selenization/sulfurization
Thin-Si	
(4) Poly-Si thin-film solar cells on foreign substrates	(4) The successful transfer of laboratory scale results to the low cost, high volume manufacturing scale (5) A significant degree of innovation at the equipment and product design

Note: These points are drawn from Chaper 2.2 and 4 primarily.

Concentrator photovoltaics

Main technology trends	Challenges to be solved
(1) Achievement of higher CPV module efficiency through: - Employement of small unit concept (each submodule is of small active area) - Switching from high to low-mid concentration	(1) adoption of innovative'lift-off' concept that allows multiple uses of expensive substrates for growth of thin epitaxial layers (2) high alignment accuracy needs to be maintained in both laboratory conditions and real operation

Note: These points are drawn from Chaper 2.3 and 4 primarily.

Conclusion 3: Current mature technologies do and will co-exist with emerging technologies and novel concepts

Conclusion 3 is based on the following:

Main technology trends	Challenges to be solved
(1) The business potential of orgnanic solar cells is large, however, the current performance leaves little room for competition with other thin film technologies. (2) Dye sensitizes solar cells need an increase in power-conversion efficiencies and develop ultralow-cost architectures that are stable over 20 years (3) Different device concepts, especially based on molecular and nanoparticulate materials, generates more thorough understanding of the fundamental mechanisms of PV devices may be applied to conventional solar technologies.	(1) The power conversion efficiency, operational lifetime, and cost would all need to be much better before a significant market share can be anticipated. (2) better matching the energy levels at the heterojunction, using more strongly absorbing dyes in thinner films and further inhibiting recombination losses, pushing efficiencies to 19% with a dye capable of absorbing out to 920 nm (3) a thorough understanding of the overall lifetimes and degradation mechanisms

Note: These points are drawn from Chaper 2.4 and 4 primarily.

Conclusion 4: Currently immature energy storage technologies are a missing link hindering the contribution of intermittent renewable energy sources like wind and solar to the transition of the European power system towards decarbonization

Conclusion 4 is based on the following:

Main technology trends	Challenges to be solved
(1) Battery energy storage systems are mainly used as ancillary services or for supporting the large scale solar and wind integration in the existing power system	(1) Batteries with new electrolytes operating at room temperature (2) Improvement of cycle life, including cases of deep discharge, efficiency and energy density (3) Increased safety and abuse tolerance
(2) Supercapacitors are foreseen for short-term storage	(4) The technology for material synthesis is still facing a challenge in establishing controllable fabrication of nanostructures with the fully desired morphology, structure, facets, surface chemistry, etc. More insightful understanding of the relationship between (5) The device performance and the material structure, including the chemical properties, with the aim to further develop the merits of nanostructured materials for enhancing the device performance in terms of reaction activity, electron or ion transport, etc., is needed. (6) An optimization of the existing nanostructures to maximize the contribution resulting from nanostructures is also necessary. (7) New mechanisms relying on nanostructures are anticipated to increase power density (8) Developing new material and structures (9) The major barriers for practical implementation of nanostructured materials are cost-effective processing, assembly and packaging

Note: These points are drawn from Chaper 3 primarily.